



Universitat Autònoma de Barcelona

ADVERTIMENT. L'accés als continguts d'aquesta tesi queda condicionat a l'acceptació de les condicions d'ús establertes per la següent llicència Creative Commons:  http://cat.creativecommons.org/?page_id=184

ADVERTENCIA. El acceso a los contenidos de esta tesis queda condicionado a la aceptación de las condiciones de uso establecidas por la siguiente licencia Creative Commons:  <http://es.creativecommons.org/blog/licencias/>

WARNING. The access to the contents of this doctoral thesis it is limited to the acceptance of the use conditions set by the following Creative Commons license:  <https://creativecommons.org/licenses/?lang=en>



Universitat Autònoma de Barcelona

Formation, transformation and inhibition
of calcium oxalate nephroliths:
in vitro studies and speciation by
synchrotron radiation techniques

Iris Henríquez Valido

Doctoral Thesis

Doctorate Program in Chemistry

Director: Assoc. Prof. Montserrat López-Mesas

Tutor: Prof. Manuel Valiente

Department of Chemistry
Faculty of Science

2020



Universitat Autònoma de Barcelona

Report submitted to aspire for the Doctor Degree by

Iris de la Trinidad Henríquez Valido

Approval:

Director: Assoc. Prof. Montserrat
López-Mesas

Tutor: Prof. Manuel Valiente

Bellaterra, 17/12/2020

*“It is not because things are difficult that we do not dare,
but because we do not dare, things are difficult”*

Lucius Annaeus Seneca

FINANCIAL SUPPORT

The PhD thesis presented in this document has been developed thanks to public founding through:

- Pre-doctoral grant, PIF-2016, Universitat Autònoma de Barcelona
- CHEMNEXUS, CTM2015-65414-C2-1-R, Ministerio de Economía y Competitividad de España (MINECO)
- Synchrotron proposals, 2015091387, 2016021675, 2016021706 and 2018022777, ALBA Synchrotron (Spain)
- Synchrotron proposals, 20150877 and 20151226, SOLEIL Synchrotron (France)



Chemistry Department

Universitat Autònoma de Barcelona,
Spain



AGUASOCIAL (612633-FP7)

NEOSETAC (GA778325)

Horizon 2020, European Union
funding for research & innovation,
Marie Curie Actions.



CLAESS, MIRAS and MSPD
beamlines scientists

ALBA Synchrotron



SMIS beamline scientists

SOLEIL Synchrotron

ACKNOWLEDGEMENTS

Well, I cannot believe I am writing this already. After all the time working on this project, there are so many people to thank and I do not know how to do it. I will try to keep it short; the first part is addressed to my family in Spanish.

Primero y más importante, quiero agradecerle a mi madre, porque sin su apoyo, su empeño y su sacrificio nunca habría llegado aquí. Las dos sabemos a lo que me refiero. La oportunidad de poder estudiar en Barcelona y poder estar lejos de casa para acabar haciendo este doctorado es, principalmente, gracias a ti mamá. Y no sólo eso, a pesar la distancia física que nos separa, siempre has estado ahí para apoyarme y hacerme sentir que todo va a salir bien y que crees en mí. Así que mamá, esta tesis va principalmente dedicada a ti (sobretudo el artículo 6, que no se habría podido hacer sin tus historias sobre las piedras de riñón en la familia y el “contrabando” de planta jeje). Te quiero mucho.

En segundo lugar, a mi hermano Pedro, por tu apoyo y ánimos, por estar siempre ahí a pesar de estar lejos. Por el amor y el “¿cómo vas por ahí bichillo?” cuando sabes que estoy estresada. Por todo lo que haces, que, aunque parezca que no tiene relación (los dos miramos piedras de alguna manera jajaja), tiene mucha, directa e indirectamente. Gracias también por tu ayuda para poder completar el final de esta tesis, mira que la dichosa plantita no querer tener flores, ¡vaya telita! Pero gracias a tus gestiones, aquí está, un artículo más en la tesis. ¿Te quiero bro!, lo creas o no, eres el mejor.

Elena. Sobrevivir emocionalmente sin los findes de pelis y los paseítos, no habría sido posible sin ti. Te considero familia más que amiga, siempre estás ahí para lo bueno y lo malo. Aunque la vida de mil vueltas, espero que me traiga de nuevo a Barcelona para seguir con nuestras pelis (en serio, la lista de pendientes es cada vez más larga).

Now, going back to the English writing part. I want to start thanking to the group that open arms to welcome me, just a little antisocial and distant girl, at that time. GTS (Montse, Mon, Vero, M Angels, Clara, Nurlin, Elena Victor, Manu, Sandra, Jorge, Laia, Roberto, Mari, Gus, Manolo, Cristina, M Dolors, Alba, Jingjing, Tingting, Lou, Dong, Nithya, Albert, Sergi... and sorry if I left someone out), you are, with all my heart, my second family. The marvelous people in this group makes me believe Barcelona is also my home (you even made me social, somehow). I will try to cover all that I want to say, but I know words will not make justice to what I feel.

There is one person that I need to thank first; she is my Thesis Director, my boss (title shared with my mom, sorry), and a role model for me. Yes Montse, you read

it right. Since my second year in the university, to the master and now the PhD, you have been there, opening the doors to the research world, giving me the chance to make this study and to learn about the synchrotron (I will never forget the opportunities you open for me during these many years) among many things. Moreover, thank you for all the things you taught me, in science and in life. You are amazing and a wonderful person.

Writing about role models and inspiration, the name that comes to my mind is Mon. Really, you are one of the most amazing person I have ever met, without doubts. Traveling with you to Brazil has been my best experience whatsoever (I made thinks I had never though on doing, you encourage me to leave fear, or whatever is my OCT, behind and enjoy life). You are the glue on the group. I love you!!! (even if I don't give a massage jeje).

Manolo, I want also to thank you for all the opportunities you have given me. I learned a lot during this period on your group, not only on my work line, but also in many others. I appreciate what you have done for me and for my career.

Now, when I started in the group I was known to be "borde" and distant (I still am, just a little less), but one person was able to break that wall. Vero, I do not know how to thank you, not only for being my friend, but also for being an important influence of how I am today. The rest, I will tell you with a hug (yep, this will be a written prove that I will be the one giving the hug, not "puercoespín" time).

Nurlin, even if we did not share a lot of time during this thesis, you were there in the beginning. I remember how you helped me start, and all the talk and learning, even with my bad English (worse than now), and the notes through the ICP window while we were working on different sites of the crystal. You really made me feel like I could do it when everything went wrong. I miss you.

M Angels, what to say, long nights will be the best description. From the synchrotrons to the lab, working late is better if it is with you. I already miss you, the adventures and the craziness (I will not tell any of the synchrotron adventures).

Another important person since the beginning, Clara, we started almost together, and it seems that we will finish pretty close. We have shared office and many brainstorming sessions; you taught me the importance of coffee break (also to bring short sleeve in winter so you could turn the office heat up). It will be very difficult to find a better lab partner (excluding the chaos zone, of course).

Special mention also to the craziest part of GTS, I am pleased to say I love ginfaxi team. Jorge and Sandra, we have encounter many troubles in these years but, I do not know how, we have figured it out. The Sweden experience was, how to say it shortly, amazing and frustrating at the same time (ginfaxi tattoo to prove it), even if I had to repeat the videos because you two were singing behind me (I think than

the “*explendida gestión*” of the almost “sugar crush” compensates it), and so many other things. I will miss you, and I hope to have more adventures with you.

Manu! Oh Manu my savior! The only way I have to thank you for all your help will be with tons of chocolate. You have helped me in the lab more times that I can count or remember. The writing of this thesis would not have been possible to accomplish without your help. A part of that, you are the sweetest person in the world, just for you to know it.

Laia, my gym partner. Thank you for being there on the moments of stress, for waking up early to hit the boxing bag with me. You have been a great support. I am going to miss you (and your desserts, of course).

To my Chinese Team (Jingjing, Tingting, Lou and Dong), thank you for all the experiences. The opportunity to know you and to celebrate with you have been amazing (and your dumplings, we cannot forget about the dumplings).

Roberto, I think this thesis already reflects the impact that you had in my work and in my life. You make me see things from a different perspective, and question everything until the end. For me, you are also a mentor, and I hope to continue learning from you.

To Gus and Mari, for the help with the projects stuff. People take for granted these things, but it is really difficult, stressful and full of acronyms. I have learned a lot from you. Thank you.

Page 3 is almost finish, and I know that this person will be thinking I forget about him, but not. From minion to friend, Victor, how could I forget about you? I think I taught you all that I could, but in the end, I can proudly say, you have surpassed me. We will always have time for a coffee break, for sure.

Furthermore, I want to thank to all the minions that have participated in this thesis, whom, believe it or not, have taught me more than I have taught them.

Moreover, I want to thank Hector, Giovana and Jair, as well as Felipe and Leonard, for the experiences in the Amazonas, from personal to the lab. The experiences with you made me, not only learn a lot, but also improve as a person. I will be forever grateful.

To finish I want to make and special mention to Cris, Kimo, Raquel and Aida. Cris, you were my first friend, literally, and to date I know that I can always count with you (and you with me), I love you. Kimo, we know each other since the beginning, even if we cannot be lab partners, we can publish papers together (wink an eye). Raquel, what to say? Cooking time is life (I think that this summarize it pretty well), we will always have skype. Finally, Aida, we survived a quarantine together and ended up with a cat; for the long chats, the catwalks and the laughs, thank you.

CONTRIBUTIONS TO CONGRESSES AND SEMINARS

The results presented in this Thesis Dissertation have been previously made public in the following events:

Oral presentations:

- H.Valido, I., Fuentes-Cebrian, V., Vallcorba, O., Boada, R., Valiente, M., López-Mesas, M. *Differentiating oxalocalcic phases on kidney stones.* (08-11/10/2019) IX AUSE congress and IV ALBA users' meeting, Barcelona, Spain.
- H.Valido, I., Resina-Gallego, M., Valiente, M., López-Mesas, M. *Study of calcium oxalate hydrates transformation and the role of the organic matter on their development by synchrotron-based μ FTIR spectroscopy.* (22-24/05/2019) Jornades Doctorals 2019, Department of Chemistry, Universitat Autònoma de Barcelona, Spain. (First prize)
- H.Valido, I., López-Mesas, M. *Study of calcium oxalate hydrates nephrolith: formation, transformation and stabilization process and their potential inhibition by natural products.* (02/11/2018) Renal Medicine and Baxter Novum Seminars, Karolinska Instituted, Sweden.
- López-Mesas, M. (Babot, C., H.Valido, I.). *Synchrotron-based FTIR microspectroscopy application of human kidney stones and teeth.* (01-02/10/2018) FTIR microspectroscopy Workshop (MIRAS beamline), ALBA synchrotron, Barcelona, Spain.
- H.Valido, I., Boada, R., Vallcorba, O., Resina-Gallego, M., Luque-Gálvez, M.P., Valiente, M., López-Mesas, M. *Estudio de la importancia de la correcta caracterización de cálculos renales de origen oxalocálcico para la prevención de la recidiva.* (13-14/04/2018) XXI Simposi de la Societat Catalana d'Urologia, Barcelona, Spain.

Poster presentation:

- H.Valido, I., Fuentes-Cebrian, V., Valiente, M., López-Mesas, M. *Transformation of oxalocalcic kidney stones: influence of common urine inhibitors.* (05-06/03/2020) 1st European NECTAR Conference, Belgrade, Serbia.
- H.Valido, I., Fuentes-Cebrian, V., Vallcorba, O., Boada, R., Valiente, M., López-Mesas, M., *Study of phosphate affecting the transformation of calcium oxalate kidney stones.* (01-05/03/2020) Pittcon, Chicago, Illinois, USA.

- Vidimce-Risteski, V., Galindo-Casas, M., Zheng, W., Tallian-Langer, C., Sanchez-Alberola, N., Teixidó-Devesa, L., Zhao, Y., H.Valido, I., Rodríguez-Martínez, J., Diez-García, S., Sansegundo-Barbosa, L., Ribitsch, D., Sánchez-Martín, M.J., Hassan, M., Valiente, M. *NEOSETAC [New Selenium-based Targeted Nanocapsules to treat Breast Cancer]*. (18-20/11/2019) European summit of industrial biotechnology (esib), Graz, Austria
- H.Valido, I., Resina-Gallego, M., Valiente, M., López-Mesas, M. *Study of the calcium oxalate hydrates transformation and the role of organic matter on their development by synchrotron-based μ FTIR spectroscopy*. (8-11/10/2019) IX AUSE congress and IV ALBA users' meeting, Barcelona, Spain.
- Fuentes-Cebrian, V., H.Valido, I., Boada, R., Vallcorba, O., Valiente, M., López-Mesas, M. *Monitoring the weddellite transformation in renal calculi by synchrotron-based μ XRD*. (8-11/10/2019) IX AUSE congress and IV ALBA users' meeting, Barcelona, Spain. (Second prize)
- H.Valido, I., Fuentes-Cebrian, V., Valiente, M., López-Mesas, M. *Transformation of calcium oxalate Dihydrate to monohydrate crystallites*. (11-14/06/2019) International Symposium of Metal Complexes (ISMEC2019), Debrecen, Hungary.
- H.Valido, I., Resina-Gallego, M., Valiente, M., López-Mesas, M. *Study of calcium oxalate hydrates transformation and the role of the organic matter on their development by synchrotron-based μ FTIR spectroscopy*. (22-24/05/2019) Jornades Doctorals 2019, Department of Chemistry, Universitat Autònoma de Barcelona, Spain. (First prize)
- H.Valido, I., Pell, A., Díaz-Rovira, A.M., Resina-Gallego, M., Subirana-Manzanares, M.A., Marini, C., Simonelli, L., Valiente, M., López-Mesas, M. *Kidney stones studies by synchrotron radiation: application of imaging techniques*. (09-11/10/2017) VIII AUSE Congress and III ALBA User's Meeting 2017, Madrid, Spain. (Second prize)
- H.Valido, I., Pell, A., Subirana-Manzanares, M.A., Resina-Gallego, M., Valiente, M., López-Mesas, M. *Synthesis of references samples of kidney stones for synchrotron studies*. (07-10/06/2016) 43th International Symposium on Metal Complexes (ISMEC2016), Barcelona, Spain.

SHORT-TERM STAYS

During the development of this Thesis, three short-term stays, in two institutions, has been performed, from which valuable collaborations has been made, as well as the acquisition of new knowledge in different disciplines:

- 28/06-18/09/2017. Grupo de Pesquisas em Metabolômica e Espectrometria de Massas, Universidade do Estado do Amazonas, Manaus, Brasil. With the European Project AGUASOCIAL (Social Innovation in the Water Treatment Sector in the Amazon)
- 01/09/-30/11/2018. Karolinska Cell Therapy Center, Karolinska University Hospital, Huddinge, Sweden. With the European Project NEOSETAC (New Selenium-based Targeted Nanocapsules to treat Breast Cancer)
- 08/06-07/07/2019. Karolinska Cell Therapy Center, Karolinska University Hospital, Huddinge, Sweden. With the European Project NEOSETAC (New Selenium-based Targeted Nanocapsules to treat Breast Cancer)

SUMMARY

Nephrolithiasis is a painful disease caused by calculi formation in the kidney. It has an incidence of around 5-12% and a recurrence with a relapse rate of 50% in 5 years and 80-90% in 10 years, generating millions of euros per year of expenses for the health care system. Kidney stones are classified into seven major groups by morpho-constitutional analysis guidelines, where calcium oxalate stones, considering both the mono- (COM) and the dihydrated (COD) species, represents around 60-70%, being the most prevalent type. However, due to its low stability, COD suffers a crystalline conversion (transformation) into COM, which is the thermodynamically stable species. Hence, calcium oxalate monohydrate in renal calculi can be either formed directly as COM or as the resulting product after the transformation from COD (hereafter named TRA). These different formation origins are related with different pathologies, for example, COM is usually related to hyperoxaluria while COD is related to hypercalciuria.

The aim of the multidisciplinary work presented in this Thesis Dissertation is to understand the basis behind the stone formation, crystalline conversion and inhibition of calcium oxalate nephroliths by the application of in vitro studies, as well as to determine the speciation of these species, in the renal calculi by using synchrotron radiation based techniques. To achieve the main goal, the work is presented in six studies:

1. The characterization of synthetic calcium oxalate hydrates by X-ray diffraction (XRD), X-ray absorption spectroscopy (XAS), infrared (IR) and raman spectroscopy, and the application of a density functional theory (DFT) computational study with the objective of performing an unambiguous assignment of the vibrations, thus providing the appropriate parameters required to monitor and characterize the COD transformation process.

2. Determination of organic matter (proteins and lipids) distribution along the oxalocalcic calculi by synchrotron-based IR microspectroscopy, in order to establish their role as promoters or inhibitors in the stone formation, as well as their participation in the stabilization of COD.
3. Distinguish the formation origin of calcium oxalate monohydrate in stones with the application of synchrotron microdiffraction, resolving it with the analysis of the 2D diffraction patterns and its correlation with the level of texture of COM and TRA.
4. Study the effect of common urine inhibitors in the COD crystalline conversion by in vitro incubations in synthetic media containing citrate, magnesium, phosphate or phytate, and their combinations with calcium, which will help to better understand the COD transformation and stabilization processes in urine.
5. Development of a new fast and affordable risk index, Urine Inhibitory Capacity (UIC), which is related with the capacity of the urine inhibitors to interact with the promoters and avoid the formation of calcium oxalate crystals. It is presented in comparison with the Relative Supersaturation (RSS) since it presents a two major drawbacks: the amount of analytical work required to determine it and the wide “grey zone” of values between stone formers and healthy subjects (range of data that comprehend both groups).
6. Study of the antioxidative properties and the effect of different extract fractions from a plant traditionally used as kidney stone breaker and diuretic on the Canary Islands, *Lepidium latifolium* L., also known as “rompepiedras” (“stone breaker”), on the calcium oxalate formation. With the preliminary results, the extracts derived from this plant could be considered as a potential treatment and/or prevention of oxalocalcic kidney stones.

RESUMEN

Nefrolitiasis es una enfermedad dolorosa causada por la formación de piedras en el riñón. Tiene una incidencia en torno al 5-12% y una recurrencia con una tasa recaída del 50% en 5 años y 80-90% en 10 años, generando un coste de millones de euros al sistema de salud. Las piedras del riñón se clasifican en siete grupos mayoritarios según las directrices del análisis morfoconstitutcional, donde las piedras de oxalato de calcio, considerando tanto la especie mono- (COM) como la dihidratada (COD), representan el 60-70%, siendo el grupo más prevalente. No obstante, debido a su baja estabilidad, COD sufre una conversión cristalina (transformación) a COM, que es la especie termodinámicamente estable. Por consiguiente, el oxalato de calcio monohidratado en los cálculos renales puede ser formado directamente como COM o como el producto resultante tras la transformación del COD (denominado en este trabajo TRA). Estas diferencias en el origen de formación están relacionadas con diferentes patologías, por ejemplo, COM está generalmente relacionado con hiperoxaluria mientras que COD lo está con hipercalciuria.

El objetivo del trabajo multidisciplinar presentado en esta Tesis es entender las bases tras la formación, conversión cristalina e inhibición de los nefrolitos compuestos por oxalato de calcio mediante la aplicación de estudios *in vitro*, así como la determinación de la especiación de éstas especies, en los cálculos renales, mediante el uso de técnicas con radiación sincrotrón. Para conseguir dicho objetivo principal, el trabajo se presenta en seis estudios:

1. La caracterización de hidratos de calcio sintéticos mediante difracción de rayos X (XRD), absorción de rayos X (XAS) y espectroscopia infrarroja (IR) y raman, así como la aplicación de estudios computacionales de teoría funcional de la densidad (DFT), proporcionando así los parámetros apropiados que se requieren para monitorizar y caracterizar el proceso de transformación del COD.

2. Determinación de la distribución de la materia orgánica (proteínas y lípidos) a lo largo de los cálculos oxalocálcicos mediante microespectroscopia infrarroja basada en radiación sincrotrón, con el objetivo de establecer su papel como promotores o inhibidores en la formación de las piedras, así como su participación en la estabilización de COD.
3. Distinguir el origen de formación del oxalato de calcio monohidratado en piedras con la aplicación microdifracción basada en radiación sincrotrón, resolviéndolo mediante el análisis de los patrones de difracción 2D y su correlación con los niveles de textura de COM y TRA.
4. Estudiar el efecto de inhibidores comúnmente presentes en la orina en la conversión cristalina de COD mediante incubaciones *in vitro* en medios sintéticos que contienen citrato, magnesio, fosfato o fitato, así como sus combinaciones con calcio, lo que ayudará a entender mejor la transformación de COD y los procesos de estabilización en la orina.
5. Desarrollo de un nuevo índice de riesgo rápido y asequible, Capacidad Inhibidora de la Orina (UIC), el cual está relacionado con la capacidad de los inhibidores presentes en la orina de interactuar con los promotores y evitar la formación de cristales de oxalato de calcio. Está presentado en comparación con la Supersaturación Relativa (RSS) ya que ésta presenta dos grandes inconvenientes: la cantidad de trabajo analítico que se requiere para calcularlo, y la amplia “zona gris” de valores que comprenden los formadores de cálculos y los sujetos sanos (rango de datos que comprende ambos grupos).
6. Estudio de las propiedades antioxidantes y el efecto de diferentes fracciones de extracto de una planta tradicionalmente usada como “rompedora” de cálculos renales y diurética en las Islas Canarias, *Lepidium latifolium L.*, también conocida como “rompepiedras”, en la formación de oxalatos de calcio. Con los resultados preliminares, los extractos derivados de esta planta podrían ser considerados como un tratamiento potencial de las piedras de riñón oxalocálcicas.

GLOSARY

μXRD	micro X-ray Diffraction	EAU	European Association of Urology
2D	two dimensions	EXAFS	Extended X-ray absorption spectroscopy
AAE	Ascorbic acid equivalent	FBS	Fetal bovine serum
ACP	Amorphous calcium phosphate	FE-SEM	Field emission scanning electron microscope
AHU	Artificial human urine	FRAP	Ferric reducing antioxidant potential
ANOVA	Analysis of variance	FT	Fourier transform
ATR-FTIR	Attenuated total reflectance Fourier transformed infrared spectroscopy	FTIR	Fourier transform infrared spectroscopy
ATTC	American Type Culture Collection	FTP	First turning point
AUA	Uric acid anhydrous	FWHM	Full width at half maximum
AUD	Uric acid dihydrate	HAP	Hydroxyapatite
BRI	Bonn-risk index	HEK	Human embryonic kidney
BSA	Bovine serum albumin	IDs	Insertion devices
CA	Chemical analysis	IR	Infrared
CaOx	Calcium oxalate	KK	Kramer-Kronig
CaP	Calcium Phosphate	KM	Kubelka-Munk
Cit	Citrate	K _{SP}	Solubility product
COD	Calcium oxalate dihydrate	LINAC	Linear accelerator
COM	Calcium oxalate monohydrate	LMWP	Low-molecular weight proteins
CT	Computed tomography	MCR	Multivariate curve resolution
DFT	Density Functional Theory	MCT	Mercury-Cadmium-Telluride
DMEM	Dulbecco's modified eagle medium	MET	Medical expulsive therapy
DPPH	2,2-diphenyl-1-picrylhydrazyl		

NIPALS	Nonlinear iterative partial square	SR- μ FTIR	Synchrotron radiation-based Fourier transform infrared spectroscopy
NTU	Nephelometric turbidity units	SR- μ XRD	Synchrotron radiation-based micro X-ray diffraction
OM	Organic matter		
OPN	Osteopontin	SS	Supersaturation
OS	Oxidative stress	STR	Struvite
Ox	Oxalate	SWL	Shock wave lithotripsy
PCA	Principal component analysis	$t_{1/2}$	half-time
Phos	Phosphate	TPTZ	2,4,6-Tris(2-pyridyl)-s-triazine
Phyt	Phytate	TRA	Transformed calcium oxalate dihydrate
PNL	Percutaneous nephrolithotomy	tts- μ XRD	Through-the-substrate micro X-ray diffraction
Q	Ionic product		
ROS	Reactive oxygen species	UIC	Urine inhibitory capacity
rpm	revolutions per minute	ULM	Upper limit metastability
RRFA	Robertson risk factor algorithms	URS	Ureterorenoscopy
RSS	Relative supersaturation	UV-Vis	Ultraviolet-visible
SEM	Scanning electron microscopy	XANES	X-ray absorption near edge structure
		XAS	X-ray absorption
SI	Support information	XRD	X-ray diffraction

PREFACE

The contents of this Thesis have been organized in different chapters as follows:

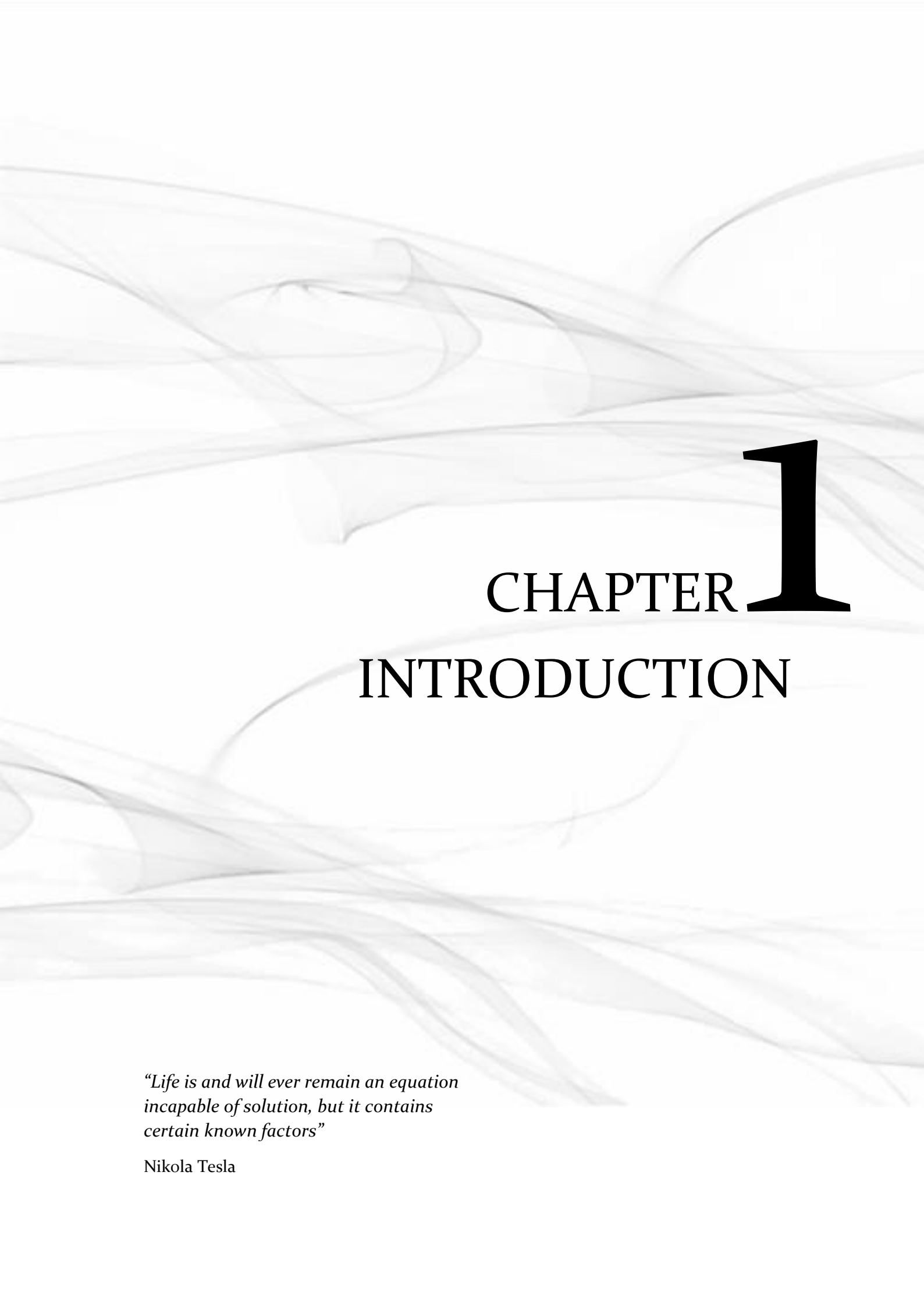
- **Chapter 1:** the introduction
- **Chapter 2:** presents the obtained results on this Thesis as a compilation of articles
- **Chapter 3:** contains further insights, derived from the work described in the previous chapter. In order to maintain the structure cohesion, this section is also presented as articles.
- **Chapter 4:** a general discussion of the results presented in Chapter 2 and 3
- **Chapter 5:** Main conclusions of the Thesis
- **Chapter 6:** briefly description of the future perspectives

Note: the UAB Guidelines for the presentation of a PhD dissertation as a compilation of peer-reviewed articles does not list at “Experimental Section” chapter. However, the experimental details for each work is given in the corresponding articles (Chapter 2 and 3).

CONTENT

Summary	XI
Resumen.....	XIII
Glossary	XV
Preface	XVII
Chapter 1. Introduction	1
1.1. Formation hypothesis.....	4
1.2. Epidemiology and cost for the health care system.....	6
1.3. Kidney stone classification.....	7
1.3.1. The case of calcium oxalate hydrates	9
1.4. Medical diagnosis and treatment.....	10
1.4.1. Diagnosis in the hospital.....	10
1.4.2. Treatment of patients with kidney stones.....	12
1.4.2.1. Surgical management	12
1.4.2.2. Prophylactic treatments	15
1.5. Experimental techniques.....	20
1.5.1. Use of synchrotron radiation	20
1.6. Objectives.....	23
1.7. References	24
Chapter 2. Compilation of articles	33
2.1. Characterization of calcium oxalate hydrates and the transformation process	35
2.2. Calcium oxalate kidney stones, where is the organic matter?: A synchrotron based infrared microspectroscopy study	63
Chapter 3. Further insights	75

3.1. Discriminating the formation origin of calcium oxalate monohydrate in kidney stones via synchrotron microdiffraction	77
3.2. Understanding the crystalline conversion of oxalocalcic kidney stones: effect of common urine inhibitors <i>in vitro</i>	97
3.3. <i>In vitro</i> study of the promoters/inhibitors influence in oxalocalcic nephroliths formation: approach for the development of Urine Inhibitory Capacity (UIC) as a risk index	119
3.4. A comparative study of the <i>Lepidium latifolium</i> , L. (<i>Rompepiedras</i>) extract effects on calcium oxalate crystallization <i>in vitro</i>	137
Chapter 4. General discussion of the results	151
Chapter 5. Conclusions	165
Chapter 6. Future perspectives	171



CHAPTER **1**

INTRODUCTION

*“Life is and will ever remain an equation
incapable of solution, but it contains
certain known factors”*

Nikola Tesla

Lithiasis is a painful disease caused by the alteration of the normal crystallization conditions of urine in the urinary tract¹. Hence, since the present work is based on different aspects of the stones formation, some basic details regarding the urinary system anatomy and physiology will be described in this section.

The urinary tract is composed by four main parts: kidneys, ureter, bladder and urethra (Figure 1A), which are the responsible for the periodically collection, transport, store and excretion of urine². The two kidneys are organs located in the upper urinary-collecting system, and are connected, from the renal pelvis to the lower system, by the ureters (Figure 1B). The kidneys are key organs in the homeostasis, since their main function is to regulate the fluid, electrolyte and pH balance on the body³, as well as perform the excretion of the metabolism waste products and reabsorption of some molecules present in the blood through the urine⁴. The blood filtration is carried out in the glomerular filtration barrier, situated in the glomerular capsule of the nephrons (Figure 1C), which are located in the kidney pyramid, partly in the cortex and partly in the renal medulla (intersection also known as “cortex-medulla junction”)⁴. Therefore, urine production is the result of two process: renal-glomerular filtration and tubular reabsorption².

Due to the filtration/reabsorption process previously mentioned, and the urine concentration produced in the loop of Henle⁵, urine becomes a complex matrix with around 158 chemical constituents that goes from electrolytes to organic compounds, being only 68 of them the ones that form the 99% of the urine solutes⁶.

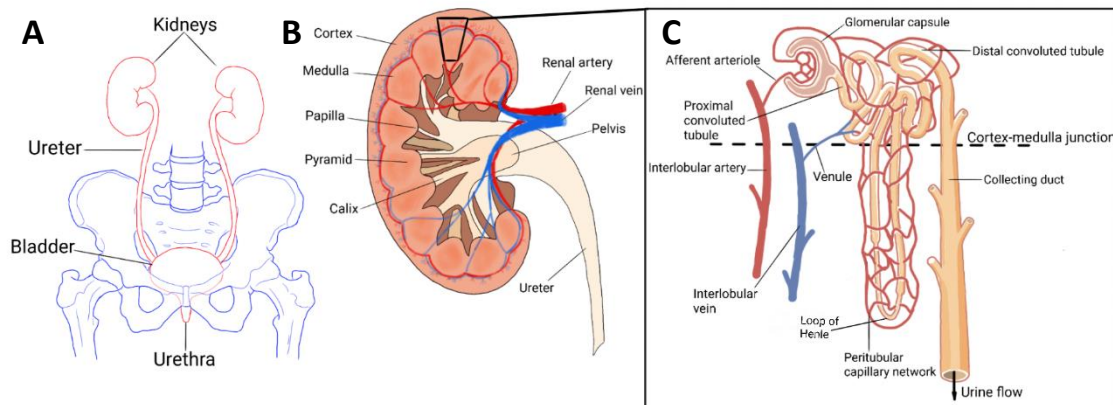


Figure 1. Schematic drawing of the urinary tract (A), kidney section (B) and nephron (C) with their main parts. The used images are adaptations from “National Institute of Diabetes and Digestive and Kidney Diseases” (A), “a level biology student” (B), and “Anatomy & Physiology. Oregon State University” (C), all of them under a CC license.

1.1. Formation hypotheses

Nephrolithiasis is a disease well known since ancient times, which symptoms and treatments were originally mentioned in the medical texts of *Asutu in Mesopotamia* (3200-1200 BC)⁷. Regarding the stone formation, it was described around 600 BC in the ancient Indian book *Sushruta Samhita* as “*Bigger stones form in the same fashion as the precipitate that occurs after some time when even clear water is kept in a new pitcher*”⁷. Even if it seems as a simple statement, the observational science practice along history is close to the more recent definitions of how kidney stones are formed based on the crystallization thermodynamics. In summary, this means that the ionic product (Q) of the reactants in urine exceed its solubility product (K_{SP}), which is the equivalent to: urine is a supersaturated solution for certain components⁸.

The authors in this research area⁹⁻¹⁶ agree that the fact that urine is a supersaturated matrix with respect to some of its components, such as calcium or oxalate, is one of the primary factors of risk for the stone formation.. Moreover, kidney stones are, by definition, the formation of microcrystals aggregates, being the first step the production of microscopic particles by the association of free ions in the supersaturated solution (nucleation), followed by their agglomeration (aggregation) and/or their growth.^{14,15} It is important to remark that, even a primary nucleation is needed, these three processes occur simultaneously in the

medium, as it happens in biomineralized structures in nature⁸. Furthermore, each stage is affected not only by the urine supersaturation, but also by the presence of other components that can affect the crystallization kinetics, commonly known as promoters or inhibitors. There are many studies regarding the mechanism of the kidney stone formation, being the supersaturation and the three formation stages common steps for all of them but with different complexity^{5,10,16-22}.

As it was mentioned before, the different constituents present in the urine (promoters/inhibitors), in combination with the urine pH and flow, will play an important role on the nucleation, grow and aggregation kinetics, as well as in the crystalline orientation during this processes^{8,15,20-23}. A short list of promoters and inhibitors is listed in Table 1, where it can be observed that “organic matter” appears in both groups. This is due to the high presence of organic macromolecules in the nephroliths matrix, being 2-3% of their weight and consisting mostly in proteins, lipids (phospholipids, cholesterol and glycolipids) and glycosaminoglycans^{10,15,22}, and there are discrepancies in studies regarding their capacity as promoters or inhibitors of the stone formation^{20,22,24}. This is the case of osteopontin (OPN), a well studied protein regarding its impact in the renal calculi development, which has been found to be a promoter²⁵⁻²⁷ and an inhibitor²⁸⁻³⁰ of calcium stones, indicating that OPN can act as promoter or inhibitor depending on the medium and experiment conditions, the mineral and the formation stage studied.

Table 1. Classification of urine constituents as promoting or inhibiting factors^{15,20,22,23}.

Inhibitors	Promoters
Citrate ($C_3H_5O_7^{3-}$)	Calcium (Ca^{2+})
Magnesium (Mg^{2+})	Sodium (Na^+)
Pyrophosphate ($P_2O_7^{4-}$)	Oxalate ($C_2O_4^{2-}$)
Phytate ($C_6H_6O_{24}P_6^{12-}$)	Urate ($C_5H_4N_4O_3$)
Organic matter	Cystine ($C_6H_{12}N_2O_4S_2$)
	Organic matter

However, taking into account that these compounds are correlated with the type of stone and that every individual is different (some stone formers do not present identifiable abnormalities)¹⁵, there is not a clear common cause of kidney stone formation.

In addition to the urine supersaturation level, and the presence of some promoters and inhibitors of the stone formation/development, several authors report the importance of the reactive oxygen species (ROS), and the development of oxidative stress (OS) in the kidneys, in that mechanism^{5,14,16,31}. There are several approaches to this hypothesis: 1) urinary conditions, such as hyperoxaluria, hypercalciuria or renal oxidative stress, trigger the formation of osteoblastic phenotypes coming from the transformation of renal epithelial cells, which promotes the deposition of calcium phosphate crystals in the renal papilla, known as Randall's plaques¹⁴; 2) the ROS are one factor involved in the renal cell injury ("crystal-induced stress"), which promotes the release of substances, such as low molecular weight proteins (e.g. prothrombin fragment-1), that induces the agglomeration of COM crystals^{5,31}; 3) the ROS also generates lipids peroxides³², products that have been found at high levels in stone former patients³³.

1.2. Epidemiology and cost for the health care system

It is well known that renal lithiasis presents multifactor pathogenesis, that comprises the combination of socio-economical (e.g. geographical location, environmental, socio-economic level, diet) and individual factors (e.g. age, sex, race/ethnicity, genetics)³⁴. It has a prevalence of 7-15% in men and 3-6% in women³⁴, being notably higher in industrially developed countries³⁵. The prevalence in Spain, according to the Registro del Grupo de Urolitiasis de la Asociación Española de Urología (Registry of the Urolithiasis Group of the Spanish Association of Urology) is around the 4%, which is the same as Germany and in the range of the United States (3-7%)³⁶. Furthermore, there is a high recurrence rate (formation of a new calculus) of 30-50% in the next 5 to 10 years after the first episode, and up to 75% after 20 years^{5,37}. The tendency of the incidence, prevalence and recurrence

along the years is troubling, since there are evidences that suggest that those factors are increasing globally³⁸.

The development of a kidney stone often causes a nephritic colic episode, which must be treated at emergency services. The treatment of patients with lithiasis, involves the cost of the visit, followed by the diagnostic, medical and/or surgical treatment, follow-up visits and the indirect cost for the patients³⁹. This disease has an economic cost of \$2-5.3 billion/year in the United States, and around €54 million in Germany³⁴. Moreover, according to a study performed using data from the National Health and Nutrition Examination Survey (NHANES) of the United States, performed to estimate the economic projection of the prevalence cost, it shows that, by 2030 the cost for the health care system will increase by \$1.24 billion/year⁴⁰. The presented cost for the health care system can be reduced if the risk factor, as well as the metabolic and nutritional ones, of patients are identified are properly managed, hence avoiding the recurrence (preventing a new stone episode)^{34,35}.

1.3. Kidney stone classification

To reduce the recurrence, the European Association of Urology (EAU) advises that the nephrolith of all first-time stone formers should be analyzed⁴¹. To perform the compositional analysis of the renal calculi, different techniques such as infrared spectroscopy (IR), X-ray diffraction (XRD) and chemical analysis (CA) have been used, although the latter is currently considered almost obsolete due to the poor results obtained⁴². In order to perform the aforementioned compositional analysis, it is necessary to powder the samples, which results in a bulk analysis. Due to the high heterogeneity of the nephroliths, important information about the stone formation origin and the growth history is lost. Moreover, the chemical information obtained is insufficient to give a differential treatment to the patient in order to avoid further stones (recurrence). To overcome this problem, the morpho-constitutional analysis of the expelled stone⁴³, which combines morphological examination of the surface (e.g. color, form, size and aspect (e.g. smooth or rough)), section (e.g. color, organization (layers, compactness, loose or

poorly organized)) and nucleus (location and aspect) of the stones with the composition analysis by FTIR, has been proposed^{43,44}. This methodology allows correlating the type of renal calculi with the main etiologic factors related to its formation^{43,44}, information that assists the urologist with the prescription of individualized treatment to prevent further stones. However, this methodology requires a skilled technician; being a long and expensive analysis.

Considering their chemical composition, urinary stones can be classified as calcium oxalate (CaOx, 66% of incidence), uric acid (15%), struvite (9%), hydroxyapatite (HAP, 7%), brushite (1%), cystine (1%) and others, which can be produced, for example, by drugs or artifacts (<1%)⁴⁵. A diagram with the groups' distribution according to their chemical composition can be seen in Figure 2. However, they are divided in several subgroups depending on the results of the morpho-constitutional analysis application^{43,44}. These subgroups are the ones that will narrow down the pathology suffered by the patient (e.g. calcium oxalate monohydrate is related to hyperoxaluria while calcium oxalate dihydrate is related to hypercalciuria⁴⁶)^{43,44}.

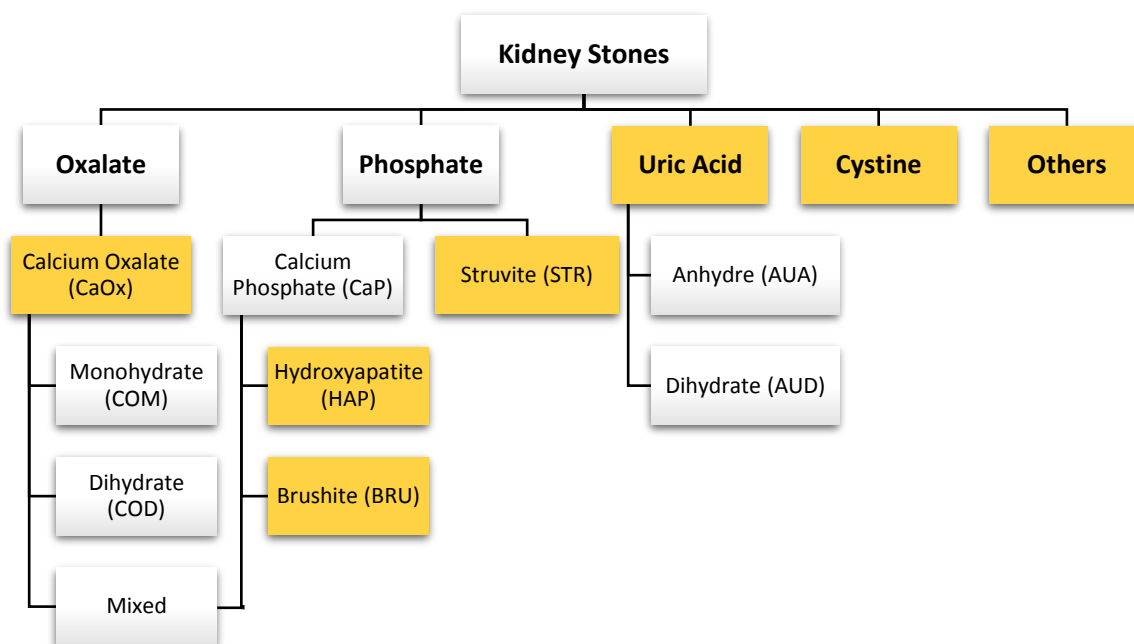


Figure 2. Diagram of the seven kidney stones groups (calcium oxalate, hydroxyapatite, brushite, struvite, uric acid, cystine and others) distributed by their main chemical composition.

1.3.1. The case of calcium oxalate hydrates

As mentioned before, calcium oxalate nephroliths present the higher incidence (66%) among the 7 major types⁴⁵, being represented mainly by two crystallographic species: calcium oxalate monohydrate (COM) or whewellite ($\text{CaC}_2\text{O}_4 \cdot \text{H}_2\text{O}$), which is the thermodynamically stable and the kinetically favorable calcium oxalate dihydrate (COD) or weddellite ($\text{CaC}_2\text{O}_4 \cdot 2\text{H}_2\text{O}$). A third species, calcium oxalate trihydrate, known as caoxite ($\text{CaC}_2\text{O}_4 \cdot 3\text{H}_2\text{O}$), can be also found, but it is rarely observed^{47,48}. Due to its low stability, COD suffers a crystalline conversion (transformation), produced over time in the medium, into COM which is the thermodynamically stable species^{46,49-51}. Hence, calcium oxalate monohydrate in renal calculi can be either formed directly as COM or as the resulting product after the transformation from COD (hereafter named TRA to distinguish between the origins of the two calcium oxalate monohydrates and to facilitate the discussion in this work). TRA is chemically and crystallographically monohydrated (COM), however, it has been suggested in a previous study that it is possible to identify oxalocalcic kidney stone that has suffered this crystalline conversion by IR characterization since there is a modification of the absorption bands and the morphological characteristics differ respect to COM, which could be related with the presence of amorphous whewellite, which has been recently synthesized^{46,52}.

The crystalline conversion of COD starts with the change in the “zeolitic water” channel sites configuration, which acts as the driving force of the transformation⁵³, resulting in the monohydrate species. Many authors have studied this process by thermogravimetry^{50,54,55} and under different humidity conditions^{49,53}. They determined that the instability of COD could be due to the presence of the zeolitic water and the large size of its channels⁵³, while other unknown factors, independent of the humidity, could drive the transformation process⁴⁹. Why is it important to study this transformation process and to differentiate between COM and TRA? The answer is simple, but solving it is not. When analyzing COD kidney stones by Fourier Transform Infrared (FTIR) spectra and Scanning Electron Microscopy (SEM), the presence of COM in COD stones provides contradictory

results. FTIR shows characteristic bands of COM, whereas SEM reveals the presence of bipyramidal crystals, characteristics of COD⁴⁶. Since both species are related to different pathologies (for example, COM to hyperoxaluria and COD to hypercalciuria), distinguish the origin of the crystal grown is important to associate the kidney stones with the corresponding etiology and treatment^{1,46,56}. On the other hand, COD is not always transformed. Therefore, the study of this transformation process, as well as the stabilization of the dihydrated species, is very important to understand the physiopathology, to propose adequate treatment and, to prevent the patients' recurrence^{46,57,58}.

1.4. Medical diagnosis and treatment

1.4.1. Diagnosis in the hospital

When a person arrives to a hospital with an excruciating abdominal pain in the lower abdomen, symptom also produced by other causes such as appendicitis, colitis, hernias or constipation, the first step carried out by the physician is to perform a physical examination. If a renal colic is suspected, the next step will be to use an imaging technique in order to find out if there is a stone and where is it located. The selection between the different techniques available will depend on the patient condition and/or history, as it is shown in Figure 3⁵⁹. Parallel to those tests, a blood analysis to measure creatinine, sodium, potassium, chloride, calcium and parathyroid hormone, and an urinalysis to determine the urine volume, pH, calcium, oxalate, uric acid, citrate, sodium and magnesium, should be performed^{41,59,60}. The measurement of the mentioned urine parameters will help the physician to perform a follow up on the patient condition and treatment⁶⁰.

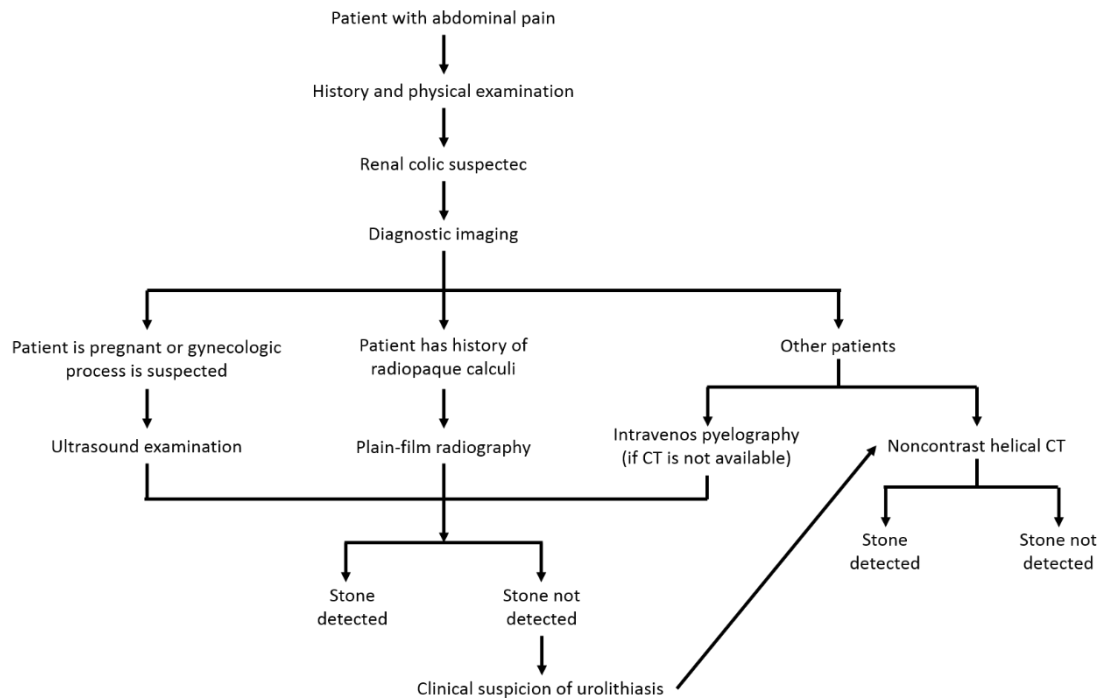


Figure 3. Scheme describing the diagnostic approach followed in hospital when a renal colic is suspected⁵⁹. CT means Computed Tomography.

Moreover, in order to determine the risk of an individual to form a nephrolith, risk indices are commonly used. These are useful, not only for the prediction of having a stone, but also to monitor the patient evolution during the treatment⁶¹. There are many risk indices, based on the urine saturation, reported in the literature¹¹, being the most common ones:

- Bonn-Risk-Index (BRI) is based on the induced crystallization in a urine sample, “simulating” the stone formation within the urine, which takes into account the effect of major and minor urinary constituents, as well as their interactions, during the crystallization process⁶². As an example, the BRI is measured in a CaOx stone forming urine by calculating the ratio of the calcium concentration (mmol/L) in the tested urine divided by the amount of oxalate (mmol/L) needed to initiate crystallization in 200 mL of sample⁶³.
- Upper Limit Metastability (ULM) makes reference to the supersaturation point at which the crystallization is initiated when the process is induced by additions of, for example, calcium or oxalate, to the urine⁹.

- Relative Supersaturation (RSS) can be defined as the concentration of the dissolved salt divided by the solubility of that salt at physiological temperature⁹. For its calculation, a more complete approach that involve a minimum of twelve urinary components taking into account interactions and equilibrium processes of some promoters and inhibitors, is used⁶⁴. This index is not directly measured in the sample, it is calculated using computer programs that consider the mentioned interactions of the components measured in the urine (usually from a 24-hour excretion)⁶⁵. Considering that it is possible to determine the RSS for different types of stones at the same time, by using softwares such as EQUIL^{66,67} (the first one and the most used in the literature), SUPERSAT, SEQUIL, URSUS, MINEQL and JESS⁶⁴, the RSS is the most used method to predict and/or monitor the risk of forming a kidney stone.

Even it has been widely recommended and studied, the use of urine analysis on stone formers is not generally performed, being few of the specialist centers the only that carry out calculation of the supersaturation levels of the urinary salts in order to determine the patients risk to perform more stones⁶⁰. This lack of use could be explained by two main factors: the high analysis cost necessary to determine the different analytes needed to calculate the RSS with the software, and the large overlap of the RSS values from stone formers and healthy individuals (grey zone of values), which means that it cannot distinguish between the two groups⁶⁴.

1.4.2. Treatment of patients with kidney stones

1.4.2.1. Surgical treatment

When a patient arrives to the hospital with an obstructed kidney, which usually includes evidence of urinary tract infection, it is considered a urological emergency. In this case, the obstructed collecting system needs to be urgently decompressed, being two the options: placement of an indwelling ureteral stent or percutaneous placement of a nephrostomy tube (Figure 4)^{41,59}.

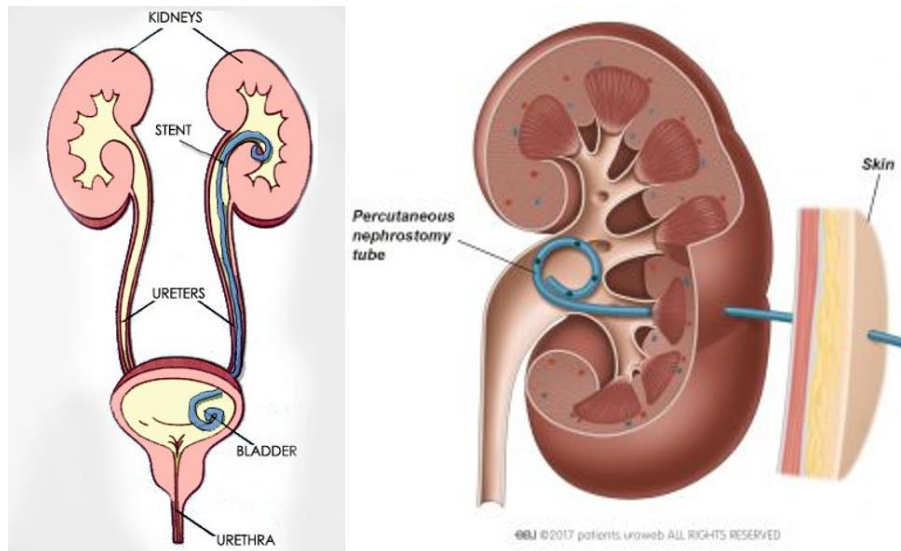


Figure 4. Comparison between indwelling ureteral stent (left) and percutaneous nephrostomy tube (right). ©Standard of Care 2020 (left) and ©2020 – European Association of Urology (right).

If the patient situation is not the mentioned emergency scenario, and after the renal colic has been treated with the use of the suitable analgesic, the physician must plan a strategy for the stone management based on the stone size and location (Table 2)⁵⁹. When the stone has a better probability to be expelled from the body (regarding its size and location) and the patient has been properly informed, a medical expulsive therapy (MET) will be applied, which involves the administration of drugs, such as alpha-blockers, calcium channel blockers, corticosteroids or phosphodiesterase type 5 inhibitors, to improve the spontaneous stone passage, avoiding the surgical intervention^{41,68}.

Table 2. Probability of stone passage (%) depending on its size and the location⁵⁹.

	Proximal ureter (closer to the kidney)	Middle section of ureter	Distal ureter (closer to the bladder)
> 5 mm	0	0	25
5 mm	57	20	45
< 5 mm	53	38	74

In the case that an active stone removal is indicated, there are different management techniques that can be applied and different recommendations depending on the consulted guideline. In order to determine the level of consensus for the surgical treatment of urolithiasis, Zumstein et al. (2018)⁶⁹ performed a comparative study between six guidelines: European Association of Urology⁴¹, American Urological Association^{70,71}, Sociedad Argentina de Urologia^{72,73}, French Association of Urology⁷⁴, German Society for Urology⁷⁵, and Singapore Urological Association⁷⁶. The results of this comparison (see Figure 5) is a mode tree that list the level of the cited guidelines regarding the use of the three main therapeutic options: extracorporeal shock wave lithotripsy (SWL), ureterorenoscopy (URS) and percutaneous nephrolithotomy (PNL)⁶⁹. A drawing of these techniques can be found in Figure 6.

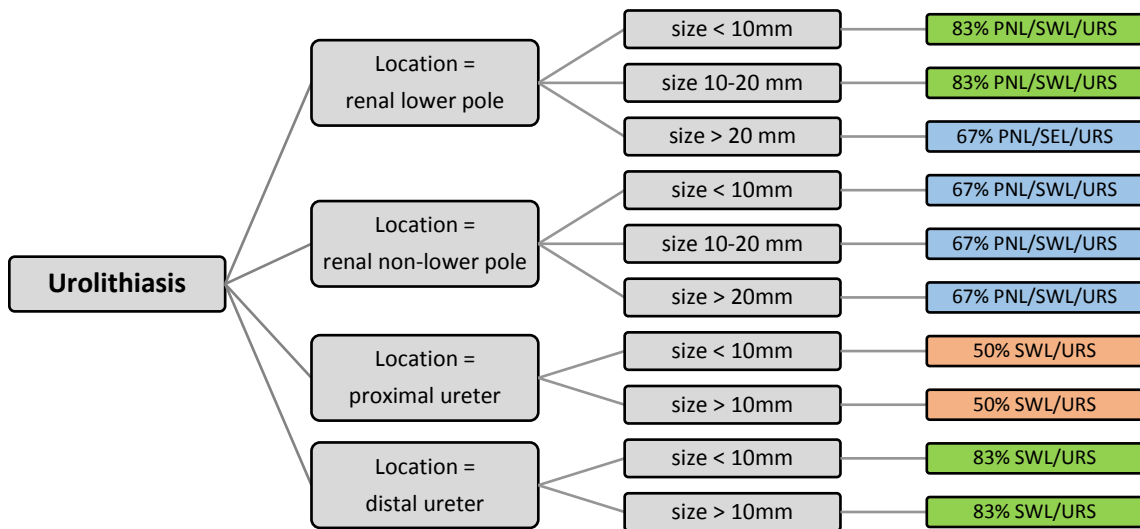


Figure 5. Mode tree that shows the level of agreement (green = high; blue = intermediate; orange = low) between the different guidelines regarding the use of three urolithiasis management techniques: extracorporeal shock wave lithotripsy (SWL), ureterorenoscopy (URS) and percutaneous nephrolithotomy (PNL). Figure adapted from the paper of Zumstein et al. (2018)⁶⁹.

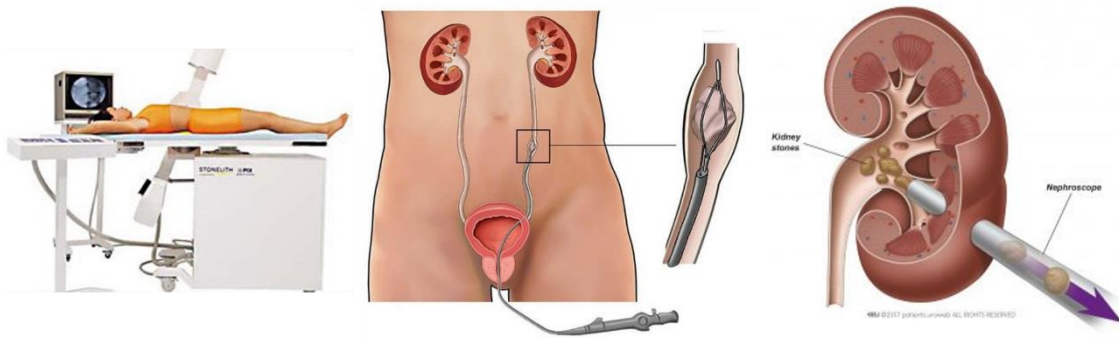


Figure 6. Images of the techniques used for the surgical management of lithiasis: left, extracorporeal shock wave lithotripsy (SWL); middle, ureterorenoscopy (URS); and right, percutaneous nephrolithotomy (PNL). ©2019 Broward Urology Center (left), ©2018 MedPort International (middle), and ©2020 – European Association of Urology.

1.4.2.2. Prophylactic treatment

As it was stated by Robertson (2006): “Continuing to allow patients to form stones and removing them by means of new technologies without providing any form of medical management other than the classical Hippocratic advice to “drink more fluids” is, in the long run, an expensive way to manage the problem...”³⁵. Hence, the use of prophylactics, treatments to prevent a disease, are necessary in order to decrease the recurrence of the patients, and therefore, the cost for the health care system. These treatments are based on the use of drugs and the modification of the nutritional habits, which could influence the formation of the stone in the patients’ history and help avoiding it by its modulation.

Nowadays, the use of individualized drug therapies are in crescendo, even being well known for centuries, as it was well expressed by Sir William Osler in a letter to the New Haven Medical Association on 1903: “Variability is the law of life, and as no two faces are the same, so no two bodies are alike, and no two individuals react alike and behave alike under abnormal conditions which we know as disease”⁷⁷. Consequently, the treatment selection will depend on the urine and metabolic analysis results, which will indicate the pathophysiological factor that influence the nephrolith formation, as well as the patient individual characteristics. Examples of some medical treatments applied for different pathophysiological

factors, related with the different types of kidney stones, can be found in Table 3^{46,78,79}.

Table 3. Pharmacological and dietary treatments of nephroliths depending on the associated pathological factors^{46,78,79}

Pathophysiological factor	Stone composition	Dietary modification	Pharmacological treatment
Low urine volume	All stones	Increase fluid intake	
Hypercalciuria	Calcium oxalate monohydrate or calcium phosphate	Sodium moderation/restriction	Hydrochlorthiazide or indapamide + potassium alkali
		Protein moderation	
Hypocitraturia	Calcium oxalate dihydrate or calcium phosphate	Protein moderation	Potassium citrate
		Consumption of lemon, lime, melon and/or oranges	
Hyperoxaluria	Calcium oxalate	Oxalate restriction	Pyridoxine for primary hyperoxaluria
		Limit consumption of spinaches, nuts and/or berries	
		Avoidance of calcium restriction	
Hyperuricosuria	Calcium oxalate or uric acid	Purine restriction	Allopurinol
		Protein moderation	
Low urinary pH	Uric acid	Protein restriction	Potassium citrate
		Increase the consumption of fruits and vegetables	
Cystinuria	Cystine	High fluid intake	Potassium citrate
			D-penicillamine
			B-mercaptopyrionyl-glycine
Urinary tract infection	Struvite		Antibiotics

The use or restriction of supplements can be also useful on the disease management. For example, Vitamin C can increase urine oxalate concentration since it is the product of ascorbic acid metabolism, while Vitamin B-6 (pyridoxine) is commonly used to treat hyperoxaluria (Table 3) since it may reduce urinary oxalate⁷⁹. Another example is the prescription of fish oil to patients with hypercalciuria, as the consumption of 1,200 mg/d has been associated with the reduction of calcium and oxalate concentration in urine⁷⁹. Furthermore, several *in vitro* studies describe the effects of crystallization inhibitors (Table 1), such as citrate, magnesium and phytate, and their potential use as supplements for the treatment of calcium oxalate kidney stones⁸⁰⁻⁸³.

Besides the possibility of using drugs, most common in higher-risk patients, there is a high interest on the use of nutrition as possible treatment^{1,84-86}. The problem with this remedy is the duration of the patients compliance with it, which it seems to be related with the complexity of the metaphylactic protocol⁸⁷. This means that the patients usually see these treatments as “diets” (more difficult to adhere to it), and not as a lifestyle change, being estimated that only 15-40% of kidney stone formers stick to the nutritional recommendations, performing a real lifestyle change^{87,88}. Therefore, is it important for the urologist to keep these protocols as simple as possible and to offer an appropriate follow up cycle that motivates the patient to continue with it⁸⁷.

A popular trend on the past decades is to go back to the use of natural products on life, with around 20-30% of the medicines in the market derived from them⁸⁹, and the prevention/treatment of lithiasis is not an exception. In this topic, there are two branches that can be follow: 1) the study of fruits or plant extracts that are “trendy” or known for their positive activities in other medical aspects; 2) the study of plant extracts that has been used for different cultures in their traditional medicine along history, also known as ethnomedicine, being the written evidence of their medicinal use a Sumerian clay slab from Nagpur (around 5000 years old)⁹⁰.

In the first group, the use of fruit extracts, such as lemon and orange⁹¹, raspberry, bitter orange, mastic or pomegranate⁹² are commonly studied, as well as extracts from parts of the plants or fruits, like avocado leaves⁹³ or grape seeds⁹⁴ has been

also studied for its antilithiatic effect. Moreover, nutritional plants, generally used as culinary spices, such as parsley, oregano and black-cumin^{92,95}, have been also studied for their use to prevent and treat kidney stones. The use of leaves for infusions, like green tea, has been studied for their inhibitory effect on urinary stone formation and antioxidative properties^{92,96}; however, other research performed by Wu Zhing Biao et. al (2017) remarks that the tea consumption in Northern China is associated with a higher risk of kidney stones⁹⁷. The use of these extracts/remedies are mainly associated with their high polyphenol content, since their antioxidant, anti-inflammatory and diuretic properties seems to contributed to the prevention of urolithiasis, being most of the studies focus on calcium oxalate⁹⁸.

In the second group, there are many plants traditionally used to treat urolithiasis for their diuretic effects, among others. There are many reviews and research papers listing the herbal medicines used in different regions with the preparation methods used and properties^{89,92,99-111}. There are two plants that had showed to be effective on the inhibition of calcium oxalate stones in *in vitro* experiments, in rat models, and in some studies with calcium stone forming patients, which are: *Phyllanthus niruri*, from the Euphorbiaceae family and widely used in folk medicine in Brazil to treat urolithiasis¹¹²⁻¹¹⁷; and *Herniaria hirsuta*, from the Caryophyllaceae family and used in Morocco to treat kidney stones¹¹⁸⁻¹²¹.

It is interesting the case of *Lepidium latifolium* (Figure 7), from the Brassicaceae family, which is used in the folk medicine of the Canary Islands and, really far away, in the Ladakh region in India, for the treatment of renal disorders¹²²⁻¹²⁴. In Canary Islands it is known as “Rompepiedra” (Stone breaker) and it is well known among the older population for its properties. In 2017, Jaime Gil González and collaborators performed a study of the wild plants uses in Gran Canaria (“Estudio de los usos de las plantas silvestres en Gran Canaria”)¹²⁵, where they carried out a series of interviews to the oldest population in order to preserve the knowledge that has been transmitted orally over centuries. In the mentioned work, there are testimonies based on the experience of the interviewed people¹²⁵, below some examples with the translations in brackets:

“Eso es pa’ piedra en el riñón, pa’ tomar, guisar y tomar agua por lo visto. [...]. En varias casas sí lo había [de antes]. Dice la gente pa’l que padece del riñón la... la guisa pa’ tomar agua” (“That is for stones in the kidney, to drink, to stew (infuse) and drink water apparently. [...]. In several houses there was [before]. People say that for those suffering from kidney, they stew it (infuse it) to drink with water”).

“[...] que cuando tiene piedras en el riñón o algo d’eso bebe mucha agua guisaa d’esta...” (“...that when someone has stone in the kidney or something of that, drink a lot of stewed (infused) water from that (with rompepiedra)”).

“La rompe piedras es muy buena pa’... pa’ las piedras del riñón, sí, y el perejil, la ríza del perejil. Yo guiso la rompe piedras, la raíz de perejil y la cola caballo juntas” (“The rompepiedra (stonebreaker) is very good for... for stones in the kidney, yes, and the parsley, the parsley root. I stew (infuse) the rompepiedra, the parsley root and the field horstail together”).

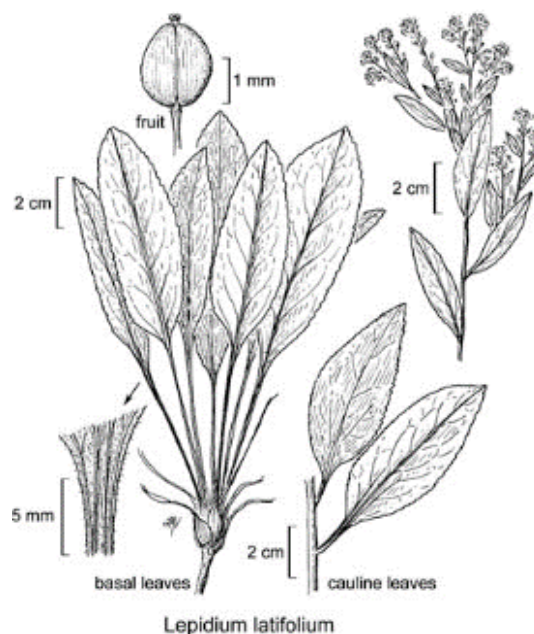


Figure 7. Botanical illustration of *Lepidium latifolium* (©Regents of the University of California).

This plant has been also reported for its use as stomach tonic, diuretic, anti-hypertensive, against renal lithiasis and other kidney disorders and against prostatic hyperplasia¹²³, being its aqueous extract diuretic properties just fully studied on one research paper¹²², to the knowledge of the author of this thesis. However, due to its popular use, there are several commercial products based on the leaves extracts or in the dried powdered leaves. Hence, due to its wide extension worldwide and its mentioned properties, it is worth to study the *Lepidium latifolium*, leaf extracts as a possible inhibitor/treatment of calcium oxalate nephroliths.

1.5. Experimental techniques

Most of the techniques used during the elaboration of this thesis can be considered of basic use on a laboratory, such as infrared spectroscopy, UV-vis spectroscopy, X-ray diffraction and/or scanning electron microscopy. Hence, the theoretical basis of those will not be explained in this introduction. However, synchrotron radiation, and the techniques associated to it, are not of common use, which is why a brief description on how it works and its advantages are described below.

1.5.1. Use of synchrotron radiation

Synchrotron facilities are large circular buildings (about the size of a football field) composed by different parts (Figure 8), each one with a specific purpose from generating and accelerating electrons, to analyze by different techniques, passing by the security parts necessary to prevent injuries to the personal and users. In these facilities, synchrotron radiation is generated and used for analysis purposes.

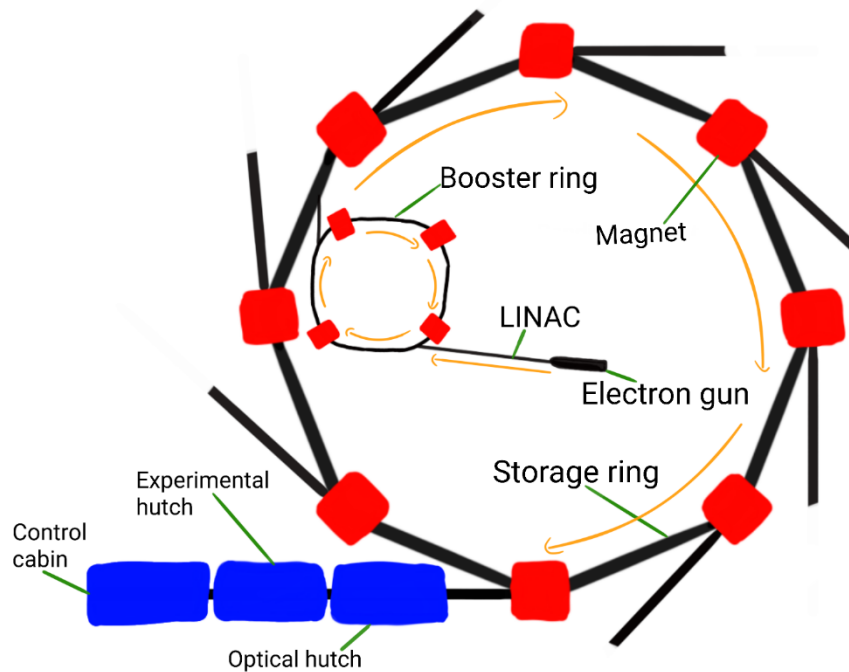


Figure 8. Schematic representation of the most important components from a modern synchrotron facility. Arrows in orange represents the direction of the electrons.

The process to generate synchrotron radiation is briefly as follows. Electrons are generated in what is known as *electron gun*, by thermionic emission from a hot filament, and are then accelerated to around 100 MeV using a linear accelerator (LINAC). These supply electrons regularly to the booster ring which, as the name states, boosts/accelerates the electrons to the energy of the storage ring, where the electrons are periodically injected¹²⁶. As it can be observed in Figure 8, the storage ring is not circular, like it will be imagined by observing the building, it is rather a higher-order polyhedron with bending magnets in each vertex. These magnets are the key factor to produce the radiation, since the electrons, travelling almost at the speed of light, are forced to deviate from their trajectory what results in the release of radiation in a broad spectrum of photon energy¹²⁷. There are other types of magnets, such as wigglers and undulators, which are composed by many magnets placed in opposing polarity^{126,127}. The periodic arrays of this magnets on the straight parts of the storage ring, also known as insertion devices (IDs), are characteristics of third-generation synchrotrons and they provide a higher photon flux, which translates as higher brightness, which in turn allows to perform measurements with a greater signal-to-noise ratio^{126,127}. The next steps happen in the beamlines,

which are located tangentially to the storage ring and the bending magnets (see Figure 8)¹²⁶. Beamlines are divided in four parts: front end, optical and experimental hutches and control cabin. The front end is located between the optical hutch and the storage ring and has several functions including safety features (e.g. isolates the beamline vacuum from the storage ring vacuum, or block, when required, the radiation from the ring to the beamline). In the optical hutch, the beam is focused and/or monochromatized, which will depend on the type of analysis to perform¹²⁶. The only two sections that the users can access to are the experimental hutch and the control cabin, where the samples are located for analysis and the experiment are monitored, respectively.

As it was mentioned in the previous paragraph, depending on the radiation energy adapted in the optical hutch, the beamlines are designed for different techniques and can be divided in four groups: Infrared, UV/Visible, soft X-rays and hard X-rays. In the present work, the techniques used with synchrotron radiation were: infrared microspectroscopy (μ -IR) from the Infrared group, X-ray absorption spectroscopy (XAS) and micro X-ray diffraction (μ -XRD) both from the hard X-rays group.

So, in summary, why to use synchrotron radiation in samples like kidney stones? These types of samples can have a size of a few millimeters and be heterogeneous. If the distribution of the different species along the stone wants to be determined, then two factors must be considered: the sample cannot be analyzed in bulk, which means made powder and destroy it; and, regardless the techniques used, it is required a small spot size (microns), with a high spectral brightness, also known as brilliance or brightness¹²⁸, in order to be able to differentiate the regions with different composition.

1.6. Objectives

The main objective of this Thesis is to fill in the knowledge gap regarding the crystalline conversion of calcium oxalate dihydrate, as well as the appropriate identification of the calcium oxalate monohydrate formation origin. In the case of the present work, the mentioned knowledge is focused in kidney stones, where it has been proven necessary to understand the basic science behind the mentioned processes in order to give the adequate feedback to physicians, reducing calcium oxalate stones recurrence and improving the patient's quality of life.

In order to accomplish the main objective, the following goals have been defined:

- Understand how the crystalline conversion occurs by performing a complete characterization of the synthetic calcium oxalate hydrates.
- Determine if it is possible to differentiate between COM and TRA in kidney stones with the help of SR- μ FTIR.
- Analyze the organic matter distribution on COM stone (surface and nucleus) by SR- μ FTIR to determine which are promoters and which are inhibitors.
- Since not all COD stones are transformed, study its stabilizing by SR- μ FTIR.
- Solve the identification problem between COM and TRA by evaluating their crystallographic textures, with the application of SR- μ XRD, and correlating the results with the morpho-constitutional analysis applied for their classification.
- By performing *in vitro* incubations, determine which components participate in the stabilization of COD, avoiding its transformation.
- Correlate the RSS of calcium oxalate stones with the formation steps, in this case nucleation and crystalline conversion, by *in vitro* studies with AHU
- Investigate the inhibitory potential of extracts from *Lepidium latifolium* on the formation of calcium oxalate stones.

As can be seen in the different objectives, this is a multidisciplinary work. Hence, to achieve the best results, collaborations with field experts have been carried out. Moreover, taking into account that the final goal of this kind of research is to be translated to the society, the results have been presented in seminars and conferences of different fields, including urology and nephrology

1.7. References

- (1) Grases, F.; Costa-Bauza, A.; Prieto, R. M. *Renal Lithiasis and Nutrition*. *Nutr. J.* 2006, 5 (1), 1–7. <https://doi.org/10.1186/1475-2891-5-23>.
- (2) Hickling, D. R.; Sun, T.-T.; Wu, X.-R. *Anatomy and Physiology of the Urinary Tract: Relation to Host Defense and Microbial Infection*. *Urin. Tract Infect.* 2016, 3 (4), 1–25. <https://doi.org/10.1128/9781555817404.ch1>.
- (3) Wallace, M. A. *Anatomy and Physiology of the Kidney*. *AORN J.* 1998, 68 (5), 799–800. [https://doi.org/10.1016/S0001-2092\(06\)62377-6](https://doi.org/10.1016/S0001-2092(06)62377-6).
- (4) Rayner, H.; Milford, D.; Thomas, M. *Understanding Kidney Diseases*; 2016. <https://doi.org/10.1007/978-3-319-23458-8>.
- (5) Alelign, T.; Petros, B. *Kidney Stone Disease: An Update on Current Concepts*. *Adv. Urol.* 2018, Feb 4. <https://doi.org/10.1155/2018/3068365>.
- (6) Putnam, D. *Composition and Concentrative Properties of Human Urine*; 1971.
- (7) Tefekli, A.; Cezayirli, F. *The History of Urinary Stones: In Parallel with Civilization*. *Sci. World J.* 2013, 2013. <https://doi.org/10.1155/2013/423964>.
- (8) De Yoreo, J. J. *Principles of Crystal Nucleation and Growth*. *Rev. Mineral. Geochemistry* 2003, 54 (1), 57–93. <https://doi.org/10.2113/0540057>.
- (9) Asplin, J. R.; Parks, J. H.; Coe, F. L. *Dependence of Upper Limit of Metastability on Supersaturation in Nephrolithiasis*. *Kidney Int.* 1997, 52 (6), 1602–1608. <https://doi.org/10.1038/ki.1997.491>.
- (10) Grases, F.; Costa-Bauzá, A.; García-Ferragut, L. *Biopathological Crystallization: A General View about the Mechanisms of Renal Stone Formation*. *Adv. Colloid Interface Sci.* 1998, 74 (1–3), 169–194. [https://doi.org/10.1016/S0001-8686\(97\)00041-9](https://doi.org/10.1016/S0001-8686(97)00041-9).
- (11) Robertson, W. G. *Methods for Diagnosing the Risk Factors of Stone Formation*. *Arab J. Urol.* 2012, 10 (3), 250–257. <https://doi.org/10.1016/j.aju.2012.03.006>.
- (12) Siener, R.; Hesse, A. *The Effect of Different Diets on Urine Composition and the Risk of Calcium Oxalate Crystallisation in Healthy Subjects*. *Eur. Urol.* 2002, 42 (3), 289–296. [https://doi.org/10.1016/S0302-2838\(02\)00316-0](https://doi.org/10.1016/S0302-2838(02)00316-0).
- (13) Daudon, M.; Letavernier, E.; Frochot, V.; Haymann, J. P.; Bazin, D.; Jungers, P. *Respective Influence of Calcium and Oxalate Urine Concentration on the Formation of Calcium Oxalate Monohydrate or Dihydrate Crystals*. *Comptes Rendus Chim.* 2016, 19 (11–12), 1504–1513. <https://doi.org/10.1016/j.crci.2016.08.009>.
- (14) Khan, Saeed R.; Pearle, Margaret S.; Robertson, William G.; Gambaro, Giovanni; Canales, Benjamin K.; Doizi, Steeve; Traxer, Olivier; Tiselius, H.-G. *Kidney Stones*. *Nat Rev Dis Prim.* 2016, 2 (16008). <https://doi.org/10.1038/nrdp.2016.8.Kidney>.
- (15) Ratkalkar, V. N.; Kleinman, J. G. *Mechanisms of Stone Formation*. *Clin. Rev. Bone Miner. Metab.* 2011, 9 (3–4), 187–197. <https://doi.org/10.1007/s12018-011-9104-8>.
- (16) Aggarwal, K. P.; Narula, S.; Kakkar, M.; Tandon, C. *Nephrolithiasis: Molecular Mechanism of Renal Stone Formation and the Critical Role Played by Modulators*. *Biomed Res. Int.* 2013, 2013. <https://doi.org/10.1155/2013/292953>.

- (17) Halbritter, J.; Seidel, A.; Müller, L.; Schönauer, R.; Hoppe, B. Update on Hereditary Kidney Stone Disease and Introduction of a New Clinical Patient Registry in Germany. *Front. Pediatr.* 2018, 6 (March). <https://doi.org/10.3389/fped.2018.00047>.
- (18) Espinosa-Ortiz, E. J.; Eisner, B. H.; Lange, D.; Gerlach, R. Current Insights into the Mechanisms and Management of Infection Stones. *Nat. Rev. Urol.* 2019, 16 (1), 35–53. <https://doi.org/10.1038/s41585-018-0120-z>.
- (19) Chutipongtanate, S. Breaking the Ice: Urine Proteomics of Medullary Sponge Kidney Disease. *Kidney Int.* 2017, 91 (2), 281–283. <https://doi.org/10.1016/j.kint.2016.10.032>.
- (20) Basavaraj, D. R.; Biyani, C. S.; Browning, A. J.; Cartledge, J. J. The Role of Urinary Kidney Stone Inhibitors and Promoters in the Pathogenesis of Calcium Containing Renal Stones{A Figure Is Presented}. *EAU-EBU Updat. Ser.* 2007, 5 (3), 126–136. <https://doi.org/10.1016/j.eeus.2007.03.002>.
- (21) Fleisch, H. Inhibitors and Promoters of Stone Formation. *Kidney Int.* 1978, 13 (5), 361–371. <https://doi.org/10.1038/ki.1978.54>.
- (22) Ryall, R. L. The Possible Roles of Inhibitors, Promoters, and Macromolecules in the Formation of Calcium Kidney Stones. *Urin. Tract Stone Dis.* 2010, 31–60. https://doi.org/https://doi.org/10.1007/978-1-84800-362-0_4.
- (23) Gupta, M.; Bhayana, S.; Sikka, S. K. Role of Urinary Inhibitors and Promoters in Calcium Oxalate Crystallisation. *Ijrpc* 2011, 1 (4).
- (24) Campbell, A. A.; Ebrahimpour, A.; Perez, L.; Smesko, S. A.; Nancollas, G. H. The Dual Role of Polyelectrolytes and Proteins as Mineralization Promoters and Inhibitors of Calcium Oxalate Monohydrate. *Calcif. Tissue Int.* 1989, 45 (2), 122–128. <https://doi.org/10.1007/BF02561411>.
- (25) Liu, C. C.; Huang, S. P.; Tsai, L. Y.; Wu, W. J.; Juo, S. H. H.; Chou, Y. H.; Huang, C. H.; Wu, M. T. The Impact of Osteopontin Promoter Polymorphisms on the Risk of Calcium Urolithiasis. *Clin. Chim. Acta* 2010, 411 (9–10), 739–743. <https://doi.org/10.1016/j.cca.2010.02.007>.
- (26) Konya, E.; Umekawa, T.; Iguchi, M.; Kurita, T. The Role of Osteopontin on Calcium Oxalate Crystal Formation. *Eur. Urol.* 2003, 43 (5), 564–571. [https://doi.org/10.1016/S0302-2838\(03\)00088-5](https://doi.org/10.1016/S0302-2838(03)00088-5).
- (27) Okada, A.; Nomura, S.; Saeki, Y.; Higashibata, Y.; Hamamoto, S.; Hirose, M.; Itoh, Y.; Yasui, T.; Tozawa, K.; Kohri, K. Morphological Conversion of Calcium Oxalate Crystals into Stones Is Regulated by Osteopontin in Mouse Kidney. *J. Bone Miner. Res.* 2008, 23 (10), 1629–1637. <https://doi.org/10.1359/jbmr.080514>.
- (28) Hunter, G. K. Role of Osteopontin in Modulation of Hydroxyapatite Formation. *Calcif. Tissue Int.* 2013, 93 (4), 348–354. <https://doi.org/10.1007/s00223-013-9698-6>.
- (29) Kleinman, J. G.; Wesson, J. A.; Hughes, J. Osteopontin and Calcium Stone Formation. *Nephron - Physiol.* 2004, 98 (2), 43–48. <https://doi.org/10.1159/000080263>.
- (30) Steitz, S. A.; Speer, M. Y.; McKee, M. D.; Liaw, L.; Almeida, M.; Yang, H.; Giachelli, C. M. Osteopontin Inhibits Mineral Deposition and Promotes Regression of Ectopic Calcification. *Am. J. Pathol.* 2002, 161 (6), 2035–2046. [https://doi.org/10.1016/S0002-9440\(10\)64482-3](https://doi.org/10.1016/S0002-9440(10)64482-3).

- (31) Bazin, D.; Daudon, M.; Combes, C.; Rey, C. Characterization and Some Physicochemical Aspects of Pathological Microcalcifications. *Chem. Rev.* 2012, 112 (10), 5092–5120. <https://doi.org/10.1021/cr200068d>.
- (32) Khan, S. R. Reactive Oxygen Species, Inflammation and Calcium Oxalate Nephrolithiasis. *Transl. Androl. Urol.* 2014, 3 (3), 256–276. <https://doi.org/10.3978/j.issn.2223-4683.2014.06.04>.
- (33) Selvam, R. Calcium Oxalate Stone Disease: Role of Lipid Peroxidation and Antioxidants. *Urol. Res.* 2002, 30 (1), 35–47. <https://doi.org/10.1007/s00240-001-0228-z>.
- (34) Ferrari, P.; Piazza, R.; Ghidini, N.; Bisi, M.; Galizia, G.; Ferrari, G. Lithiasis and Risk Factors. *Urol. Int.* 2007, 79 (SUPPL. 1), 8–15. <https://doi.org/10.1159/000104435>.
- (35) Robertson, W. G. Is Prevention of Stone Recurrence Financially Worthwhile? *Urol. Res.* 2006, 34 (2), 157–161. <https://doi.org/10.1007/s00240-005-0030-4>.
- (36) Burgos, F. J.; Gomez, V.; Dapena, F. Controversias Actuales En La Litiasis Urinaria. *Nefrologia* 1998, 18 (SUPPL. 6), 62–70.
- (37) Curhan, G. C. Epidemiology of Stone Disease. *Urol. Clin. North Am.* 2007, 34, 287–293. <https://doi.org/10.1016/j.ucl.2007.04.003>.
- (38) Romero, V.; Akpınar, H.; Assimos, D. G. Kidney Stones: A Global Picture of Prevalence, Incidence, and Associated Risk Factors. *Rev. Urol.* 2010, 12 (2–3), e86–96. <https://doi.org/10.3909/riu0459>.
- (39) Trinchieri, A. Epidemiological Trends in Urolithiasis: Impact on Our Health Care Systems. *Urol. Res.* 2006, 34 (2), 151–156. <https://doi.org/10.1007/s00240-005-0029-x>.
- (40) Raheem, O. A.; Khandwala, Y. S.; Sur, R. L.; Ghani, K. R.; Denstedt, J. D. Burden of Urolithiasis: Trends in Prevalence, Treatments, and Costs. *Eur. Urol. Focus* 2017, 3 (1), 18–26. <https://doi.org/10.1016/j.euf.2017.04.001>.
- (41) Türk, C.; Neisius, A.; Petrik, A.; Seitz, C.; Skolarikos, A.; Thomas, K. EAU Guidelines on Urolithiasis. *Eur. Assoc. Urol.* 2018, 69 (3), 475–482. <https://doi.org/10.1016/j.eururo.2015.07.041>.
- (42) Siener, R.; Buchholz, N.; Daudon, M.; Hess, B.; Knoll, T.; Osther, P. J.; Reis-Santos, J.; Sarica, K.; Traxer, O.; Trinchieri, A. Quality Assessment of Urinary Stone Analysis: Results of a Multicenter Study of Laboratories in Europe. *PLoS One* 2016, 11 (6). <https://doi.org/10.1371/journal.pone.0156606>.
- (43) Daudon, M.; Dessombz, A.; Frochot, V.; Letavernier, E.; Haymann, J. P.; Jungers, P.; Bazin, D. Comprehensive Morpho-Constitutional Analysis of Urinary Stones Improves Etiological Diagnosis and Therapeutic Strategy of Nephrolithiasis. *Comptes Rendus Chim.* 2016, 19 (11–12), 1470–1491. <https://doi.org/10.1016/j.crci.2016.05.008>.
- (44) Grases, F.; Costa-Bauzá, A.; Ramis, M.; Montesinos, V.; Conte, A. Simple Classification of Renal Calculi Closely Related to Their Micromorphology and Etiology. *Clin. Chim. Acta* 2002, 322 (1–2), 29–36. [https://doi.org/10.1016/S0009-8981\(02\)00063-3](https://doi.org/10.1016/S0009-8981(02)00063-3).
- (45) Lorenzo, V.; Torres, A.; Hernández, D.; Ayus, J. C. *Manual de Nefrología*, 2nd ed.; Elsevier, España, 2002.

- (46) Bazin, D.; Leroy, C.; Tielens, F.; Bonhomme, C.; Bonhomme-Coury, L.; Damay, F.; Le Denmat, D.; Sadoine, J.; Rode, J.; Frochot, V.; Letavernier, E.; Haymann, J. P.; Daudon, M. *Hyperoxaluria Is Related to Whewellite and Hypercalciuria to Weddellite: What Happens When Crystalline Conversion Occurs?* *Comptes Rendus Chim.* 2016, 19 (11–12), 1492–1503. <https://doi.org/10.1016/j.crci.2015.12.011>.
- (47) Walton, R. C.; Kavanagh, J. P.; Heywood, B. R.; Rao, P. N. *Calcium Oxalates Grown in Human Urine under Different Batch Conditions.* *J. Cryst. Growth* 2005, 284 (3–4), 517–529. <https://doi.org/10.1016/j.jcrysgro.2005.06.057>.
- (48) Zhang, D.; Qi, L.; Ma, J.; Cheng, H. *Morphological Control of Calcium Oxalate Dihydrate by a Double-Hydrophilic Block Copolymer.* *Chem. Mater.* 2002, 14 (6), 2450–2457. <https://doi.org/10.1021/cm010768y>.
- (49) Conti, C.; Casati, M.; Colombo, C.; Realini, M.; Brambilla, L.; Zerbi, G. *Phase Transformation of Calcium Oxalate Dihydrate-Monohydrate: Effects of Relative Humidity and New Spectroscopic Data.* *Spectrochim. Acta - Part A Mol. Biomol. Spectrosc.* 2014, 128, 413–419. <https://doi.org/10.1016/j.saa.2014.02.182>.
- (50) Kloprogge, J. T.; Boström, T. E.; Weier, M. L. *In Situ Observation of the Thermal Decomposition of Weddellite by Heating Stage Environmental Scanning Electron Microscopy.* *Am. Mineral.* 2004, 89 (1), 245–248. <https://doi.org/10.2138/am-2004-0129>.
- (51) Ihli, J.; Wang, Y. W.; Cantaert, B.; Kim, Y. Y.; Green, D. C.; Bomans, P. H. H.; Sommerdijk, N. A. J. M.; Meldrum, F. C. *Precipitation of Amorphous Calcium Oxalate in Aqueous Solution.* *Chem. Mater.* 2015, 27 (11), 3999–4007. <https://doi.org/10.1021/acs.chemmater.5b01642>.
- (52) Hajir, M.; Graf, R.; Tremel, W. *Stable Amorphous Calcium Oxalate: Synthesis and Potential Intermediate in Biomineralization.* *Chem. Commun.* 2014, 50 (49), 6534–6536. <https://doi.org/10.1039/c4cc02146k>.
- (53) Conti, C.; Brambilla, L.; Colombo, C.; Dellasega, D.; Gatta, G. D.; Realini, M.; Zerbi, G. *Stability and Transformation Mechanism of Weddellite Nanocrystals Studied by X-Ray Diffraction and Infrared Spectroscopy.* *Phys. Chem. Chem. Phys.* 2010, 12 (43), 14560–14566. <https://doi.org/10.1039/c0cp00624f>.
- (54) Christy, A. A.; Nodland, E.; Burnham, A. K.; Kvalheim, O. M.; Dahl, B. *Determination of Kinetic Parameters for the Dehydration of Calcium Oxalate Monohydrate by Diffuse Reflectance FT-IR Spectroscopy.* *Appl. Spectrosc.* 1994, 48 (5), 561–568. <https://doi.org/10.1366/0003702944924916>.
- (55) Frost, R. L.; Weier, M. L. *Thermal Treatment of Whewellite—a Thermal Analysis and Raman Spectroscopic Study.* *Thermochim. Acta* 2004, 409 (1), 79–85. [https://doi.org/10.1016/S0040-6031\(03\)00332-0](https://doi.org/10.1016/S0040-6031(03)00332-0).
- (56) Daudon, M.; Bader, C. A.; Jungers, P.; Robertson, W. G.; Tiselius, H. G.; Hess, B.; Asplin, J. R. *Urinary Calculi: Review of Classification Methods and Correlations with Etiology.* *Scanning Microscopy.* 1993, pp 1081–1106.
- (57) Daudon, M.; Jungers, P.; Bazin, D.; Williams, J. C. *Recurrence Rates of Urinary Calculi According to Stone Composition and Morphology.* *Urolithiasis* 2018, 46 (5), 459–470. <https://doi.org/10.1007/s00240-018-1043-0>.

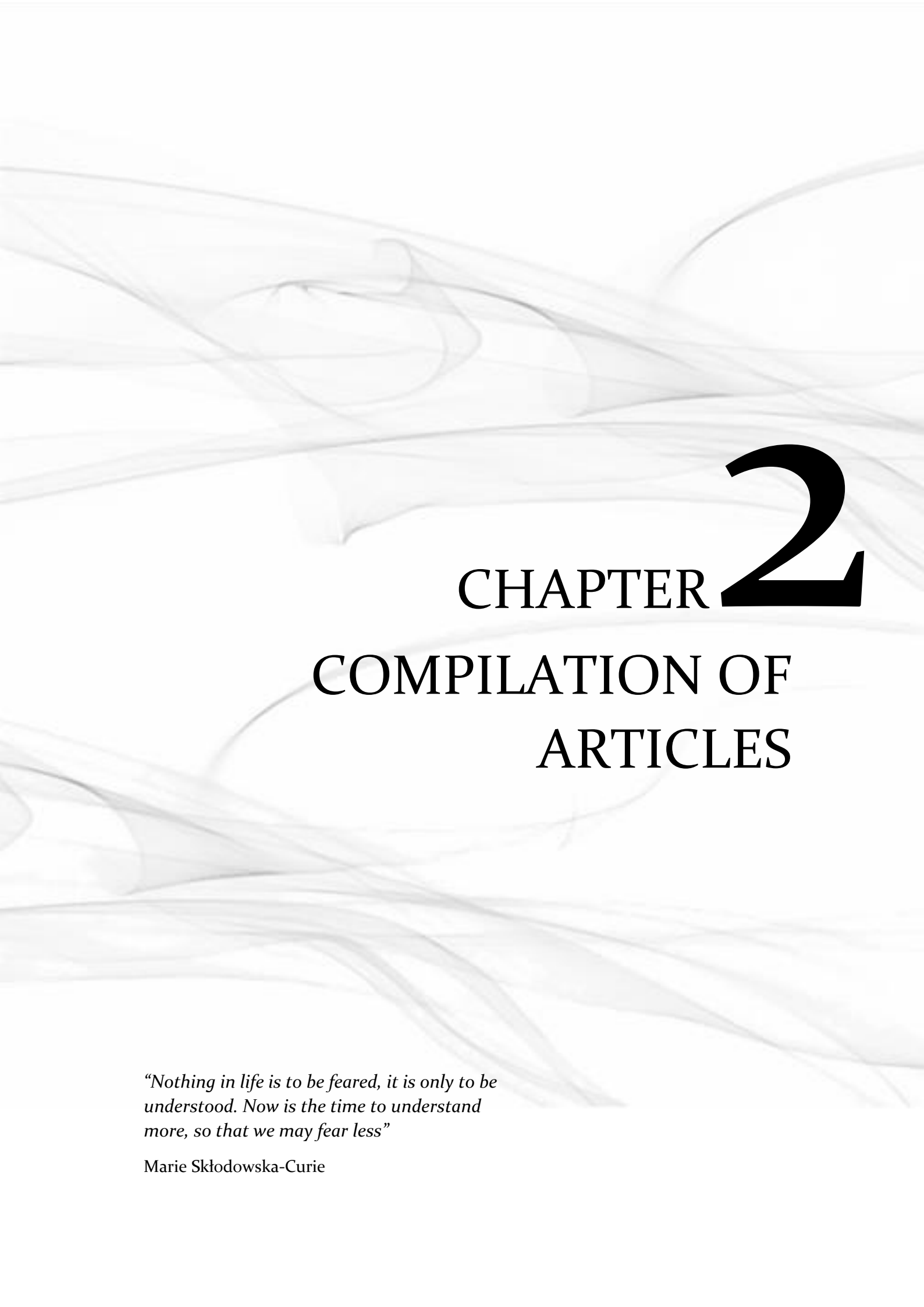
- (58) Daudon, M.; Jungers, P.; Bazin, D. Stone Morphology: Implication for Pathogenesis. *AIP Conf. Proc.* 2008, 1049, 199–215. <https://doi.org/10.1063/1.2998023>.
- (59) Portis, A. J.; Sundaram, C. P. Diagnosis and Initial Management of Kidney Stones. *Am. Fam. Physician* 2001, 63 (7), 1329–1338.
- (60) Williams, J. C.; Gambaro, G.; Rodgers, A.; Asplin, J.; Bonny, O.; Costa-Bauzá, A.; Ferraro, P. M.; Fogazzi, G.; Fuster, D. G.; Goldfarb, D. S.; Grases, F.; Heilberg, I. P.; Kok, D.; Letavernier, E.; Lippi, G.; Marangella, M.; Nouvenne, A.; Petrarulo, M.; Siener, R.; Tiselius, H. G.; Traxer, O.; Trinchieri, A.; Croppi, E.; Robertson, W. G. Urine and Stone Analysis for the Investigation of the Renal Stone Former: A Consensus Conference. *Urolithiasis* 2020, No. 0123456789. <https://doi.org/10.1007/s00240-020-01217-3>.
- (61) Laube, Norbert; Kleinen, L. Risk Indices. In *Urinary Tract Stone Disease*; 2011; pp 355–368. https://doi.org/10.1007/978-1-84800-362-0_30.
- (62) Laube, N.; Berg, W.; Knoll, T.; Busch, H. The Bonn-Risk-Index for Determination of the Risk of Urolith Formation and Other Metabolic Diseases. *EPMA J.* 2014, 5 (S1), A63. <https://doi.org/10.1186/1878-5085-5-s1-a63>.
- (63) Kavanagh, J. P.; Laube, N. Why Does the Bonn Risk Index Discriminate between Calcium Oxalate Stone Formers and Healthy Controls? *J. Urol.* 2006, 175 (2), 766–770. [https://doi.org/10.1016/S0022-5347\(05\)00145-X](https://doi.org/10.1016/S0022-5347(05)00145-X).
- (64) Rodgers, A. L. Urinary Saturation: Casual or Causal Risk Factor in Urolithiasis? *BJU Int.* 2014, 114 (1), 104–110. <https://doi.org/10.1111/bju.12481>.
- (65) Prochaska, M.; Taylor, E.; Ferraro, P. M.; Curhan, G. Relative Supersaturation of 24-Hour Urine and Likelihood of Kidney Stones. *J. Urol.* 2018, 199 (5), 1262–1266. <https://doi.org/10.1016/j.juro.2017.10.046>.
- (66) Werness, P. G.; Brown, C. M.; Smith, L. H.; Finlayson, B. Equil 2: A BASIC Computer Program for the Calculation of Urinary Saturation. *J. Urol.* 1985, 134 (6), 1242–1244. [https://doi.org/10.1016/S0022-5347\(17\)47703-2](https://doi.org/10.1016/S0022-5347(17)47703-2).
- (67) Brown, C. M.; Purich, D. L.; Ackermann, D. K. EQUIL 93: A Tool for Experimental and Clinical Urolithiasis. *Urol. Res.* 1994, 22 (2), 119–126. <https://doi.org/10.1007/BF00311003>.
- (68) De Coninck, V.; Antonelli, J.; Chew, B.; Patterson, J. M.; Skolarikos, A.; Bultitude, M. Medical Expulsive Therapy for Urinary Stones: Future Trends and Knowledge Gaps. *Eur. Urol.* 2019, 76 (5), 658–666. <https://doi.org/10.1016/j.eururo.2019.07.053>.
- (69) Zumstein, V.; Betschart, P.; Abt, D.; Schmid, H. P.; Panje, C. M.; Putora, P. M. Surgical Management of Urolithiasis - A Systematic Analysis of Available Guidelines. *BMC Urol.* 2018, 18 (1), 1–8. <https://doi.org/10.1186/s12894-018-0332-9>.
- (70) Assimos, D.; Krambeck, A.; Miller, N. L.; Monga, M.; Murad, M. H.; Nelson, C. P.; Pace, K. T.; Pais, V. M.; Pearle, M. S.; Preminger, G. M.; Razvi, H.; Shah, O.; Matlaga, B. R. Surgical Management of Stones: American Urological Association/Endourological Society Guideline, PART I. *J. Urol.* 2016, 196 (4), 1153–1160. <https://doi.org/10.1016/j.juro.2016.05.090>.
- (71) Assimos, D.; Krambeck, A.; Miller, N. L.; Monga, M.; Murad, M. H.; Nelson, C. P.; Pace, K. T.; Pais, V. M.; Pearle, M. S.; Preminger, G. M.; Razvi, H.; Shah, O.; Matlaga, B. R. Surgical Management of Stones: American Urological

- Association/Endourological Society Guideline, PART II. *J. Urol.* 2016, 196 (4), 1161–1169. <https://doi.org/10.1016/j.juro.2016.05.091>.
- (72) Hernandez, R. *Guías En Tratamiento de Litiasis Renal.* Soc. Argentina Urol. 2014.
- (73) Hernandez, R. *Guías Para El Tratamiento de La Litiasis Renal y Ureteral.* Soc. Argentina Urol. 2014.
- (74) Conort, Pierre; Dore, Bertrand; Saussine, C. *Comite Lithiase de l'Association Francaise DU. Guidelines for the Urological Management of Renal and Ureteric Stones in Adults.* *J. L'association Fr. D'urologie la Soc. Fr. D'urologie* 2014, 4 (6), 1095–1102.
- (75) Knoll, T.; Bach, T.; Humke, U.; Neisius, A.; Stein, R.; Schönthaler, M.; Wendt-Nordahl, G. *Szk-Leitlinie Zur Diagnostik, Therapie Und Metaphylaxe Der Urolithiasis (AWMF 043/025): Kurzfassung.* *Urol.* 2016, 55 (7), 904–922. <https://doi.org/10.1007/s00120-016-0133-2>.
- (76) SUA (Singapore Urological Association). *The Management of Urolithiasis.* 2001.
- (77) Lesko, L. J.; Schmidt, S. *Individualization of Drug Therapy: History, Present State, and Opportunities for the Future.* *Clin. Pharmacol. Ther.* 2012, 92 (4), 458–466. <https://doi.org/10.1038/clpt.2012.113>.
- (78) Moe, O. W. *Kidney Stones: Pathophysiology and Medical Management.* *Lancet* 2006, 367 (9507), 333–344. [https://doi.org/10.1016/S0140-6736\(06\)68071-9](https://doi.org/10.1016/S0140-6736(06)68071-9).
- (79) Gul, Z.; Monga, M. *Medical and Dietary Therapy for Kidney Stone Prevention.* *Korean J. Urol.* 2014, 55 (12), 775–779. <https://doi.org/10.4111/kju.2014.55.12.775>.
- (80) Grases, F.; Rodriguez, A.; Costa-Bauza, A. *Efficacy of Mixtures of Magnesium, Citrate and Phytate as Calcium Oxalate Crystallization Inhibitors in Urine.* *J. Urol.* 2015, 194 (3), 812–819. <https://doi.org/10.1016/j.juro.2015.03.099>.
- (81) Muñoz, J. A.; López-Mesas, M.; Valiente, M. *Inhibitors of Oxalocalcic Lithiasis: Effects of Their Interactions on Calcium Oxalate Crystallization.* *Urology* 2012, 80 (5), 1163.e13–1163.e18. <https://doi.org/10.1016/j.urology.2012.04.040>.
- (82) Costa-Bauzá, A.; Isern, B.; Perelló, J.; Sanchis, P.; Grases, F. *Factors Affecting the Regrowth of Renal Stones in Vitro: A Contribution to the Understanding of Renal Stone Development.* *Scand. J. Urol. Nephrol.* 2005, 39 (3), 194–199. <https://doi.org/10.1080/00365590510031101>.
- (83) Chow, K.; Dixon, J.; Gilpin, S.; Kavanagh, J. P.; Rao, P. N. *Citrate Inhibits Growth of Residual Fragments in an in Vitro Model of Calcium Oxalate Renal Stones.* *Kidney Int.* 2004, 65 (5), 1724–1730. <https://doi.org/10.1111/j.1523-1755.2004.00566.x>.
- (84) Icer, M. A.; Gezmen-Karadag, M. *The Potential Effects of Dietary Food and Beverage Intakes on the Risk of Kidney Stone Formation.* *Rev. Nutr.* 2019, 32, 1–14. <https://doi.org/10.1590/1678-9865201932E190029>.
- (85) Heilberg, I. P.; Goldfarb, D. S. *Optimum Nutrition for Kidney Stone Disease.* *Adv. Chronic Kidney Dis.* 2013, 20 (2), 165–174. <https://doi.org/10.1053/j.ackd.2012.12.001>.
- (86) Taylor, E. N.; Curhan, G. C. *Role of Nutrition in the Formation of Calcium-Containing Kidney Stones.* *Nephron - Physiol.* 2004, 98 (2), 55–64. <https://doi.org/10.1159/000080265>.

- (87) Fritsche, H. M.; Dötzer, K. Improving the Compliance of the Recurrent Stone-Former. *Arab J. Urol.* 2012, 10 (3), 342–346. <https://doi.org/10.1016/j.aju.2012.07.003>.
- (88) Parks, J. H.; Coe, F. L. Evidence for Durable Kidney Stone Prevention over Several Decades. 2010, 103 (9), 1238–1246. <https://doi.org/10.1111/j.1464-410X.2008.08170.x.Evidence>.
- (89) González, A. F.; Pieters, L.; Hernández, R. D. Effectiveness of Herbal Medicine in Renal Lithiasis: A Review. *Siriraj Med. J.* 2020, 72 (2), 188–194. <https://doi.org/10.33192/Smj.2020.25>.
- (90) Petrovska, B. B. Historical Review of Medicinal Plants' Usage. *Pharmacogn. Rev.* 2012, 6 (11), 1–5. <https://doi.org/10.4103/0973-7847.95849>.
- (91) Aassem, Y.; Bouha, M.; Bouhdadi, R.; Bir, M. E. L.; Gamouh, A.; Mbarki, M. Effet Inhibiteur d'Extraits Aqueux de Pulpes de Caroube, de Citron et d'Orange Sur La Cristallurie de Patients Lithiasiques [Inhibitory Effect of Aqueous Extracts for Carob, Lemon and Orange Pulp on the Crystalluria of Lithiasic Patients]. 2019, 27 (2), 678–685.
- (92) Nirumand, M. C.; Hajialyani, M.; Rahimi, R.; Farzaei, M. H.; Zingue, S.; Nabavi, S. M.; Bishayee, A. Dietary Plants for the Prevention and Management of Kidney Stones: Preclinical and Clinical Evidence and Molecular Mechanisms. *Int. J. Mol. Sci.* 2018, 19 (3). <https://doi.org/10.3390/ijms19030765>.
- (93) WIENTARSIH, I.; MADYASTUTI, R. I. N. I.; PRASETYO, B. F.; ALDOBRATA, A. Anti Lithiasis Activity of Avocado (*Persea Americana* Mill) Leaves Extract in White Male Rats. *HAYATI J. Biosci.* 2012, 19 (1), 49–52. <https://doi.org/10.4308/hjb.19.1.49>.
- (94) Grases, F.; Prieto, R. M.; Fernandez-Cabot, R. A.; Costa-Bauzá, A.; Tur, F.; Torres, J. J. Effects of Polyphenols from Grape Seeds on Renal Lithiasis. *Oxid. Med. Cell. Longev.* 2015, 2015. <https://doi.org/10.1155/2015/813737>.
- (95) Ardakani Movaghati, M. R.; Yousefi, M.; Saghebi, S. A.; Sadeghi Vazin, M.; Iraj, A.; Mosavat, S. H. Efficacy of Black Seed (*Nigella Sativa* L.) on Kidney Stone Dissolution: A Randomized, Double-Blind, Placebo-Controlled, Clinical Trial. *Phyther. Res.* 2019, 33 (5), 1404–1412. <https://doi.org/10.1002/ptr.6331>.
- (96) Jeong, B. C.; Kim, B. S.; Kim, J. I.; Kim, H. H. Effects of Green Tea on Urinary Stone Formation: An in Vivo and in Vitro Study. *J. Endourol.* 2006, 20 (5), 356–361. <https://doi.org/10.1089/end.2006.20.356>.
- (97) WU, Z. B.; JIANG, T.; LIN, G. B.; WANG, Y. X.; ZHOU, Y.; CHEN, Z. Q.; XU, Y. M.; YE, H. B.; CHEN, B. J.; BAO, X. Z.; ZHANG, C. M. Tea Consumption Is Associated with Increased Risk of Kidney Stones in Northern Chinese: A Cross-Sectional Study. *Biomed. Environ. Sci.* 2017, 30 (12), 922–926. <https://doi.org/10.3967/bes2017.124>.
- (98) Ahmed, S.; Hasan, M. M.; Khan, H.; Mahmood, Z. A.; Patel, S. The Mechanistic Insight of Polyphenols in Calcium Oxalate Urolithiasis Mitigation. *Biomed. Pharmacother.* 2018, 106 (July), 1292–1299. <https://doi.org/10.1016/j.biopha.2018.07.080>.
- (99) Miyaoka, R.; Monga, M. Use of Traditional Chinese Medicine in the Management of Urinary Stone Disease. *Int. Braz J Urol* 2009, 35 (4), 396–405. <https://doi.org/10.1590/S1677-55382009000400002>.

- (100) Butterweck, V.; Khan, S. R. *Herbal Medicines in the Management of Urolithiasis: Alternative or Complementary? Planta Med.* 2009, 75 (10), 1095–1103. <https://doi.org/10.1055/s-0029-1185719>.
- (101) Kieley, S.; Dwivedi, R.; Monga, M. *Ayurvedic Medicine and Renal Calculi. J. Endourol.* 2008, 22 (8), 1613–1616. <https://doi.org/10.1089/end.2008.0020>.
- (102) Ballabh, B.; Chaurasia, O. P.; Ahmed, Z.; Singh, S. B. *Traditional Medicinal Plants of Cold Desert Ladakh-Used against Kidney and Urinary Disorders. J. Ethnopharmacol.* 2008, 118 (2), 331–339. <https://doi.org/10.1016/j.jep.2008.04.022>.
- (103) Gürocak, S.; Küpeli, B. *Consumption of Historical and Current Phytotherapeutic Agents for Urolithiasis: A Critical Review. J. Urol.* 2006, 176 (2), 450–455. <https://doi.org/10.1016/j.juro.2006.03.034>.
- (104) Beto, J. A. *Herbal Use in the Nutrition Management of Kidney Stones; Han, H.; Mutter, W.; Nasser, S., Ed.; Cham Humana, 2019.* https://doi.org/10.1007/978-3-030-15534-6_22.
- (105) Dhole, A. R.; Yeligar, V. C. *Urolithiasis and Its Herbal Remedies. Int. J. Sci. Res. Sci. Technol.* 2018, 4 (11), 150–156. <https://doi.org/10.32628/ijrst1840116>.
- (106) Kasote, D. M.; Jagtap, S. D.; Thapa, D.; Khyade, M. S.; Russell, W. R. *Herbal Remedies for Urinary Stones Used in India and China: A Review. J. Ethnopharmacol.* 2017, 203, 55–68. <https://doi.org/10.1016/j.jep.2017.03.038>.
- (107) Bahmani, M.; Baharvand-Ahmadi, B.; Tajeddini, P.; Rafieian-Kopaei, M.; Naghdi, N. *Identification of Medicinal Plants for the Treatment of Kidney and Urinary Stones. J. Ren. Inj. Prev.* 2016, 5 (3), 129–133. <https://doi.org/10.15171/jrip.2016.27>.
- (108) Ahmed, S.; Hasan, M. M.; Alam, Z. *In-Vitro Urolithiasis Models: An Evaluation of Prophylactic Management against Kidney Stones. J. Pharmacogn. Phytochem.* 2016, 5 (3), 28–35.
- (109) Delfan, B.; Baharvand-Ahmadi, B.; Bahmani, M.; Mohseni, N.; Saki, K.; Rafieian-Kopaei, M.; Shahsavari, S.; Naghdi, N.; Taherikalani, M.; Ghafourian, S. *An Ethnobotanical Study of Medicinal Plants Used in Treatment of Kidney Stones and Kidney Pain in Lorestan Province, Iran. J. Chem. Pharm. Sci.* 2015, 8 (4), 693–699.
- (110) Sharma, N.; Tanwer, B. S.; Vijayvergia, R. *Study of Medicinal Plants in Aravali Regions of Rajasthan for Treatment of Kidney Stone and Urinary Tract Troubles. Int. J. PharmTech Res.* 2011, 3 (1), 110–113.
- (111) NOUMI, E. *Potentiality of Medicinal Plants in Treating Urinary Lithiasis in Littoral Region, Cameroon. European J. Med. Plants* 2011, 1 (3), 74–87. <https://doi.org/10.9734/ejmp/2011/234>.
- (112) Freitas, A. M.; Schor, N.; Boim, M. A. *The Effect of Phyllanthus Niruri on Urinary Inhibitors of Calcium Oxalate Crystallization and Other Factors Associated with Renal Stone Formation. BJU Int.* 2002, 89 (9), 829–834. <https://doi.org/10.1046/j.1464-410X.2002.02794.x>.
- (113) Barros, M. E.; Lima, R.; Mercuri, L. P.; Matos, J. R.; Schor, N.; Boim, M. A. *Effect of Extract of Phyllanthus Niruri on Crystal Deposition in Experimental Urolithiasis. Urol. Res.* 2006, 34 (6), 351–357. <https://doi.org/10.1007/s00240-006-0065-1>.

- (114) Barros, M. E.; Schor, N.; Boim, M. A. *Effects of an Aqueous Extract from Phyllanthus Niruri on Calcium Oxalate Crystallization in Vitro*. *Urol. Res.* 2003, 30 (6), 374–379. <https://doi.org/10.1007/s00240-002-0285-y>.
- (115) Nishiura, J. L.; Campos, A. H.; Boim, M. A.; Heilberg, I. P.; Schor, N. *Phyllanthus Niruri Normalizes Elevated Urinary Calcium Levels in Calcium Stone Forming (CSF) Patients*. *Urol. Res.* 2004, 32 (5), 362–366. <https://doi.org/10.1007/s00240-004-0432-8>.
- (116) Pucci, N. D.; Marchini, G. S.; Mazzucchi, E.; Reis, S. T.; Srougi, M.; Evazian, D.; Nahas, W. C. *Effect of Phyllanthus Niruri on Metabolic Parameters of Patients with Kidney Stone: A Perspective for Disease Prevention*. *Int. Braz J Urol* 2018, 44 (4), 758–764. <https://doi.org/10.1590/S1677-5538.IBJU.2017.0521>.
- (117) Boim, M. A.; Heilberg, I. P.; Schor, N. *Phyllanthus Niruri as a Promising Alternative Treatment for Nephrolithiasis*. *Int. Braz J Urol* 2010, 36 (6), 657–664. <https://doi.org/10.1590/S1677-55382010000600002>.
- (118) Atmani, F.; Khan, R. *Effects of an Extract from Herniaria Hirsuta on Calcium Oxalate Crystallization in Vitro*. 2000, 621–625.
- (119) Atmani, F.; Slimani, Y.; Mimouni, M.; Hacht, B. *Prophylaxis of Calcium Oxalate Stones by Herniaria Hirsuta on Experimentally Induced Nephrolithiasis in Rats*. *BJU Int.* 2003, 92 (1), 137–140. <https://doi.org/10.1046/j.1464-410X.2003.04289.x>.
- (120) Atmani, F.; Farell, G.; Lieske, J. C. *Extract from Herniaria Hirsuta Coats Calcium Oxalate Monohydrate Crystals and Blocks Their Adhesion to Renal Epithelial Cells*. *J. Urol.* 2004, 172 (4 I), 1510–1514. <https://doi.org/10.1097/01.ju.0000131004.03795.c5>.
- (121) Fouada, A.; Yamina, S.; Nait, M. A.; Mohammed, B.; Abdlekrim, R. *In Vitro and in Vivo Antilithiasic Effect of Saponin Rich Fraction Isolated from Herniaria Hirsuta*. *J. Bras. Nefrol.* 2006, 28 (4), 199–203.
- (122) Navarro, E.; Alonso, J.; Rodriguez, R.; Trujillo, J.; Boada, J. *Diuretic Action of an Aqueous Extract of Lepidium Latifolium L.* *J. Ethnopharmacol.* 1994, 41 (1–2), 65–69. [https://doi.org/10.1016/0378-8741\(94\)90059-0](https://doi.org/10.1016/0378-8741(94)90059-0).
- (123) Verma, A. K.; Goyal, Y.; Dev, K. *Medicinal Value and Mechanism of Light Adaptation in Lepidium Latifolium in Ladakh Region*. 2019, 20 (3), 49–55.
- (124) Tabassum, N.; Ahmad, F. *Role of Natural Herbs in the Treatment of Hypertension*. 2011, 5 (9). <https://doi.org/10.4103/0973-7847.79097>.
- (125) González, J. G. *Estudio de Los Usos Culturales de Las Plantas Silvestres En Los Campos de Gran Canaria*. 2017, 111.
- (126) Willmott, P. *An Introduction to Synchrotron Radiation: Techniques and Applications, Second Edi.*; John Wiley & Sons Ltd, 2019.
- (127) Duncan, D. A. *Synchrotron-Based Spectroscopy in on-Surface Polymerization of Covalent Networks*; Elsevier, 2018. <https://doi.org/10.1016/B978-0-12-409547-2.13768-0>.
- (128) Mills, D. M.; Helliwell, J. R.; Kvik, Å.; Ohta, T.; Robinson, I. A.; Authier, A. *Report of the Working Group on Synchrotron Radiation Nomenclature - Brightness, Spectral Brightness or Brilliance?* *J. Synchrotron Radiat.* 2005, 12 (3), 385. <https://doi.org/10.1107/S090904950500796X>.

The background of the page is a soft, ethereal image of white fabric or smoke flowing across the frame, creating a sense of movement and lightness. The fabric is translucent and layered, with some areas appearing more dense than others, giving it a dreamlike quality.

CHAPTER 2

COMPILATION OF ARTICLES

“Nothing in life is to be feared, it is only to be understood. Now is the time to understand more, so that we may fear less”

Marie Skłodowska-Curie

Characterization of calcium oxalate hydrates and the transformation process

Iris H. Valido^a, Joaquim M. Rius-Bartra^b, Roberto Boada^a, Montserrat Resina-Gallego^a, Manuel Valiente^a, and Montserrat López-Mesas^{a*}

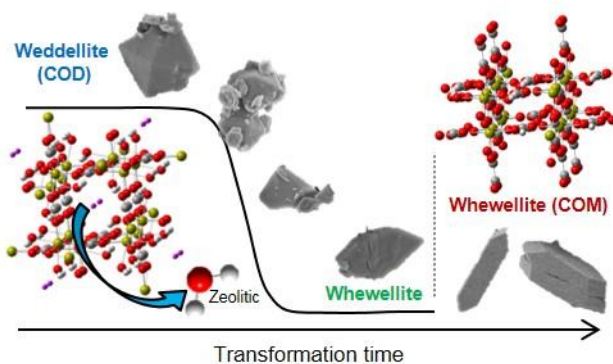
^a Centre Grup de Tecniques de Separacio en Quimica (GTS), Departament de Quimica, Universitat Autònoma de Barcelona, Facultat de Ciències, Edifici CN. 08193, Bellaterra, Barcelona, Spain

^b Departament de Quimica, Universitat Autònoma de Barcelona, Facultat de Ciències, Edifici CN. 08193, Bellaterra, Barcelona, Spain

*Montserrat.lopez.mesas

Journal: ChemPhysChem
doi.org/10.1002/cphc.202000684
First published: 28 August 2020
Version of Record online: 23 October 2020
Issue Online: 18 November 2020

Reproduced with permission from ChemPhysChem. Copyright © 1990-2020 John Wiley & Sons



Characterization of calcium oxalate hydrates and the transformation process

Iris H. Valido^a, Joaquim M^a Rius-Bartra^b, Roberto Boada^a, Montserrat Resina-Gallego^a, Manuel Valiente^a, Montserrat López-Mesas^{a*}

^a Centre Grup de Tècniques de Separació en Química (GTS), Departament de Química, Universitat Autònoma de Barcelona, Facultat de Ciències, Edifici CN, 08193, Bellaterra, Spain

^b Departament de Química, Universitat Autònoma de Barcelona, Facultat de Ciències, Edifici CN, 08193, Bellaterra, Barcelona, Spain

KEYWORDS: *weddellite; whewellite; DFT computational calculations; FTIR spectroscopy; Raman spectroscopy; X-ray diffraction; X-ray absorption spectroscopy*

ABSTRACT: Calcium oxalate can be found in humans as kidney stones and in cultural heritage as films in two crystallographic species, dihydrate (COD/weddellite) and/or monohydrate (COM/whewellite). Due to its instability, COD is transformed into COM. Study this crystalline conversion provides information about the origin of the monohydrated species, which will help in the assessment of prevention measurements in order to avoid their formation. In the present study, the synthesis of calcium oxalate hydrates microcrystals has been carefully performed to avoid mixture of phases in the final products; the long and short range order structure of both species have been studied by X-ray Diffraction (XRD) and X-ray Absorption Spectroscopy (XAS) respectively. This structural information was considered in the Density Functional Theory (DFT) computational study performed to assign the characteristic vibrational IR and Raman frequencies found. This detailed characterization allows an unambiguous assignment of the vibrations, thus providing the appropriate parameters required to monitor the transformation process, and to characterize the transformation process.

INTRODUCTION

Calcium oxalate hydrates commonly crystallize in nature, being found on sediments, plants and animals. They are represented by three crystallographic species: calcium oxalate monohydrate (COM) or whewellite ($\text{CaC}_2\text{O}_4 \cdot \text{H}_2\text{O}$), which is the thermodynamically stable; the kinetically favorable calcium oxalate dihydrate (COD) or weddellite ($\text{CaC}_2\text{O}_4 \cdot 2\text{H}_2\text{O}$); and calcium oxalate trihydrate, known as caoxite ($\text{CaC}_2\text{O}_4 \cdot 3\text{H}_2\text{O}$), which is rarely observed.^[1,2]

In the field of medicine, calcium oxalate is the main component of urinary stones, representing 70% of cases in Western countries.^[3] Although both COM and COD are found in renal stones, COM is more frequently observed, maybe due to its stability.^[4] Calcium oxalate is also known in the field of cultural heritage, since films of this material have been found on the surface of ancient monuments,^[5] being an indicator of weathering

process and/or decay of the monument substrates,^[6] where both forms can also be observed.

One of the most controversial issues in the chemistry of oxalates is the process which accounts for the transformation of calcium oxalate dihydrate into the monohydrated species.^[5,7] This process starts with the change in the “zeolitic water” channel sites configuration, which acts as the driving force of the transformation,^[5] resulting in the monohydrate species. In order to facilitate the discussion through this manuscript, the product obtained during the crystalline conversion of COD will be named TRA (with the transformation time between brackets). The study of this crystalline conversion is important since it provides information about the different origin of the monohydrated species. Many authors have studied this process by thermogravimetry^[8-10] and under different humidity conditions.^[5,7] They determined that the instability of COD could be due to the presence of the zeolitic water and the large size of its channels,^[5] while

other unknown factors, independent of the humidity, could drive the transformation process.^[7]

When analyzing COD kidney stones by Fourier Transform Infrared (FTIR) spectra and Scanning Electron Microscopy (SEM), the presence of COM in COD stones provides contradictory results. FTIR shows characteristic bands of COM, whereas SEM reveals the presence of bipyramidal crystals, characteristics of COD.^[11] Since both species are related to different pathologies (for example, COM to hyperoxaluria and COD to hypercalciuria), distinguish the origin of the crystal grown is important to associate the kidney stones with the corresponding etiology and treatment.^[11] On the other hand, COD is not always transformed. Hence, it is present as weddellite in renal calculi and, in the same way, weddellite is often detected in oxalate films occurring on the surface of several ancient monuments.^[7]

The aim of this work is to characterize the transformation process from the dihydrated to the monohydrated calcium oxalate species. The synthesis of calcium oxalate hydrates microcrystals has been carefully performed to avoid mixture of phases. Thus, the resulting materials were studied by different structural characterization techniques, such as X-ray Diffraction (XRD), X-ray Absorption Spectroscopy (XAS), vibrational spectroscopy (Infrared and Raman) and scanning electron microscopy (SEM). A Density Functional Theory (DFT) computation study was also performed to assign the characteristics frequencies in the vibrational spectra. This characterization of the oxalocalcic hydrates is essential to further characterize the transformation mechanism.

RESULTS AND DISCUSSION

Characterization of the Synthetized Species

Long-range order study: X-ray diffraction

In order to confirm the crystallographic phases of the samples, profile matching refinement^[12] of the diffraction patterns obtained was performed by starting with the structures reported in the literature for weddellite (COD) and whewellite (COM) determined from single crystal fragments extracted from kidney stones.^[13] COM/whewellite (monoclinic, $P2_1/c$), which correspond to a low temperature structure (COM-LT),^[14] has more reflections than COD/weddellite (tetragonal (bipyramidal), $I4/m$) since the space group

has less symmetry elements and, therefore, fewer equivalent reflections. Figure 1 shows the results obtained from the refinement of the synthetic COM (top) and the synthetic COD (bottom). The lattice parameters and the fitting results can be found in section 1 and 2 of the Supporting Information respectively. This confirms that the synthesized samples have the expected single phase structure (the secondary phase observed in the synthetic COM correspond to weddellite and it is less than 1%).

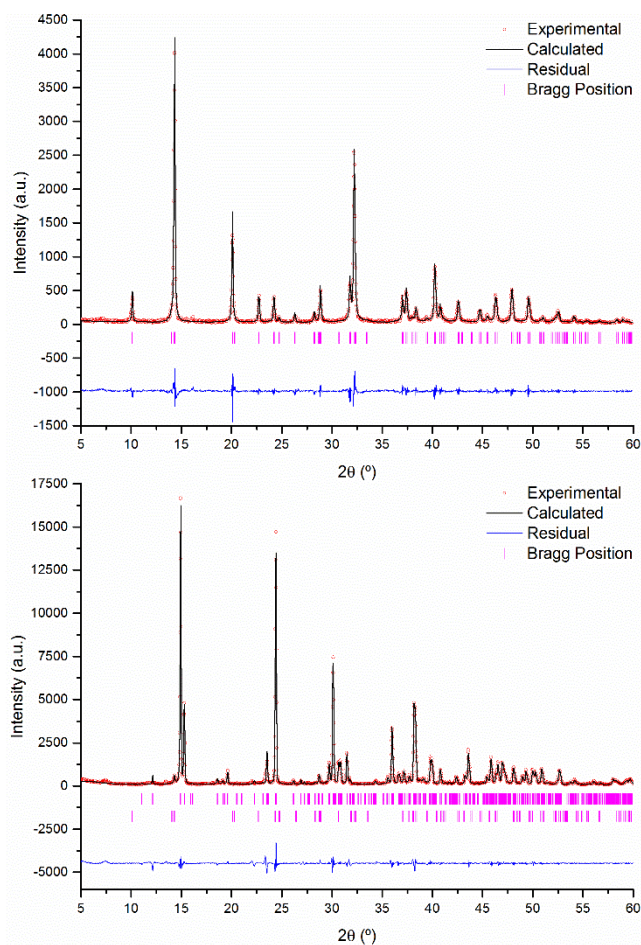


Figure 1. XRD patterns of the synthesized COM (top) and COD (bottom) after the profile matching.

Short-range order study: X-ray Absorption Spectroscopy

XAS measurements were performed to study the differences in the local coordination environment of calcium in the two calcium oxalate hydrates. As shown in top panel of Figure 2, subtle differences between the two hydrates, COD and COM, are observed in the normalized Ca K-edge X-ray absorption near edge structure (XANES) spectra. Since the XANES region of the spectra which is more sensitive to the chemical state and the stereochemical arrangement of the atoms

around Ca, these subtle differences can be attributed to the difference in bond angles of the oxalate molecules and the coordination geometry around Ca atom. On the other hand, as shown in the bottom panel of Figure 2, the EXAFS signal is rather complex, especially for COM, and it is not dominated by a single frequency contribution.

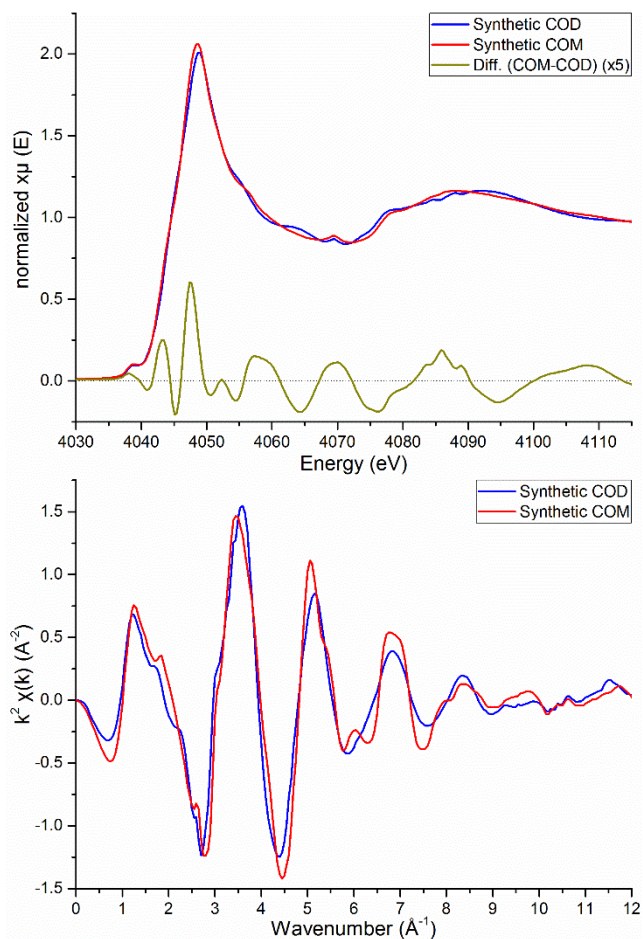


Figure 2. Normalized Ca K-edge XAS spectra with the difference (COM-COD) signal (amplified $\times 5$) to appreciate the differences between both phases (top) and k_2 -weighted EXAFS signal (bottom) of COD (blue) and COM (red).

The pseudo-radial distribution function obtained after performing the Fourier Transform (FT) of the EXAFS signal (Figure 3), suggests that, despite the spread of the Ca-O distances of the 8 nearest neighbor oxygen atoms around Ca and the two Ca sites in the case of the whewellite structure, Ca_1 and Ca_2 (see Tables in section 3 of the Support Information), both hydrates show a similar first coordination shell. The slightly decrease in amplitude of COD respect to COM can be attributed to the fact that, in weddellite, respect to whewellite, calcium is coordinated to one less oxalic

group and one more water molecule which may introduce some structural disorder in the first coordination sphere. The main changes are found in the second and further coordination spheres. In our case, COM shows a marked second sphere contribution around 3.5 \AA (not phase shift corrected) which is not that pronounced in COD which denotes a different in the local geometry around the Ca atom respect to COM. In order to better understand these differences and to confirm that the structures reported by Tazzoli et al. (1980), for Weddellite and Whewellite describe the short-range order details of COD and COM hydrates, respectively, the EXAFS data was modelled using those reported structures as the starting atomic model. It is worth mentioning that Whewellite structure has two different crystallographic sites for calcium, Ca_1 and Ca_2 , however, from the point of view of the scattering contributions considered for the EXAFS modelling, the most important contributions (according to ranking performed considering their spectral weight within the fitting range considered in k -space, $3\text{-}10.5 \text{ \AA}^{-1}$) are rather similar which allow us to simplify the modelling considering only one Ca site, Ca_1 . In addition, to avoid overparameterizing the fit due to the relative short k -range available for performing the EXAFS fitting, the distortion of Ca-O nearest neighbor polyhedron composing the first coordination sphere has been simply modelled by a single oxygen type and a single distance to account for the different Ca-O contributions (see more details in section 3 of the Support Information). In a similar fashion, for the COM sample, a single Ca-Ca contribution has been considered instead of the three different Ca-Ca distances which differ less than $\pm 0.05 \text{ \AA}$ among them.

Results from the fitting refinement of the EXAFS are reported in Table 1 and Figure 4. Even this simplified model allows getting a reasonably good fit of the experimental data. The mismatch at the extremes of the k -range considered for the refinement is due to the presence of weak artifacts at 2.7 , 3.7 and 10.3 \AA^{-1} which are attributed to three absorption edges corresponding to the multielectron excitations of the $\text{KM}_{\text{II,III}}$, KM_{I} , and $\text{KL}_{\text{II,III}}$ transitions, respectively.^[15] Hence, this confirms that COM and COD can be described also at short-range distances by the structures reported by Tazzoli et al. (1980). The fitting results suggests that the Ca-Ca contributions in COD are not as important as the ones in COM since the obtained mean-square displacement is much larger than in COD than in COM.

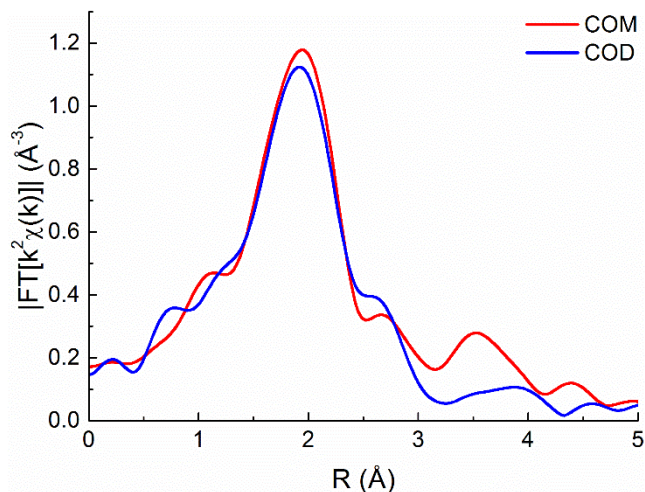


Figure 3. Pseudo-radial distribution function from the Fourier Transform (FT) of the EXAFS signal of COM (red) and COD (blue).

Vibrational study: Infrared and Raman Spectroscopy

In order to assign the vibrational bands, it is first necessary to understand the vibrations happening to the oxalate anion. Therefore, the symmetry of the different anion coordination was studied, from the free oxalate on solution to the three coordination symmetries of the calcium oxalate hydrates of the present work.

The symmetry group of the studied oxalates enables the understanding of the allowed vibrations in the infrared (IR) and Raman spectra. In solution, the oxalate ion has a D_{2d} symmetry group (dihedral), characterized by a vibration activity of $\Gamma=3A_1+B_1+2B_2+3E$, where only the modes $2B_2$ and $3E$ are IR active, while all of them are Raman active.^[16,17] It has been previously reported that, the most stable conformation for an isolated oxalate anion is a non-planar D_{2h} symmetry,^[18] which means that the twist of the C-C bond does not achieve the 90° , but it is not completely planar either. Furthermore, a study with different cations in solution demonstrated that the counter-ions interaction in solution increases as the cation size decreases.^[18-20]

According to Tazzoli et al. (1980), the crystalline structure of the dihydrated species contains equivalent

planar units of oxalate, while the monohydrated species contains one planar and other barely twisted (with a shorted C-C distance) oxalate. The oxalate ion coordination on both species,^[13] are shown in Figure 5. With this information, it can be elucidated that the “barely twisted” oxalate of COM corresponds to the non-planar D_{2h} point group (Figure 5c), which has been previously reported as planar by other authors.^[21,22] In this case, the irreducible representation of the vibrational activity will be $\Gamma=7A_g+3B_{1g}+3B_{2g}+5B_{3g}+3A_u+7B_{1u}+7B_{2u}+4B_{3u}$, being the gerade modes Raman actives and the ungerade modes IR actives. Moreover, the point group of the monohydrated species’ second oxalate corresponds to a planar C_{2h} (Figure 5b), with a vibrational activity $\Gamma=5A_g+B_g+2A_u+4B_u$ (gerade modes Raman actives and the ungerade modes IR actives).^[23] Due to the presence of a center of symmetry (inversion center) on the D_{2h} and C_{2h} point groups, both Raman and IR frequencies are exclusives.^[16] On the other hand, owing to the bidentate-like coordination of the oxalate ion on the COD species, the assigned point group is C_{2v} (Figure a), with a vibrational activity of $\Gamma=6A_1+2A_2+5B_1+2B_2$, being all the vibrational modes both Raman and IR active.^[16,17]

Table 1. Results from EXAFS fitting R-space (k -range from 3-10.6 \AA^{-1} and R -range in 1.3-4.5 \AA).

COM			
R-factor=0.008; $E_0(\text{eV})=0.4\pm 1.4$; $S_0^2=1.16\pm 0.18$			
shell	N	R (\AA)	$\sigma^2(\text{\AA}^2)$
Ca1-O	8	2.44 ± 0.01	0.014 ± 0.002
Ca1-C	4	3.22 ± 0.02	0.07 ± 0.08
Ca1-Ca	3	3.85 ± 0.02	0.012 ± 0.002
Ca1-C-O (forward triangle)	8	4.73 ± 0.12	0.032 ± 0.022
COD			
R-factor=0.010; $E_0(\text{eV})=-1.6\pm 1.3$; $S_0^2=0.98\pm 0.12$			
shell	N	R (\AA)	$\sigma^2(\text{\AA}^2)$
Ca-O	8	2.43 ± 0.01	0.014 ± 0.002
Ca-C	4	3.20 ± 0.04	0.014 ± 0.006
Ca-Ca	2	3.98 ± 0.02	0.04 ± 0.06
Ca-C-O (forward triangle)	8	4.56 ± 0.06	0.022 ± 0.014

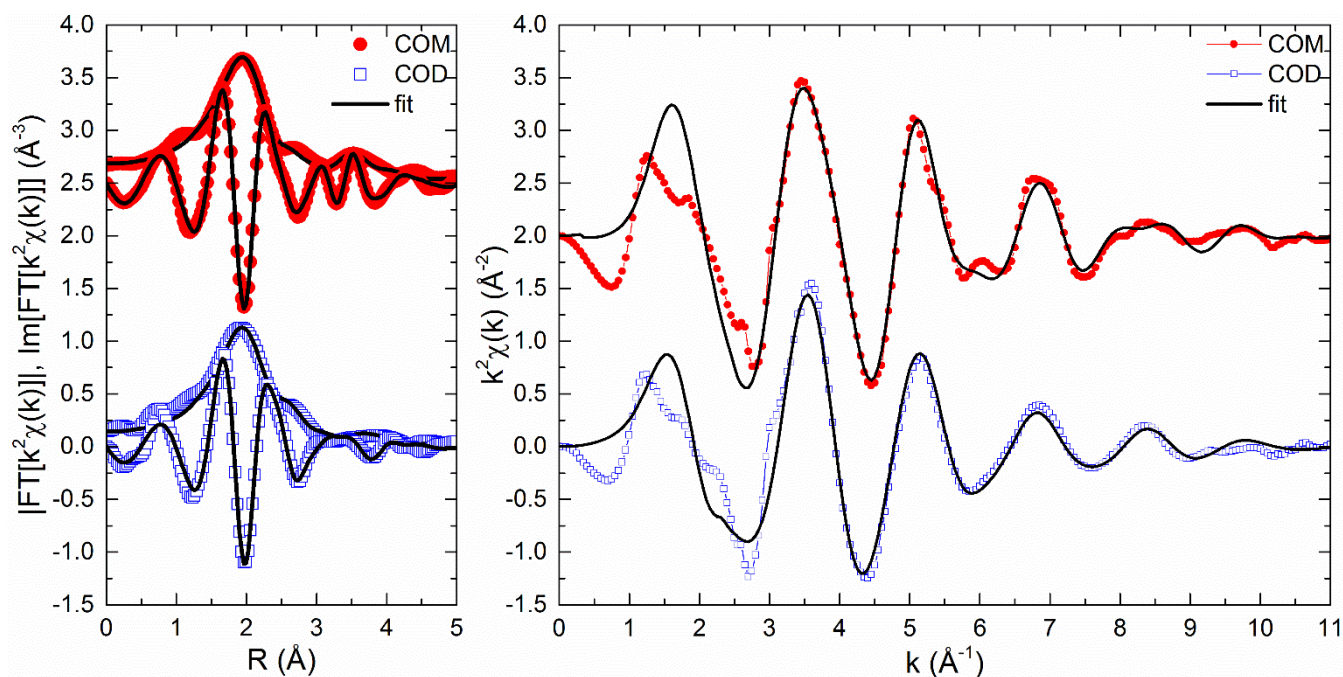


Figure 4. EXAFS signal fitting results of the Fourier transformation (Left panel) and corresponding to the Ca K-edge EXAFS signal (Right panel) collected on COM and COD samples. Black continuous line represents the best fit to the data. Results from the fits are included in Table 1. See text for details

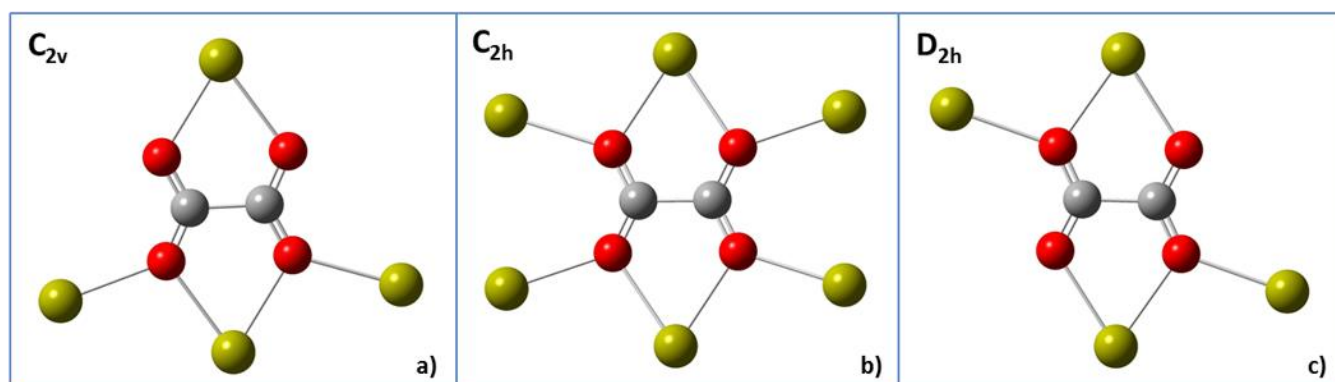


Figure 5. Schematic representation of the oxalate ion coordination with the correspondent symmetry group on: COD species a) C_{2v} ; and COM species b) C_{2h} and D_{2h} c).

This information has been considered in the DFT computational study performed for the vibrational frequencies assignment, as well as the results described in the previous sections (XRD and XAS) since it proves that the structures from Tazzoli et al. (1980) reproduce the results obtained from the long and short range structural characterization. A schematic representation and the coordinates of the clusters considered for the DFT calculations can be found in sections 4 and 5 of the Support Information. The IR and Raman spectra of the synthetic species are shown in Figure 6 where the

calculated frequencies are represented as vertical lines (calculated frequencies are listed in section 6 of the Supporting Information). It is necessary to notice that the differences between theoretical and the experimental frequencies could be caused by the lack of periodicity on the used cluster, since a small cluster was considered in order to understand the vibrations. The experimental bands with the corresponding assignment and a comparison with bibliographic data are showed in Table 2 (IR) and Table 3 (Raman).

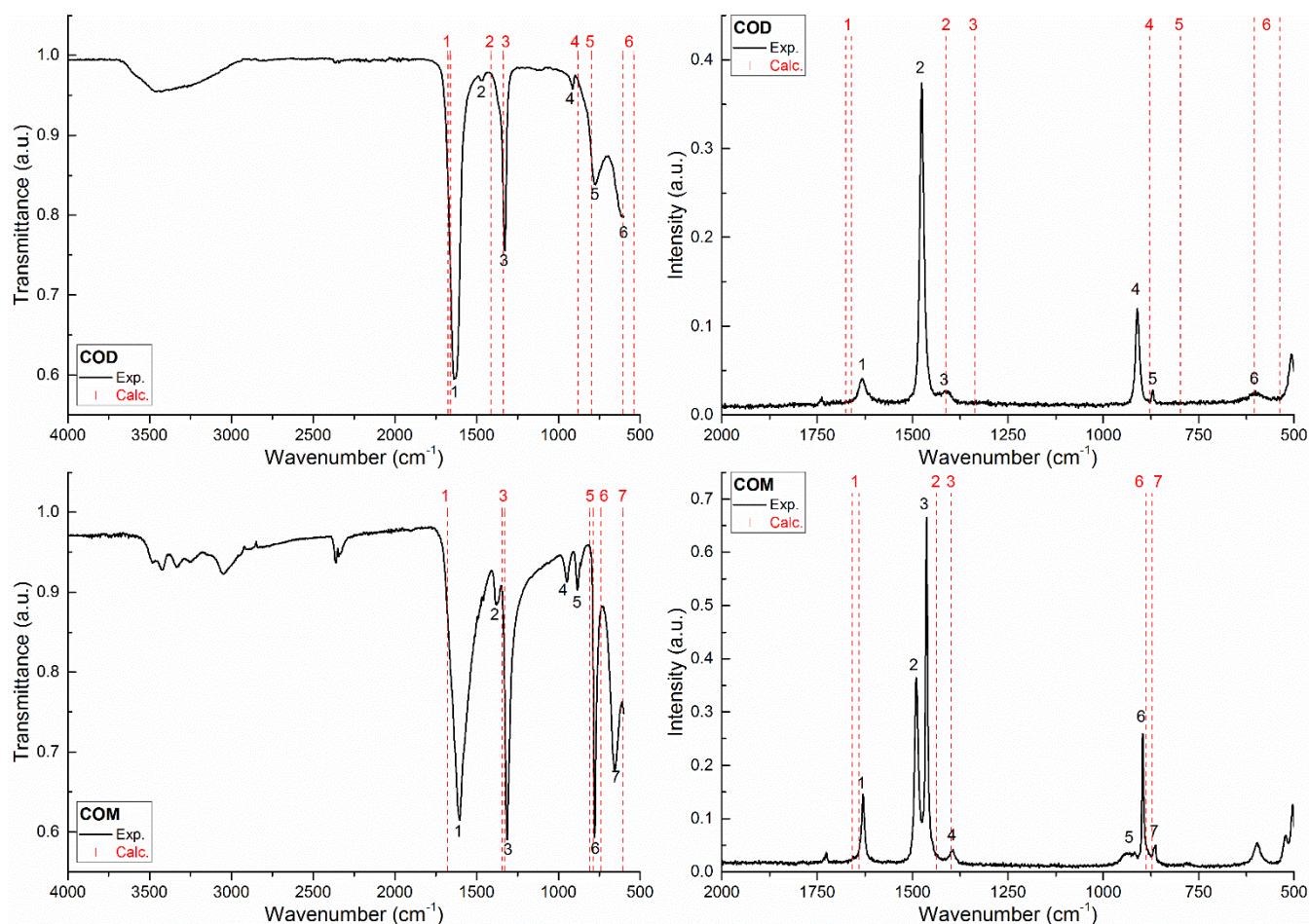


Figure 6. IR (left) and Raman (Right) of the synthesized COD (top) and COM (bottom). The vertical red dot lines correspond to the calculated frequencies, which are related with the experimental ones by numbers.

Assuming that COM had only the D_{2h} symmetry group, only one symmetric stretching (corresponding to the C-O) will occur due to the presence of four equivalent oxygen atoms. In the case of the other two coordination geometries, the symmetric and the antisymmetric stretching (both corresponding to the C-O) can occur. The differences in energy between the groups of symmetry allows the distinction of the bands in the IR spectra (frequencies displacement).^[20]

As it is well known, the water libration modes correspond to the external/rotational modes (twisting, wagging and rocking or a combination of them) of the molecule.^[24] On the case of the calcium oxalate species, only the monohydrated one has a band corresponding to this water libration mode (947.9 cm^{-1} on the Infrared and 918.6 cm^{-1} on the Raman). This effect can be justified as the structure of COM is more constrained, which restricts the water orientation. On the other hand, the

water molecules of COD have less restrictions (movement constrains) due to the zeolitic water channel of the structure, what entails more liberty to move.

The band from COM at 1380.9 cm^{-1} in the IR and 1394.5 cm^{-1} in Raman is not assigned on this work. This vibration does not appear on the computational simulation of the clusters. Considering the frequency of the vibration, it is most likely to be a contribution coming from a resonance coupling, as it is well described by Shippey et al. (1980) as a Dennison coupling band.^[21] The low frequencies do not correspond to the asymmetric stretching of the oxalates (which will be around 1600 cm^{-1}), while the symmetric stretching will be around 1300 cm^{-1} (higher frequencies if it is in combination with the C-C stretching, as it is shown on Raman).

Table 2. IR band assigned for COM (top) and COD (bottom).

Exp. Band (cm ⁻¹)	Present work	COM (IR)						
		Petrov and Šoptrajanov ²²	Christy <i>et al.</i> ⁸ Comi <i>et al.</i> ⁷	Ahmed <i>et al.</i> ²⁵	Guerra-López <i>et al.</i> ²⁶	Shippey ²¹	Kanchana <i>et al.</i> ²⁷	
3481.3		$\nu(\text{OH})$	$\nu(\text{OH})$	$\nu(\text{OH})$		$\nu(\text{OH})$		
3427.3		$\nu(\text{OH})$	$\nu(\text{OH})$	$\nu(\text{OH})$		$\nu(\text{OH})$		
3335.7	OH vibrations	$\nu(\text{OH})$	$\nu(\text{OH})$	Intermolecular hydrogen bonded	$\nu(\text{OH})$	$\nu(\text{OH})$	$\nu(\text{OH})$	$\nu(\text{OH}) + \nu(\text{OH})$
3254.7		2 $\delta(\text{HOH})$ in plane bending	2 $\delta(\text{HOH})$			2 $\delta(\text{HOH})$		
3050.2		$\nu(\text{OH})$	$\nu(\text{OH})$	$\nu(\text{OH})$		$\nu(\text{OH})$		
1604.7	$\nu(\text{C=O})$ (C _{2s})	$\nu(\text{Ox})$ antisym. stret.	$\nu(\text{C=O})$	Main $\nu(\text{C=O})$ indicating carboxylates	$\nu(\text{C-O})$ (B _{2g} mode)	$\nu(\nu(\text{C-O}))$ v ₂ ^a + v ₉	C=O vibration	
1380.9	--	$\nu(\text{Ox})$ antisym. stret.						
1313.4	$\nu(\text{C=O})$ (C _{2s}) $\nu(\text{C=O})$ (D _{2h})	$\nu_{\text{H}}(\text{Ox})$ sym. Stret.	$\nu(\text{C=O})$		$\nu(\text{OCCO})$ (B _{2g} mode by C _{2s} symmetry species)	$\nu(\nu(\text{C-O}))$	C-O vibration	
947.9	Water libration			$\nu(\text{C-H})$		R ₁ (H ₂ O)		
883.3	$\delta(\text{C=O})$ scissoring + $\nu(\text{M-O})$ (C _{2s}) $\delta(\text{C=O})$ scissoring + $\nu(\text{M-O})$ (D _{2h})	$\nu(\text{H}_2\text{O})$ Water libration	water libration	$\nu(\text{C-C})$ (presence of two carboxylates anions/existence of the oxalate group)	combination modes $\nu(\text{C-O}) + \delta(\text{O-C=O})$	R ₁ ^a (H ₂ O)	$\nu(\text{C-C})$	
778.2	$\delta(\text{C=O})$ wagging (D _{2h})	$\nu_2(\text{Ox})$ in-plane deformation		$\delta(\text{C-H})$	$\delta(\text{O-C=O}) + \nu(\text{M-O})$	$\nu_2(\delta(\text{O-C-O}))$	$\delta(\text{C-H})$	
656.7	$\delta(\text{C=O})$ rocking (C _{2s})	$\nu(\text{H}_2\text{O})$ Water libration			Water libration	R ₃ (H ₂ O)	$\delta(\text{O-H})$	
COD (IR)								
Exp. Band (cm ⁻¹)	Present work	Guerra-López <i>et al.</i> ²⁶	Frost ¹⁶					
3429.2	OH vibrations	$\nu(\text{OH})$	$\nu(\text{OH})$					
1637.4	$\nu(\text{C=O})$ $\nu(\text{OCC-C=O})$	$\nu(\text{C-O})$ (B _{2g} mode)	$\nu(\text{C=O})$					
1469.6	$\nu(\text{C-O}) + \nu(\text{C=O})$		$\nu(\text{C=O})$					
1328.8	$\nu(\text{C=O})$	$\nu(\text{OCCO})$ (B _{2g} mode by C _{2s} symmetry species)	$\nu(\text{C-O}) + \delta(\text{O-C=O})$					
912.3	$\nu(\text{C-C}) + \delta(\text{C=O})$ scissoring + $\nu(\text{M-O})$	combination modes $\nu(\text{C-O}) + \delta(\text{O-C=O})$	$\nu(\text{C-C}) + \delta(\text{O-C=O})$					
773.4	$\delta(\text{C=O})$ scissoring + $\nu(\text{M-O})$	$\delta(\text{O-C=O}) + \nu(\text{M-O})$	$\delta(\text{O-C=O}) + \nu(\text{M-O})$					
605.6	$\delta(\text{C=O})$ rocking	Water libration	water libration					

Nomenclature: Stretching (ν); asymmetric stretching (ν_a); symmetric stretching (ν_s); bending (δ); in-plane bending (δ_i); out-of-plane bending (δ_o)

Table 3. Raman band assigned for COM (top) and COD (bottom). Comparison with bibliographic data

COM (RAMAN)					
Exp. Band (cm ⁻¹)	Present work	Shippey ²¹	Edwards <i>et al.</i> ¹⁷	Kontoyanis <i>et al.</i> ²³	Carmona <i>et al.</i> ²⁹
1629.8	$\nu_a(\text{OOC-COO}) (\text{C}_{2h})$ $\nu_d(\text{COO}) (\text{D}_{2h})$	$\nu_{10}(\nu_d(\text{C-O}))$	$\nu(\text{CO})$	$\nu_d(\text{C-O})$	$\nu_d(\text{C-O})$
1490.4	$\nu(\text{C-C}) + \nu_d(\text{COO}) (\text{C}_{2h})$	$\nu_1(\nu_d(\text{C-O}))$	$\nu(\text{CO})$	$A_1(\nu_1) \rightarrow D_{2d}$	
1463.4	$\nu(\text{C-C}) + \nu_d(\text{COO}) (\text{D}_{2h})$	$\nu_{11}(\nu_d(\text{C-O}))$	$\nu(\text{CO})$	$\nu_d(\text{C-O})$	doublet: $\nu_d(\text{C-O})$
1394.5	---	$\nu_2^1 + \nu_1^1$			
918.6	Water libration	$R_1(\text{H}_2\text{O})$	$\nu(\text{CC})$	$A_1(\nu_3) \rightarrow C_{2v}$	
896.9	$\delta_s(\text{COO})$ scissoring (C_{2h})	$\nu_2(\nu(\text{C-C}))$	$\nu(\text{CC})$	$\nu(\text{C-C})$	$\nu(\text{C-C})$
863.2	$\nu(\text{C-C}) + \delta_s(\text{COO})$ scissoring (D_{2h})	$\nu_2^*(\nu(\text{C-C}))$	$\nu(\text{CC})$	$A_1(\nu_4) \rightarrow C_{2v}$	
COD (RAMAN)					
Exp. Band (cm ⁻¹)	Present work	Carmona <i>et al.</i> ²⁹			
1633.1	$\nu_d(\text{COO})$ $\nu_d(\text{OOC-COO})$	$\nu_d(\text{C-O})$			
1476.0	$\nu(\text{C-C}) + \nu_d(\text{COO})$	$\nu_d(\text{C-O})$			
1413.6	$\nu_d(\text{COO})$				
910.9	$\nu(\text{C-C}) + \delta_s(\text{COO})$ scissoring + $\nu(\text{M-O})$	$\nu(\text{C-C})$			
870.4	$\delta_s(\text{COO})$ scissoring + $\nu(\text{M-O})$				
600.9	$\delta_s(\text{COO})$ rocking				
Nomenclature: Stretching (ν); asymmetric stretching (ν_a); symmetric stretching (ν_s); bending (δ); in-plane bending (δ_i); out-of-plane bending (δ_o)					

Scanning Electron Microscopy

The SEM images were used to characterize the morphology and the size of the synthesized crystallites. As can be seen in Figure 7 (top), COM has relatively big and well-defined monoclinic shaped crystallites (around 1-10 μm).^[30] On the other hand, in Figure 7 (bottom), COD shows smaller crystallites (around 0.2-1 μm) with rather flat tetragonal bipyramids shape, as expected.

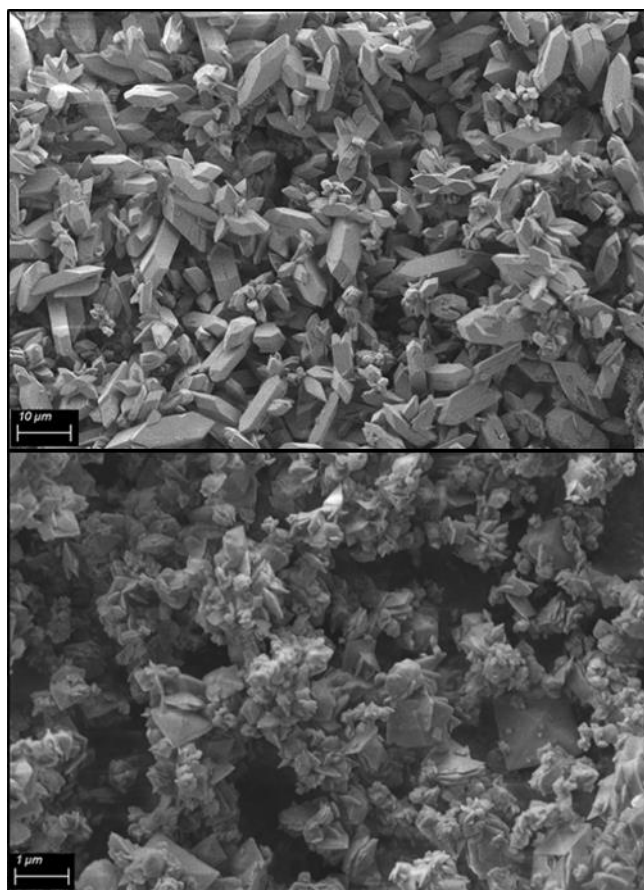


Figure 7. SEM images of synthetic COM (top) and COD (bottom). Notice the difference in the scale, 10 μm for COM and 1 μm for COD.

Calcium Oxalate Dihydrate Transformation to Monohydrate

Monitoring the transformation process by IR Spectroscopy

With the aim of monitoring the transformation process from dihydrated to monohydrated calcium oxalate, a Multivariate Curve Resolution (MCR) analysis of the IR spectra collected at different stages of the transformation was performed. The analysis was performed in the region from 1000 to 820 cm^{-1} where, as shown in Figure 6, the largest spectral differences between the two calcium oxalate species are found. The

spectrum from each step of the transformation can be seen on the section 7 of the Supporting Information. The information obtained with the MCR analysis can be divided in two parts: the first one is the Estimated Concentrations, Figure 8 (top), which shows the profile of each pure component through the sample (in this case, incubation time); the second one is the Estimated Spectra, Figure 8 (bottom), which is a simulation/estimation of each pure component spectrum (for the range included in the analysis).

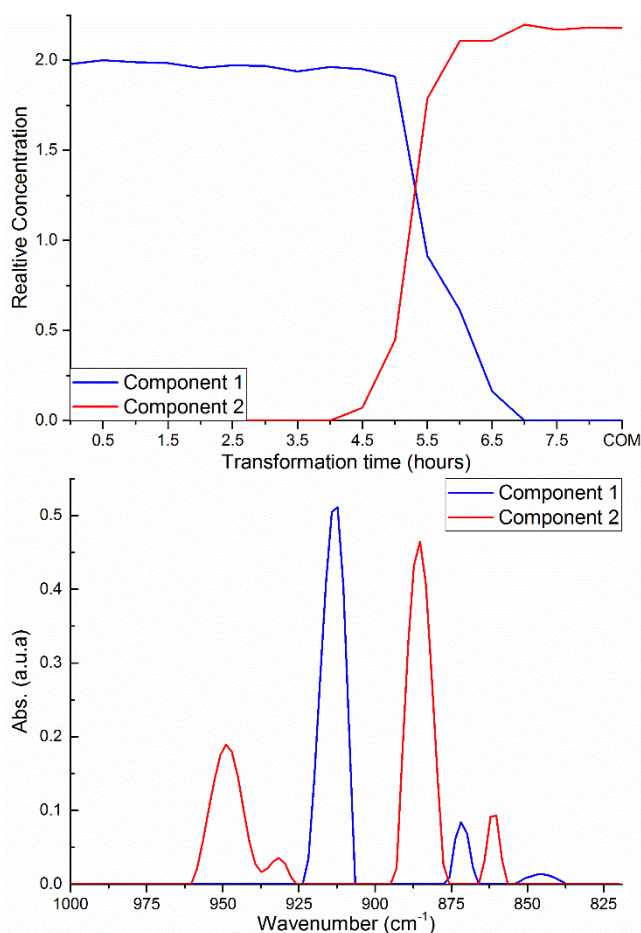


Figure 8. Component Concentration image (top) and Component Spectra (bottom), with Component 1 (blue) and Component 2 (red) characteristic of dihydrated and monohydrated species respectively, from the Multivariate Curve Resolution (MCR) analysis of the selected IR region (1000-820 cm^{-1}).

As can be observed in Figure 8, the peak corresponding to the $\nu(\text{C}-\text{C}) + \delta_i(\text{COO})$ scissoring + $\nu(\text{M}-\text{O})$ at 912.3 cm^{-1} , which is characteristic of COD (marked as Component 1), disappears during the transformation; while the peaks characteristics of COM at 883.3 cm^{-1} ($\delta_i(\text{COO})$ scissoring + $\nu(\text{M}-\text{O})$) and 947.9 cm^{-1} (water libration) appears (marked as Component 2). Around five hours of incubation on water, both components can

be observed; moreover, after six hours of transformation Component 2 dominates, making the transformed COD after this point (TRA) indistinguishable from COM by their IR spectra, since both are the same species. The half-time ($t_{1/2}$) transformation has been determined by non-linear (sigmoidal) fitting of the Component 1 (COD) from the Component Concentration of the MCR, being 5.59 ± 0.06 hours for the synthesized COD crystals in water.

X-ray diffraction characterization of the transformed calcium oxalate dihydrated

By comparing the diffractograms from the transformed weddellite at two different times with the synthetic COD and COM (Figure 9), it can be observed that, after five hours of incubation (half-transformed product), the main reflections of COM start to appear; its quantitative analysis revealed that it has 63% of weddellite and 37% of whewellite. After eight hours of incubation (a higher time than the one needed to achieve total transformation, as seen in the previous section) the diffractogram of the transformed weddellite is the same as the synthetic COM (as determined by the LeBail fitting), but with peaks less intense.

Scanning Electron Microscopy

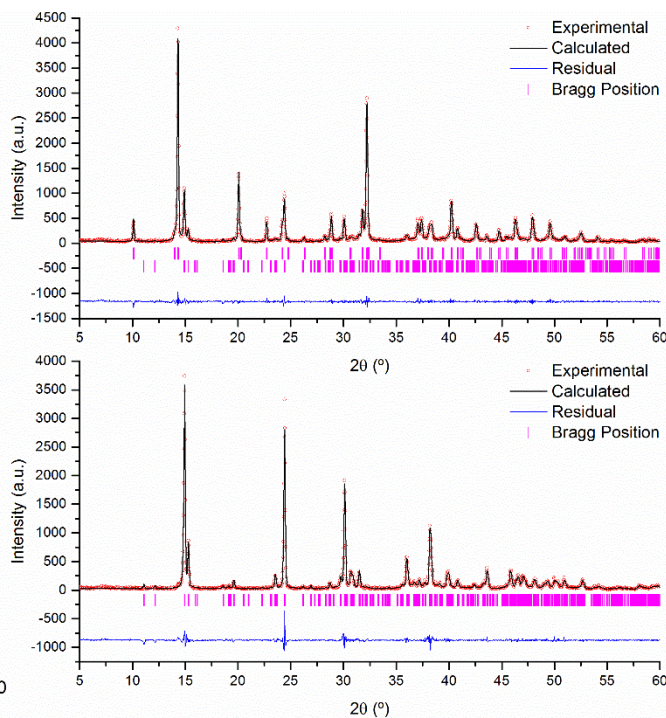
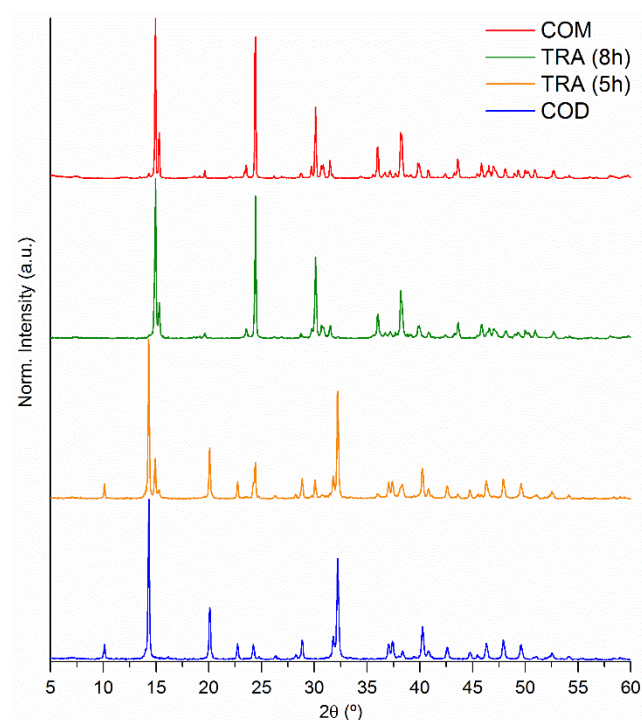


Figure 9. (Left panel) XRD patterns of TRA after 5 and 8 hours of incubation, compared with the synthetic COD and COM. (Right panel) Results of the profile matching of the TRA after 5 h (top) and after 8 h (bottom) of incubation.

SEM images of COD crystallites with different transformation degrees are shown in Figure 10. After two hours of incubation (Figure 10a), COD shaped crystallites are still present; when the incubation time is increased to five hours (Figure 10b), a mixture of COD crystallites (red arrows) and crystallites with COM/monoclinic like shapes (yellow arrows) can be appreciated. These results are consistent with the information obtained by IR and XRD analysis described on the previous sections, since the crystallites after 5 h transformation shows a mixture of well-defined phases (as described by the XRD fitting) and it is in a mid-transformation stage (as shown by the MCR analysis) with, in general, less well-defined crystallites. Finally, after eight hours of incubation (Figure 10c), COD shaped crystallites are not observed. If these transformed crystallites are compared with the synthetic COM (Figure 7 (Left panel)), it can be observed that the crystallites obtained after 8h of incubation are smaller and less defined than those of the synthetic COM. These differences are mainly related with the origin of the crystallites. It is important to consider that TRA comes from the transformation of COD, which crystallites are smaller (nanoscale) than the ones synthesized as COM (microscale).

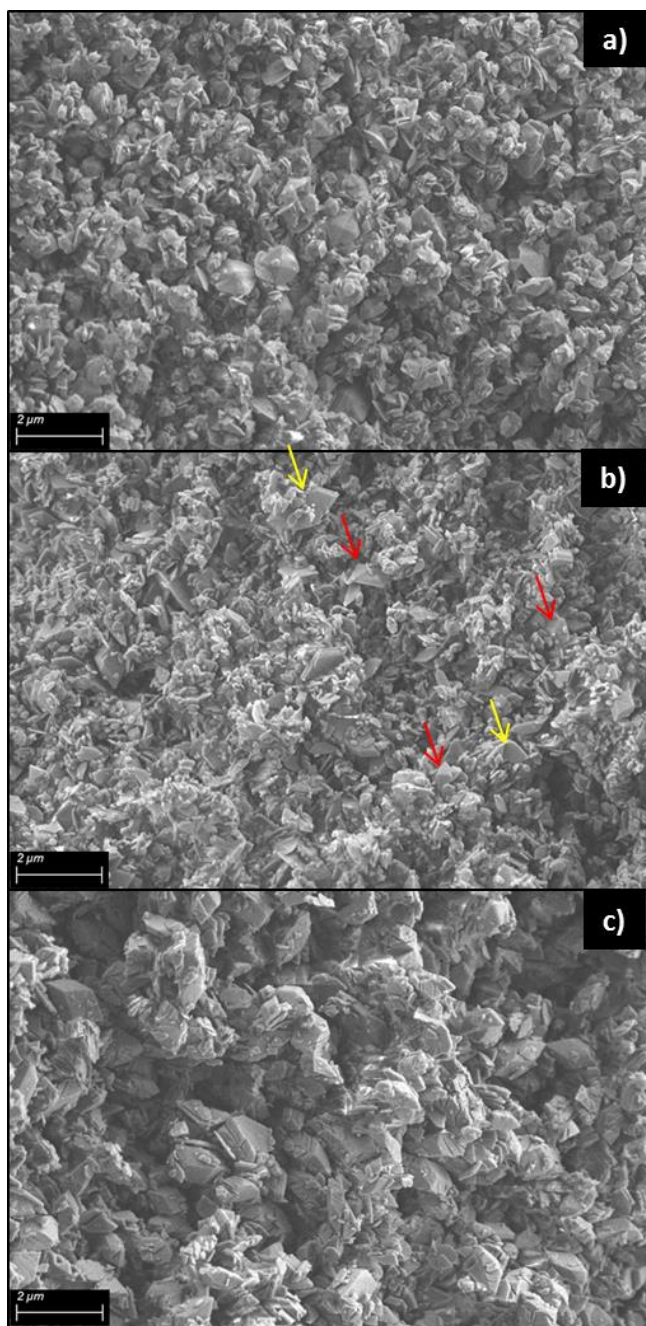


Figure 10. SEM images of COD crystallites transformation with 2 hours (a), 5 hours (b) and 8 hours (c) of incubation. Red arrows indicate COD shaped crystallites, while yellow arrows indicate COM shaped crystallites.

Characterization of the transformation process

1. The decomposition of the COD crystalline structure is produced by the alteration of the “zeolitic water” channel site occupancy, which promotes the structural rearrangement (closing the channel).^[5]
2. During the transformation (cell reorganization), the $\nu(\text{C-C})$ of the COD oxalate

is gradually restrained (associated with the symmetric $\delta_i(\text{COO})$ scissoring+ $\nu(\text{M-O})$), ending in an asymmetric scissoring of the calcium oxalate monohydrate $\delta_i(\text{COO}) + \nu(\text{M-O})$, corresponding to the more stable symmetries of the oxalate coordination (C_{2h} and D_{2h}). This behaviour can be observed on the MCR analysis performed to monitor the transformation (Figure 8), and it could explain the rearrangement of the structure to form a more stable calcium-oxalate coordination. In this step, we agree with Conti *et al.*^[5] in regards that the water molecules in the reconstructed cell comes from the medium. Hence, these steps describe the same process as Conti *et al.* studied, but from the point of view of the oxalates vibration instead of the OH ones, which provides complementary information and could help in future studies.

Taking into account the described transformation, it can be deduced that there are some aspects that could stabilize the COD structure, such as: larger crystal sizes; elements that “protects” the zeolitic channel, like organic matter or big ligands that interact with the 001 plane in order to avoid the zeolitic water exchange with the medium; elements that could interact with (stabilize) the 200 plane, like common calcium oxalate inhibitors present in the urine (citrate and phosphate among others). It is necessary a more extensive study to prove this hypothesis and to better understand the transformation mechanism and the possible stabilizing agents/properties

CONCLUSIONS

This work reports a synthesis of calcium oxalate hydrates to selectively obtain microcrystals of the two main oxalocalcic species (monohydrated and dihydrated). It has been shown that the long-range (XRD) and short-range (XAS) order characterization of the synthetic oxalocalcic species, COM and COD, agrees well with the structures reported for Whewellite and Weddellite respectively. These structures were used in the DFT computation study performed to fully understand the vibrational spectra (IR and Raman) of the two systems by assigning each characteristic band to the corresponding vibration and oxalate symmetries. With this approach, the assignments performed in the literature have been unified. In addition, SEM images show that COM have elongated crystallites (1-10 μm)

characteristic of monoclinic systems, whereas COD have rather flat tetragonal bipyramid crystallites (around 0.2-1 μm).

Moreover, the transformation process from the dihydrate to the monohydrate species in water has been studied. This process has been monitored by Infrared spectroscopy with the application of Multivariate Curve Resolution (MCR) analysis on the region between 1000-800 cm^{-1} . The analysis revealed that the half-time ($t_{1/2}$) transformation in water is 5.59 ± 0.06 hours for the 1-10 μm synthesized COD crystals. In addition, SEM images show a progressive change on the crystallites shape during the transformation process, reaching at the end a monoclinic structure but not as well defined as the synthetic COM and with a smaller crystallite size.

This study brings new information that will help on the understanding of the calcium oxalate dihydrate instability as well as the transformation process to the monohydrated species. Further studies will be necessary in order to differentiate the calcium oxalate monohydrate by its formation origin in real/complex samples, such as films from cultural heritage and kidney stones, and to determine the elements/properties participating in the COD stability, as well as their mechanisms.

EXPERIMENTAL SECTION

Reagents

: Di-sodium oxalate (Na_2Ox , Panreac, Spain, 99.5%), calcium chloride (CaCl_2 , Merck, Czech Republic, 98%), tri-sodium citrate dihydrate ($\text{Na}_3\text{Cit}\cdot 2\text{H}_2\text{O}$, Merck, Germany, 99%), tetra-sodium pyrophosphate decahydrate ($\text{Na}_4\text{Pyr}\cdot 10\text{H}_2\text{O}$, Panreac, Spain, 99%). Solutions were prepared with "ultrapure Type 1" water (Milli-Q, Millipore, 18.2 mS cm^{-1}).

Synthesis of Calcium Oxalate Monohydrate (COM)

The synthesis of COM described in the literature^[28,31] were adapted optimizing the following parameters: addition rate, pH, ageing time, temperature and volume of water in the crystallizer in order to obtain the monohydrated species, avoiding the co-precipitation of COD, and to achieve big and well defined crystallites. The final selected conditions were as follows: 250 mL of Na_2Ox 40 mM and 250 mL of CaCl_2 40 mM were adjusted to pH 6 (pH of human urine, the most common

medium of calcium oxalate precipitation^[32,33]). Both solutions were simultaneously added dropwise (2.5 mL/min) into a crystallizer containing Milli-Q water (1000 mL, degassed for 30 min by sonication), with the pH adjusted to 6 and at 75°C, under constant stirring. The obtained mother liquor was incubated at 37°C for five hours without stirring, and then vacuum filtered and washed with hot Milli-Q water (around 40-50°C). The obtained slurry was aged at 37°C for two days, obtaining a dry white powder.

Synthesis of Calcium Oxalate Dihydrate (COD)

This oxalocalcic species is the kinetically favorable, therefore it is required certain conditions to ensure that COM does not co-precipitate and that the species is stabilized (it does not transform onto the monohydrated one).^[34] To achieve this goal, tri-sodium citrate (Na_3Cit) and tetra-sodium pyrophosphate (Na_4Pyr) were used as inhibitors of the crystallization of calcium oxalate at normal conditions.^[35] The ratio between inhibitors was kept constant, following the method described by Yuzawa et al. (1998), being the optimized parameters: the crystallization temperature, the addition rate and the pH. For this synthesis, all the materials and solutions were cooled in an ice bath for 10 min previous use. Afterwards, 10 mL of CaCl_2 (40 mM, pH 6) were added dropwise (1.7 mL/min) into 30 mL of a solution containing Na_2Ox (13 mM), Na_3Cit (5 mM) and Na_4Pyr (0.2 mM), with constant stirring. The mixture was allowed to react during 5 min without stirring, subsequently centrifuged (10 min, 2000 rpm) and washed by resuspension and consecutive centrifuging two times more with cold water (5 mL) and one time with cold ethanol (5 mL). The sediment was vacuum dried using a 0.22 μm GVPP Millipore filter for one hour and stored in a sealed tube on a desiccator. Since the final product was washed and dried afterwards, there should not be any citrate or pyrophosphate present on the formed crystals, as it has been seen in the IR of the crystals (spectra not shown).

Characterization

An X-ray powder diffractometer X'Pert (XRD, Philips, Eindhoven, Netherlands) equipped with two goniometers and a copper tube was used to identify the oxalocalcic hydrates. The whole-patterns profile matching of the XRD data was performed using FULLPROF program (version 3.00 June 2015)^[12] In order to study the transformation between species (from COD

to TRA), the vibrational spectroscopy characterization was performed using an Infrared Spectrophotometer Tensor 27, equipped with an Attenuated Total Reflectance module (ATR-FTIR, Bruker, Ettlingen, Germany), with a resolution of 4 cm^{-1} ; and a Raman Spectrometer MultiRam with a Nd:YAG laser sample excitation source of 1064 nm (FT-Raman, Bruker, Ettlingen, Germany), with a resolution of 4 cm^{-1} . The analysis of the vibrational spectroscopy data was performed with the Unscrambler X[®] software. For the spectra comparison, a Savitzky-Golay second derivative was applied, followed by a Maximum Normalization in the different ranges of interest. The theoretical frequencies have been calculated via DFT with Gaussian software^[36], with the method WB97XD^[37] and basis set aug-cc-pVTZ^[38] for carbons and oxygens and Stuttgart relativistic pseudopotential ECP(18/2) basis set for calcium^[39]. The morphology of the crystals was studied by Field Emission-Scanning Electron Microscope MERLIN (FE-SEM, Zeiss, 1.4 nm resolution, 1 kV , 4 pA - 100 nA probe current, 0.2 - 30 kV accelerating voltage).

The X-ray Absorption Spectroscopy (XAS) was carried out at CLAEISS beamline^[40] from ALBA Synchrotron facility using a Si (111) monochromator operated in QXAFS mode. The monochromator was calibrated with a standard of tellurium and the maximum of the first derivative was set to 4341 eV ^[41]. The measurements were performed at the calcium K-edge in transmission mode using ionization chambers filled with 20% N₂ and 80% He for the I₀, and 98% N₂ and 2% Ar in the case of I₁, which implies an absorption of 16% and 75% of the beam, respectively. The beam size was set to $100 \times 200\ \mu\text{m}^2$ (vertical \times horizontal). For the data treatment, Athena and Artemis programs from the Demeter software package were used.^[42] Phase and amplitudes for all single scattering (SS) and multiple scattering (MS) paths were calculated by FEFF6 code.^[43] The $k^2\chi(k)$ EXAFS signals were Fourier transformed using a Hann window in the k range: 3 - $10.6\ \text{\AA}^{-1}$. The EXAFS fits were performed in R-space in the 1.3 - $4.3(4.5)\ \text{\AA}$ range for both oxalates. The number of independent points: $2\Delta k\Delta R/\pi \sim 14$. A single amplitude reduction factor, S_0^2 , and energy origin, E_0 , was considered for all the scattering paths included in each refinement.

Study of the Transformed Calcium Oxalate Dihydrated (TRA)

For the preparation of TRA, the starting point was the synthesized COD species. In order to follow up the

transformation process over time, tubes with 10 mg of COD and 2 mL of Milli-Q water were placed on an incubator at 37°C , the content of one tube was filtered every 30 minutes with a $0.22\ \mu\text{m}$ GVPP Millipore filter (Durapore membrane filter) and crystals were analyzed by ATR-FTIR, XRD and SEM. The experiment was carried out on a total time of eight hours.

AUTHOR INFORMATION

Corresponding author

*montserrat.lopez.mesas@uab.cat

Author contributions

The manuscript was written through contributions of all authors. / All authors have given approval to the final version of the manuscript.

ACKNOWLEDGEMENTS

The authors want to acknowledge the financial support from the *Ministerio de Economía y Competitividad* (Spanish Project CMT 2015-65414-C2-1-R). Iris H. Valido acknowledges funding support from the Universitat Autònoma de Barcelona (PIF-2016 grant). Ph.D. Roberto Boada acknowledges funding support from Marie Skłodowska-Curie grant agreement No 665919 of the European Union. The XAS experiments were performed at CLAEISS beamline at ALBA Synchrotron, under proposal 2015091387, with the collaboration of ALBA staff. All the authors are grateful to the *Serveis de Suport a la Investigació* of the UAB (SM, SDRX, SAQ) for the analysis. The authors thank Prof. Santiago MasPOCH and Ph.D. Diego A. Gómez for the Raman measurements and Prof. Vicenç Branchadell for the access to the cluster to perform the computational study.

REFERENCES

- (1) Walton, R. C.; Kavanagh, J. P.; Heywood, B. R.; Rao, P. N. Calcium Oxalates Grown in Human Urine under Different Batch Conditions. *J. Cryst. Growth* **2005**, *284* (3-4), 517-529.
- (2) Zhang, D.; Qi, L.; Ma, J.; Cheng, H. Morphological Control of Calcium Oxalate Dihydrate by a Double-Hydrophilic Block Copolymer. *Chem. Mater.* **2002**, *14* (6), 2450-2457.
- (3) Cousson, A.; André, G.; Matzen, G.; Chevallier, P.; Jungers, P.; Véron, E.; Daudon, M.; Bazin, D. Examination of Whewellite Kidney Stones by Scanning

- Electron Microscopy and Powder Neutron Diffraction Techniques. *J. Appl. Crystallogr.* **2009**, *42* (1), 109–115.
- (4) Poloni, L. N.; Ward, M. D. The Materials Science of Pathological Crystals. *Chem. Mater.* **2014**, *26* (1), 477–495.
- (5) Conti, C.; Brambilla, L.; Colombo, C.; Dellasega, D.; Gatta, G. D.; Realini, M.; Zerbi, G. Stability and Transformation Mechanism of Weddellite Nanocrystals Studied by X-Ray Diffraction and Infrared Spectroscopy. *Phys. Chem. Chem. Phys.* **2010**, *12* (43), 14560–14566.
- (6) Rampazzi, L. Calcium Oxalate Films on Works of Art: A Review. *J. Cult. Herit.* **2019**.
- (7) Conti, C.; Casati, M.; Colombo, C.; Realini, M.; Brambilla, L.; Zerbi, G. Phase Transformation of Calcium Oxalate Dihydrate-Monohydrate: Effects of Relative Humidity and New Spectroscopic Data. *Spectrochim. Acta - Part A Mol. Biomol. Spectrosc.* **2014**, *128*, 413–419.
- (8) Christy, A. A.; Nodland, E.; Burnham, A. K.; Kvalheim, O. M.; Dahl, B. Determination of Kinetic Parameters for the Dehydration of Calcium Oxalate Monohydrate by Diffuse Reflectance FT-IR Spectroscopy. *Appl. Spectrosc.* **1994**, *48* (5), 561–568.
- (9) Klopogge, J. T.; Boström, T. E.; Weier, M. L. In Situ Observation of the Thermal Decomposition of Weddellite by Heating Stage Environmental Scanning Electron Microscopy. *Am. Mineral.* **2004**, *89* (1), 245–248.
- (10) Frost, R. L.; Weier, M. L. Thermal Treatment of Whewellite—a Thermal Analysis and Raman Spectroscopic Study. *Thermochim. Acta* **2004**, *409* (1), 79–85.
- (11) Bazin, D.; Leroy, C.; Tielens, F.; Bonhomme, C.; Bonhomme-Courty, L.; Damay, F.; Le Denmat, D.; Sadoine, J.; Rode, J.; Frochot, V.; Letavernier, E.; Haymann, J. P.; Daudon, M. Hyperoxaluria Is Related to Whewellite and Hypercalciuria to Weddellite: What Happens When Crystalline Conversion Occurs? *Comptes Rendus Chim.* **2016**, *19* (11–12), 1492–1503.
- (12) Rodríguez-Carvajal, J. FULLPROF: A Program for Rietveld Refinement and Pattern Matching Analysis. *Abstr. Satell. Meet. Powder Diffr. XV Congr. IUCr*, **1990**.
- (13) Tazzoli, V.; Domeneghetti, C. The Crystal Structures of Whewellite and Weddellite: Re-Examination and Comparison. *Am. Mineral.* **1980**, *65* (Table 1), 27–334.
- (14) Izatulina, A. R.; Gurzhiy, V. V.; Krzhizhanovskaya, M. G.; Kuz'Mina, M. A.; Leoni, M.; Frank-Kamenetskaya, O. V. Hydrated Calcium Oxalates: Crystal Structures, Thermal Stability, and Phase Evolution. *Cryst. Growth Des.* **2018**, *18* (9), 5465–5478.
- (15) Fulton, J. L.; Heald, S. M. Understanding the Effects of Concentration on the Solvation Structure of Ca^{2+} in Aqueous Solution. I: The Perspective on Local Structure from EXAFS and XANES. **2003**, 4688–4696.
- (16) R.L., F. Raman and FTIR Spectroscopy of Natural Oxalates: Implications for the Evidence of Life on Mars. *Chinese Sci. Bull.* **2003**, *48* (17), 1844.
- (17) Edwards, H. G. M.; Farwell, D. W.; Seaward, M. R. D. Raman Spectra of Oxalates in Lichen Encrustations on Renaissance Frescoes. *Spectrochim. Acta Part A Mol. Spectrosc.* **1991**, *47* (11), 1531–1539.
- (18) Dean, P. A. W. The Oxalate Dianion, $\text{C}_2\text{O}_4^{2-}$: Planar or Nonplanar? *J. Chem. Educ.* **2012**, *89* (3), 417–418.
- (19) Hind, A. R.; Bhargava, S. K.; Van Bronswijk, W.; Grocott, S. C.; Eyer, S. L. On the Aqueous Vibrational Spectra of Alkali Metal Oxalates. *Appl. Spectrosc.* **1998**, *52* (5), 683–691.
- (20) Peterson, K. I.; Pullman, D. P. Determining the Structure of Oxalate Anion Using Infrared and Raman Spectroscopy Coupled with Gaussian Calculations. *J. Chem. Educ.* **2016**, *93* (6), 1130–1133.
- (21) Shippey, T. A. Vibrational Studies of Calcium Oxalate Monohydrate (Whewellite) and an Anhydrous Phase of Calcium Oxalate. *J. Mol. Struct.* **1980**, *63* (2), 157–166.
- (22) Petrov, I.; Šoptrajanov, B. Infrared Spectrum of Whewellite. *Spectrochim. Acta Part A Mol. Spectrosc.* **1975**, *31* (4), 309–316.
- (23) Duval, D.; Conurate, R. A. Temperature Dependence of the Raman Spectra of Calcium Oxalate Monohydrate. *Phys. Status Solidi* **1985**, *132* (1), 83–92.
- (24) Hirsch, A.; Azuri, I.; Addadi, L.; Weiner, S.; Yang, K.; Curtarolo, S.; Kronik, L. Infrared Absorption Spectrum of Brushite from First Principles. *Chem. Mater.* **2014**, *26* (9), 2934–2942.
- (25) Ahmed, S.; Hasan, M. M.; Alam, Z. Urolithiasis in Gel: An in Vitro Approach for Whewellite Growth

- Patterns to Evaluate Risk Factors and Management of Urinary Stones. *J. Pharmacogn. Phytochem.* **2017**, *6* (2), 87–91.
- (26) Guerra-López, J. R.; Güida, J. A.; Della Védova, C. O. Infrared and Raman Studies on Renal Stones: The Use of Second Derivative Infrared Spectra. *Urol. Res.* **2010**, *38* (5), 383–390.
- (27) Kanchana, G.; Sundaramoorthi, P.; Jeyanthi, G. P. Bio-Chemical Analysis and FTIR-Spectral Studies of Artificially Removed Renal Stone Mineral Constituents. *J. Miner. Mater. Charact. Eng.* **2009**, *8* (2), 161–170.
- (28) Kontoyannis, C. G.; Bouropoulos, N. C.; Koutsoukos, P. G. Raman Spectroscopy: A Tool for the Quantitative Analysis of Mineral Components of Solid Mixtures. The Case of Calcium Oxalate Monohydrate and Hydroxyapatite. *Vib. Spectrosc.* **1997**, *15* (1), 53–60.
- (29) Carmona, P.; Bellanato, J.; Escolar, E. Infrared and Raman Spectroscopy of Urinary Calculi: A Review. *Biospectroscopy* **1997**, *3* (5), 331–346.
- (30) Millan, A. Crystal Growth Shape of Whewellite Polymorphs: Influence of Structure Distortions on Crystal Shape. *Cryst. Growth Des.* **2001**, *1* (3), 245–254.
- (31) Walton, R. C.; Kavanagh, J. P.; Heywood, B. R. The Density and Protein Content of Calcium Oxalate Crystals Precipitated from Human Urine: A Tool to Investigate Ultrastructure and the Fractional Volume Occupied by Organic Matrix. *J. Struct. Biol.* **2003**, *143* (1), 14–23.
- (32) Pieras, E.; Costa-Bauzá, A.; Ramis, M.; Grases, F. Papillary and Nonpapillary Calcium Oxalate Monohydrate Renal Calculi: Comparative Study of Etiologic Factors. *ScientificWorldJournal.* **2006**, *6*, 2411–2419.
- (33) Manissorn, J.; Fong-Ngern, K.; Peerapen, P.; Thongboonkerd, V. Systematic Evaluation for Effects of Urine PH on Calcium Oxalate Crystallization, Crystal-Cell Adhesion and Internalization into Renal Tubular Cells. *Sci. Rep.* **2017**, *7* (1), 1–11.
- (34) Grases, F.; Millan, A.; Conte, A. Production of Calcium-Oxalate Monohydrate, Dihydrate Or Trihydrate - a Comparative-Study. *Urol. Res.* **1990**, *18* (1), 17–20.
- (35) Yuzawa, M.; Tozuka, K.; Tokue, A. Effect of Citrate and Pyrophosphate on the Stability of Calcium Oxalate Dihydrate. *Urol. Res.* **1998**, *26* (2), 83–88.
- (36) Frisch, M. J.; Trucks, G. W.; Schlegel, H. B.; Scuseria, G. E.; Robb, M. A.; Cheeseman, J. R.; Scalmani, G.; Barone, V.; Mennucci, B.; Petersson, G. A.; Nakatsuji, H.; Caricato, M.; Li, X.; Hratchian, H. P.; Izmaylov, A. F.; Bloino, J.; Zheng, G.; So, D. J. Gaussian 09 Revision D . 01 Release Notes. *Gaussian, Inc., Wallingford CT.* **2013**, No. June, 1–13.
- (37) Chai, J. Da; Head-Gordon, M. Long-Range Corrected Hybrid Density Functionals with Damped Atom-Atom Dispersion Corrections. *Phys. Chem. Chem. Phys.* **2008**, *10* (44), 6615–6620.
- (38) Kendall, R. A.; Dunning, T. H.; Harrison, R. J. Electron Affinities of the First-Row Atoms Revisited. Systematic Basis Sets and Wave Functions. *J. Chem. Phys.* **1992**, *96* (9), 6796–6806.
- (39) Fuentealba, P.; Von Szentpaly, L.; Preuss, H.; Stoll, H. Pseudopotential Calculations for Alkaline-Earth Atoms. *J. Phys. B At. Mol. Phys.* **1985**, *18* (7), 1287–1296.
- (40) Simonelli, L.; Marini, C.; Olszewski, W.; Ávila Pérez, M.; Ramanan, N.; Guilera, G.; Cuartero, V.; Klementiev, K. CLAESS: The Hard X-Ray Absorption Beamline of the ALBA CELLS Synchrotron. *Cogent Phys.* **2016**, *3* (1), 1–10.
- (41) Thompson, A. C.; Attwood, D. T.; Gullikson, E. M.; Howells, M. R.; Kortright, J. B.; Robinson, A. L.; Underwood, J. H.; Kim, K.-J.; Kirz, J.; Lindau, I.; Pianetta, P.; Winick, H.; Williams, G. P.; Scofield, J. H. X-Ray Data Booklet. *Berkeley Natl. Lab* **2001**, *8* (4), 1125.
- (42) Ravel, B.; Newville, M. ATHENA, ARTEMIS, HEPHAESTUS: Data Analysis for X-Ray Absorption Spectroscopy Using IFEFFIT. *J. Synchrotron Radiat.* **2005**, *12* (4), 537–541.
- (43) Zabinsky, S. I.; Rehr, J. J.; Ankudinov, A.; Albers, R. C.; Eller, M. J. Multiple-Scattering Calculations of x-Ray-Absorption Spectra. *Phys. Rev. B* **1995**, *52* (4), 2995–3009.

Support Information of the manuscript:
**“Characterization of calcium oxalate hydrates
and the transformation process”**

Authors: Iris H. Valido^a, Joaquim M^a Rius-Bartra^b, Roberto Boada^a, Montserrat Resina-Gallego^a, Manuel Valiente^a, Montserrat López-Mesas^{a*}

*^a Centre Grup de Tècniques de Separació en Química (GTS), Departament de Química,
Universitat Autònoma de Barcelona, Facultat de Ciències. Edifici CN. 08193, Bellaterra,
Barcelona, Spain*

*^b Departament de Química, Universitat Autònoma de Barcelona, Facultat de Ciències. Edifici
CN. 08193, Bellaterra, Barcelona, Spain
montserrat.lopez.mesas@uab.cat*

SI1: Structural parameters of the synthesized calcium oxalates reported in this work and those from the literature taken as reference.

	COD	COM	TRA (8h)	Weddellite*	Whewellite*
Space group	I4/m, No. 87	P2 ₁ /c, No. 14	P2 ₁ /c, No. 14	I4/m, No. 87	P2 ₁ /c, No. 14
a	12.3762	6.2944	6.2934	12.371	6.290
b	12.3762	14.5884	14.5832	12.371	14.583
c	7.3497	10.1189	10.1132	7.357	10.116
alpha	90	90	90	90	90
beta	90	109.458	109.445	90	109.46
gamma	90	90	90	90	90
Volume	1125.742	876.111	875.228	1125.927	874.904

(*) as reported by Tazzoli et al. 1980 ^[1]

SI2: XRD fitting results

COD	
	Weddellite
Bragg R-factor	1.20
Vol	1125.742 (0.063)
Rf-factor	0.976
ATZ	2081.665
Chi2	3.29
Overall scale factor	0.000011482
Zero-point	0.0570 (0.0010)
a	12.37616 (0.00043)
b	12.37616 (0.00043)
c	7.34966 (0.00021)
Preferred orientation (G1)	-1.03420 (0.00333)
Eta_0	1.84857 (0.03501)
U	0.00302 (0.00333)
V	0.00152 (0.00216)
W	0.00219 (0.00027)
X parameter	0.00360 (0.00102)
Asym1	-0.01915 (0.00342)
Asym2	-0.00186 (0.00151)

COM		
	Whewellite	Weddellite
Bragg R-factor	1.37	3.90
Vol	876.111 (0.105)	1121.112 (0.534)
Rf-factor	1.58	3.77
ATZ	1163.154	2081.665
Chi2	7.49	
Fract (%)	99.9	0.1
Overall scale factor	0.000410090	0.000000125
Zero-point	-0.0078 (0.0026)	
a	6.29441 (0.00048)	12.38221 (0.00282)
b	14.58842 (0.00100)	12.38221 (0.00282)
c	10.11894 (0.00064)	7.31228 (0.00257)
beta	109.45753 (0.00270)	
Preferred orientation (G1)	-1.79545 (0.00272)	-0.64829 (0.02623)
Eta_0	0.65057 (0.02960)	1.74891 (0.20320)
U	0.03648 (0.00739)	0.00413 (0.00000)
V	0.02902 (0.00163)	-0.00762 (0.00000)
W	0.00000 (0.00000)	0.00625 (0.00000)
X parameter	-0.01284 (0.00105)	-0.00750 (0.00829)
Asym1	0.03648 (0.00739)	-0.00107 (0.01871)
Asym2	0.02902 (0.00163)	0.00000 (0.00000)

TRA_5h		
	Weddellite	Whewellite
Bragg R-factor	0.804	2.57
Vol	1125.314	877.901
Rf-factor	1.22	3.80
ATZ	2081.665	1163.154
Chi2	1.74	
Fract (%)	62.6	37.4
Overall scale factor	0.000016307	0.000022385
Zero-point	0.0136 (0.003)	
a	12.37254 (0.00105)	6.30022 (0.00091)
b	12.37254 (0.00105)	14.59523 (0.00157)
c	7.35116 (0.00055)	10.12222 (0.00142)
beta		109.40423 (0.01593)
Preferred orientation (G1)	-4.64386 (0.00285)	-0.43210 (0.00714)
Eta_0	0.67918 (0.03154)	1.13679 (0.09525)
U	0.07028 (0.02595)	0.61050 (0.10036)
V	-0.00294 (0.01312)	-0.24766 (0.04646)
W	0.01659 (0.00151)	0.04409 (0.00535)
X parameter	-0.00824 (0.00109)	-0.03294 (0.00372)
Asym1	0.04822 (0.00605)	0.01286 (0.00828)
Asym2	0.01513 (0.00125)	0.00682 (0.00322)

TRA_8h	
	Whewellite
Bragg R-factor	
Vol	
Rf-factor	
ATZ	
Chi2	
Overall scale factor	0.000089208
Zero-point	0.0095 (0.0045)
a	6.29344 (0.00087)
b	14.58316 (0.00179)
c	10.11318 (0.00116)
beta	109.44503 (0.00606)
Preferred orientation (G1)	-1.26661 (0.00334)
Eta_0	0.71778 (0.04040)
U	0.37497 (0.04144)
V	-0.17379 (0.02026)
W	0.03942 (0.00246)
X parameter	-0.01159 (0.00152)
Asym1	0.02297 (0.00858)
Asym2	0.02496 (0.00180)

S13: Details of the EXAFS modelling for the different calcium environments:

The following tables detail the different Ca-O distances within the first coordination shell found in the structure as reported by Tazzoli et al. . For the EXAFS refinement analysis, a single Ca-O contribution with the appropriate degeneracy to account for all the oxygen neighbours has been considered to avoid over parametrizing the fit. The notation for the atoms follows the one used by Tazzoli in the CIF files.

- Whewellite:

Path	R (Å)
Ca1-OW2	2.397
Ca1-O6	2.428
Ca1-O1	2.433
Ca1-O4	2.436
Ca1-O5	2.446
Ca1-O4	2.450
Ca1-O3	2.461
Ca1-O7	2.479

Path	R (Å)
Ca-O2	2.420
Ca-O2	2.423
Ca-O7	2.426
Ca-O8	2.433
Ca-O3	2.439
Ca-O6	2.448
Ca-O1	2.453
Ca-OW1	2.540

- Weddellite:

Path	R (Å)
Ca-OW1	2.391
Ca-O2 (x2)	2.446
Ca-OW2	2.453
Ca-O1 (x2)	2.461
Ca-O1 (x2)	2.501

S14: Images of the different cluster used in the frequency calculations.

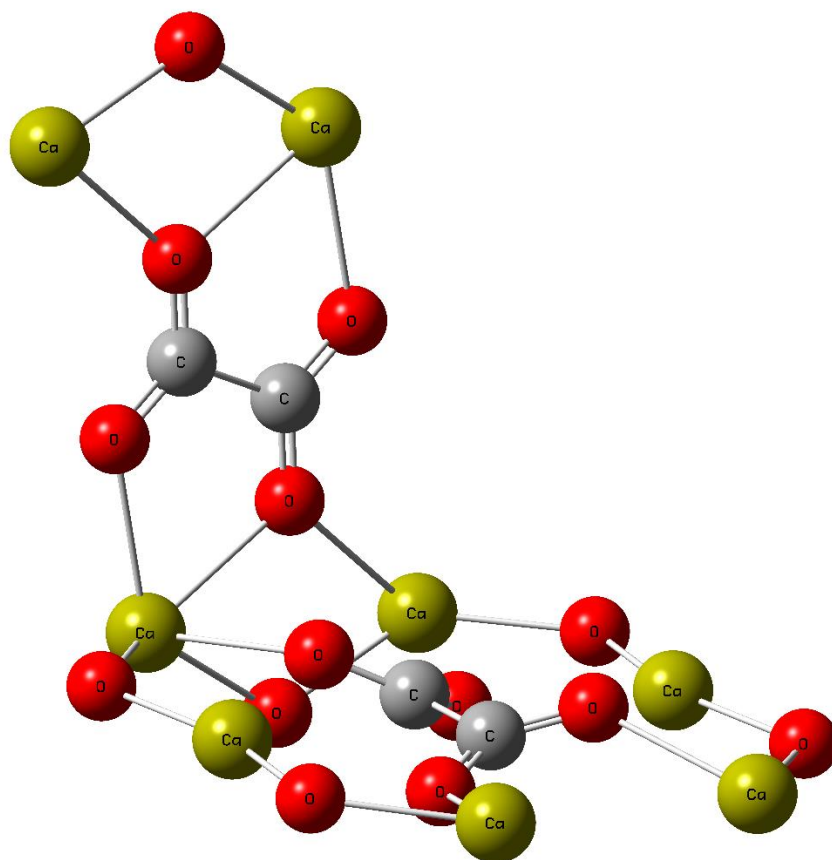


Figure 2: Cluster simulating COM structure with both type of oxalate, C_{2h} and D_{2h} .

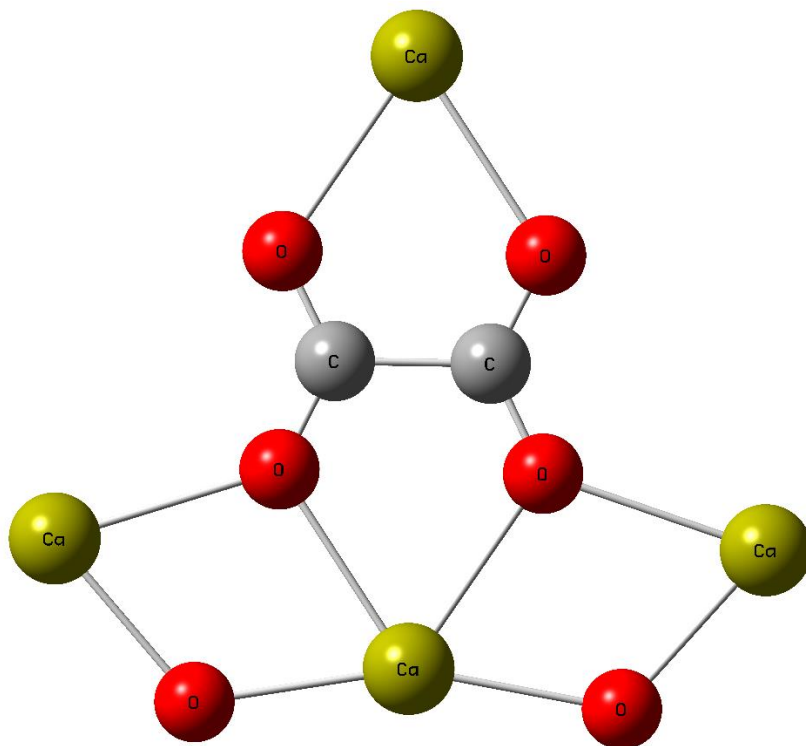


Figure 3: Cluster simulating COD structure (C_{2v}).

S15: Cartesian coordinates of the cluster structures

Table 1: Cartesian coordinates of the COM cluster structure

(A) COM structure	X	Y	Z
Ca	-1.250855	3.00756	-1.1437867
Ca	-4.4214016	3.0861408	1.1161895
O	-3.0622349	1.4667623	-0.2083495
O	-0.4502079	0.5888051	-0.9468447
Ca	-5.3177902	-0.4254678	2.1204625
C	-2.6339601	0.3318026	0.1222569
C	-1.3770988	-0.2295674	-0.7188244
O	-3.072504	-0.4159976	1.0329313
O	-1.4371711	-1.4350993	-1.0708719
Ca	-2.760204	-2.9053248	0.5472192
O	-4.5727497	-2.4900986	1.8009262
O	-2.8826843	4.1307443	-0.0925462
O	0.5616908	2.5923339	-2.3974936
O	-1.1283747	-4.0285091	-0.5040212
Ca	4.7442758	-1.3554956	2.2935752
O	3.0211534	-1.960851	0.6571653
O	4.2895067	0.4513879	0.6992728
Ca	0.3380824	-3.1215507	-1.7619733
C	2.6777116	-1.1362706	-0.2276897
C	3.4283634	0.2913691	-0.2027692
O	1.8165683	-1.2962894	-1.1297317
O	3.0849216	1.1159495	-1.0876243
Ca	1.3617992	0.5105941	-2.7240341
Ca	5.7679926	2.2766492	1.3315143
O	0.1307402	-1.3338841	-3.0585637
O	5.9753349	0.4889826	2.6281047

Table 2: Cartesian coordinates of the COD cluster structure

(B) COD structure	X	Y	Z
Ca	0	0	4.1086554
O	0	1.3628453	2.0700049
O	0	-1.3628453	2.0700049
Ca	0	3.6759584	-0.9379568
C	0	0.8065752	0.9424336
C	0	-0.8065752	0.9424336
O	0	1.3628453	-0.1851377
O	0	-1.3628453	-0.1851377
Ca	0	0	-2.2237882
Ca	0	-3.6759584	-0.9379568
O	0	2.2103851	-2.6028844
O	0	-2.2103851	-2.6028844

S16: Calculated frequencies at WB97XD/aug-cc-pvtz.

Table 3: Comparison of the calculated and experimental frequencies of IR (left) and Raman (right) bands of COM.

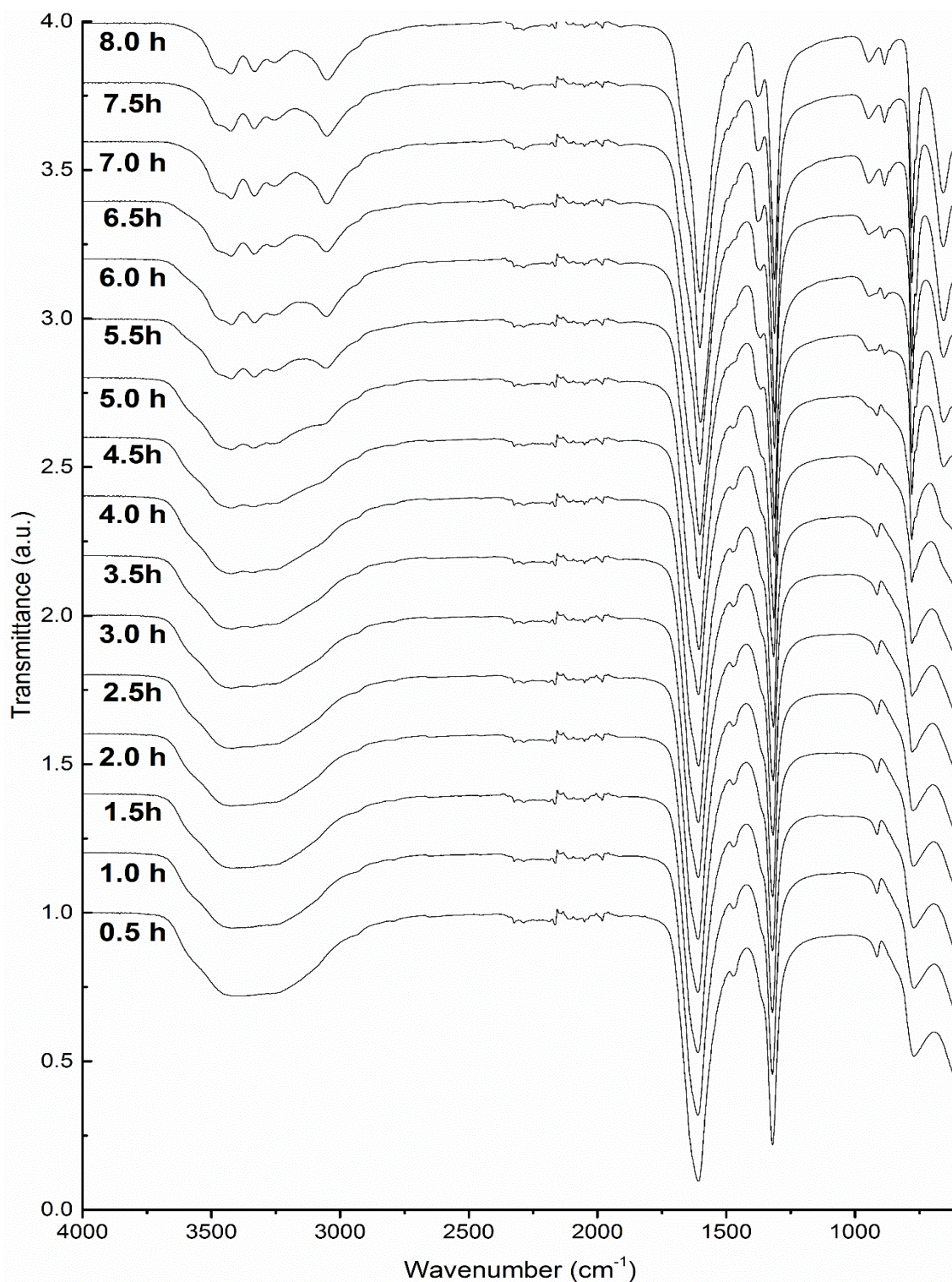
COM (IR)			COM (Raman)		
Exp. (cm ⁻¹)	Calc. (cm ⁻¹)	Assignment	Exp. (cm ⁻¹)	Calc. (cm ⁻¹)	Assignment
1604.7	1677.2	$\nu_a(\text{COO})$ (C _{2h})	1629.8	1657.9	$\nu_a(\text{OOC-COO})$ (C _{2h})
1380.9	--	--		1640.3	$\nu_a(\text{COO})$ (D _{2h})
1313.4	1343.1	$\nu_s(\text{COO})$ (C _{2h})	1490.4	1436.9	ν (C-C) + $\nu_s(\text{COO})$ (C _{2h})
	1330.4	$\nu_s(\text{COO})$ (D _{2h})	1463.4	1399.5	ν (C-C) + $\nu_s(\text{COO})$ (D _{2h})
947.9		Water libration	1394.5	--	--
883.3	808.8	$\delta_i(\text{COO})$ scissoring + $\nu(\text{M-O})$ (C _{2h})	918.6		Water libration
	785.9	$\delta_i(\text{COO})$ scissoring + $\nu(\text{M-O})$ (D _{2h})	896.9	888.1	$\delta_i(\text{COO})$ scissoring (C _{2h})
778.2	604.7	$\delta_o(\text{COO})$ wagging (D _{2h})	863.2	872.8	$\nu(\text{C-C})$ + $\delta_i(\text{COO})$ scissoring (D _{2h})
656.7	549.1	$\delta_i(\text{COO})$ rocking (C _{2h})			

Table 4: Comparison of the calculated and experimental frequencies of IR (left) and Raman (right) bands of COD

COD (IR)			COD (Raman)		
Exp. (cm ⁻¹)	Calc. (cm ⁻¹)	Assignment	Exp. (cm ⁻¹)	Calc. (cm ⁻¹)	Assignment
1637.4	1675.9	$\nu_a(\text{COO})$	1633.1	1675.0	$\nu_a(\text{COO})$
	1659.8	$\nu_a(\text{OOC-COO})$		1659.8	$\nu_a(\text{OOC-COO})$
1469.6	1412.8	$\nu(\text{C-C})$ + $\nu_s(\text{COO})$	1476.0	1412.8	ν (C-C) + $\nu_s(\text{COO})$
1328.8	1337.0	$\nu_s(\text{COO})$	1413.6	1337.0	$\nu_s(\text{COO})$
912.3	878.3	$\nu(\text{C-C})$ + $\delta_i(\text{COO})$ scissoring+ $\nu(\text{M-O})$	910.9	878.7	$\nu(\text{C-C})$ + $\delta_i(\text{COO})$ scissoring + $\nu(\text{M-O})$
773.4	797.7	$\delta_i(\text{COO})$ scissoring + $\nu(\text{M-O})$	870.0	797.7	$\delta_i(\text{COO})$ scissoring + $\nu(\text{M-O})$
605.6	604.7	$\delta_i(\text{COO})$ rocking	600.9	604.7	$\delta_i(\text{COO})$ rocking

S17: IR spectra from each step of the transformation

The Figure shows the IR spectra of synthesized COD with different transformation times (from 0.5 to 8 hours). As can be observed, the major changes are in the OH vibration regions, where the single broad band of the dihydrated calcium oxalate, becomes the 5 peaks of the monohydrated species. On the other hand, the peak corresponding to the $\nu(\text{C-C}) + \delta(\text{COO})$ scissoring+ $\nu(\text{M-O})$ at 912.3 cm^{-1} , which is characteristic of COD, disappears during the transformation; while the peaks characteristics of COM at 883.3 cm^{-1} ($\delta(\text{COO})$ scissoring + $\nu(\text{M-O})$) and 947.9 cm^{-1} (water libration) appears.



Calcium oxalate kidney stones, where is the organic matter?: A synchrotron based infrared microspectroscopy study

Iris H. Valido^a, Montserrat Resina-Gallego^a, Ibraheem Yousef^b, Maria Pilar Luque-Gálvez^c, Manuel Valiente^a, and Montserrat López-Mesas^{a*}

^a Centre Grup de Tecniques de Separacio en Quimica (GTS), Departament de Quimica, Universitat Autònoma de Barcelona, Facultat de Ciències, Edifici CN. 08193, Bellaterra, Barcelona, Spain

^b MIRAS beamline BLO1, ALBA-CELLS Synchrotron, Cerdanyola del Vallès, Spain.

^c Urology Department, Hospital Clínic Barcelona, Barcelona, Spain

**Montserrat.lopez.mesas*

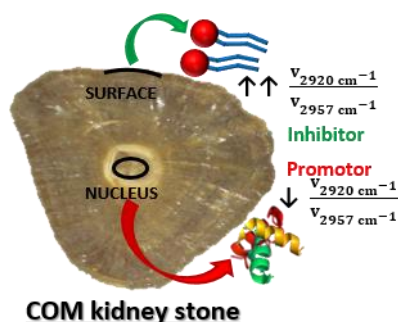
Journal: Journal of Biophotonics

doi.org/10.1002/jbio.202000303

Manuscript accepted: 03 September 2020

Version of Record online: 18 September 2020

Reproduced with permission from Journal of Biophotonics. Copyright © 1990-2020 John Wiley & Sons



Calcium oxalate kidney stones, where is the organic matter?: A synchrotron based infrared microspectroscopy study

Iris H. Valido^a, Montserrat Resina-Gallego^a, Ibraheem Yousef^b, Maria Pilar Luque-Gálvez^c, Manuel Valiente^a, Montserrat López-Mesas^{a*}

^a Centre Grup de Tècniques de Separació en Química (GTS), Departament de Química, Universitat Autònoma de Barcelona, Facultat de Ciències, Edifici CN, 08193, Belaterra, Spain.

^b MIRAS beamline BLo1, ALBA-CELLS Synchrotron, Carrer de la Llum 2-26, 08290, Cerdanyola del Vallès, Spain.

^c Urology Department, Hospital Clinic Barcelona, Calle Villarroel 170, 08036, Barcelona, Spain.

KEYWORDS: kidney stones; nephrolithiasis; synchrotron FTIR microspectroscopy; calcium oxalate stones; organic matter

ABSTRACT: Kidney stones are collections of microcrystals formed inside the kidneys, which affect 6-12% of the population worldwide, with an increasing recurrence (50-72%) after the first episode. The most abundant type is calcium oxalate (66%), described as monohydrated (COM) and dihydrated (COD). An issue in their chemistry is the transformation process of the metastable specie (COD) into the stable one, which is chemically, and in appearance, monohydrated. Since the origin of these species is different, it is important to differentiate between the transformation stage (and what stabilize COD) to understand the physiopathology and prevent the patients' recurrence. This work focuses on the organic matter distribution along these nephroliths, by Synchrotron Radiation-Based Infrared Microspectroscopy. Differences in the asymmetric stretching of the aliphatic hydrocarbons suggest that lipids may participate in the stabilization of COD and as inhibitors of COM formation/development; however, the presence of proteins in the nucleus could indicate a promoting role.

INTRODUCTION

Renal Nephrolithiasis is a clinical condition that implies the formation of microcrystals aggregates on the kidney. This disease affects approximately 6-12% of the population with a recurrence between 30-50% in the following five years from the first episode^{1,2}, being more than 72% after 20 years². Kidney stones are classified into seven major groups by morpho-constitutional analysis guidelines^{3,4}, where calcium oxalate stones, considering both the mono- (COM) and the dihydrated (COD) species, represents around 60-70% of the kidney stone population (most prevalent type)⁴⁻⁶. COD is the fastest species to be formed (kinetically favourable), but it is unstable in the medium, which induce a conversion into the stable monohydrated calcium oxalate (thermodynamically stable)^{7,8}. The stone resulting after this transformation (named TRA) has one water molecule being chemically COM, but its nucleation corresponds to a calcium oxalate dihydrated species,

COD⁹. It has been previously reported that the crystalline structure of TRA is the same as COM (monoclinic, $P2_1/c$)¹⁰, while other works report that it could indicate the presence of amorphous whewellite, which has been recently synthesized^{9,11}. The differentiation between COM (being formed as monohydrated) and TRA (coming from the transformation of COD), in any of the transformation stages, is of great importance since their origins are caused by different pathologies, for example, COD nephroliths are related to hypercalciuria, while COM ones are related to hyperoxaluria^{9,12,13}. Therefore, the study of this transformation process, as well as the stabilization of the dihydrated species, is very important to understand the physiopathology, to propose adequate treatment and, to prevent the patients' recurrence^{9,14,15}.

The matrix of kidney stones, including the oxalocalcic ones, is not only formed by crystalline

phases; there are also macromolecules (organic matter), such as proteins, lipids, carbohydrates and glycosaminoglycans¹⁶, as well as trace elements such as Zn and Sr ions¹⁷, incorporated into the crystals structures. The role of those molecules is not fully understood, since they can act as promoters or inhibitors of the renal calculi development by participating on any of the formation steps (nucleation, aggregation and/or growth)^{18,19}.

Due to the binding capacity of COM crystals to several urine/kidney proteins²⁰, it is possible to find a large number of these on COM stones, with a high relative abundance of inflammatory proteins²¹. This could be related with an oxidative stress process produced in the kidneys during the kidney stones formation and/or development^{22,23}, but further studies need to be carried out, specifically, the location of those inflammatory proteins.

The presence of organic matter (OM) into the nucleus has been previously observed by Synchrotron Radiation-Based Fourier Transform Infrared Microspectroscopy (SR- μ FTIR) of kidney stones in reflectance mode, where the characteristic band of the amide II (around 1500 cm^{-1}) was reported²⁴. In this work, a comparison of the organic matter composition of the surface and nucleus of COM stones was performed by SR- μ FTIR with the objective of understanding their distribution along the oxalocalcic nephroliths. Moreover, since kidney stones containing COD are commonly found (not only COM or the already transformed (TRA) COD), and the study of the stabilizing factors are of great importance in several research areas²⁵, the presence of OM on the COD crystallites, with and without transformation, was also studied.

EXPERIMENTAL

Preparation of calcium oxalate hydrate references

The process used to synthesize the calcium oxalate hydrates references, was previously developed in our research group¹⁰.

Sample preparation

Fourteen kidney stones were collected from the research group nephrolithiasis library. The studied samples were previously classified by morpho-

constitutional analysis^{3,4} and chosen only those belonging to the three main groups: COD, COM and TRA (examples can be found on Figure 1).

For the SR- μ FTIR spectroscopy study in reflectance mode, 7 samples were embedded in EpoFix resin[®], cut and polished to have a flat surface; the measurements were performed in grids along the polished surface of the samples. For the transmission mode SR- μ FTIR spectroscopy study, crystals from different samples sections (7 samples) were selected and placed in a Diamond EX'Press II Cell (S. T. Japan-Europe GmbH) in order to be compressed in a measurable thickness in transmission; the measurements were performed in lines, grides or points depending on the crystallites size and zones of interest.

Synchrotron-based Fourier transform infrared microspectroscopy (μ FTIR) and Data Acquisition

μ FTIR coupled to synchrotron radiation (SR- μ FTIR) experiment in reflectance mode was performed at SMIS beamline at SOLEIL synchrotron (Saint-Aubin, France). The IR Continuum microscope was coupled to a 5700 Nicolet FTIR spectrometer (Thermo-Nicolet) with a Mercury-Cadmium-Telluride (MCT-A) detector, collecting in the Mid-IR range from 4000 to 600 cm^{-1} . The synchrotron IR light is focused on the sample using a 32x Schwarzschild objective (NA = 0.65) coupled to a 32x Schwarzschild condenser (for optical light illumination of the sample). The spectra were recorded using Omnic 8.0 software (Thermo Scientific) at a spectral resolution of 4 cm^{-1} , a 12x12 μm^2 aperture size and 128 co-added scans per spectrum to achieve a good S/N ratio. Background spectra were collected from a ZnSe slide. In some samples, due to the light scattering produced by the sample surface (presence of nano/micro crystals and the natural porosity of the sample), the aperture was opened to 25x25 μm^2 . In reflection mode, the high brilliance (concentration of photons) of the synchrotron light is important since the possibility of reflecting more photons from a rough surface will be much higher comparing with to the conventional source, and accordingly better spectral quality will be achieved.

SR- μ FTIR experiment in transmission mode was carried out at MIRAS beamline of ALBA synchrotron light source (Cerdanyola del Vallès, Spain) using a Hyperion 3000 Microscope coupled to a Vertex 70

spectrometer (Bruker, Germany) and equipped with a Mercury-Cadmium-Telluride (MCT) detector. The microscope is utilizing a 36x Schwarzschild objective (NA = 0.52) coupled to a 36x Schwarzschild condenser to focus the synchrotron IR light on the sample. The spectra were recorded using OPUS 7.5 software (Bruker, Germany) at a spectral resolution of 4 cm^{-1} , within a measuring range of 4000–600 cm^{-1} , a 10x10 μm^2 masking aperture size and a co-addition of 512 scans per spectrum to obtain a good S/N ratio. Background spectra were collected from a clear area of the Diamon EX'Press II Cell that does not contain a sample.

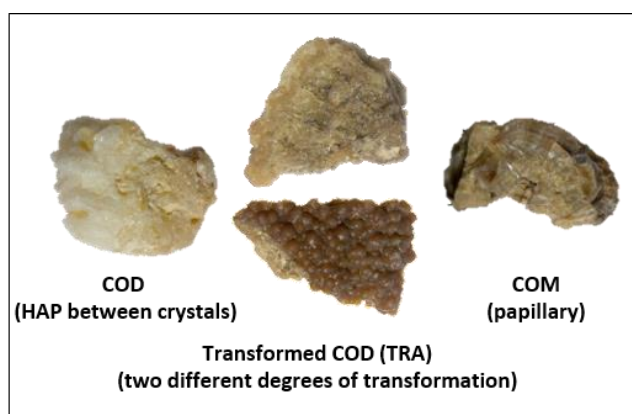


Figure 1. Examples of the CaOx stones selected by morpho-constitutional analysis for this study. In the left, COD (with HAP between crystals); in the middle, two TRA stones (COD stones with two different degrees of transformation); and in the right, a papillary COM stone.

The number of spectra collected from each sample will depend on the experiment (reflectance or transmission) as well as the sample itself, having a minimum of 100 points (taking into account that some spectra needed to be discarded due to the poor quality, problem mostly produced by the sample roughness and thickness in the reflectance and the transmission experiments respectively).

Fourier transform (FTIR) data analysis

To correct the optical dispersion of the spectra with specular reflection, in the reflectance mode SR- μ FTIR study, Kramer-Kronig (KK) correction²⁶ was applied in the range of 2000–730 cm^{-1} . Since the spectra presented both the specular and the diffuse reflection, KK correction cannot be directly applied²⁷; hence, Kubelka-Munk (KM) conversion²⁸ needs to be executed first in the same range.

For data processing, the Unscrambler X 10.3 software (CAMO Software, Oslo, Norway) was used. Savitsky-

Golay algorithm for second derivative (2D-SG), with a polynomial order of three and nine points smoothing filter, was applied to the spectra to eliminate the baseline contribution. Unit vector normalization was applied after the 2D-SG on the 1800–1190 cm^{-1} range for the calcium oxalate hydrates differentiation in the reflectance mode experiment, and on the 3000–2800 cm^{-1} for the organic matter differentiation in the transmittance mode experiment. Principal Component Analysis (PCA) was performed to the spectra in the selected ranges, using the Nonlinear Iterative Partial Least Square (NIPALS) algorithm on mean centred data, with the same software package. Note that, since the spectra were pre-processed using the second derivative algorithm, the relation between the PCA score plot and the loadings are inverted (positive scores correlates with negative loadings and vice versa). To study the significances of the differences observed in the PCA, a one-way analysis of variance (ANOVA) test was carried out with OriginLab software (OriginLab Corp., Northampton, MA, USA). The criterion for statistical significance for all comparison was $p < 0.05$.

RESULTS AND DISCUSSION

Calcium oxalate hydrates differentiation

To differentiate between calcium oxalate species, the measurements performed in reflectance mode with SR- μ FTIR of three different set of samples (COD, COM and TRA) were analysed by applying PCA (Figure 2). As can be observed in the scores distribution of the principal components PC-1 and PC-3 (Figure 2A), it is possible to differentiate between monohydrated and dihydrated species but it is difficult to distinguish between the two monohydrated components (COM and TRA). It is possible to observe differences between them (small shift to lower wavenumber in the case of TRA) as can be seen in the 2nd Derivative representation, of the averaged spectra, in Figure 3. However, as it is observed in the spectra of all the points represented (Figure 3), there is a high variability in each species individually. This high variability is also observed in the PCA analysis. For example, COM is evenly distributed through PC-1 and around 35% of the points characterized as COM overlaps with the ones characterized as TRA.

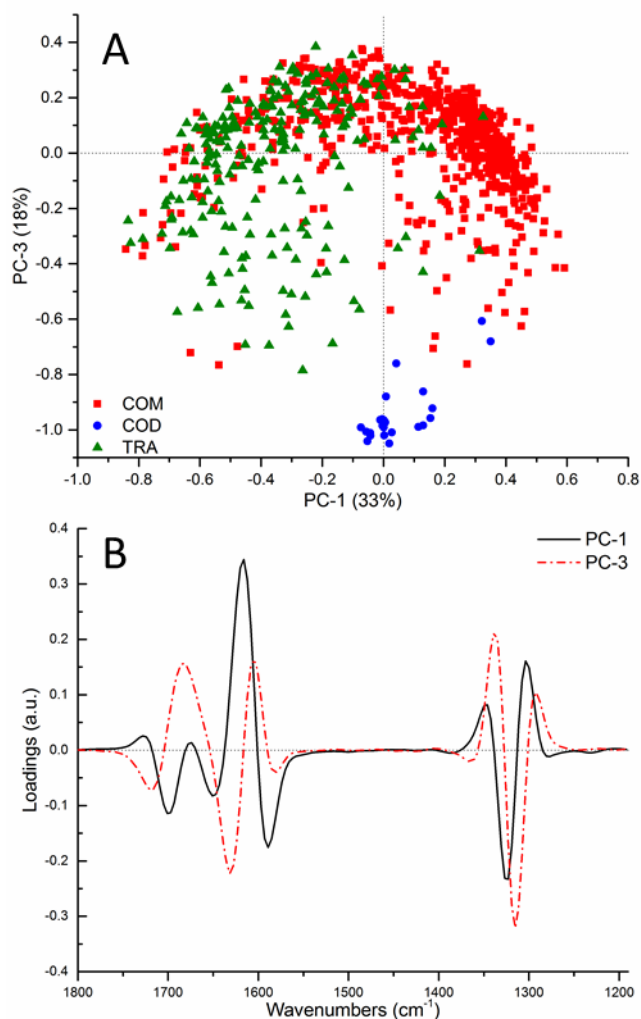


Figure 2. Principal Component Analysis (PCA) of the region between $1800\text{--}1190\text{ cm}^{-1}$ (unit vector normalization of the second derivative) corresponding to kidney stones samples previously classified as COM (red squares), COD (blue circles) and TRA (green triangles) by morpho-constitutional analysis: (A) scores graph and (B) PC-1 and PC-3 loadings of the PCA.

The loadings of PC-1 and PC-3 (Figure 2B) describe the major differences shown in the scores. COD samples are located in the PC-3 negative, which is represented with a higher contribution of the wavenumber 1338 cm^{-1} , while most of the monohydrated species (COM and TRA) are in the PC-3 positive, with a characteristic wavenumber of 1315 cm^{-1} , vibrations that correspond to the $\nu_s(\text{COO})$ of the COD and COM references respectively^{10,29}. Moreover, the presence of a high contribution of the wavenumber 1631 cm^{-1} for the PC-3 positive (Figure 3) can be attributed to the presence of the second peak observed in that region for the majority of the calcium oxalate monohydrated species (COM and TRA); however, the contribution of the wavenumbers

1605 and 1681 cm^{-1} for the PC-3 negative can be due to the high ratio variability of these two peaks, indicating a high presence/distribution of the monohydrated species in this score plot section. This has been proven by the results of the one-way ANOVA test of COM spectra, distributed along PC-3, which indicates significant differences in the population means, at the 0.05 level, for the peak ratio $1681/1605$ between the ones located in PC-3 positive, and the ones located in PC-3 negative. The PC-1 represents a higher variability on the 1616 cm^{-1} (PC-1 positive) and 1326 cm^{-1} (PC-1 negative), which correspond to the $\nu_a(\text{COO})$ and the $\nu_s(\text{COO})$ respectively^{10,29}. This effect is more related with these peaks ratio and shifts on the calcium oxalate monohydrate species observed on Figure 3 (as explained before). Furthermore, this effect has been also studied by one-way ANOVA test of COM and TRA spectra, distributed along PC-1. In the case of the comparison of COM and TRA from PC-1 negative, the population means are not significantly different, at the 0.05 level, for the position of the peak 1326 cm^{-1} as well as for the peak ratio $1616/1326$. However, when comparing COM from PC-1 positive vs. negative, these two factors are significantly different, proving the previous statement.

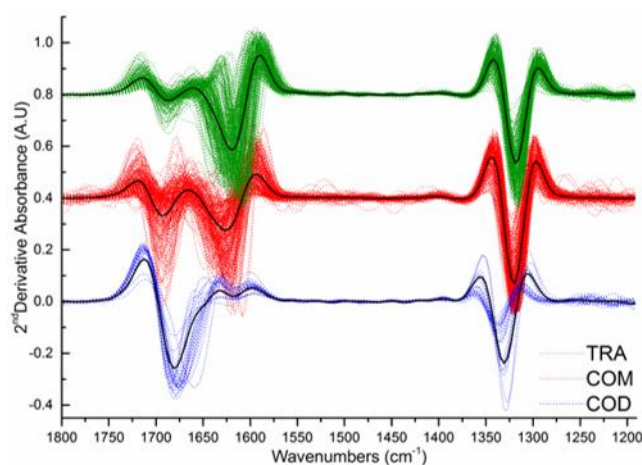


Figure 3. Second derivative spectra of the samples analysed in the PCA (Figure 2) on the region between 1800 and 1190 cm^{-1} . Groups are divided in COD (blue-bottom), COM (red-middle), and TRA (green-top) according to the sample classification by morpho-constitutional analysis. The black lines represent the average of each group.

Organic matter distribution

There are significant differences between proteins and lipids regarding their FTIR spectra³⁰. Both components concur in the asymmetric stretching of the aliphatic $-\text{CH}_3$ ($\sim 2957\text{ cm}^{-1}$) and $-\text{CH}_2$ ($\sim 2920\text{ cm}^{-1}$)^{31,32}, so

the intensity ratios between ν_{2920}/ν_{2957} ($-\text{CH}_2/-\text{CH}_3$) can be associated to the differences in structure between lipids and proteins. In this sense, the presence of long $-\text{CH}_2$ chains in lipids means a higher ν_{2920}/ν_{2957} , being the opposite for proteins. These differences have been used to identify lipid and proteins in the measurements performed in transmittance mode with SR- μFTIR .

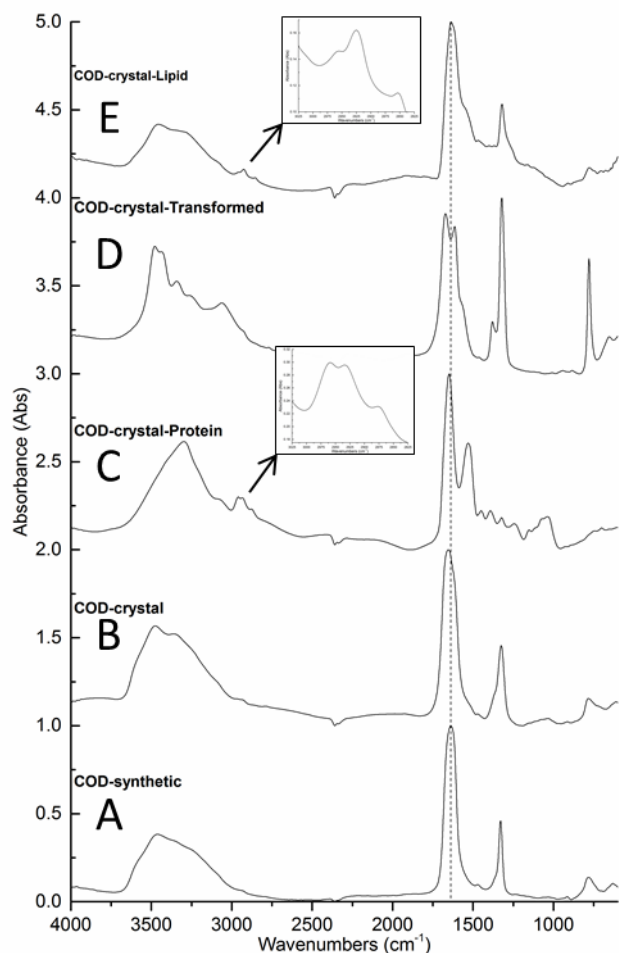


Figure 4. Examples of synchrotron FTIR spectra of synthetic COD (A), a typical crystal of COD (B), protein (C) and transformed COD (D) found in COD crystallites undergoing the transformation process, and of lipids (E) found on a non-transformed COD crystal

In the case of calcium oxalate dihydrate, twelve crystals from non-transformed COD kidney stones and from nephroliths undergoing the transformation process were studied. An example of the different spectra found is represented in Figure 4, alongside with the spectrum of a synthetic COD as a reference (Figure 4A). In the case of the transformation process, three different types of spectra were found: the typical COD (Figure 4B), the presence of proteins inside the analysed crystallites (Figure 4C) and the transformed calcium

oxalate (Figure 4D), which spectrum corresponds to calcium oxalate monohydrate. On the other hand, the organic matter spectra observed in the non-transformed COD crystallites is mostly represented by lipids (Figure 4E). The major differences between the proteins and lipids on the COD crystallites spectra in region of the asymmetric stretching of the aliphatic $-\text{CH}_2$ and $-\text{CH}_3$ can be found magnified, inside a frame, in Figure 4.

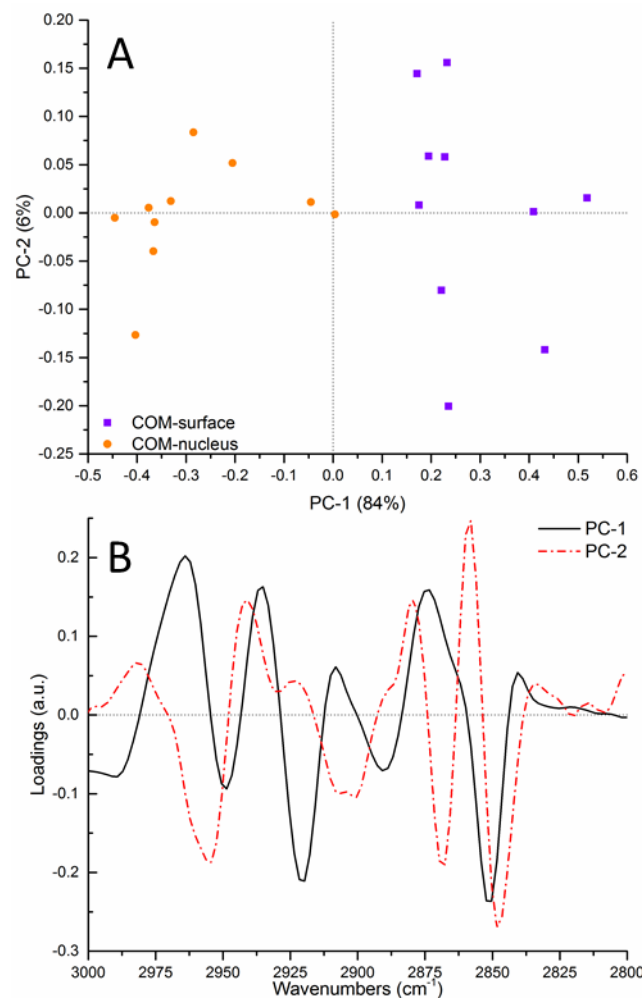


Figure 5. Principal Component Analysis (PCA) of the region between $3000\text{--}2800\text{ cm}^{-1}$ (unit vector normalization of the second derivative) corresponding to COM crystals selected from the nucleus (orange) and surface (purple) of a quiescent kidney stone: (A) scores graph and (B) PC-1 and PC-2 loadings of the PCA.

The distribution of organic matter throughout calcium oxalate monohydrate (COM) has been also studied. With this purpose, the spectra of crystals from the nucleus and the surface of quiescent COM kidney stones (without a white/grayish film on their surface)³ were analysed by PCA of the asymmetric $-\text{CH}_2$ and $-\text{CH}_3$ stretching region. The scores distributions and the

loadings (for PC-1 and PC-2) are shown in Figure 5A and Figure 5B respectively. Samples from the surface and from the nucleus are grouped by PC-1, where the negative region is represented by a high contribution in the ν_{2920} , and the positive region by a high contribution of the ν_{2957} , as it is shown by the loadings (inverse relation between scores and loadings as explained before). This behaviour explains the distribution of the OM in the samples since, as described before, lipids present an intense $-\text{CH}_2$ peak (higher ν_{2920}/ν_{2957}), while aliphatic chain of proteins have an intense $-\text{CH}_3$ with a $-\text{CH}_2$ of the same or lower intensity.

The results presented in this work are in agreement with the ones described in the literature, where proteins have been found in the nucleus of calcium oxalate kidney stones^{22,33}. However, other studies reveal that the same proteins can act as promoters or inhibitors of this type of stones, still existing a controversy in the subject⁸. For example, osteopontin (OPN) has been reported to act as a CaOx growth modulator by interacting with {100} faces of COM crystals, thus inhibiting their growth³⁴; however, similar studies show that OPN acts as a promotor of the formation and aggregation of CaOx crystals³⁵. With the results of this work, it is not possible to characterize the type of proteins found in the nucleus. However, it could be related with low-molecular-weight proteins (LMWP) that, as has been described elsewhere^{22,23}, could be also derived from an oxidative stress produced in the kidney during the formation process, which generates reactive oxygen species (ROS). Moreover, these ROS do not only generate LMWP, but also lipid peroxides²². The presence of the lipid peroxidation products have been found in stone former patients in high levels³⁶. Furthermore, it is common to find in the literature works that simulate in vitro the interaction between lipids and calcium oxalate crystals by using lipids monolayers^{37,38}, concluding that their role is as promoters of calcium oxalate nucleation. These kinds of studies tend to simulate the crystal nucleation on the epithelial cell surface, but they do not consider the behaviour of free lipids in urine, like fatty acids. The presence of lipids in the surface of COM stones found in this study, suggest that some types of lipids could participate in the renal calculi formation as an inhibitor. Taking into account that lipids have a strong binding capacity with calcium ions^{39,40}, it makes sense that they could interact with the calcium in the surface of the oxalocalcic stones, or with the free calcium in the urine, making it less available to

interact with the oxalate ions. Therefore, the oxidative stress in the kidney, described previously^{22,23}, could favour the calcium oxalate stone formation by two different means: the loss of an inhibitory potential (lipids breakdown), and the formation of promoters (products of the lipid peroxidation and the formation of LMWP).

CONCLUSIONS

This study has demonstrated the applicability of SR- μ FTIR to the in situ analysis of kidney stones components. By using the reflectance mode on three groups of samples (COM, COD and TRA) previously characterized by morpho-constitutional analysis, it was observed that mono- and dihydrated species can be differentiated; however, due to high variability on the calcium oxalate monohydrated spectra, the slight differences between the two components (COM and TRA) described in this work are not considered enough to distinguish between them with the used technique. Hence, further studies will be needed to determine the differences between COM and TRA, being able to characterize this type of kidney stones by their origin, which is of great importance, since both have different underlying causes related with their origins. Differentiating both types of lithiasis would help to propose different therapeutic approaches in order to treat the disease and prevent future recurrences.

On the case of the transmittance mode experiment, the distribution of the organic matter throughout calcium oxalate nephroliths was studied. A comparison between proteins and lipids was performed by analysing the asymmetric stretching of the aliphatic $-\text{CH}_2$ and $-\text{CH}_3$. In the case of COD, it was observed that lipids participate in the stabilization of the crystallites, while proteins have been found in crystals undergoing the transformation process. Knowing what promotes or inhibits the transformation of COD to the thermodynamically stable species could help to further relate the different transformation stages with the patients' pathologies or plan adjusted treatments. Regarding the formation of COM stones, lipids and proteins were found in the surface and nucleus of inactive stones respectively. These findings are in agreement with the hypothesis that the formation of kidney stones could be related with an oxidative stress process^{22,23}, in which LMWP and the products of lipid peroxidation could act as promoters of the calculi formation, while the inhibitory potential of the lipids

could come from the strong binding capacity with the calcium ions. This is the first time that lipidic macromolecules are proposed as inhibitors of the oxalocalcic kidney stone development and not as a promoter, since not all the lipids in the urine come from the cell membranes (phospholipids). With these findings, further studies could be performed in order to determine the type of lipids that can participate in the inhibition, such as fatty acids, and what type of proteins are located in the nucleus and can act as promoters, with the objective of developing new treatments for calcium oxalate stone formers to prevent, not only its formation, but its growth in the kidneys. Moreover, since these types of calcifications can be found in other organs, like breast, prostate or thyroid⁴¹, it could be interesting to follow a similar approach to understand the stability of COD and how it affects to the associated diseases on those organs^{42,43}.

AUTHOR INFORMATION

Corresponding Author

* montserrat.lopez.mesas@uab.cat

Author Contributions

The manuscript was written through contributions of all authors. / All authors have given approval to the final version of the manuscript.

ACKNOWLEDGEMENTS

This work was supported by the Ministerio de Economía y Competitividad (Spanish Project CMT 2015-65414-C2-1-R). Iris H. Valido acknowledges funding support from the Universitat Autònoma de Barcelona (PIF-2016 grant). SR- μ FTIR experiments were performed at SMIS beamline at SOLEIL Synchrotron (Saint-Aubin, France) and at MIRAS beamline at ALBA Synchrotron (Cerdanyola del Vallès, Spain), with the collaboration of SOLEIL and ALBA staff. This work has been funded by SOLEIL and ALBA synchrotron through granted proposal.

REFERENCES

- (1) Curhan, G. C. Epidemiology of Stone Disease. *Urol. Clin. North Am.* **2007**, *34* (3), 287–293.
- (2) Bartoletti, R.; Cai, T.; Mondaini, N.; Melone, F.; Travaglini, F.; Carini, M.; Rizzo, M. Epidemiology and Risk Factors in Urolithiasis. *Urol. Int.* **2007**, *79* (SUPPL. 1), 3–7.
- (3) Daudon, M.; Dessombz, A.; Frochot, V.; Letavernier, E.; Haymann, J. P.; Jungers, P.; Bazin, D. Comprehensive Morpho-Constitutional Analysis of Urinary Stones Improves Etiological Diagnosis and Therapeutic Strategy of Nephrolithiasis. *Comptes Rendus Chim.* **2016**, *19* (11–12), 1470–1491.
- (4) Grases, F.; Costa-Bauzá, A.; Ramis, M.; Montesinos, V.; Conte, A. Simple Classification of Renal Calculi Closely Related to Their Micromorphology and Etiology. *Clin. Chim. Acta* **2002**, *322* (1–2), 29–36.
- (5) Worcester, E. M. Pathophysiology of Kidney Stone Formation. In *Nutritional and Medical Management of Kidney Stones*; Han, H., Mutter, W. P., Nasser, S., Eds.; Springer International Publishing: Cham, 2019; pp 21–42.
- (6) Sakhaee, K. Kidney Stones 2019: Epidemiology, Clinical Pathophysiology, and Treatment. *Intern. Med. Gd. Rounds* **2019**.
- (7) Conti, C.; Casati, M.; Colombo, C.; Realini, M.; Brambilla, L.; Zerbi, G. Phase Transformation of Calcium Oxalate Dihydrate-Monohydrate: Effects of Relative Humidity and New Spectroscopic Data. *Spectrochim. Acta - Part A Mol. Biomol. Spectrosc.* **2014**, *128*, 413–419.
- (8) Klopogge, J. T.; Boström, T. E.; Weier, M. L. In Situ Observation of the Thermal Decomposition of Weddellite by Heating Stage Environmental Scanning Electron Microscopy. *Am. Mineral.* **2004**, *89* (1), 245–248.
- (9) Bazin, D.; Leroy, C.; Tielens, F.; Bonhomme, C.; Bonhomme-Coury, L.; Damay, F.; Le Denmat, D.; Sadoine, J.; Rode, J.; Frochot, V.; Letavernier, E.; Haymann, J. P.; Daudon, M. Hyperoxaluria Is Related to Whewellite and Hypercalciuria to Weddellite: What Happens When Crystalline Conversion Occurs? *Comptes Rendus Chim.* **2016**, *19* (11–12), 1492–1503.
- (10) H. Valido, I.; Rius-Bartra, J. M.; Boada, R.; Resina-Gallego, M.; Valiente, M.; López-Mesas, M. Characterization of Calcium Oxalate Hydrates and the Transformation Process. *ChemPhysChem* **2020**.
- (11) Hajir, M.; Graf, R.; Tremel, W. Stable Amorphous Calcium Oxalate: Synthesis and Potential Intermediate in Biomineralization. *Chem. Commun.* **2014**, *50* (49), 6534–6536.
- (12) Daudon, M.; Bader, C. A.; Jungers, P.; Robertson, W. G.; Tiselius, H. G.; Hess, B.; Asplin, J. R. Urinary Calculi: Review of Classification Methods and

- Correlations with Etiology. *Scanning Microscopy*. 1993, pp 1081–1106.
- (13) Grases, F.; Costa-Bauza, A.; Prieto, R. M. Renal Lithiasis and Nutrition. *Nutr. J.* **2006**, *5* (1), 1–7.
- (14) Daudon, M.; Jungers, P.; Bazin, D.; Williams, J. C. Recurrence Rates of Urinary Calculi According to Stone Composition and Morphology. *Urolithiasis* **2018**, *46* (5), 459–470.
- (15) Daudon, M.; Jungers, P.; Bazin, D. Stone Morphology: Implication for Pathogenesis. *AIP Conf. Proc.* **2008**, *1049*, 199–215. <https://doi.org/10.1063/1.2998023>.
- (16) Alelign, T.; Petros, B. Kidney Stone Disease: An Update on Current Concepts. *Adv. Urol.* **2018**, Feb 4.
- (17) Bazin, D.; Chevallier, P.; Matzen, G.; Jungers, P.; Daudon, M. Heavy Elements in Urinary Stones. *Urol. Res.* **2007**, *35* (4), 179–184.
- (18) Bihl, G.; Meyers, A. Recurrent Renal Stone Disease - Advances in Pathogenesis and Clinical Management. *Lancet* **2001**, *358* (9282), 651–656.
- (19) Wesson, J. A.; Ward, M. D. Pathological Biomineralization of Kidney Stones. *Elements* **2007**.
- (20) Chiangjong, W.; Thongboonkerd, V. A Novel Assay to Evaluate Promoting Effects of Proteins on Calcium Oxalate Crystal Invasion through Extracellular Matrix Based on Plasminogen/Plasmin Activity. *Talanta* **2012**, *101*, 240–245.
- (21) Canales, B. K.; Anderson, L.; Higgins, L.; Slaton, J.; Roberts, K. P.; Liu, N.; Monga, M. Second Prize: Comprehensive Proteomic Analysis of Human Calcium Oxalate Monohydrate Kidney Stone Matrix. *J. Endourol.* **2008**, *22* (6), 1161–1168.
- (22) Khan, S. R. Reactive Oxygen Species, Inflammation and Calcium Oxalate Nephrolithiasis. *Transl. Androl. Urol.* **2014**, *3* (3), 256–276.
- (23) Aggarwal, K. P.; Narula, S.; Kakkar, M.; Tandon, C. Nephrolithiasis: Molecular Mechanism of Renal Stone Formation and the Critical Role Played by Modulators. *Biomed Res. Int.* **2013**, 2013.
- (24) Blanco, F.; Ortiz-Alfás, P.; López-Mesas, M.; Valiente, M. High Precision Mapping of Kidney Stones Using μ -IR Spectroscopy to Determine Urinary Lithogenesis. *J. Biophotonics* **2015**, *8* (6), 457–465.
- (25) Izatulina, A. R.; Punin, Y. O.; Shtukenberg, A. G.; Frank-Kamenetskaya, O. V.; Gurzhiy, V. V. Formation and Stability of Calcium Oxalates, the Main Crystalline Phases of Kidney Stones. In *Minerals as Advanced Materials II*; 2012.
- (26) Stuart, B. Infrared Spectroscopy. *Kirk-Othmer Encyclopedia of Chemical Technology*. April 15, 2005.
- (27) Arrizabalaga, I.; Gómez-Laserna, O.; Aramendia, J.; Arana, G.; Madariaga, J. M. Applicability of a Diffuse Reflectance Infrared Fourier Transform Handheld Spectrometer to Perform in Situ Analyses on Cultural Heritage Materials. *Spectrochim. Acta - Part A Mol. Biomol. Spectrosc.* **2014**, *129*, 259–267.
- (28) Hecht, H. G. Interpretation of Diffuse Reflectance Spectra. *J Res Natl Bur Stand Sect A Phys Chem* **1976**, *80 A* (4), 567–583.
- (29) Petit, I.; Belletti, G. D.; Debrouse, T.; Llansola-Portoles, M. J.; Lucas, I. T.; Leroy, C.; Bonhomme, C.; Bonhomme-Coury, L.; Bazin, D.; Daudon, M.; Letavernier, E.; Haymann, J. P.; Frochot, V.; Babonneau, F.; Quaino, P.; Tielens, F. Vibrational Signatures of Calcium Oxalate Polyhydrates. *ChemistrySelect* **2018**, *3* (31), 8801–8812.
- (30) Lozano, M.; Rodríguez-Ulibarri, P.; Echeverría, J. C.; Beruete, M.; Sorolla, M.; Beriain, M. J. Mid-Infrared Spectroscopy (MIR) for Simultaneous Determination of Fat and Protein Content in Meat of Several Animal Species. *Food Anal. Methods* **2017**, *10* (10), 3462–3470.
- (31) Benseny-Cases, N.; Klementieva, O.; Cotte, M.; Ferrer, I.; Cladera, J. Microspectroscopy (MFTIR) Reveals Co-Localization of Lipid Oxidation and Amyloid Plaques in Human Alzheimer Disease Brains. *Anal. Chem.* **2014**, *86* (24), 12047–12054.
- (32) Mecozzi, M.; Pietrantonio, E.; Pietroletti, M. The Roles of Carbohydrates, Proteins and Lipids in the Process of Aggregation of Natural Marine Organic Matter Investigated by Means of 2D Correlation Spectroscopy Applied to Infrared Spectra. *Spectrochim. Acta - Part A Mol. Biomol. Spectrosc.* **2009**, *71* (5), 1877–1884.
- (33) Selvam, R.; Kalaiselvi, P. Oxalate Binding Proteins in Calcium Oxalate Nephrolithiasis. *Urol. Res.* **2003**, *31* (4), 242–256.
- (34) Grohe, B.; O'Young, J.; Ionescu, D. A.; Lajoie, G.; Rogers, K. A.; Karttunen, M.; Goldberg, H. A.; Hunter, G. K. Control of Calcium Oxalate Crystal Growth by Face-Specific Adsorption of an Osteopontin

- Phosphopeptide. *J. Am. Chem. Soc.* **2007**, *129* (48), 14946–14951.
- (35) Konya, E.; Umekawa, T.; Iguchi, M.; Kurita, T. The Role of Osteopontin on Calcium Oxalate Crystal Formation. *Eur. Urol.* **2003**, *43* (5), 564–571.
- (36) Selvam, R. Calcium Oxalate Stone Disease: Role of Lipid Peroxidation and Antioxidants. *Urol. Res.* **2002**, *30* (1), 35–47.
- (37) Khan, S. R.; Glenton, P. A.; Backov, R.; Talham, D. R. Presence of Lipids in Urine, Crystals and Stones: Implications for the Formation of Kidney Stones. *Kidney Int.* **2002**, *62* (6), 2062–2072.
- (38) Talham, D. R.; Backov, R.; Benitez, I. O.; Sharbaugh, D. M.; Whipps, S.; Khan, S. R. Role of Lipids in Urinary Stones: Studies of Calcium Oxalate Precipitation at Phospholipid Langmuir Monolayers. *Langmuir* **2006**, *22* (6), 2450–2456. <https://doi.org/10.1021/la052503u>.
- (39) Melcrová, A.; Pokorna, S.; Pullanchery, S.; Kohagen, M.; Jurkiewicz, P.; Hof, M.; Jungwirth, P.; Cremer, P. S.; Cwiklik, L. The Complex Nature of Calcium Cation Interactions with Phospholipid Bilayers. *Sci. Rep.* **2016**, *6*, 1–12.
- (40) Huster, D.; Arnold, K.; Gawrisch, K. Strength of Ca²⁺ Binding to Retinal Lipid Membranes: Consequences for Lipid Organization. *Biophys. J.* **2000**, *78* (6), 3011–3018.
- (41) Bazin, D.; Daudon, M.; Combes, C.; Rey, C. Characterization and Some Physicochemical Aspects of Pathological Microcalcifications. *Chem. Rev.* **2012**, *112* (10), 5092–5120.
- (42) Oyama, T.; Sano, T.; Hikino, T.; Xue, Q.; Iijima, K.; Nakajima, T.; Koerner, F. Microcalcifications of Breast Cancer and Atypical Cystic Lobules Associated with Infiltration of Foam Cells Expressing Osteopontin. *Virchows Arch.* **2002**, *440* (3), 267–273.
- (43) Mathonnet, M.; Dessombz, A.; Bazin, D.; Weil, R.; Frédéric, T.; Pusztaszeri, M.; Daudon, M. Chemical Diversity of Calcifications in Thyroid and Hypothetical Link to Disease. *Comptes Rendus Chim.* **2016**, *19* (11–12), 1672–1678.



CHAPTER 3

FURTHER INSIGHTS

“Principles for the development of a complete mind: study the art of science, study the science of art, develop your senses-especially learn how to see, realize that everything is connected to everything else”

Leonardo da Vinci



Discriminating the formation origin of calcium oxalate monohydrate in kidney stones via synchrotron microdiffraction

Iris H. Valido^{a‡}, Victor Fuentes-Cebrian^{a‡}, Roberto Boada^a, Oriol Vallcorba^b, Montserrat Resina-Gallego^a, Manuel Valiente^a, and Montserrat López-Mesas^{a*}

^a *Centre Grup de Tècniques de Separació en Química (GTS), Departament de Química, Universitat Autònoma de Barcelona, Facultat de Ciències, Edifici CN. 08193, Bellaterra, Barcelona, Spain*

^b *ALBA synchrotron Light Source, Cerdanyola del Vallès, Barcelona, Spain*

**Montserrat.lopez.mesas*

‡ These authors contributed equally to this work

Submitted

Dicriminating the formation origin of calcium oxalate monohydrate in kidney stones via synchrotron microdiffraction

Iris H. Valido^{a‡}, Victor Fuentes-Cebrian^{a‡}, Roberto Boada^a, Oriol Vallcorba^b, Montserrat Resina-Gallego^a, Manuel Valiente^a, Montserrat López-Mesas^{a*}

^a Centre Grup de Tècniques de Separació en Química (GTS), Departament de Química, Universitat Autònoma de Barcelona, Facultat de Ciències, Edifici CN, 08193, Belaterra, Spain.

^b ALBA Synchrotron Light Source, Cerdanyola del Vallès, Barcelona, Spain

KEYWORDS: kidney stones; calcium oxalate hydrates; whewellite; weddellite crystalline conversion; synchrotron based μ XRD

ABSTRACT: Nephrolithiasis is a multifactor disease that produces nephroliths in the kidney. Calcium oxalate hydrated (dihydrated, COD, or monohydrated, COM) stones are the most common ones with more than sixty percent incidence worldwide. They are related with different pathologies, COD with hypercalciuria and COM with hyperoxaluria. COD is the unstable species and transforms into COM (herein named as TRA to distinguish the origin of the monohydrated species). TRA and COM are chemically and crystallographically identical leading to a misdiagnose and to a recurrence increase. In the current study, the composition and crystalline structure of several calcium oxalate stones, classified by morpho-constitutional analysis, were examined by IR and synchrotron through-the-substrate micro X-ray diffraction (tts- μ XRD). Both, IR and linear diffractogram studies, were able to distinguish between the monohydrated and dihydrated phases but not between COM and TRA, as expected. The analysis of the 2D diffraction patterns revealed that TRA showed lower degree of crystallinity and less texture respect to COM which can be used as a signature to distinguish between the two. This study confirms that despite the subtle differences between COM and TRA, the origin of the monohydrate oxalates can be unraveled using tts- μ XRD. This valuable information should be taken into account in order to improve the patients' diagnose and reduce the recurrence by considering and treating the origin of the formed stone.

INTRODUCTION

Urolithiasis is a disease caused by the formation of stones in different parts of the urinary tract (renal pyelocaliceal system, ureter, bladder and urethra). Urinary stones can be classified in seven types by considering their chemical composition as calcium oxalate (66% of incidence), uric acid (15%), struvite (9%), hydroxyapatite (HAP, 7%), brushite (1%), cysteine (1%) and others (<1%)¹. However, its incidence is highly dependent on several factors, such as genetic, dietary, ethnic, geographical and climatic. It has been reported that countries with the highest standard of life present a prevalence of renal stone higher than 10%, being higher in men (12%) than in women (6%)². In addition, there is an elevated recurrence rate of 30-50% in the next 5 to 10 years after the first episode, and up to 75% after 20 years^{3,4}. Although there are plenty of epidemiological

studies on these factors, only few emphasize the importance of determining the relationship between stone type and the risk of recurrence⁵. To reduce the recurrence, the European Association of Urology (EAU) advises that the nephrolith of all first-time stone formers should be analyzed². To perform the compositional analysis of the renal calculi, different techniques such as infrared spectroscopy (IR), X-ray diffraction (XRD) and chemical analysis (CA) have been used, although the latter is currently considered almost obsolete due to poor results⁶. In order to perform the aforementioned compositional analysis, it is necessary to powder the samples, which results in a bulk analysis. Due to the high heterogeneity of the nephroliths, important information about the stone formation origin and the growth history is lost. To overcome this problem, the morpho-constitutional analysis⁷, which

combines morphological examination of the surface (e.g. color, form, size and aspect (e.g. smooth or rough)), section (e.g. color, organization (layers, compactness, loose or poorly organized)) and nucleus (location and aspect) of the stones with the composition analysis by FTIR, has been proposed^{7,8}. This methodology allows correlating the type of renal calculi with the main etiologic factors related to its formation^{7,8}. Among nephroliths types, calcium oxalate has the highest prevalence (60-70%) and it is found in two forms: monohydrated (COM, whewellite, $\text{CaC}_2\text{O}_4 \cdot \text{H}_2\text{O}$) and dihydrated (COD, weddellite, $\text{CaC}_2\text{O}_4 \cdot 2\text{H}_2\text{O}$)^{8,9}. Due to its low stability, COD suffers a crystalline conversion (transformation), produced over time in the medium, into COM which is the thermodynamically stable species¹⁰⁻¹³. Hence, calcium oxalate monohydrate in renal calculi can be either formed directly as COM or as the resulting product after the transformation from COD. This different formation origin is related with different pathologies since COM is usually related to hyperoxaluria while COD is related to hypercalciuria¹². Therefore, identifying the origin of the stone formation is of great importance in order to prevent its recurrence. However, determining this important factor is difficult since the product of this transformation (hereafter named TRA to distinguish between the origin of the two calcium oxalate monohydrates and to facilitate the discussion in this work) is chemically and crystallographically COM, as concluded in our previous work where we characterized this transformation process and showed that TRA has the same space group as COM ($\text{P}2_1/\text{c}$)¹⁴. It has been suggested in a previous work that it is possible to identify a kidney stone that has suffered this crystalline conversion by IR characterization since there is a modification of the absorption bands and the morphological characteristics differ respect to COM¹². Nevertheless, in a previous study performed by applying μFTIR spectroscopy with synchrotron radiation over calcium oxalate stones samples, we determined that due to the high variability on the COM spectra measured, the subtle differences found in the IR spectra between COM and TRA were not significantly different to distinguish them¹⁵. Hence, the interpretation of the IR results can be a difficult task due to the high variability of the samples.

Since it has not been possible to solve the identification problem between COM and TRA by the conventional techniques, a new approach is proposed in this work, based on a qualitative evaluation of the

calcium oxalate monohydrates (COM/TRA) crystallographic texture, since it has been observed that TRA is more fragile than COM when cutting the stone. In this sense, an analysis based on the azimuthal plot of characteristic reflections from the 2D XRD data images obtained by synchrotron through-the-substrate microdiffraction technique (tts- μXRD)¹⁶ has been correlated with the morpho-constitutional analysis applied to classify oxalocalcic kidney stones.

EXPERIMENTAL SECTION

Sample preparation

Kidney stones were collected from hospitals of the Barcelona area. The studied samples were previously classified by morpho-constitutional analysis^{7,8} as calcium oxalate hydrates (COM, COD and with different degrees of transformation, Table 1). For tts- μXRD analysis, samples were embedded in EpoFix resin[®], cut in half, fixed on a glass substrate (1.5 mm thickness) and polished to reduce the sample thickness down to ~ 30 μm and to have a flat surface. From the same samples, a representative fraction was powdered in order to perform the infrared spectroscopy analysis. The synthetic calcium oxalate hydrates references were prepared using the procedure previously optimized in our research group¹⁴.

Infrared spectroscopy analysis

To determine the calcium oxalate hydrate (CaOx) composition of the kidney stones, Attenuated Total Reflectance Fourier Transform Infrared Spectroscopy (ATR-FTIR) measurements were performed on a representative portion of seven of the fourteen selected samples, since there were not enough fragments of all the samples to pulverize (Table 1). An Infrared Spectrophotometer Tensor 27 equipped with an Attenuated Total Reflectance module (ATR-FTIR, Bruker, Ettlingen, Germany), with a resolution of 4 cm^{-1} and 64 scans (region between $4000\text{-}600 \text{ cm}^{-1}$) was used. A Savitzky-Golay second derivative, with a polynomial order 3 and 9 total smoothing points, was applied to the transmittance spectra of the synthetic references and the selected samples (Unscrambler X[®] software), followed by the application of Equation 1 to determine the contribution of each oxalocalcic hydrates in the samples. This equation represents the relative concentration of each hydrate with respect to the total calcium oxalate present in the sample, and not

considering the contribution of other components, such as HAP.

$$\frac{\nu_{CaOx}}{\nu_{COD} + \nu_{COM}} \cdot 100 \quad \text{Equation 1}$$

The wavenumbers used as characteristics for each species were 912 cm^{-1} ($\nu(\text{C-C}) + \delta_i(\text{COO}) + \nu(\text{M-O})$) for COD and 883 cm^{-1} ($\delta_i(\text{COO}) + \nu(\text{M-O})$) for COM, since those are the major differences between both species observed¹⁴.





























Synchrotron μ XRD data collection and data analysis

Synchrotron μ XRD measurements were performed at the Materials Science and Powder Diffraction Beamline (MSPD)¹⁷ at ALBA synchrotron facility (Cerdanyola del Vallès, Barcelona, Spain). This beamline is equipped with Kirkpatrick-Baez mirrors providing a monochromatic focused beam of $15 \times 15 \mu\text{m}^2$ size at full width at half maximum (FWHM) and a Rayonix SX165 CCD detector (round active area of 165 mm diameter, frame size 2048×2048 pixels, 79 mm pixel size, dynamic range 16 bit). The $30 \mu\text{m}$ thickness sections were measured in transmission through the glass substrate¹⁶ with a rotation from -5 to 5° in the vertical axis during measurement to improve grain statistics. The data collection strategy for the stones consisted of measuring a 2D diffraction pattern at a series of points contained on lines from the outside to the inside of the kidney stone and separated $15 \mu\text{m}$ between them. The energy used was 29.2 keV ($\lambda = 0.4246 \text{ \AA}$) determined from the Sn absorption K-edge. The instrumental calibration was performed with a LaB_6 standard (NIST SRM 660b). Synthetic CaOx samples were loaded into 0.7 mm borosilicate glass capillaries and measured at the high-resolution end station of the

same beamline using the Mythen-II detector at a wavelength of 0.95349 \AA .

The profile matching of the powder XRD data was performed using FULLPROF program (version 3.00 June 2015)¹⁸. The diffraction data from the samples was processed using the d1Dplot and d2Dplot programs¹⁹, including the azimuthal plots, defined as the pixel intensity evolution along and ellipse specified by the 2θ angle and a given tolerance. The results were further analyzed with the Unscrambler X[®] software to perform Principal Component Analysis (PCA) of the diffractograms in the regions of interest (2.5 - 9.5° (Bragg angle)). Moreover, a Multivariate Curve Resolution (MCR) was performed with the Unscrambler X[®] software to study the evolution of the different components throughout the collected diffraction patterns along each measured line from the surface to the inside of the samples. This analysis allows to solve the mixture composition of a sample along time or distance on a sample, providing the calculated concentration and response profiles of the mixture components extracted from the given data (in this case, the X-ray diffractograms). The classification of compounds represented in the MCR was done following the morphological analysis of the measured areas in combination with the obtained μ XRD diffractograms. Regarding the MCR patterns, it is well known that COD is transformed over time in the medium^{10,14,20}, therefore the transformation occurs along the crystal growth (oldest sections are more transformed) what is described in this work as a Correlated transformation, since it is proportional to the formation time. The transformation that is not proportional to the formation time is described in this work as non-Correlated.

Table 1. Samples used in the present work, classified by morpho-constitutional analysis^{7,8}. Abbreviations: COD = calcium oxalate dihydrate; COM = calcium oxalate monohydrated; HAP = hydroxyapatite; OM = organic matter.

Sample name/ Description	Surface	Section	Sample name/ Description	Surface	Section
S21/ Mixed COD+HAP, layered			S27/ COM (cavity) with core COM+OM and superficial deposit of COD		
S22/ Pure COD with transformation			S28/ Pure COD with transformation		
S23/ COM (cavity) with core HAP+OM			S29/ COD with HAP between crystals		
S24/ COM (cavity) with core COM+OM and superficial deposit of COD			S30/ COD with HAP between crystals		
S25/ Pure COD totally transformed			S31/ COD with HAP between crystals (with transformation)		
S26A/ COD with core HAP (totally transformation)			S32/ COM (cavity) with core COM+OM		
S26B/ COD with core HAP (with transformation)			S33/ COM (papillary) with core HAP+OM		

RESULTS AND DISCUSSION

IR analysis of kidney stone samples

The ATR-FTIR analysis of the selected kidney stones was used to determine the contribution of each oxalocalcic species in the samples, which has been represented in Figure 1 as relative CaOx concentration (calculated with Equation 1) together with the synthetic samples as references. Based on the morphological analysis of the samples, it will be expected that samples

classified as COD or COM will have relative concentration of 100% of the respective oxalocalcic species. This was observed in sample S32, classified as COM (see Table 1) but not in the ones classified as COD by the aforementioned technique, as can be seen in Figure 1. Two samples classified as COD with transformation and core HAP (S26A and S26B), and one classified as pure COD with transformation (S22), present a relative CaOx concentration of 100% COM, which means that they are totally transformed into the monohydrated species, even if the presence of crystals,

identified as COD from their shape and color, are observed with the stereomicroscope¹². On the other hand, three samples present a mixture of COD and COM, one classified as pure COD with a low level transformation (S28) and two classified as COD with HAP between crystals with (S31) and without (S29) transformation, presenting a COD:COM ratio of 61:39, 19:81 and 99:1, respectively (Figure 1). These results suggest that stones formed as COD with HAP between crystals are less transformed or more stable over the formation/development time. Furthermore, the results clearly show the great difficulty to differentiate between COM and those CaOx monohydrated that come from the transformation of the unstable COD by using ATR-FTIR, as reported in a previous study¹⁵.

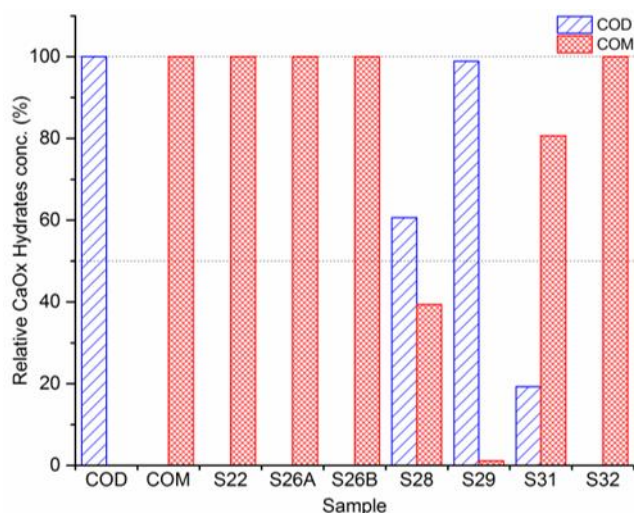


Figure 1. Graphic representation of the relative CaOx concentration (%) of the synthetic references (COD and COM) and seven of the kidney stones samples classified as COM (S32) and COD (S22, S26A, S26B, S28, S29 and S31) with different degrees of transformation. The relative CaOx concentration (%) was calculated using Equation 1.

The tts- μ XRD approach

XRD data analysis

Powder XRD data of synthetic CaOx measured in capillaries were used as references for the renal calculi study. A full pattern matching¹⁸ starting with the crystallographic parameters of weddellite (COD) and whewellite (COM) reported in the literature²¹ was performed. The fitting confirms that the crystallographic phase of COD/weddellite is tetragonal (bipyramidal, space group $I4/m$) while COM/whewellite is monoclinic (space group $P2_1/c$), corresponding to the reported low temperature phase (COM-LT)²². The

results obtained from the refinement can be found in the Support Information (SI1). The comparison of the powder data of the synthetic species with the powder patterns of the samples morpho-constitutionally classified as COM and COD obtained from the 2D μ XRD data shows the same characteristic reflections in both cases. Figure 2 displays examples of the most common reflections observed in CaOx nephroliths, together with the synthetic references. However, not all the reflections are present in the renal calculi samples due to the preferential orientation of the crystallites in the stone as a consequence of its formation/growth²³.

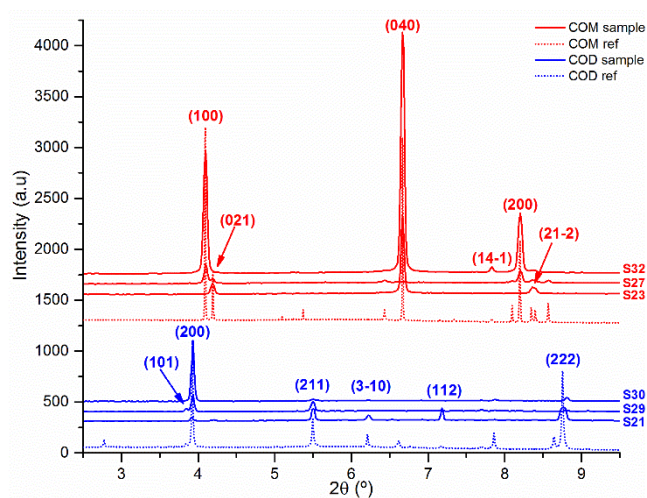


Figure 2. Example of diffractograms for COM (top-red) and COD (bottom-blue), showing reflections, for samples S23, S27 and S32 for COM and S21, S29 and S30 for COD, analyzed by tts- μ XRD, together with the synthetic references (dotted lines).

In order to determine if there are significant differences between the powder diffraction patterns of COM and TRA from kidney stones, a Principal Component Analysis (PCA) was performed in the regions of interest ($2\theta=2.5-9.5^\circ$). In Figure 3, the Scores (top) and Loadings (bottom) of this analysis are represented. In the Scores, each point represents a diffraction pattern performed over samples classified by morpho-constitutional analysis as COD, COM and TRA. Additionally, MIX refers to points with a mixture of components or to an intermediate point on the transformation process. As can be observed, COD is easily separated from the monohydrated species along PC-3, being distributed in its negative region with a major contribution, described in the Loadings, of the reflections (200) and (222) of COD, while the principal contribution in the positive region of PC-3 is the reflection (021) of the monohydrated CaOx. It can be

noted in Figure 3-top that the characteristics points/patterns of COM and TRA are mixed over PC-1 and PC-2, with the reflections that describe them being characteristic of the monohydrated species, such as: (100), (040) and (200) on PC-1 positive; (100) and (200) on PC-2 positive; and (040) on PC-2 negative. The performed PCA is not able to differentiate between COM and TRA since both are the same crystallographic phase (space group $P2_1/c$)¹⁴. The observed differences between PC-1 and PC-2 might be related with the orientation that can be found in monohydrated calcium oxalate species.

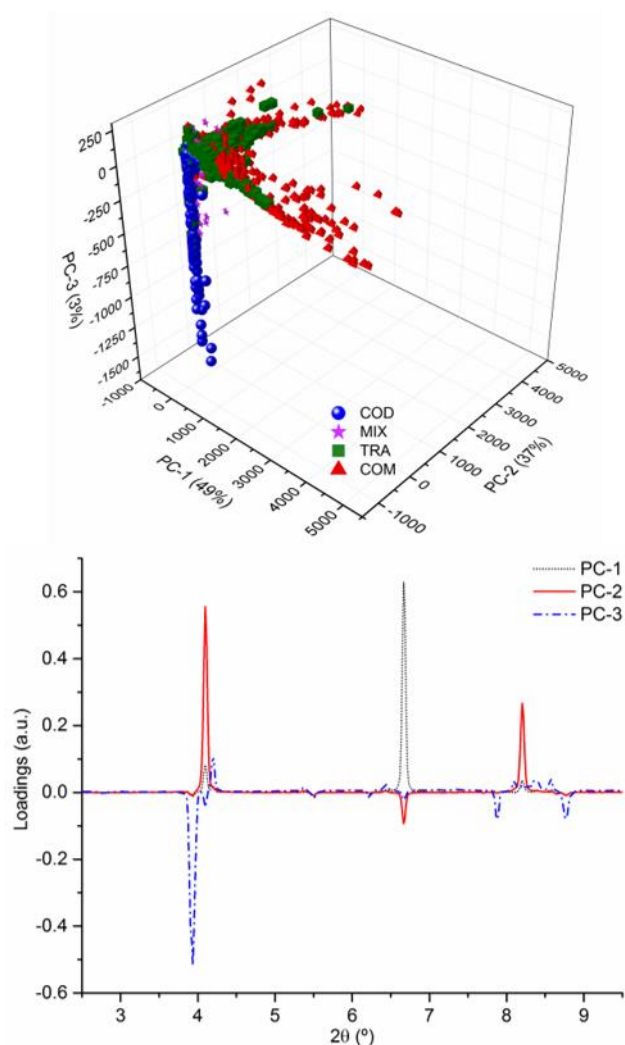


Figure 3. Principal Component Analysis (PCA) of the diffraction patterns obtained from *tts*- μ XRD of the samples classified by morpho-constitutional analysis as COM, COD and TRA (MIX refers to points with a mixture of components or to an intermediate point on the transformation process). 3D graphical representations of the scores distribution along PC-1, PC-2 and PC-3 (Top panel) and their loadings (Bottom panel).

Inspection of the 2D μ XRD images

In the previous section, it was discussed the impossibility to differentiate between COM and TRA by their diffraction patterns since they are crystallographically equivalent. However, the collected 2D μ XRD images provide also information regarding the sample texture, orientation degree and graininess affecting how the intensity of the reflections are distributed along the Debye rings²⁴. In this aspect, differences can be observed in the 2D diffraction images of four representative points of calcium oxalate hydrates in kidney stones previously classified by morpho-constitutional analysis (Figure 4). As can be seen for the COD stone, exemplified with a diffractogram taken on sample S30, the individual reflections appear as small spots, characteristic of single crystals at a specific orientation. In the COM stone, exemplified with a diffractogram taken on sample S23, the image shows elongated spots following partially the Debye ring and representing a distribution of close orientations, corresponding to a textured sample with a clear distribution of orientations²⁴. However, after the transformation process, TRA, exemplified in Figure 4 with a diffractogram taken on sample S26A, does not present the same degree of texture than its monohydrated homologue COM. For TRA stone, the intensity of the reflections are more distributed along the Debye ring, approaching the behavior of random oriented polycrystalline samples²⁴. A fourth distribution has been observed in the 2D diffraction patterns, and it has been defined as MIX, exemplified in Figure 4 with a diffractogram taken on sample S27 (on the intersection of the superficial deposit with the COM stone), since those are points where there is a contribution of the signals of weddellite (COD) and whewellite (COM or TRA). This mixed signal can come from a point where both species are present, such as in the intersection of the superficial deposit of COD with the COM stone (S24 and S27), where there is COD with TRA (totally transformed COD, for example S31), or where there is some level of transformation, but not completed. The results shown in Figure 4 are observed in all samples with the corresponding classification.

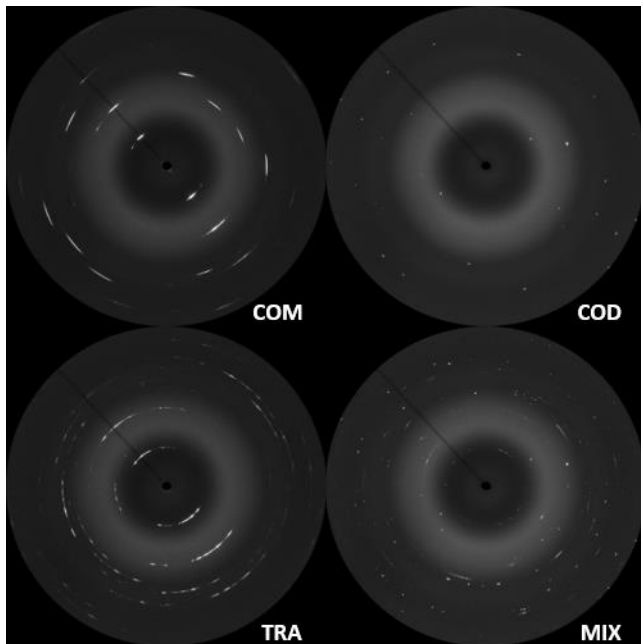


Figure 4. 2D- μ XRD images of four representative points from calcium oxalate kidney stones, namely COM (top-left), COD (top-right), TRA (bottom-left) and MIX (bottom-right).

Azimuthal plot analysis

In order to have a better representation and a systematic method to analyze the different orientation behavior of the species, the evolution of the azimuthal intensity of selected reflections has been plotted to obtain a linear representation of the pixel intensity evolution along the ellipse specified by the 2θ angle (Debye ring)¹⁹. The azimuthal plots of two reflections, (100) and (040), were selected for this analysis since they are the most prevalent ones observed in the calcium oxalate monohydrate kidney stones, Figure 5 left and right panel, respectively. To evaluate the differences in the texture degree along each stone, the azimuthal plot of each point measured along the lines drawn in the stones has been represented (described lines can be seen in the Support Information (SI₂)). An example of a kidney stone classified as COM (S₂₃) is represented in

Figure 5 (top). A clear orientation can be observed, since the pattern is repeated every 180° of the azimuthal angle. Moreover, it is interesting to note that the outer zone of the stone has peaks on the (040) reflection, while the inner has more intense peaks on the (100) reflection, meaning that the nucleus and the surface have different orientations. The same tendency has been observed in other stones with the same classification, being also distributed in layers (Support Information (SI₂)). However, if this behavior is compared with the one of a nephrolith classified as TRA (S_{26A}), depicted in Figure 5 (middle), it can be observed that there is no clear tendency in the distribution in any of the angles (this behavior has been observed in all samples classified as TRA, to confirm it, another example can be found in the Support Information (SI₂)). These results prove that, even being the same calcium monohydrated species, COM and TRA kidney stones can be differentiated by these variations on their texture degree, given that they differ in the formation origin, being COM formed directly as whewellite and TRA coming from the transformation of weddellite.

The azimuthal plot of a nephrolith classified as papillary COM with HAP and organic matter in the nucleus (S₃₃) (see Table 1) is shown in Figure 5 (bottom). When examining the stone with the stereomicroscope (Support Information (SI₂)), several areas raised doubts about the formation origin, as those present differences in texture. As can be observed, marked with red dot-lines, there are two regions characterized as COM, since they seem to have clear orientation. However, the central part of the represented line is characterized by a non-clear pattern, which matches with the TRA behavior. The different regions of the analyzed line classified by the azimuthal plot are marked on the kidney stone section image and can be found in the Support Information (SI₂, Figure 2C), correlating the observed behavior with the obtained results.

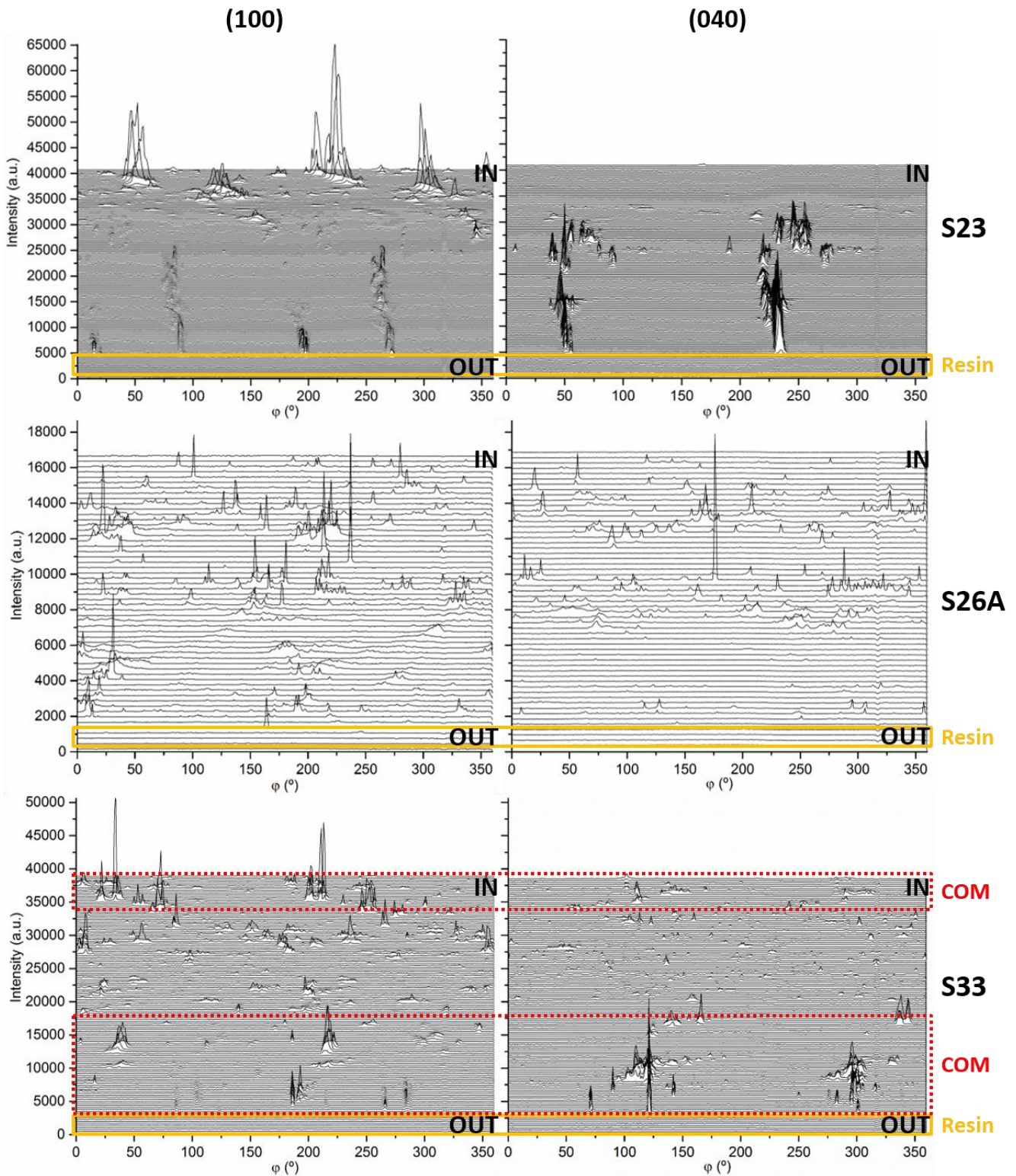


Figure 5. Representation of the azimuthal plots for three samples, one representative of COM (top, S23), one representative of TRA (middle, S26A) and a test sample (bottom, S33), at reflections (100) and (040), left and right panels respectively. The orange square (bottom of each plot) represents the resin where the stones are embedded, and the red dot-lines the two regions characterized as COM. The separation between points is of 300 a.u. on the y-axis

Multivariate Curve Resolution analysis for the transformation monitoring

An example of the MCR analysis is represented in Figure 6 (top), for sample S27, classified as COM (nucleus) with an external deposit of COD (see Table 1). The transformation of the COD deposit was studied. COD was found, as expected, and TRA (at different transformation degrees) and COM at the beginning of the deposit. As can be observed in the components distribution graph (Figure 6 (top) left panel), in the external part of the deposit, only reflections characteristics of COD are observed, represented by Component-1 in the simulated pattern (Figure 6 (top) right panel), like the reflection 211. Along the analyzed

line, the relative concentration of COD starts decreasing while, appearing the components characteristics of the monohydrated species (around 275 μm from the surface), which has been named as MIX, as it was previously described in the $\text{tts-}\mu\text{XRD}$ section (Figure 4 (bottom) right panel). After the complete transformation, the components present are characteristics of the monohydrated phases, with a negligible relative concentration of COD, being the most representative reflections 100 and 200 for Component-2, 040 for Component-3 and 021 and 121 for Component-4, among others. Another sample, S24, with a similar composition to S27 and, hence, behavior, can be found in the Support Information (SI₃), which corroborates the obtained results.

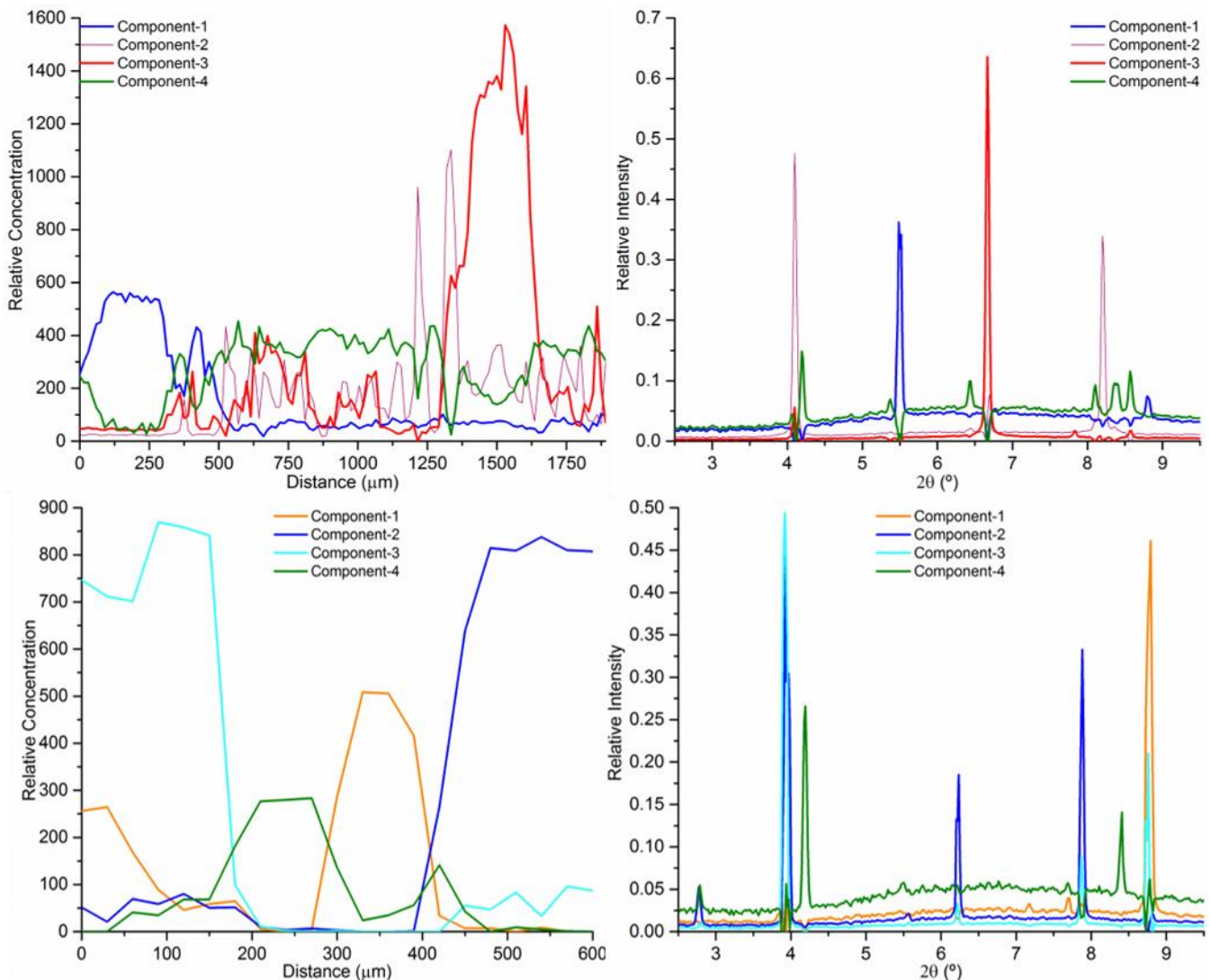


Figure 6. Examples of MCR analysis of the diffractograms from a Correlated (top) and a non-Correlated (bottom) transformation from samples S27 and S29 respectively. In the left panel, the evolution of the four components along the diffraction analysis (from the surface to the inside of the stone) is represented, while on the right panel the simulated patterns for each component is shown.

Furthermore, another transformation behavior has been observed, which has been named non-Correlated transformation. An example showing this behavior is represented in Figure 6 (bottom), representing a line performed in sample S29, a kidney stone classified as COD with HAP between crystals. In this case, the majority of the reflections are characteristic of COD, with exception of the ones represented by Component-4 (reflections 021 and 21-2 of COM) and partially by Component-1 (reflection 14-1 of COM), as can be observed in Figure 6 ((bottom) right panel), which have a higher concentration approximately between 200-400 μm (Figure 6 (bottom) left panel).

These two different features found in kidney stones classified as COD suggest that the level of transformation is not only related with the time after the formation of the crystals (or the contact time with the medium), but also with the presence of certain components that could act as stabilizers of the dihydrated species, as has been described in a previous study⁵.

CONCLUSIONS

The Principal Component Analysis (PCA) approach described in the present work, using the diffraction peaks of CaOx stones, does not allow to distinguish between COM and TRA. Nevertheless, it is possible to differentiate them, and so, their formation origin, by studying the crystalline texture degree of the CaOx species in renal calculi with a qualitative analysis of the azimuthal plots of selected reflections from 2D μXRD data. This approach shows that nephroliths originally formed as COM have well oriented structures, while TRA does not present the same level of texture. With this method, it is possible to correlate the obtained results with the observations of the samples from the stereomicroscope, which could improve the morpho-constitutional analysis. Furthermore, with the MCR analysis, it was possible to analyze the crystalline conversion of COD in situ, being able to differentiate between two behaviors: Correlated, where COD has been transformed over the time (oldest sections are more transformed), and non-Correlated. These results suggest that the transformation level is not only related with the crystal time in the medium, but it is also affected by the presence of other components (e.g. HAP) that could stabilize the dihydrated species. Hence, the use of synchrotron radiation based μXRD is a useful tool to improve the knowledge applied to perform the

morpho-constitutional analysis used to classify oxalocalcic kidney stones, which could help to reduce the patients' recurrence.

ASSOCIATED CONTENT

Supporting Information.

SI1: XRD fitting results

SI2: Examples of azimuthal plot

SI3: Multivariate Curve Resolution Analysis of the transformation monitoring

AUTHOR INFORMATION

Corresponding Author

* montserrat.lopez.mesas@uab.cat

Author Contributions

The manuscript was written through contributions of all authors. / All authors have given approval to the final version of the manuscript.

‡These authors contributed equally.

ACKNOWLEDGMENT

The authors want to acknowledge the financial support from the Ministerio de Economía y Competitividad (Spanish Project CMT 2015-65414-C2-1-R). Iris H. Valido acknowledges funding support from the Universitat Autònoma de Barcelona (PIF-2016 grant). Roberto Boada acknowledges funding support from Marie Skłodowska-Curie grant agreement No 665919 of the European Union. The XRD experiments were performed at MSPD beamline at ALBA Synchrotron, under proposal 2018o22777, with the collaboration of ALBA staff. All the authors are grateful to the Serveis de Suport a la Investigació of the UAB (SAQ) for the FTIR equipment.

ABBREVIATIONS

ATR-FTIR, Attenuated Total Reflectance Transformed Infrared Spectroscopy; CA, chemical analysis; CaOx, calcium oxalate hydrates; COD, calcium oxalate dihydrate; COM, calcium oxalate monohydrate; EAU, European Association of Urology; IR, infrared spectroscopy; OM, organic matter; PCA, Principal Component Analysis; MCR, Multivariate Curve Resolution; TRA, transformed calcium oxalate dihydrate; μXRD , through-the-substrate micro X-ray diffraction; XRD, X-ray diffraction.

REFERENCES

- (1) Lorenzo, V.; Torres, A.; Hernández, D.; Ayus, J. C. *Manual de Nefrología*, 2nd ed.; Elsevier, España, 2002.
- (2) Türk, C.; Neisius, A.; Petrik, A.; Seitz, C.; Skolarikos, A.; Thomas, K. EAU Guidelines on Urolithiasis. *Eur. Assoc. Urol.* **2018**, *69* (3), 475–482. <https://doi.org/10.1016/j.eururo.2015.07.041>.
- (3) Curhan, G. C. Epidemiology of Stone Disease. *Urol. Clin. North Am.* **2007**, *34* (3), 287–293.
- (4) Alelign, T.; Petros, B. Kidney Stone Disease: An Update on Current Concepts. *Adv. Urol.* **2018**, Feb 4.
- (5) Daudon, M.; Jungers, P.; Bazin, D.; Williams, J. C. Recurrence Rates of Urinary Calculi According to Stone Composition and Morphology. *Urolithiasis* **2018**, *46* (5), 459–470.
- (6) Siener, R.; Buchholz, N.; Daudon, M.; Hess, B.; Knoll, T.; Osther, P. J.; Reis-Santos, J.; Sarica, K.; Traxer, O.; Trinchieri, A. Quality Assessment of Urinary Stone Analysis: Results of a Multicenter Study of Laboratories in Europe. *PLoS One* **2016**, *11* (6).
- (7) Daudon, M.; Dessombz, A.; Frochot, V.; Letavernier, E.; Haymann, J. P.; Jungers, P.; Bazin, D. Comprehensive Morpho-Constitutional Analysis of Urinary Stones Improves Etiological Diagnosis and Therapeutic Strategy of Nephrolithiasis. *Comptes Rendus Chim.* **2016**, *19* (11–12), 1470–1491.
- (8) Grases, F.; Costa-Bauzá, A.; Ramis, M.; Montesinos, V.; Conte, A. Simple Classification of Renal Calculi Closely Related to Their Micromorphology and Etiology. *Clin. Chim. Acta* **2002**, *322* (1–2), 29–36.
- (9) Worcester, E. M. Pathophysiology of Kidney Stone Formation. In *Nutritional and Medical Management of Kidney Stones*; Han, H., Mutter, W. P., Nasser, S., Eds.; Springer International Publishing: Cham, 2019; pp 21–42.
- (10) Conti, C.; Casati, M.; Colombo, C.; Realini, M.; Brambilla, L.; Zerbi, G. Phase Transformation of Calcium Oxalate Dihydrate-Monohydrate: Effects of Relative Humidity and New Spectroscopic Data. *Spectrochim. Acta - Part A Mol. Biomol. Spectrosc.* **2014**, *128*, 413–419.
- (11) Klopogge, J. T.; Boström, T. E.; Weier, M. L. In Situ Observation of the Thermal Decomposition of Weddellite by Heating Stage Environmental Scanning Electron Microscopy. *Am. Mineral.* **2004**, *89* (1), 245–248.
- (12) Bazin, D.; Leroy, C.; Tielens, F.; Bonhomme, C.; Bonhomme-Courry, L.; Damay, F.; Le Denmat, D.; Sadoine, J.; Rode, J.; Frochot, V.; Letavernier, E.; Haymann, J. P.; Daudon, M. Hyperoxaluria Is Related to Whewellite and Hypercalciuria to Weddellite: What Happens When Crystalline Conversion Occurs? *Comptes Rendus Chim.* **2016**, *19* (11–12), 1492–1503.
- (13) Ihli, J.; Wang, Y. W.; Cantaert, B.; Kim, Y. Y.; Green, D. C.; Bomans, P. H. H.; Sommerdijk, N. A. J. M.; Meldrum, F. C. Precipitation of Amorphous Calcium Oxalate in Aqueous Solution. *Chem. Mater.* **2015**, *27* (11), 3999–4007.
- (14) H. Valido, I.; Rius-Bartra, J. M.; Boada, R.; Resina-Gallego, M.; Valiente, M.; López-Mesas, M. Characterization of Calcium Oxalate Hydrates and the Transformation Process. *ChemPhysChem* **2020**. <https://doi.org/10.1002/cphc.202000684>.
- (15) H. Valido, Iris; Resina-Gallego, Montserrat; Yousef, Ibraheem; Luque-Gálvez, Maria Pilar; Valiente, Manuel; López-Mesas, M. Calcium Oxalate Kidney Stones, Where Is the Organic Matter?: A Synchrotron Based Infrared Microspectroscopy Study. *J. Biophotonics* **2020**.
- (16) Rius, J.; Vallcorba, O.; Frontera, C.; Peral, I.; Crespi, A.; Miravittles, C. Application of Synchrotron Through-the-Substrate Microdiffraction to Crystals in Polished Thin Sections. *IUCrJ* **2015**, *2*, 452–463.
- (17) Fauth, F.; Peral, I.; Popescu, C.; Knapp, M. The New Material Science Powder Diffraction Beamline at ALBA Synchrotron. In *Powder Diffraction*; 2013.
- (18) Rodríguez-Carvajal, J. FULLPROF: A Program for Rietveld Refinement and Pattern Matching Analysis. *Abstr. Satell. Meet. Powder Diffr. XV Congr. IUCr*, **1990**.
- (19) Vallcorba, O.; Rius, J. D2Dplot: 2D X-Ray Diffraction Data Processing and Analysis for through-the-Substrate Microdiffraction. *J. Appl. Crystallogr.* **2019**, *52* (2), 478–484.
- (20) Conti, C.; Brambilla, L.; Colombo, C.; Dellasega, D.; Gatta, G. D.; Realini, M.; Zerbi, G. Stability and Transformation Mechanism of Weddellite Nanocrystals Studied by X-Ray Diffraction and Infrared Spectroscopy. *Phys. Chem. Chem. Phys.* **2010**, *12* (43), 14560–14566.

- (21) Tazzoli, V.; Domeneghetti, C. The Crystal Structures of Whewellite and Weddellite: Re-Examination and Comparison. *Am. Mineral.* **1980**, *65* (Table 1), 27–334.
- (22) Izatulina, A. R.; Gurzhiy, V. V.; Krzhizhanovskaya, M. G.; Kuz'Mina, M. A.; Leoni, M.; Frank-Kamenetskaya, O. V. Hydrated Calcium Oxalates: Crystal Structures, Thermal Stability, and Phase Evolution. *Cryst. Growth Des.* **2018**, *18* (9), 5465–5478.
- (23) Al-Atar, U.; Bokov, A. A.; Marshall, D.; Teichman, J. M. H.; Gates, B. D.; Ye, Z. G.; Branda, N. R. Mechanism of Calcium Oxalate Monohydrate Kidney Stones Formation: Layered Spherulitic Growth. *Chem. Mater.* **2010**, *22* (4), 1318–1329.
- (24) Widjonarko, N. Introduction to Advanced X-Ray Diffraction Techniques for Polymeric Thin Films. *Coatings* **2016**, *6* (4), 54.

Support Information of the manuscript:
“Discriminating the formation origin of calcium oxalate monohydrate in kidney stones via synchrotron microdiffraction”

Authors: Iris H. Valido^{a‡}, Victor Fuentes-Cebrian^{a‡}, Roberto Boada^a, Oriol Vallcorba^b, Montserrat Resina-Gallego^a, Manuel Valiente^a, Montserrat López-Mesas^{a*}

^a *Centre Grup de Tècniques de Separació en Química (GTS), Departament de Química, Universitat Autònoma de Barcelona, Facultat de Ciències. Edifici CN. 08193, Bellaterra, Barcelona, Spain*

^b *ALBA Synchrotron Light Source, Cerdanyola del Valle`s, Barcelona, Spain*

* *montserrat.lopez.mesas@uab.cat*

‡ *These authors contributed equally to this work*

S11: XRD fitting results

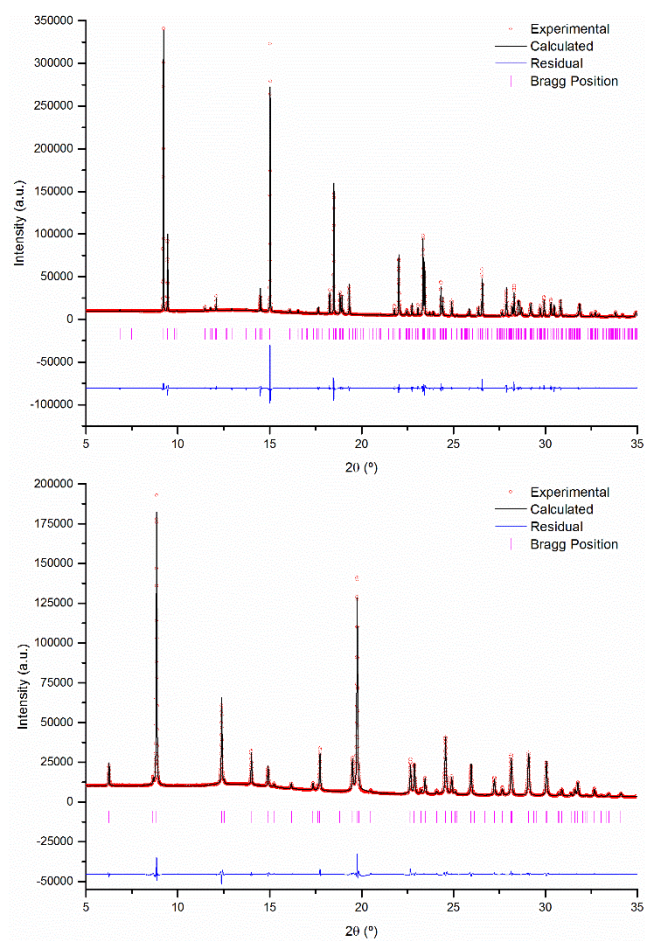


Figure 4. XRD pattern of the synthesized COD (top) and COM (bottom) after the profile matching

Table 5. XRD fitting results of the synthesized calcium oxalate hydrates reported in this work

	COD	COM
	Weddellite	Whewellite
Space group	I4/m, No. 87	P2 ₁ /c, No. 14
Bragg R-factor	0.638	0.155
Vol	1126.292 (0.018)	876.317 (0.005)
Rf-factor	0.336	0.114
Chi2	3.29	7.49
Zero-point	-0.0216 (0.0000)	-0.0139 (0.0000)
a	12.37721 (0.00011)	6.29536 (0.00002)
b	12.37721 (0.00011)	14.58995 (0.00004)
c	7.35200 (0.00008)	10.11883 (0.00004)
beta		109.45900 (0.00036)
Preferred orientation (G1)	0.15778 (0.00149)	-2.78239 (0.00118)
Eta_0	0.75207 (0.01670)	0.15082 (0.00968)
U	0.02937 (0.00393)	0.01967 (0.00089)
V	0.01025 (0.00118)	-0.00086 (0.00026)
W	0.00086 (0.00008)	0.00053 (0.00002)
X parameter	0.00040 (0.00075)	0.01296 (0.00048)
Asym1	-0.02351 (0.00095)	0.01763 (0.00108)
Asym2	0.00062 (0.00037)	0.00369 (0.0005)

S12: Examples of azimuthal plot

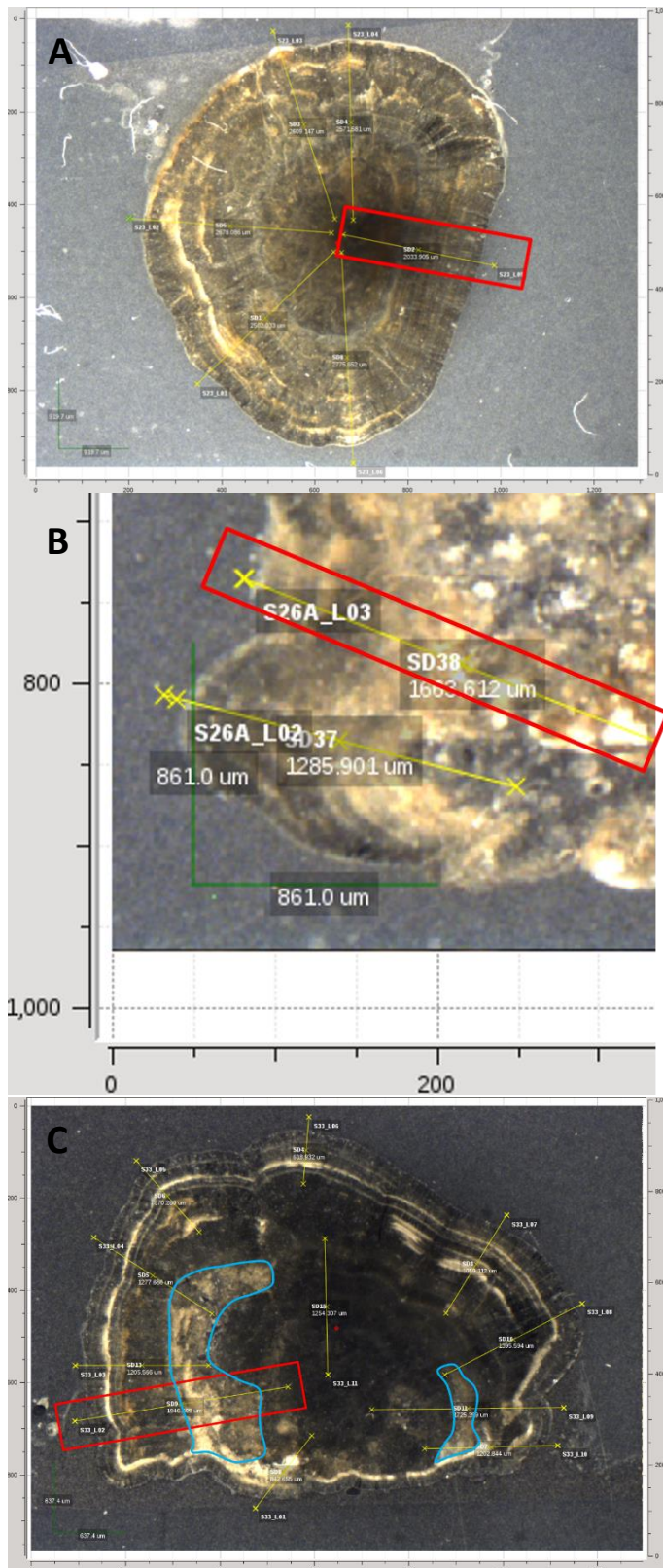


Figure 5. Images of the samples used as examples on the azimuthal Integration section of the manuscript, with the analyzed line highlighted in red. The kidney Stones are, S23 (top), S26A (middle) and S33 (bottom). In the S33, the regions marked in blue represent the ones suspected as TRA, by using the stereomicroscope, due to the differences in texture.

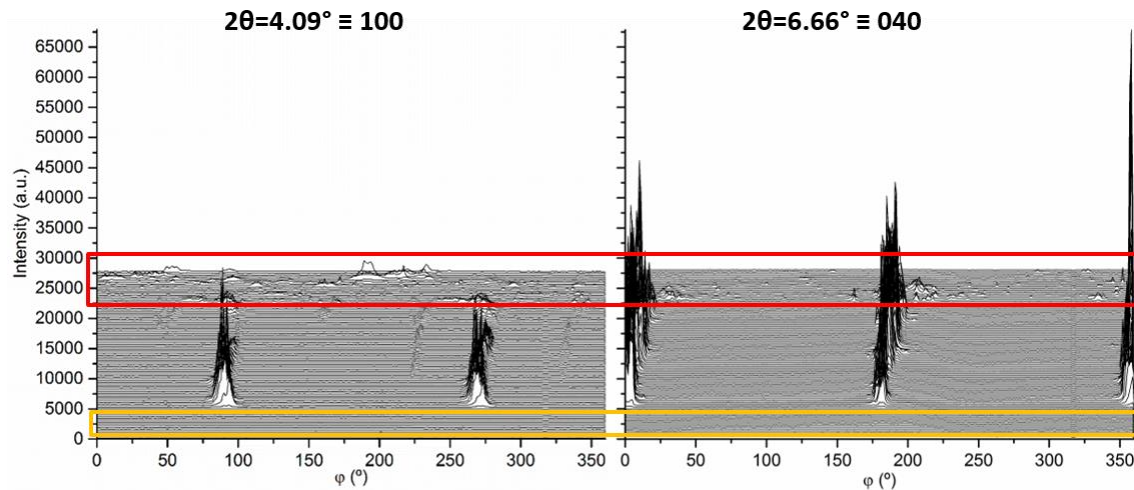


Figure 6. Representation of the azimuthal integration on the reflections (100) (Left) and (040) (Right) of a kidney classified as COM (S32). Orange square (bottom) mark the resin where the Stone is embedded, while red square represents the regions characterized as COM with organic matter. A clear orientation can be observed, since the pattern is repeated every 180° of the azimuthal angle.



Figure 7. Image of the analyzed line from sample S32 represented in Figure 6. Highlighted in red is the region described as COM with organic matter.

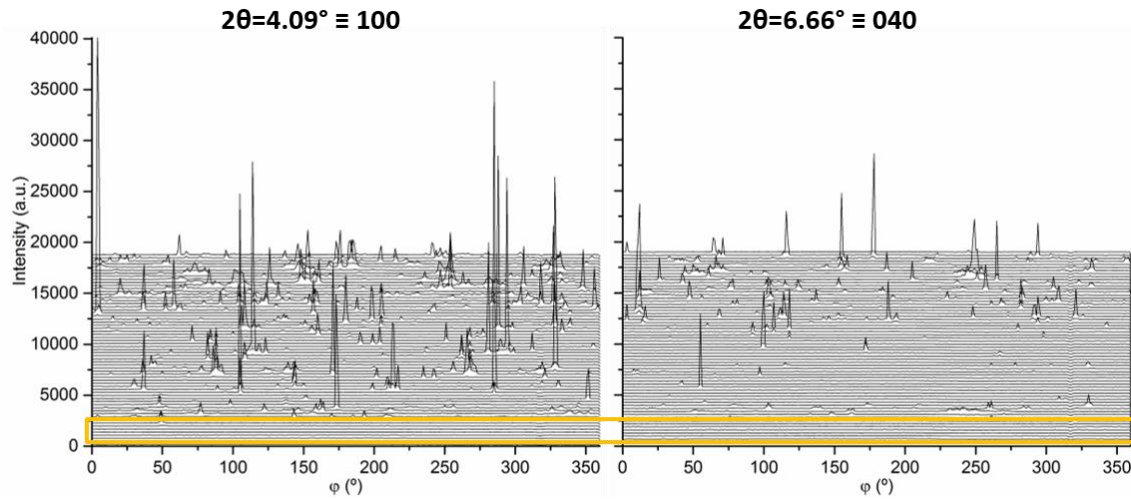


Figure 8. Representation of the azimuthal integration on the reflections (100) (Left) and (040) (Right) of a kidney classified as a transformed COD (S_{31}). Orange square (bottom) mark the resin where the Stone is embedded.



Figure 9. Image of the analyzed line from sample S_{31} represented in Figure 8, with the analyzed line highlighted in red.

S13: Multivariate Curve Resolution Analysis for the Transformation Monitoring

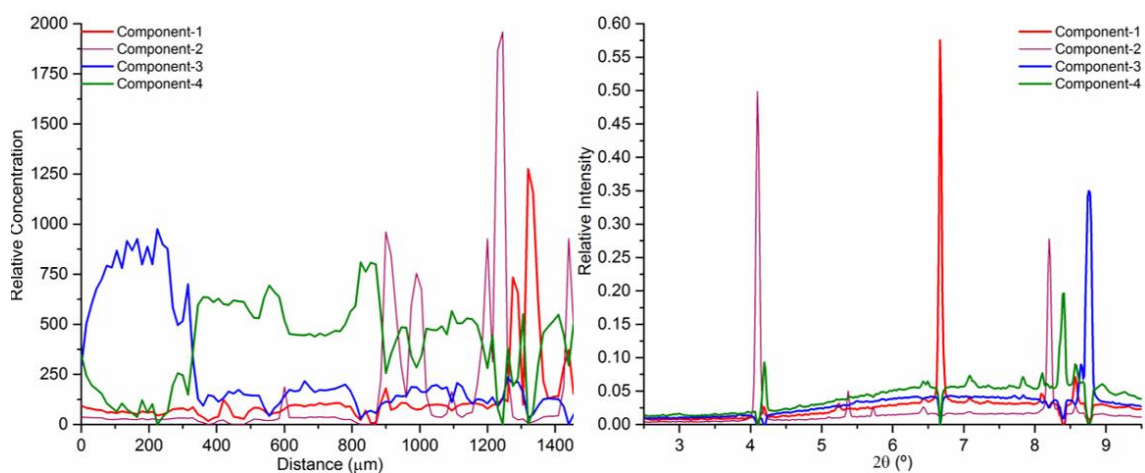



Figure 10. Example of MCR analysis of the diffractogram from a Correlated transformation from the superficial deposit of sample S24. In the left panel, the evolution of the four components along the diffraction analysis (from the surface to the inside of the stone) is represented, while on the right panel the simulated patterns for each component is shown.



Understanding the crystalline conversion of oxalocalcic kidney stones: effect of common urine inhibitors *in vitro*

Iris H. Valido, Victor Fuentes-Cebrian, Manuel Valiente, and Montserrat López-Mesas*

Centre Grup de Tecniques de Separacio en Quimica (GTS), Departament de Quimica, Universitat Autònoma de Barcelona, Facultat de Ciències, Edifici CN. 08193, Bellaterra, Barcelona, Spain

**Montserrat.lopez.mesas*

Unpublished



Understanding the crystalline conversion of oxalocalcic kidney stones: effect of common urine inhibitors *in vitro*

Iris H. Valido, Victor Fuentes-Cebrian, Manuel Valiente, Montserrat López-Mesas*

Centre Grup de Tècniques de Separació en Química (GTS), Departament de Química, Universitat Autònoma de Barcelona, Facultat de Ciències, Edifici CN, 08193, Belaterra, Spain.

KEYWORDS: *crystalline conversion; calcium oxalate dihydrate; calcium oxalate monohydrate; inhibitors; kidney stones*

ABSTRACT: Nephrolithiasis is a high prevalence and recurrence disease worldwide, specially the case of oxalocalcic nephroliths. Calcium oxalate (CaOx) kidney stones are classified into the dihydrate (COD) and monohydrate (COM), where the first type suffers a crystalline conversion into the second one in the urine. In this work, the effect of several CaOx inhibitors on the transformation of synthetic COD *in vitro* were studied. From the individual components, it was observed how phosphate promotes the transformation due to the presence of H_2PO_4^- , while citrate and magnesium did not show any effect, being phytate the best inhibitor of this process. Regarding the combinations of Ca and Mg with phosphate, the higher inhibitory capacity was shown by the Ca:Phos ratio 1:1 at pH 6, being related with the *in situ* formation of colloidal hydroxyapatite (HAP). Meanwhile, the loss of the inhibitory capacity has been related with the increase of H_2PO_4^- in the medium. Furthermore, it was determined that adding citrate to the Ca:Phos medium increases the inhibition, although it has no effect by itself, which could be associated to the capacity of citrate to promote HAP nucleation while inhibits its crystal growth. However, adding magnesium to the Ca:Phos medium decreases the inhibition potential, maybe due to its HAP crystallization inhibition capacity. Moreover, it was determined that the morphology of the crystals after the transformation in the different media is highly dependent of the medium composition, being citrate and colloidal HAP the ones that presented a higher influence. Finally, this study presents a first approach to better understand the process under the transformation and stabilization of COD in urine, which could help diagnose and treat patients with this type of nephroliths, opening the door to new studies in this area.

INTRODUCTION

Kidney stones are the cause of a painful disease with a high prevalence (1-20%) worldwide¹, being more present in men than in women and with an increasing recurrence of 30-50% in the next 5 to 10 years after the first episode^{2,3}. From the seven major groups of kidney stones classified by morpho-constitutional analysis guidelines^{4,5}, calcium oxalate hydrates represent the highest prevalent type (60-70%)⁵⁻⁷, and include the calcium oxalate monohydrate (COM) and the calcium oxalate dihydrated (COD) species. As it is well known, COD is the kinetically favorable species while COM is the thermodynamically stable one; hence, COD suffers a crystalline conversion into the monohydrated species⁸⁻¹⁰ but, even its high instability, COD is present in renal stones. The transformation process has been widely studied by thermogravimetry¹¹⁻¹³, under different humidity conditions^{8,10}, and it has been recently

monitored by infrared spectroscopy in an *in vitro* experiment in water¹⁴. The level of transformation is not only related to the contact time with the medium, but also with the presence of certain components, such as organic matter, as lipids¹⁵ or as hydroxyapatite (HAP)¹⁶ that could act as stabilizers.

On the other hand, urine is a complex matrix formed by a 95% of water and the other 5% is a mixture of organic and inorganic molecules¹⁷. A group of these molecules are known to be inhibitors of calcium oxalate nucleation and/or growth, such as citrate, magnesium and phytate^{18,19}. This project tries to determine if the common oxalocalcic inhibitors are also possible stabilizers of COD in solution, as well as if the *in situ* formation of hydroxyapatite could influence the crystalline conversion. Since COD and COM nephroliths are related to different pathologies (hypercalciuria and hyperoxaluria respectively)²⁰⁻²², it is

of great importance to determine which components participates in the stabilization or transformation of COD. This could help to find an adequate treatment for the patients, helping to prevent the recurrence^{20,22,23}.

MATERIALS AND METHODS

Reagents

Sodium dihydrogen phosphate dihydrate ($\text{NaH}_2\text{PO}_4 \cdot 2\text{H}_2\text{O}$, 99%), di-sodium hydrogen phosphate dihydrate ($\text{Na}_2\text{HPO}_4 \cdot 2\text{H}_2\text{O}$, 99%), sodium oxalate (Na_2Ox , 99%), tetra-sodium pyrophosphate decahydrate ($\text{Na}_4\text{Pyr} \cdot 10\text{H}_2\text{O}$, 99%), and magnesium chloride hexahydrate ($\text{MgCl}_2 \cdot 6\text{H}_2\text{O}$, 99%) were purchased from Panreac (Spain). Sodium citrate dihydrate ($\text{Na}_3\text{Cit} \cdot 2\text{H}_2\text{O}$, 99%) and calcium nitrate tetrahydrate ($\text{Ca}(\text{NO}_3)_2 \cdot 4\text{H}_2\text{O}$, 99%) were purchased from Merck (Germany) and calcium chloride (CaCl_2 , 98%) from Merk (Czech Republic). Phytic acid sodium salt (Phyt, >90%) was purchased from Sigma-Aldrich (USA). Solutions were prepared with “ultrapure Type 1” water (Milli-Q, Millipore, 18.2 mS cm^{-1}).

Synthesis of calcium oxalate hydrates

The synthesis of calcium oxalate hydrates used in this work was previously optimized in our research group¹⁴. Briefly, to prepare COM, equal volumes (250 mL) of Na_2Ox and CaCl_2 , both of 40 mM, were adjusted to pH 6 and simultaneously added (at 2.5 mL/min) into a crystallizer containing 1 L of degassed Milli-Q at 75°C and pH 6, with constant stirring. All the content was incubated for five hours at 37°C, after which it was vacuum filtered and washed with hot Milli-Q water; the obtained product was then aged for two days at 37°C. In the case of the preparation of the dihydrated species (COD), since it is the instable species, special care on the conditions needs to be taken in order to avoid the co-precipitation of COM or its transformation during the synthesis time. Hence, lower reaction time and temperature (solutions and material need to be cooled in an ice bath for, at least, 10 min previous use) were used, as well as inhibitors of calcium oxalate crystallization around 25°C (Na_3Cit and Na_4Pyr)²⁴. For the synthesis, 10 mL of CaCl_2 (40 mM) were added (1.7 mL/min) into 30 mL that contains Na_2Ox (13 mM), Na_3Cit (5 mM) and Na_4Pyr (0.2 mM), both at pH 6 and with constant stirring. After 5 min of reaction, the mixture was centrifuged (10 min, 2000 rpm) with washing steps of cold water (5 mL) and cold ethanol (5

mL) and the sediment was vacuum dried for one hour using a 0.22 μm GVPP Millipore filter. Since the COD crystals were thoroughly washed and dried after the synthesis, citrate or pyrophosphate do not remain on the formed crystals, as observed in the IR of the crystals (Support Information, SI1), so these compounds may not be considered as interferences in the transformation experiments.

Inhibitory media

To prepare the media for this study, the common calcium oxalate crystallization inhibitors in the urine were chosen, at their average and high concentration in healthy urine and at pH 6. The selected inhibitors were magnesium (2 and 4 mM), citrate (5 and 8 mM) and phytate (1.7 and 4.5 μM)^{18,25}. Additionally, phosphate was also evaluated as a possible inhibitor in a ratio 48:52 of $\text{Na}_2\text{HPO}_4 \cdot 2\text{H}_2\text{O}:\text{NaH}_2\text{PO}_4 \cdot 2\text{H}_2\text{O}$ (5 and 50 mM)²⁶ since hydroxyapatite ($\text{Ca}_5(\text{PO}_4)_3(\text{OH})$) is commonly found in COD stones and was previously found in stabilized crystals¹⁶. In order to determine if the inhibition effect is due to the phosphate alone or it is due to the formation of hydroxyapatite in situ, Ca:Phos in a concentration ratio 1:1 and 1:10 at pH 6 or pH 7 were also used on the transformation experiment. Moreover, it is important to determine if there is a synergistic effect between the different inhibitors, hence, the selected ratios were: Mg:Phos (1:2.5 and 1:25), Ca:Mg:Phos (1:2.5:1 and 1:2.5:10) and Ca:Cit:Phos (1:1:1 and 1:1:10); keeping Ca (5 mM), Mg (2 mM) and Cit (5 mM) in the average concentration and all tested at both pH.

Monitoring the transformation process

The crystalline conversion on different inhibitor solutions was performed following the process described in a previous study¹⁴, with variations on the medium used and the incubation times. Briefly, tubes with 10 mg of synthetic COD and 2 mL of the designated medium were incubated at 37°C and then two tubes of each medium (one sample and its duplicate) were filtered with a 0.22 μm GVPP Millipore filter (Durapore membrane filter) at the specified time. Since COD in an inhibitory medium required more time to be transformed than in water, the incubation time for each sample was optimized for each medium used. Moreover, incubation in water was used as a control to be able to compare between incubation sets. Crystals were analyzed using an Infrared Spectrophotometer Tensor 27, equipped with an Attenuated Total Reflectance

module (ATR-FTIR, Bruker, Ettlingen, Germany), with a resolution of 4 cm^{-1} . The IR data treatment was performed with the Unscrambler X[®] software. In order to monitor the crystalline conversion from COD to the monohydrated species, a Savitzky-Golay second derivative followed by a Maximum Normalization was applied, in the region from 1000 to 820 cm^{-1} , to the spectra collected at the different transformation stages. With the obtained data, a Multivariate Curve Resolution (MCR) analysis was performed to follow the loss of the peak corresponding to COD at 912 cm^{-1} ($\nu(\text{C}-\text{C}) + \delta(\text{COO})$ scissoring + $\nu(\text{M}-\text{O})$) and the appearance of the ones characteristic of COM at 883 cm^{-1} ($\delta(\text{COO})$ scissoring + $\nu(\text{M}-\text{O})$) and 948 cm^{-1} (water libration) with respect to time¹⁴. The half-time transformation ($t_{1/2}$) was determined by non-linear (sigmoidal) fitting, using Boltzmann Function on the representation of Relative Concentration of the MCR corresponding to the loss of the COD peak contribution, with the OriginLab software (OriginLab Corp., Northampton, MA, USA). An example of the MCR results and the performed fitting can be found in the Support Information (SI2). The relative $t_{1/2}$ of the transformation in each medium was calculated with respect to water, as shown in Eq. 1

$$\text{Rel. } t_{1/2} = t_{1/2}(\text{medium}) - t_{1/2}(\text{water}) \quad \text{Eq. 1}$$

Where $t_{1/2}(\text{medium})$ is the half-time transformation of the studied medium and $t_{1/2}(\text{water})$ is the half-time transformation of COD in water. If the result for Eq. 1 is negative, then the transformation is faster in the medium than in water and then the medium acts as a promoter, while if it is positive, the medium acts as an inhibitor.

To compare the morphology of the crystals before and after the crystalline conversion in the different media, Field Emission-Scanning Electron Microscope MERLIN (FE-SEM, Zeiss, 1.4 nm resolution, 1 kV , 4 pA - 100 nA probe current, 0.2 - 30 kV accelerating voltage) was used.

RESULTS AND DISCUSSION

Transformation controls performed in water

It is well known that the type, size and morphology of calcium oxalate crystals formed are determined by the conditions used for the crystallization and growth, being the most significant factors: temperature, pH, ionic strength and local environment^{27,28}. The SEM images of the synthesized COD crystallites, as well as the total

transformation in water at pH 6 and pH 7 are represented in Figure 1.

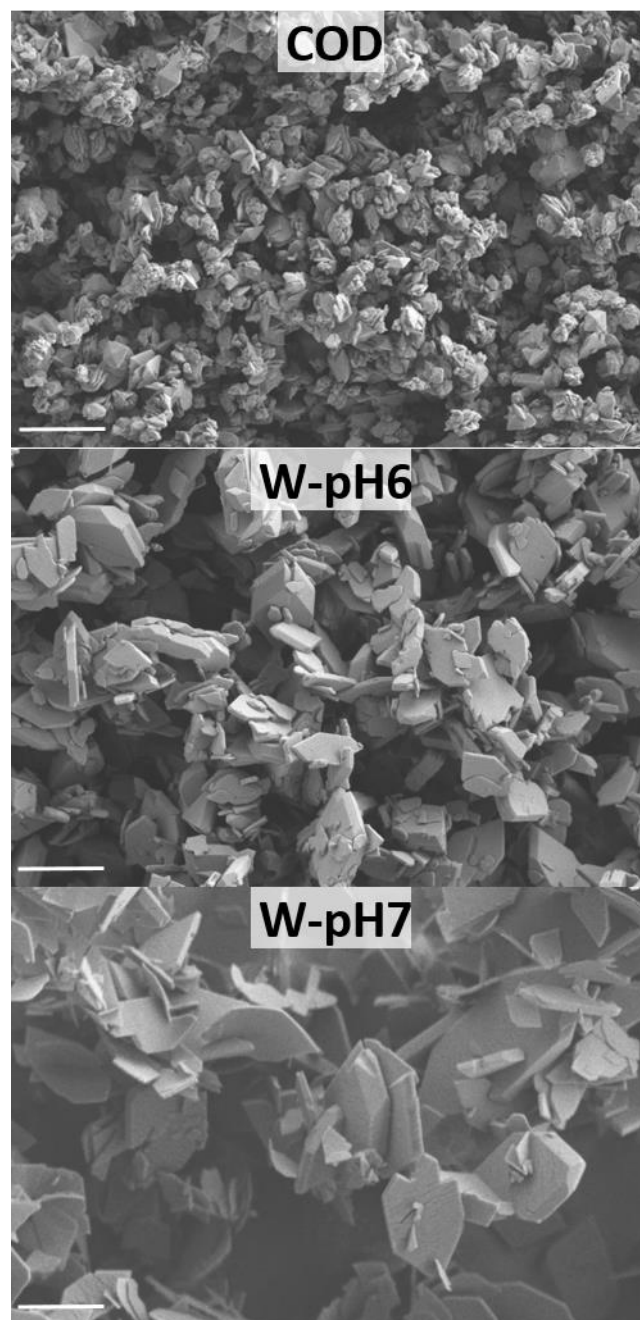


Figure 1. SEM images of synthetic COD (top), the same synthetic crystals after total transformation process in water at pH 6 (middle) and pH 7 (bottom). The scale bar represents $2\text{ }\mu\text{m}$.

As it has been described in a previous study¹⁴, COD crystallites are represented by rather flat tetragonal bipyramid shapes (Figure 1 (top)), while the product of the total transformation in water, at pH 6 and 37°C , corresponds to COM/whewellite with monoclinic shaped crystallites (Figure 1 (middle)). However, the crystallites after the total transformation in water at pH

7, are slightly bigger and flatter with respect to the ones transformed at pH 6 (Figure 1 (bottom)). Nevertheless, in both cases the transformed COD crystals have the typical morphology and crystal habit found on the direct formation of COM^{14,29}. Hence, the pH of the media affects the morphology of the transformed crystallites. These results were performed minimum by duplicate, and the resulting morphology was always the same. The $t_{1/2}$ of water can vary depending on the environment and synthetic conditions, being between 16–34 hours of incubation at the mentioned conditions in this study. Hence, the $t_{1/2}$ for the different experiments presented hereafter, are calculated with respect to the $t_{1/2}$ of COD in water, as control, by applying Eq.1.

Transformation process in different inhibitory media at pH 6

In order to compare the inhibitory potential of the different individual components, the Rel. $t_{1/2}$ are represented in Figure 2. It can be observed how phosphate presents a promoting factor while increasing the concentration, while citrate does not promote or inhibit the transformation by itself. However, when combining both in a 1:1 ratio, the promoting effect observed in phosphate is lost. This can be explained by the species present in solution. At pH 6, the majoritarian species of phosphate is dihydrogen phosphate (H_2PO_4^-); when citrate is added, there is a competition for calcium between H_2PO_4^- and HCit^{2-} , having the calcium citrate complexes a higher formation constant than the calcium phosphate ones^{30,31}, which means a higher capacity to bind to the calcium present on the crystal surfaces. The presence of magnesium in the medium increases the Rel. $t_{1/2}$, nevertheless, increasing its concentration does not increase the inhibitory capacity. Of the individual components studied, phytate presents the major inhibitory capacity, which increases at higher concentrations (COD was not totally transformed in the medium with 4.5 μM of phytate after five days of analysis). This effect could be related to the molecular structure of phytate (and the capacity of the phosphate groups on it to bind to the calcium of the crystals active sites³²). It has been previously reported that the alteration of the “zeolitic water” water channel in the COD structure is what promotes the structural rearrangement and, hence, the transformation process^{8,14}; which means that, by closing the zeolitic channel it is possible to stabilize the structure and retard the crystalline conversion.

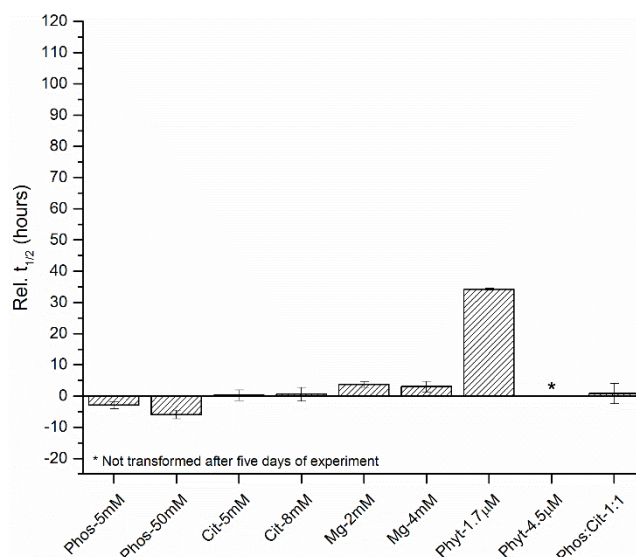


Figure 2. Normalized half-time transformation (Rel. $t_{1/2}$) of the different inhibition media studied with the common calcium oxalate inhibitors found in urine. Notice that positive values represent inhibitory potential, while negative values represent promoter potential.

The SEM images showing the product obtained, after the final time of the experiment in the different media are shown in Figure 3 (all sharing the same scale of 2 μm). The shape of the crystals in the phosphate medium resemble the ones described by Millan (2001)²⁹ as the “possible equilibrium shape of whewellite”, which could be due to the faster transformation time in comparison to water. Moreover, the crystal size decreases as the concentration of phosphate increases. The morphology of the crystals transformed in the citrate medium can be compared with the ones crystallized by Grases et. al. (2015)²⁵ in synthetic urine (180 mg/L of calcium, 35 mg/L of oxalate and 600 mg/L of citrate), and with the structure described by Millan (2001)²⁹ for the whewellite crystal growth in the presence of citric acid, which presents an elongated hexagonal platelets (being more fragmented in the case of the present study). As well as in the case of phosphate, the crystal size decreases as the citrate concentration increases. Similar behavior is observed when adding magnesium to the medium at average concentration (2 mM), however, when increasing the concentration to 4 mM, a diamond-shaped like crystals are observed, similar to the ones formed in the presence of bovine serum albumin (BSA), which binds to $\{12-1\}$ and/or $\{021\}$ faces reducing the crystal aspect ratio³³. That shape has been also reported as “rhomboid” with a dominant pinacoid $\{100\}$ and an additional facet $\{010\}$ in whewellite crystals found in Cactaceae³⁴. The crystal shape of the totally transformed

COD in presence of phytate at average concentration ($1.7 \mu\text{M}$) is similar to the one carried out in water. Meanwhile, when increasing the concentration to $4.5 \mu\text{M}$, there is a mixture of COM (with the “possible equilibrium shape” described by Millan (2001)²⁹ and also

observed in the incubation with phosphate) and COD crystals, being the COD crystals considerably smaller. This is caused by the lack of a total transformation, as can be observed in the graph of Figure 2.

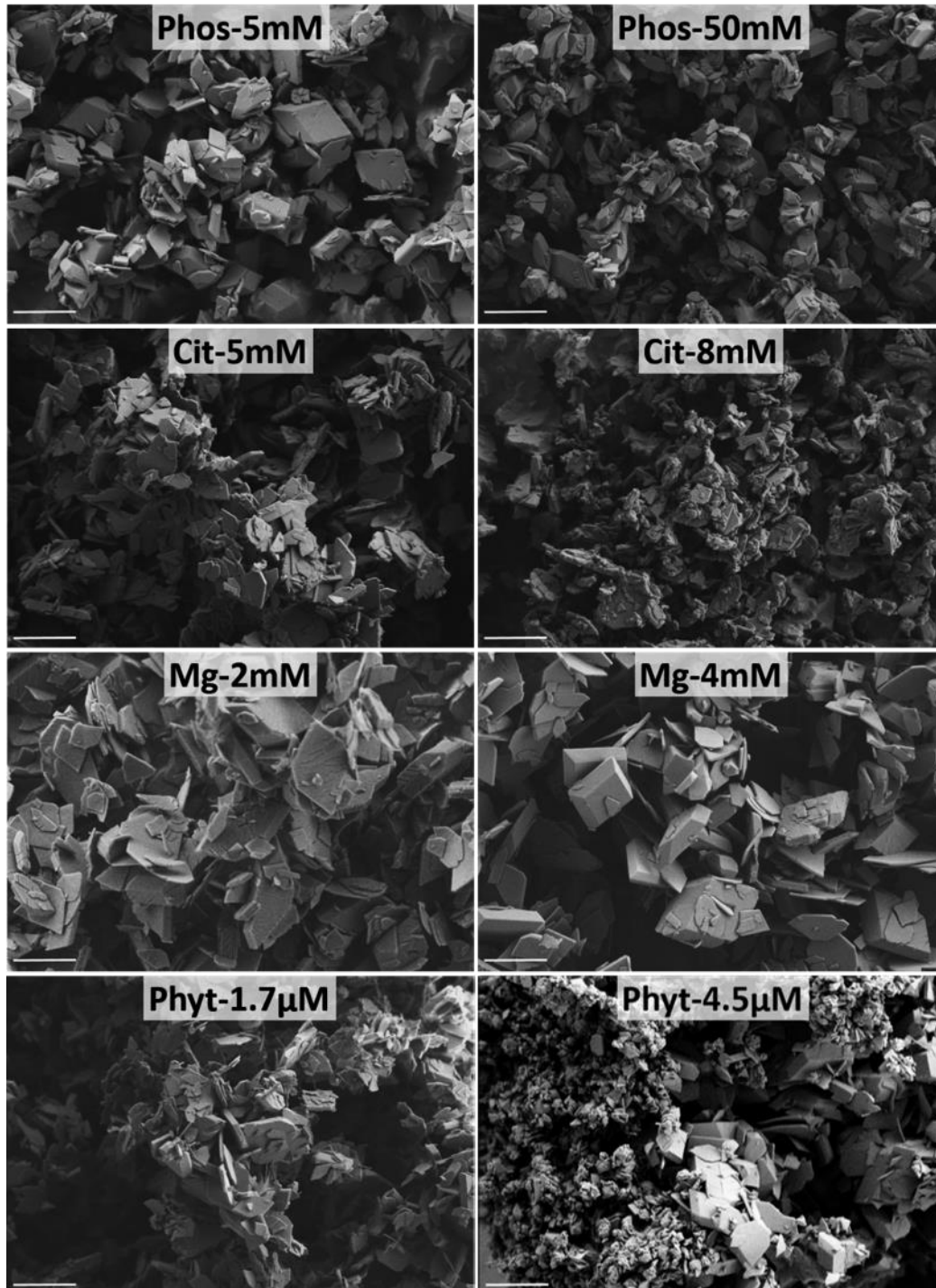


Figure 3. SEM images of the COD crystalline conversion obtained after the final time of the experiment in the studied media (phosphate, citrate, magnesium and phytate) at the average (left) and high (right) concentrations in urine. The scale bar represents $2 \mu\text{m}$.

Influence of phosphate combined with calcium or magnesium at different pH

It is common to find phosphate in CaOx kidney stones, usually as hydroxyapatite^{4,5}. In the case of COM, it is a promoter of the nucleation in the form of Randall's Plaques, while in the case of COD it is usually found between crystals or in the nucleus of the stone. In a study performed by Grases et. al. (1990)³⁵ it was observed that the presence of colloidal phosphate in the medium favored the formation of COD crystals, being of larger size when working at pH 7.2. Moreover, in a previous study it was observed the presence of hydroxyapatite in stabilized COD crystallites in kidney stones analyzed by SR- μ XRD¹⁶. However, in the previous section it was found that phosphate acts as promoter of the transformation process and not as inhibitor. Since urine is a complex medium, and the relationship between phosphate and COD is not clear, the combination of calcium and magnesium with phosphate at two different pH values were studied, keeping the concentrations of Ca (5 mM) and Mg (2 mM) constants and at two different concentrations of phosphate, the average (5 mM) and the highest one (50 mM).

The Rel. $t_{1/2}$ of these combinations are shown in Figure 4, where it can be observed that the ratio 1:1 for Ca:Phos at pH 6 (Ca:Phos-pH6-1:1) is the combination that presents the highest inhibitory capacity, which could be explained by the *in situ* formation of colloidal calcium phosphate, which according to the species equilibrium diagram (Support Information, SI3, Figure 4) corresponds to HAP. Moreover, the characteristic bands corresponding to HAP formed by the crystalline conversion of amorphous calcium phosphate (ACP)³⁶ can be observed on the spectrum of the total transformation (Figure 5 (left panel)), which proves that this component is present in the crystals. The inhibitory effect is considerably lost when increasing the concentration of phosphate in the medium Ca:Phos-pH6-1:10, which could be related once again with the presence of H_2PO_4^- and the absence of colloidal HAP, as it is shown in the equilibrium diagram in Support Information, SI3, Figure 5). Furthermore, the observed bands on the total transformation of COD in that medium are in agreement with the ones described by Sánchez-Enríquez et. al (2013)³⁷ for the $\text{Ca}(\text{H}_2\text{PO}_4)_2 \cdot \text{H}_2\text{O}$ and not with the commercial $\text{CaHPO}_4 \cdot \text{H}_2\text{O}$ (Figure 5 (right panel)), which means that part of the H_2PO_4^- interacts with the crystals but do not inhibit their

transformation. It is important to notice that the studied media are synthetic and only formed by calcium and phosphate, making possible the identification of the phosphate species by IR.

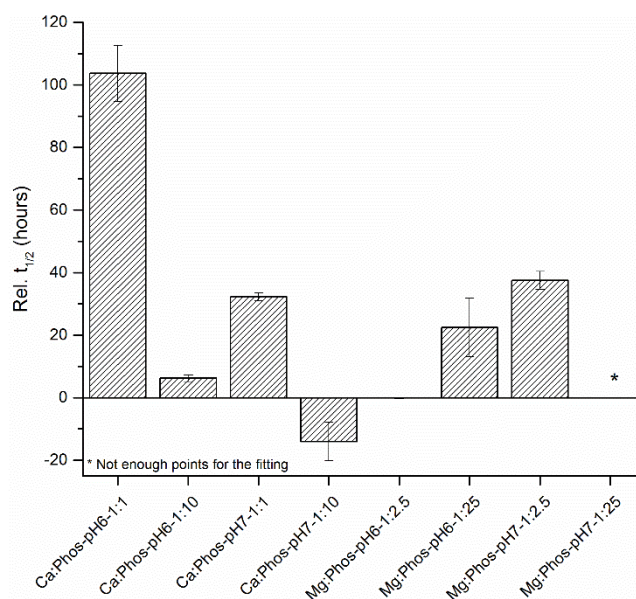


Figure 4. Normalized half-time transformation (Rel. $t_{1/2}$) of the different inhibition mediums studied with the ratios of Ca and Mg with phosphate. Notice that positive values represent inhibitory potential, while negative values represent promoter potential.

There is also a loss in the inhibitory effect when the pH is increased from 6 to 7 at both phosphate concentration, which could be related to the higher stability of HAP at pH 7. Furthermore, as has been explained previously, the promoting effect observed when the phosphate is increased at pH 7 is also related to the higher amount of H_2PO_4^- . As can be observed in Figure 6, the spectra of the total transformation, on the Ca:Phos media at pH 7, present the characteristic bands of HAP nanoparticles as described by Sadat-Shojai (2009)³⁸, which appear at similar wavenumbers than the commercial HAP but with different ratios. These findings corroborate that colloidal HAP acts as a COD stabilizer in aqueous media. In the case of the Mg:Phos-pH6-1:2.5, there is no inhibition or promotion of the transformation due to the formation of magnesium phosphate complexes in the medium (Support Information, SI4, Figure 6). When the phosphate concentration is increased (ratio 1:25), there is some inhibitory effect, which could be associated to the formation of colloidal newberyite, a magnesium phosphate mineral ($\text{MgHPO}_4 \cdot 3\text{H}_2\text{O}$) also found in renal stones³⁹, and formed between pH 6 and 9 (Support

Information, SI4, Figure 7), which could also explain the higher inhibition at pH 7 (data for incubation at pH 7 not shown in Figure 4 for the lack of results for the fitting, but the results of the ATR-FTIR spectra showed a higher inhibitory effect than at pH 6 (it did not presented the characteristic, and well defined, five bands of the OH between 3500-300 cm^{-1} , neither the peaks corresponding to COM at 948 and 883 cm^{-1}). In

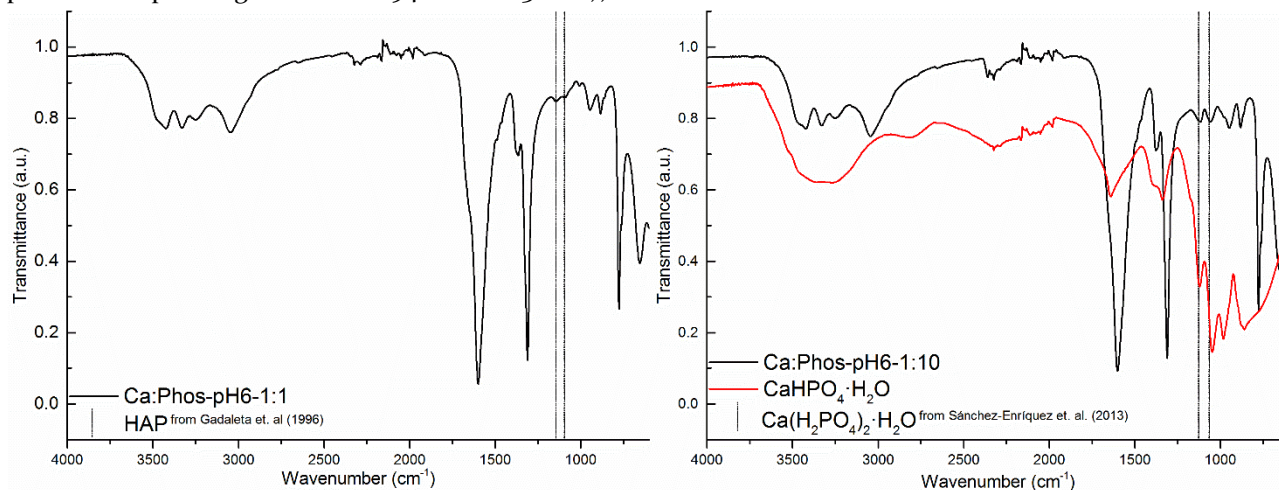


Figure 5. ATR-FTIR spectrum of the total transformation of COD on: Ca:Phos-pH6-1:1 medium, with vertical dot lines representing the characteristic bands of HAP formed from the conversion of ACP as described by Gadaleta et al. (1996)³⁶ (left panel); and Ca:Phos-pH6-1:10 medium and the commercial $\text{CaHPO}_4 \cdot \text{H}_2\text{O}$, with vertical dot lines representing the characteristic bands of $\text{Ca}(\text{H}_2\text{PO}_4)_2 \cdot \text{H}_2\text{O}$ as described by Sánchez-Enríquez et al. (2013)³⁷ (right panel).

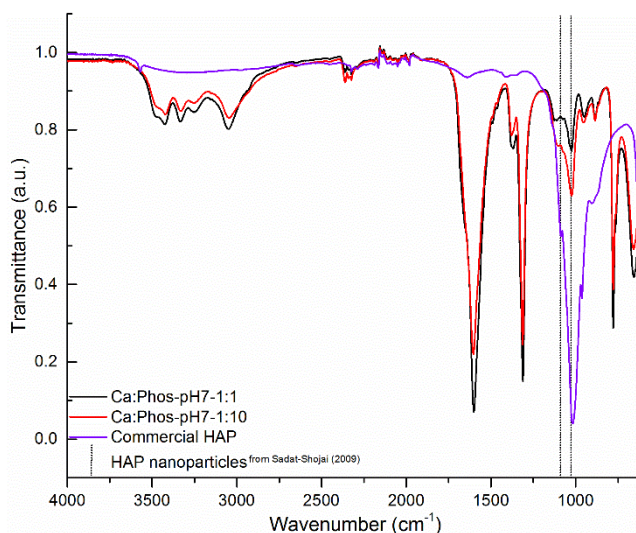


Figure 6. ATR-FTIR spectra of the total transformation of COD on the Ca:Phos-pH7-1:1 (black) and Ca:Phos-pH7-1:10 (red) media, and the commercial HAP (purple), with vertical dot lines representing the characteristic bands of HAP nanoparticles as described by Sadat-Shojai (2009)³⁸

Regarding the morphologies of the crystals formed after the total transformation of COD in the media

the equilibrium diagram (Support Information, SI4, Figure 7), newberyite appears around pH 6.2 to pH 8.5, while other authors reports its stability under physiological conditions around or below pH 6^{40,41}, hence, the presented hypothesis needs further experiment to prove the formation of this species when working in the conditions of the present study.

combining calcium or magnesium with phosphate, the results are shown in Figure 7. As can be observed, in the ratio Ca:Phos-pH6-1:10 the crystallites present similar morphology and size than the incubations with just 5 mM of phosphate (Figure 3), being caused, as explained before, by the presence of H_2PO_4^- . The morphology observed in the ratio Ca:Phos-pH7-1:10 is similar to the previous one, with the addition of the presence of amorphous deposits, which could indicate the presence of HAP, as can be seen in the IR spectra on Figure 6. Regarding the Ca:Phos 1:1 ratios, crystals are elongated hexagonal platelets, like the ones observed in the previous section in the incubations with citrate, being of smaller size at pH 6 than pH 7. For the ratios of Mg:Phos at pH 6, the observed morphology is similar to the one described by Millan (2001)²⁹ as the possible equilibrium shape found in natural samples, with the only difference of the presence of smaller crystallites for the 1:25 ratio. At pH 7, the Mg:Phos ratio 1:2.5 present a mixture of few larger crystals, with similar morphology than at pH 6, with the smallest crystals observed in these combinations. However, the ratio 1:25 does not present a clear whewellite shape.

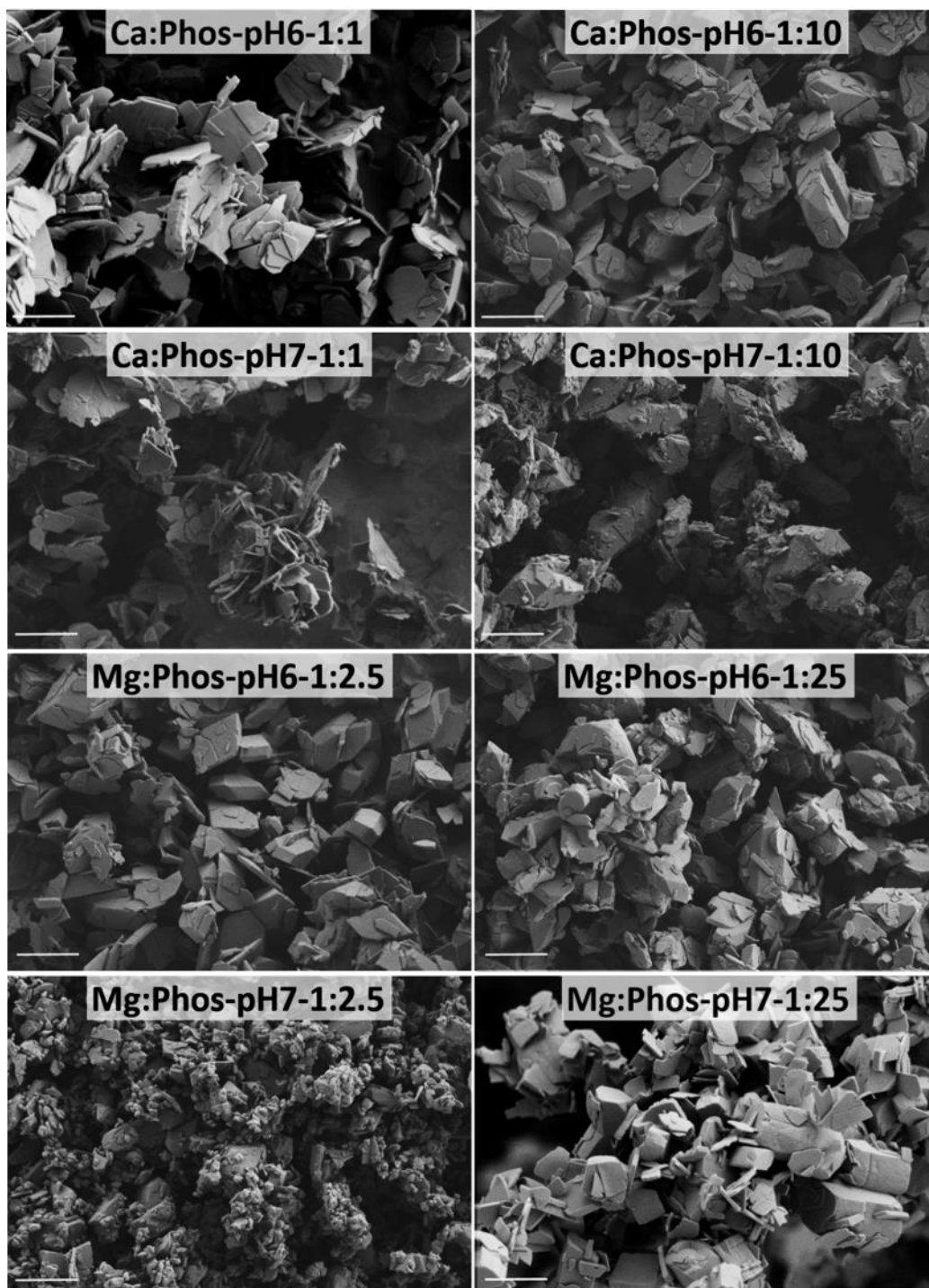


Figure 7. Figure 7. SEM images of synthetic COD totally transformed in media with calcium (5 mM) or magnesium (2 mM) with phosphate at concentrations 5 mM (left) and 50 mM (right) at pH 6 or 7 (as specified). The scale bar represents 2 μm.

Influence of the Ca:Phos ratio combined with magnesium or citrate at two different pH

Urine is a complex medium, so synergistic effects between compounds are expected but, are those positive or negative on the stabilization of COD? In order to evaluate this possibility, the results of the Rel. $t_{1/2}$ for the incubations of COD with different combinations of

calcium and phosphate with magnesium or citrate are shown in Figure 8.

The Ca:Mg:Phos-pH6-1:2.5:1 combination shows a good inhibition effect, despite that, if it is compared with the same ratio without magnesium (Figure 4), some of this effect is lost. This is due to the fact that

magnesium inhibits the crystallization of HAP by being adsorbed in the surface of its precursor, the ACP⁴²⁻⁴⁴.

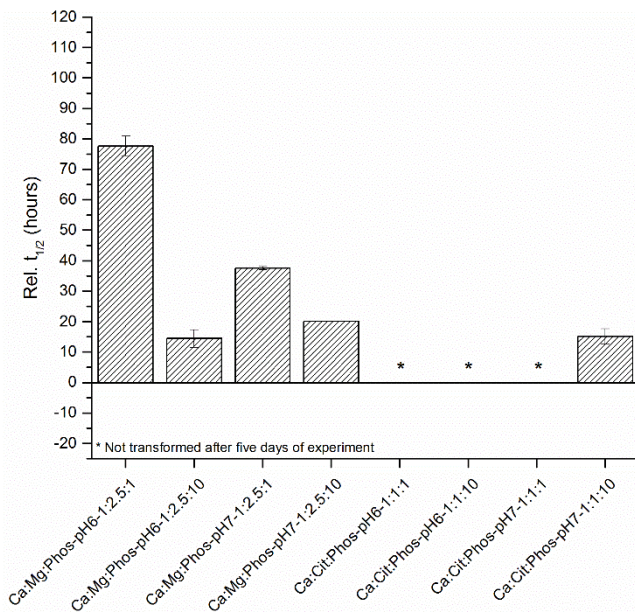


Figure 8. Normalized half-time transformation (Rel. $t_{1/2}$) of the different inhibition media studied for possible synergistic effect between inhibitors.

When the pH is increased to 7, no difference is observed between adding or not magnesium, due to the higher stability of the formed HAP in combination with the formation of newberyite. The presence of HAP nanoparticles can be observed on the IR spectra of the total transformed COD on Ca:Mg:Phos-pH7-1:2.5:1 (Figure 9(left panel)). On the other hand, when the phosphate concentration is increased, there is an improvement in the inhibition effect when comparing to the Ca:Phos-pH6-1:1:10, being caused by the magnesium complexation with the excess of phosphate, avoiding the presence of free H_2PO_4^- in the medium. When only adding citrate to the medium (Figure 2) no effect was observed, while when adding it to the Ca:Phos mixture, there is a remarkable improvement of the inhibition (Rel. $t_{1/2}$) while compared with its absence. This is caused by the fact that citrate is a promoter of HAP nucleation while it inhibits its crystal growth^{45,46}, while it also aid in the stabilization of HAP hydrocolloids⁴⁶, which can be observed on the IR spectra of these media (Figure 9(right panel)), which have the characteristic bands of the HAP formed by the crystalline conversion of ACP³⁶. These findings could mean that the hydroxyapatite involved in the stabilization of COD (found stabilized kidney stones COD crystallites¹⁶), are small colloids of certain characteristics.

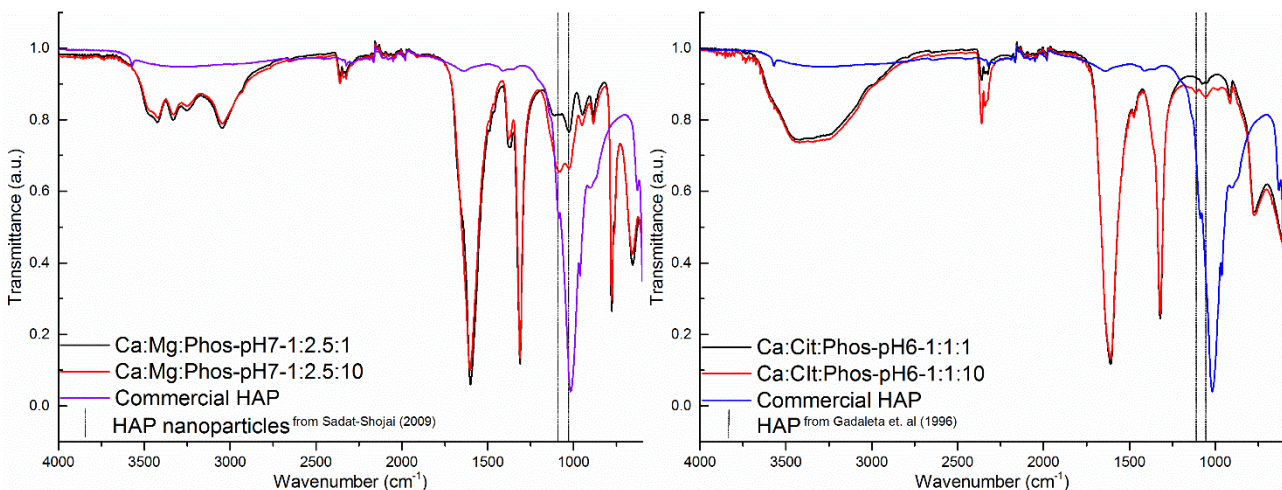


Figure 9. ATR-FTIR spectrum of the total transformation of COD on: the Ca:Mg:Phos medium at pH 7, with vertical dot lines representing the characteristic bands of HAP nanoparticles as described by Sadat-Shojai (2009)³⁸(left panel); and the Ca:Cit:Phos medium at pH 6 formed from the conversion of amorphous calcium phosphate (ACP) as described by Gadaleta et. al. (1996)³⁶ (right panel).

Regarding the crystal morphology of the transformations on the combination media, the SEM images are illustrated in Figure 10. As can be noticed, the Ca:Cit:Phos ratios present mostly COD crystals, with

the exception of the Ca:Cit:Phos-pH7-1:1:10, which showed better inhibition effect comparing with the same combination but without citrate (Figure 4 and Figure 8), and presents similar crystals morphology than

the ones transformed in the 8 mM citrate medium (Figure 3), which, as was explained before, could be related with the presence of citrate and its interaction with the excess phosphate in the medium. The incubations performed in combination with magnesium show similar morphologies that the ones carried out without calcium (Mg:Phos) and shown in Figure 7, with

the exception of the combination Ca:Mg:Phos-pH6-1:1:1 that are similar to the incubations of the same ratio without magnesium, which means that it does not play a role, or it is not as significant as the Ca:Phos combination, on the crystalline conversion in the mentioned media

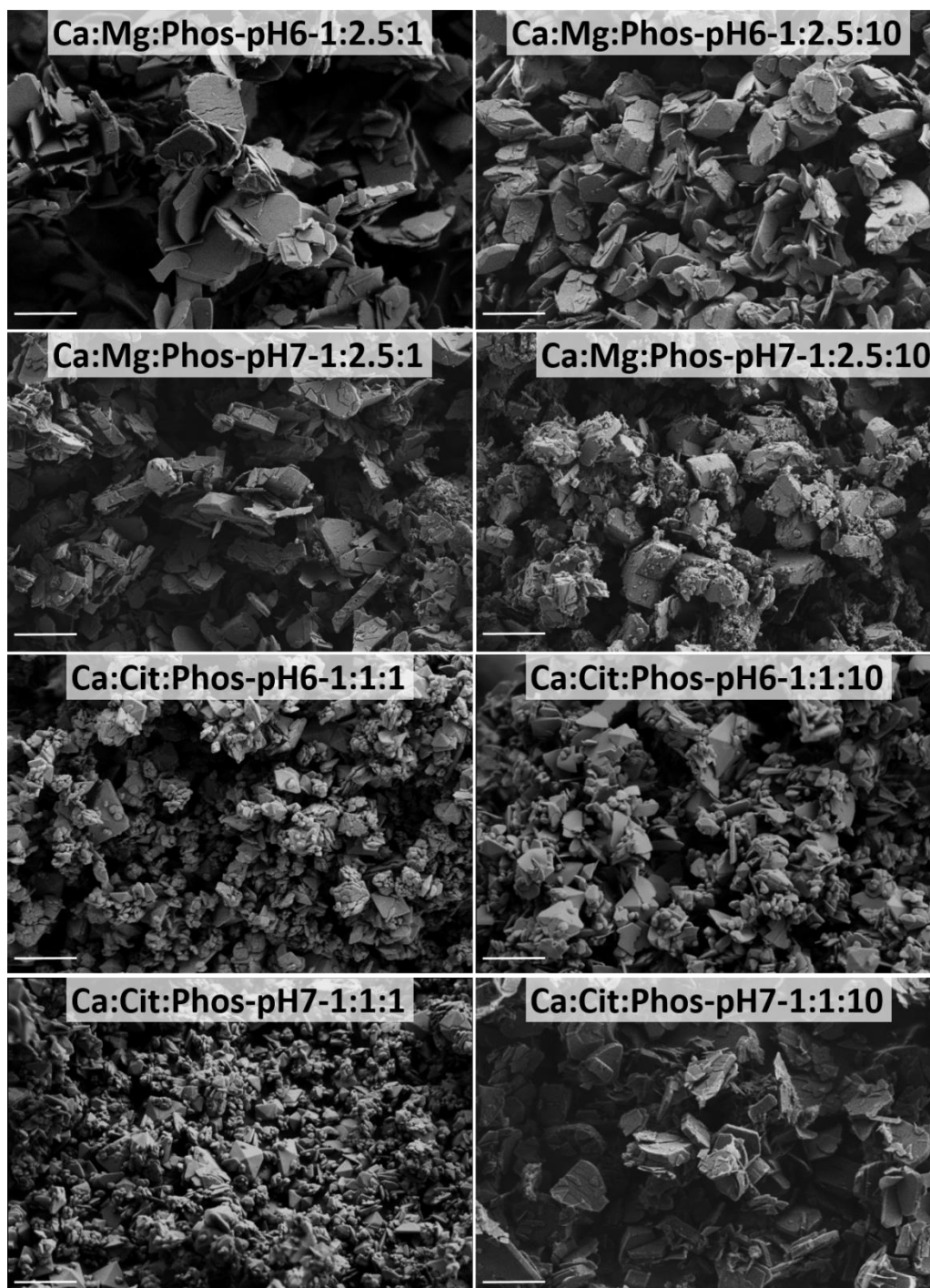


Figure 10. SEM images of the inhibitors combination to determine the possible synergistic effect, being calcium (5 mM), magnesium (2 mM), citrate (5 mM) and phosphate at average (5 mM) (left) and high (50 mM) concentrations, all studied at pH 6 and pH 7. The scale bar represent 2 μm .

CONCLUSIONS

It is possible to determine the half-time transformation ($t_{1/2}$) of COD in different media by fitting the MCR curves of the ATR-FTIR spectra, which allows monitoring the promotor or inhibitory effect of the species on the media. The use of individual components showed how phytate presents the major inhibitory capacity, maybe due to its molecular structure, and how phosphate promotes the transformation of COD, due to the presence of H_2PO_4^- in the medium (as shows the species diagram). To determine if hydroxyapatite was the responsible of the stabilization of COD reported in previous studies⁶, the combination of Ca:Phos at the two different pH studied, presented a major inhibitory effect in the 1:1 ratio and at pH 6. The results of the Ca:Phos combinations with magnesium and citrate, indicate that the small HAP colloids are the responsible of this stabilization, since the HAP formation is inhibited by magnesium but citrate only inhibits its growth, being this the cause of the HAP hydrocolloid stabilization. This research represents the first step to try to understand the presence of the unstable calcium oxalate dihydrate species (COD) in complex media such as urine, which could help on the diagnosis and treatment of patients with oxalocalcic renal stones.

ASSOCIATED CONTENT

Supporting Information.

S11: Comparison of the FTIR spectra of COD and the two inhibitors used on its synthesis, sodium pyrophosphate decahydrate ($\text{Na}_4\text{P}_2\text{O}_7 \cdot 10\text{H}_2\text{O}$) and sodium citrate dihydrate ($\text{Na}_3\text{C}_6\text{H}_5\text{O}_7 \cdot 2\text{H}_2\text{O}$).

S12: Example of the Multivariate Curve Resolution (MCR) analysis and the performed non-linear (sigmoidal) fitting.

S13: Equilibrium diagram of the Ca:Phos medium

S14: Equilibrium diagram of the Mg:Phos medium

AUTHOR INFORMATION

Corresponding Author

* montserrat.lopez.mesas@uab.cat

Author Contributions

The manuscript was written through contributions of all authors. / All authors have given approval to the final version of the manuscript.

ACKNOWLEDGMENT

The authors want to acknowledge the financial support from the Ministerio de Economía y Competitividad (Spanish Project CMT 2015-65414-C2-1-R). Iris H. Valido acknowledges funding support from the Universitat Autònoma de Barcelona (PIF-2016 grant). All the authors are grateful to the Serveis de Suport a la Investigació of the UAB (SAQ and SM).

ABBREVIATIONS

ATR-FTIR, Attenuated Total Reflectance Fourier Transform Infrared spectroscopy; CaOx, calcium oxalate hydrates; Cit, citrate; COD, calcium oxalate dihydrate; COM, calcium oxalate monohydrate; HAP; hydroxyapatite; IR, infrared; MCR, Multivariate Curve Resolution; Ox, oxalate; Phos, phosphate; Phyt, phytate; $t_{1/2}$, half-time.

REFERENCES

- (1) Türk, C.; Neisius, A.; Petrik, A.; Seitz, C.; Skolarikos, A.; Thomas, K. EAU Guidelines on Urolithiasis. *Eur. Assoc. Urol.* **2018**, *69* (3), 475–482.
- (2) Curhan, G. C. Epidemiology of Stone Disease. *Urol. Clin. North Am.* **2007**, *34* (3), 287–293.
- (3) Alelign, T.; Petros, B. Kidney Stone Disease: An Update on Current Concepts. *Adv. Urol.* **2018**, Feb 4.
- (4) Daudon, M.; Dessombz, A.; Frochot, V.; Letavernier, E.; Haymann, J. P.; Jungers, P.; Bazin, D. Comprehensive Morpho-Constitutional Analysis of Urinary Stones Improves Etiological Diagnosis and Therapeutic Strategy of Nephrolithiasis. *Comptes Rendus Chim.* **2016**, *19* (11–12), 1470–1491.
- (5) Grases, F.; Costa-Bauzá, A.; Ramis, M.; Montesinos, V.; Conte, A. Simple Classification of Renal Calculi Closely Related to Their Micromorphology and Etiology. *Clin. Chim. Acta* **2002**, *322* (1–2), 29–36.
- (6) Worcester, E. M. Pathophysiology of Kidney Stone Formation. In *Nutritional and Medical Management of Kidney Stones*; Han, H., Mutter, W. P., Nasser, S., Eds.; Springer International Publishing: Cham, 2019; pp 21–42.
- (7) Sakhaee, K. Kidney Stones 2019: Epidemiology, Clinical Pathophysiology, and Treatment. *Intern. Med. Gd. Rounds* **2019**.
- (8) Conti, C.; Brambilla, L.; Colombo, C.; Dellasega, D.; Gatta, G. D.; Realini, M.; Zerbi, G. Stability and Transformation Mechanism of Weddellite Nanocrystals

- Studied by X-Ray Diffraction and Infrared Spectroscopy. *Phys. Chem. Chem. Phys.* **2010**, *12* (43), 14560–14566.
- (9) Rampazzi, L. Calcium Oxalate Films on Works of Art: A Review. *J. Cult. Herit.* **2019**.
- (10) Conti, C.; Casati, M.; Colombo, C.; Realini, M.; Brambilla, L.; Zerbi, G. Phase Transformation of Calcium Oxalate Dihydrate-Monohydrate: Effects of Relative Humidity and New Spectroscopic Data. *Spectrochim. Acta - Part A Mol. Biomol. Spectrosc.* **2014**, *128*, 413–419.
- (11) Christy, A. A.; Nodland, E.; Burnham, A. K.; Kvalheim, O. M.; Dahl, B. Determination of Kinetic Parameters for the Dehydration of Calcium Oxalate Monohydrate by Diffuse Reflectance FT-IR Spectroscopy. *Appl. Spectrosc.* **1994**, *48* (5), 561–568.
- (12) Kloprogge, J. T.; Boström, T. E.; Weier, M. L. In Situ Observation of the Thermal Decomposition of Weddellite by Heating Stage Environmental Scanning Electron Microscopy. *Am. Mineral.* **2004**, *89* (1), 245–248.
- (13) Frost, R. L.; Weier, M. L. Thermal Treatment of Whewellite—a Thermal Analysis and Raman Spectroscopic Study. *Thermochim. Acta* **2004**, *409* (1), 79–85.
- (14) H. Valido, Iris; Rius-Bartra, Joaquim M^a; Boada, Roberto; Resina-Gallego, Montserrat; Valiente, Manuel; Lopez-Mesas, M. Characterization of Calcium Oxalate Hydrates and the Transformation Process. *ChemPhysChem* **2020**.
- (15) H. Valido, Iris; Resina-Gallego, Montserrat; Yousef, Ibraheem; Luque-Gálvez, María Pilar; Valiente, Manuel; López-Mesas, M. Calcium Oxalate Kidney Stones, Where Is the Organic Matter?: A Synchrotron Based Infrared Microspectroscopy Study. *J. Biophotonics* **2020**.
- (16) H. Valido, Iris; Fuentes-Cebrian, Victor; Boada, Roberto; Vallcorba, Oriol; Resina-Gallego, Montserrat; Valiente, Manuel; López-Mesas, M. Discriminating the Formation Origin of Calcium Oxalate Monohydrate in Kidney Stones via Synchrotron Microdiffraction. *Unpublished*.
- (17) Sarigul, N.; Korkmaz, F.; Kurultak, İ. A New Artificial Urine Protocol to Better Imitate Human Urine. *Sci. Rep.* **2019**, *9* (1), 1–11.
- (18) Basavaraj, D. R.; Biyani, C. S.; Browning, A. J.; Cartledge, J. J. The Role of Urinary Kidney Stone Inhibitors and Promoters in the Pathogenesis of Calcium Containing Renal Stones{A Figure Is Presented}. *EAU-EBU Updat. Ser.* **2007**, *5* (3), 126–136.
- (19) Muñoz, J. A.; Valiente, M. Effects of Trace Metals on the Inhibition of Calcium Oxalate Crystallization. *Urol. Res.* **2005**, *33* (4), 267–272.
- (20) Bazin, D.; Leroy, C.; Tielens, F.; Bonhomme, C.; Bonhomme-Coury, L.; Damay, F.; Le Denmat, D.; Sadoine, J.; Rode, J.; Frochot, V.; Letavernier, E.; Haymann, J. P.; Daudon, M. Hyperoxaluria Is Related to Whewellite and Hypercalciuria to Weddellite: What Happens When Crystalline Conversion Occurs? *Comptes Rendus Chim.* **2016**, *19* (11–12), 1492–1503.
- (21) Grases, F.; Costa-Bauza, A.; Prieto, R. M. Renal Lithiasis and Nutrition. *Nutr. J.* **2006**, *5* (1), 1–7.
- (22) Daudon, M.; Jungers, P.; Bazin, D.; Williams, J. C. Recurrence Rates of Urinary Calculi According to Stone Composition and Morphology. *Urolithiasis* **2018**, *46* (5), 459–470.
- (23) Daudon, M.; Jungers, P.; Bazin, D. Stone Morphology: Implication for Pathogenesis. *AIP Conf. Proc.* **2008**, *1049*, 199–215.
- (24) Yuzawa, M.; Tozuka, K.; Tokue, A. Effect of Citrate and Pyrophosphate on the Stability of Calcium Oxalate Dihydrate. *Urol. Res.* **1998**, *26* (2), 83–88.
- (25) Grases, F.; Rodriguez, A.; Costa-Bauza, A. Efficacy of Mixtures of Magnesium, Citrate and Phytate as Calcium Oxalate Crystallization Inhibitors in Urine. *J. Urol.* **2015**, *194* (3), 812–819.
- (26) Muñoz, J. A.; López-Mesas, M.; Valiente, M. Inhibitors of Oxalocalcic Lithiasis: Effects of Their Interactions on Calcium Oxalate Crystallization. *Urology* **2012**, *80* (5), 1163.e13–1163.e18.
- (27) Qiu, S. R.; Wierzbicki, A.; Salter, E. A.; Zepeda, S.; Orme, C. A.; Hoyer, J. R.; Nancollas, G. H.; Cody, A. M.; De Yoreo, J. J. Modulation of Calcium Oxalate Monohydrate Crystallization by Citrate through Selective Binding to Atomic Steps. *J. Am. Chem. Soc.* **2005**, *127* (25), 9036–9044.
- (28) Thongboonkerd, V.; Semangoen, T.; Chutipongtanate, S. Factors Determining Types and Morphologies of Calcium Oxalate Crystals: Molar Concentrations, Buffering, PH, Stirring and Temperature. *Clin. Chim. Acta* **2006**, *367* (1–2), 120–131.

- (29) Millan, A. Crystal Growth Shape of Whewellite Polymorphs: Influence of Structure Distortions on Crystal Shape. *Cryst. Growth Des.* **2001**, *1* (3), 245–254.
- (30) Pearce, K. N. Formation Constants for Magnesium and Calcium Citrate Complexes. *Aust. J. Chem.* **1980**, *33* (7), 1511–1517.
- (31) Giocondi, J. L.; El-Dasher, B. S.; Nancollas, G. H.; Orme, C. A. Molecular Mechanisms of Crystallization Impacting Calcium Phosphate Cements. *Philos. Trans. R. Soc. A Math. Phys. Eng. Sci.* **2010**, *368* (1917), 1937–1961.
- (32) Grases, F.; Costa-Bauza, A. Key Aspects of Myo-Inositol Hexaphosphate (Phytate) and Pathological Calcifications. *Molecules* **2019**, *24* (24).
- (33) Farmanesh, S.; Ramamoorthy, S.; Chung, J.; Asplin, J. R.; Karande, P.; Rimer, J. D. Specificity of Growth Inhibitors and Their Cooperative Effects in Calcium Oxalate Monohydrate Crystallization. *J. Am. Chem. Soc.* **2014**, *136* (1), 367–376.
- (34) Hartl, W. P.; Klapper, H.; Barbier, B.; Ensikat, H. J.; Dronskowski, R.; Müller, P.; Ostendorp, G.; Tye, A.; Bauer, R.; Barthlott, W. Diversity of Calcium Oxalate Crystals in Cactaceae. *Can. J. Bot.* **2007**, *85* (5), 501–517.
- (35) Grases, F.; Millan, A.; Conte, A. Production of Calcium-Oxalate Monohydrate, Dihydrate Or Trihydrate - a Comparative-Study. *Urol. Res.* **1990**, *18* (1), 17–20.
- (36) Gadaleta, S. J.; Paschalis, E. P.; Betts, F.; Mendelsohn, R.; Boskey, A. L. Fourier Transform Infrared Spectroscopy of the Solution-Mediated Conversion of Amorphous Calcium Phosphate to Hydroxyapatite: New Correlations between X-Ray Diffraction and Infrared Data. *Calcif. Tissue Int.* **1996**, *58* (1), 9–16.
- (37) Sánchez-Enríquez, J.; Reyes-Gasga, J. Obtaining $\text{Ca}(\text{H}_2\text{PO}_4)_2 \cdot \text{H}_2\text{O}$, Monocalcium Phosphate Monohydrate, via Monetite from Brushite by Using Sonication. *Ultrason. Sonochem.* **2013**, *20* (3), 948–954.
- (38) Sadat-Shojai, M. Preparation of Hydroxyapatite Nanoparticles: Comparison between Hydrothermal and Solvo-Treatment Processes and Colloidal Stability of Produced Nanoparticles in a Dilute Experimental Dental Adhesive. *J. Iran. Chem. Soc.* **2009**, *6* (2), 386–392.
- (39) Frost, R. L.; Palmer, S. J.; Pogson, R. E. Thermal Stability of Newberyite $\text{Mg}(\text{PO}_3\text{OH})_3 \cdot 3\text{H}_2\text{O}$ A Cave Mineral from Skipton Lava Tubes, Victoria, Australia. *J. Therm. Anal. Calorim.* **2012**, *107* (3), 1143–1146.
- (40) Tamimi, F.; Nihouannen, D. Le; Bassett, D. C.; Ibasco, S.; Gbureck, U.; Knowles, J.; Wright, A.; Flynn, A.; Komarova, S. V.; Barralet, J. E. Biocompatibility of Magnesium Phosphate Minerals and Their Stability under Physiological Conditions. *Acta Biomater.* **2011**, *7* (6), 2678–2685.
- (41) Babić-Ivančić, V.; Kontrec, J.; Brečević, L. Formation and Transformation of Struvite and Newberyite in Aqueous Solutions under Conditions Similar to Physiological. *Urol. Res.* **2004**, *32* (5), 350–356.
- (42) Grases, F.; Söhnel, O.; Vilacampa, A. I.; March, J. G. Phosphates Precipitating from Artificial Urine and Fine Structure of Phosphate Renal Calculi. *Clin. Chim. Acta* **1996**, *244* (1), 45–67.
- (43) Bigi, A.; Falini, G.; Foresti, E.; Ripamonti, A.; Gazzano, M.; Roveri, N. Magnesium Influence on Hydroxyapatite Crystallization. *J. Inorg. Biochem.* **1993**, *49* (1), 69–78.
- (44) Ding, H.; Pan, H.; Xu, X.; Tang, R. Toward a Detailed Understanding of Magnesium Ions on Hydroxyapatite Crystallization Inhibition. *Cryst. Growth Des.* **2014**, *14* (2), 763–769.
- (45) Kim, K. C.; Hwang, I. G.; Kim, H. Y.; Song, H. L.; Kim, H. S.; Jang, K. Il; Lee, J.; Jeong, H. S. Quality Characteristics and Mineral, Oxalate and Phytate Contents of Soymilk Manufactured by Recommended Soybean Cultivars in Korea. *J. Korean Soc. Food Sci. Nutr.* **2010**, *39* (8), 1149–1155.
- (46) Li, C.; Zhao, L.; Han, J.; Wang, R.; Xiong, C.; Xie, X. Synthesis of Citrate-Stabilized Hydrocolloids of Hydroxyapatite through a Novel Two-Stage Method: A Possible Aggregates-Breakdown Mechanism of Colloid Formation. *J. Colloid Interface Sci.* **2011**, *360* (2), 341–349.

**Support Information of the manuscript:
“Understanding the crystalline conversion of
oxalocalcic kidney stones: effect of common
urine inhibitors *in vitro*”**

***Authors: Iris H.Valido, Victor Fuentes-Cebrian, Manuel Valiente,
Montserrat López-Mesas****

*^a Centre Grup de Tècniques de Separació en Química (GTS), Departament de Química,
Universitat Autònoma de Barcelona, Facultat de Ciències. Edifici CN. 08193, Bellaterra,
Barcelona, Spain*

**montserrat.lopez.mesas@uab.cat*

SI1: Comparison of the FTIR spectra of COD and the two inhibitors used on its synthesis, sodium pyrophosphate decahydrate ($\text{Na}_4\text{P}_2\text{O}_7 \cdot 10\text{H}_2\text{O}$) and sodium citrate dihydrate ($\text{Na}_3\text{C}_6\text{H}_5\text{O}_7 \cdot 2\text{H}_2\text{O}$).

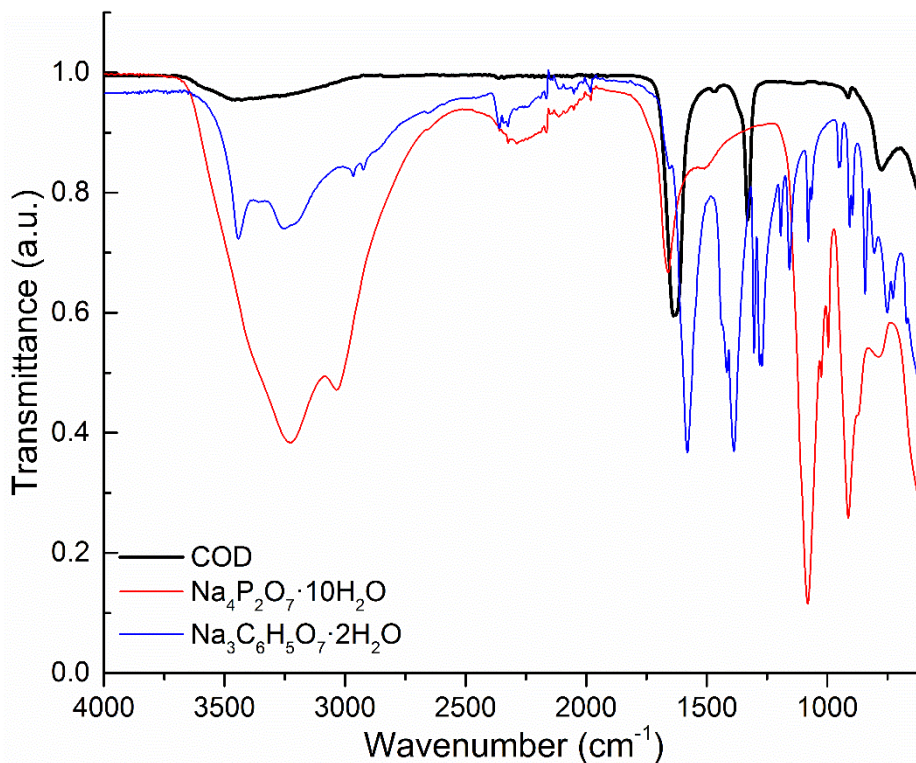


Figure 11. Infrared spectra of COD (black), sodium pyrophosphate decahydrate (red) and sodium citrate dihydrate (blue). As can be observed, the two inhibitors do not remain on the formed crystal after the synthesis and washing processes.

SI2: Example of the Multivariate Curve Resolution (MCR) analysis and the performed non-linear (sigmoidal) fitting.

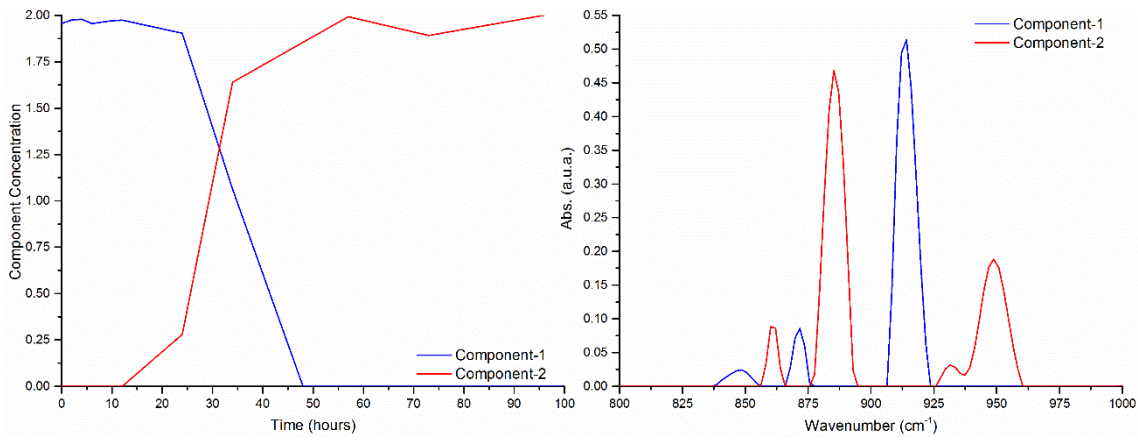


Figure 12. Component Concentration image (left) and Component Spectra (right), with Component 1 (blue) and Component 2 (red) characteristic of the dihydrated and monohydrated species respectively, from the Multivariate Curve Resolution (MCR) analysis of the selected IR region ($100\text{--}820\text{ cm}^{-1}$) from the transformation carried out in water at pH6.

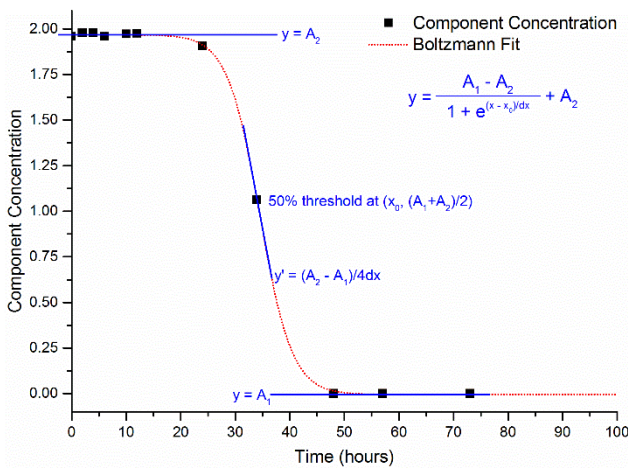


Figure 13. Example of the non-linear (sigmoidal) fitting, using Boltzmann function, performed to the Component Concentration that correspond to COD (Component 1, blue) of the MCR analysis represented in Figure 2 of this Support Information. The parameters of the fitting are represented in blue, being A_1 the initial value (minimum), A_2 the final value (maximum), x_0 the center (50% threshold), and dx the time constant.

SI3: Equilibrium diagram of the Ca:Phos medium

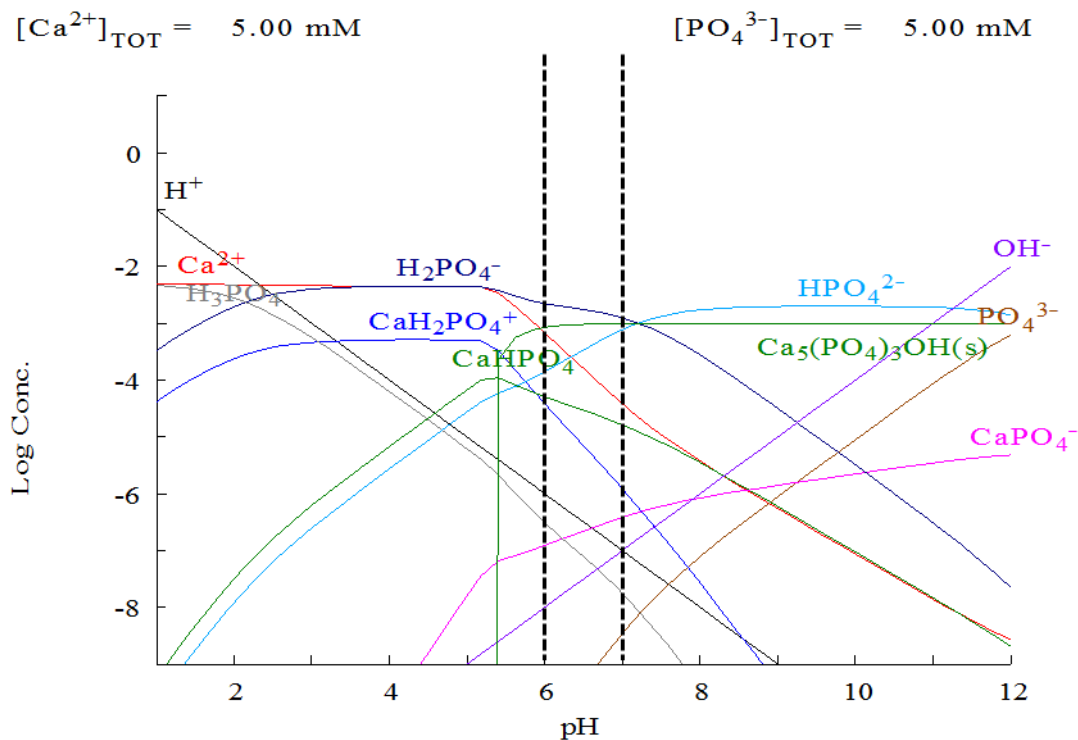


Figure 14. Equilibrium diagram performed with Medusa software of the Ca:Phos medium with the 1:1 ratio. Vertical dash lines highlight pH 6 and 7. The chemical formula of HAP is $Ca_5(PO_4)_3OH$.

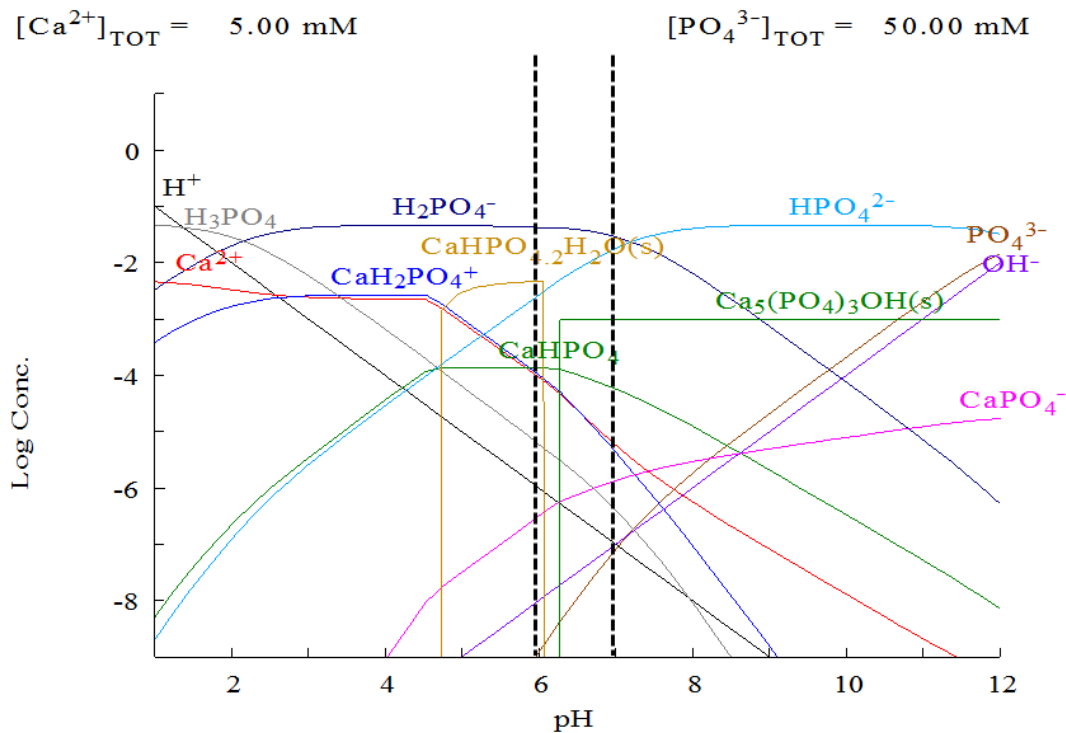


Figure 15. Equilibrium diagram performed with Medusa software of the Ca:Phos medium with the 1:10 ratio. Vertical dash lines highlight pH 6 and 7.

S14: Equilibrium diagram of the Mg:Phos medium

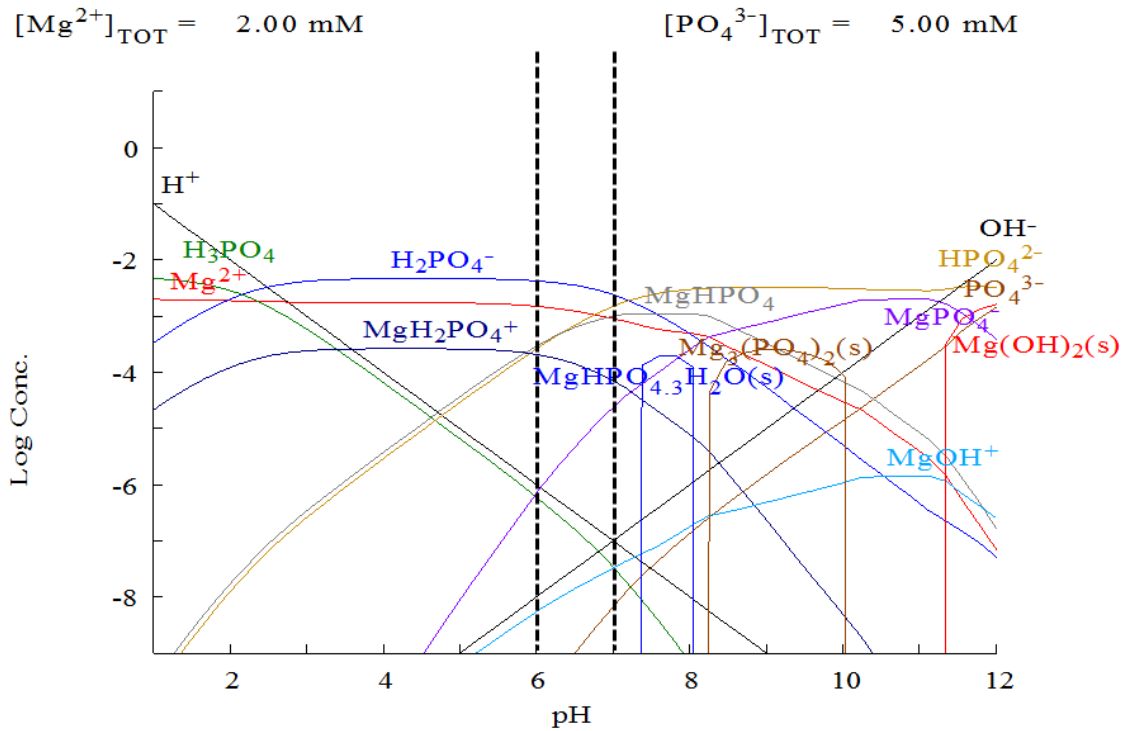


Figure 16. Equilibrium diagram performed with Medusa software of the Mg:Phos medium with the 1:2.5 ratio. Vertical dash lines highlight the pH 6 and 7.

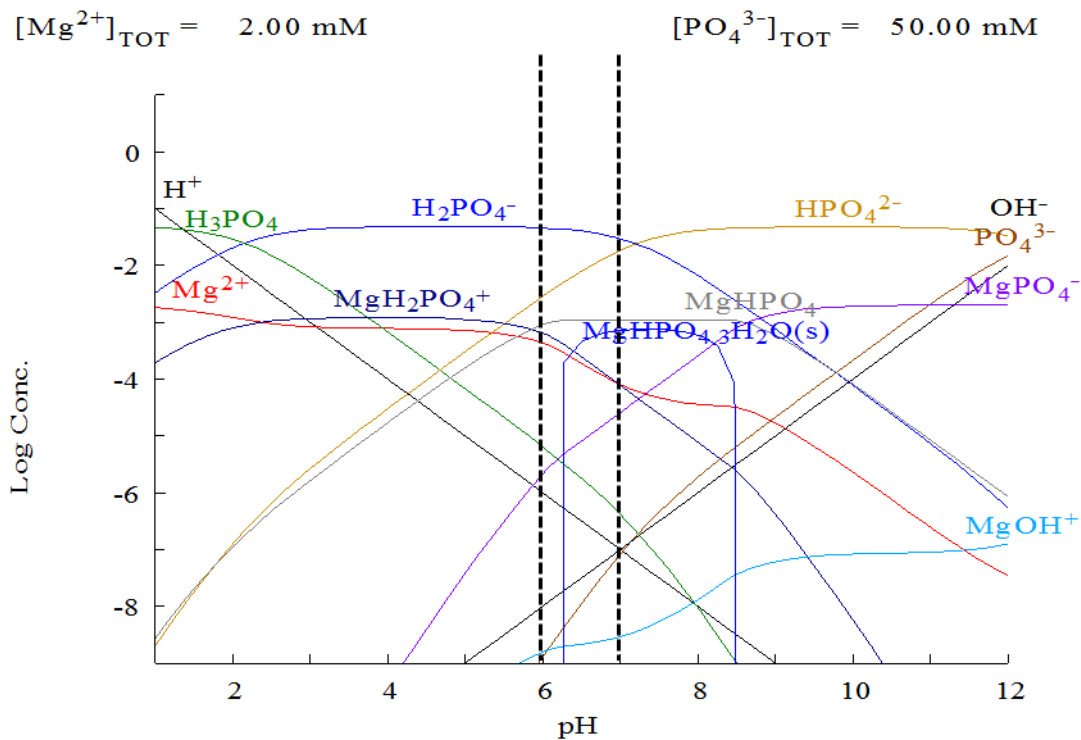



Figure 17. Equilibrium diagram performed with Medusa software of the Mg:Phos medium with the 1:25 ratio. Vertical dash lines highlight the pH 6 and 7.



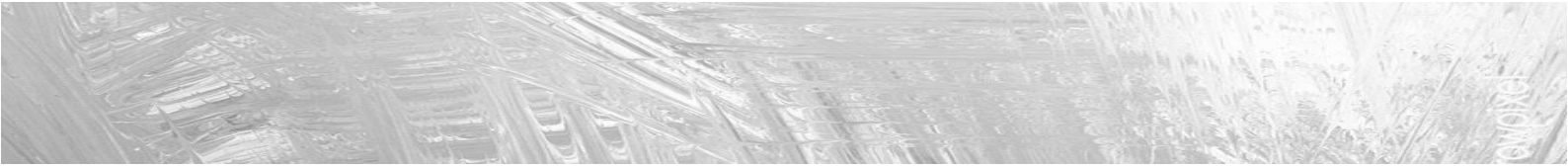
***In vitro* study of the ration
promoters/inhibitors influence in oxalocalcic
nephroliths formation: approach for the
development of Urine Inhibitory Capacity
(UIC) as a risk index**

Iris H.Valido, Daniel Patilla-Gutiérrez, Manuel Valiente, and Montserrat López-Mesas*

*Centre Grup de Tecniques de Separacio en Quimica (GTS), Departament de Quimica, Universitat
Autonoma de Barcelona, Facultat de Ciencies, Edifici CN. 08193, Bellaterra, Barcelona, Spain*

**Montserrat.lopez.mesas*

Unpublished



In vitro study of the ratio promoters/inhibitors influence in oxalocalcic nephroliths formation: Approach for the development of Urine Inhibitory Capacity (UIC) as a risk effect

Iris H. Valido, Daniel Patilla-Gutiérrez, Manuel Valiente, Montserrat López-Mesas*

Centre Grup de Tècniques de Separació en Química (GTS), Departament de Química, Universitat Autònoma de Barcelona, Facultat de Ciències, Edifici CN, 08193, Belaterra, Spain.

KEYWORDS: kidney stones; calcium oxalate; Relative Supersaturation; artificial urine; Urine Inhibitory Capacity

ABSTRACT: Nephrolithiasis is a painful disease with a high incidence (6-12%) and recurrence (30-50%) worldwide, being calcium oxalate (CaOx) the calculi with the highest incidence. From many methods to determine the risk of forming a kidney stone by analyzing the urine saturation, the calculation of the urine Relative Supersaturation (RSS) is the most used, which integrates a complex approach that involves several urine components and takes into account their interactions and equilibriums in the medium. However, even being widely recommended and studied, this method is not generally used by the specialist centers, which could be explained by the high cost of the analysis required to perform the RSS calculation and the large grey zone of values where the healthy and stone formers ranges overlap. The present study is focused in the *in vitro* comparison of the urine RSS with the CaOx stone formation process (nucleation and crystalline conversion) with the use of Artificial Human Urine (AHU). It was determined by oxalate induction of the precipitation that the type, size, morphology and level of aggregation of the formed crystallites depends on the different Ca/Ox ratios and the saturation level. Furthermore, by analyzing two samples with the same RSS but different promoters/inhibitors ratios, it was concluded that the RSS grey zone discrepancies could be solved by the calculation of the Urine Inhibitory Capacity (UIC).

INTRODUCTION

Urolithiasis is a disease caused by the formation of stones in different parts of the urinary tract, being the ones formed in the kidneys known as kidney stones, renal calculi or nephroliths. The incidence of this disease is between 6 to 12% of the population worldwide, presenting an increase of recurrence after five years of the first episode between 30 to 50%^{1,2}. Moreover, it is well known that, from the seven types of nephroliths, based on their chemical composition, calcium oxalate hydrates (CaOx) represent the highest incidence (around 66%), being divided in two species: whewellite (COM, $\text{CaC}_2\text{O}_4 \cdot \text{H}_2\text{O}$) and weddellite (COD, $\text{CaC}_2\text{O}_4 \cdot 2\text{H}_2\text{O}$)³. Furthermore, COD endures a crystalline conversion into the monohydrated species (the thermodynamically stable one)⁴⁻⁶, process not only affected by the humidity conditions^{4,5} and the contact time with the medium⁶, but also by the presence of certain components that can act as stabilizers of the

COD species, such as organic matter (lipids) or hydroxyapatite (HAP)^{7,8}.

There are many methods to determine the risk of forming a kidney stone, based on the urine saturation, known as BONN-Risk index (BRI), Relative Supersaturation (RSS), Upper Limit Metastability (ULM) and Tiselius Indices and Robertson Risk Factor Algorithms (RRFA)⁹. The most used method is the calculation of the RSS, since it becomes a more suitable parameter since the development of the EQUIL software^{10,11} (in its different versions), as well as other similar softwares: SUPERSAT, SEQUIL, URSUS, MINEQL and JESS². In summary, the urine saturation can be defined as the concentration of the dissolved salt divided by the solubility of that salt at physiological temperature¹³, which is more extensively described by the EQUIL software, since it integrates a more complete approach that involves several urinary components taking into account interactions and equilibrium

processes¹². In summary, to calculate the RSS with the aforementioned software, it is necessary to measure at least twelve parameters in the urine, including pH, calcium, oxalate, phosphate and citrate among others. Then, the software considers the introduced concentrations to calculate the concentration of multiple soluble ion complexes, as well as the activity products of the stone-forming salts. The ratios of the activity products to the thermodynamic solubility products define the RSS of the different stone components¹⁴. Even it has been widely recommended and studied, the use of urine analysis on stone formers it is not generally used, being few of the specialist centers the only that perform calculation of the supersaturation (SS) levels of the urinary salts in order to determine the patients risk to perform more stones¹⁵. This lack of use could be explained by two main factors: the high analysis cost necessary to determine the different analytes needed to calculate the RSS (also known only as SS) with the software, and the large overlap of the RSS values from stone formers and healthy individuals (grey zone of values), which means that it cannot distinguish between the two groups¹². On the other hand, these methods are based in the analysis of individual parameters and their interaction by using the equilibrium constants, but human urine contains many other compounds that could act as inhibitors or promoters. The objective of the present work is to determine the influence of the promoters/inhibitors ratio in the formation of oxalocalcic nephroliths. Moreover, this approach will help to develop a simple method to measure the risk of a particular urine to develop a kidney stone, taking into consideration all the compounds present in the urine, by the induction of the precipitation of CaOx in the urine, what we have called the Urine Inhibitory Capacity (UIC).

MATERIALS AND METHODS

Reagents

All the chemicals used in this project were of analytical grade. From Merck (Germany): ammonium chloride (NH₄Cl, 99.5%), calcium nitrate tetrahydrate (Ca(NO₃)₂·4H₂O, 99%), sodium citrate dihydrate (Na₃C₆H₅O₇, Na₃Citrate·2H₂O, 99%) and creatinine (C₄H₇N₃O, 99%). From Panreac (Spain): potassium chloride (KCl, 99.5%), sodium chloride (NaCl, 95%), sodium dihydrogen phosphate dihydrate (NaH₂PO₄·2H₂O, 95%), sodium hydrogen phosphate dihydrate (Na₂HPO₄·2H₂O, 95%), sodium oxalate

(Na₂C₂O₄, Na₂Ox, 95%), sodium sulfate (Na₂SO₄, 99%). From Sigma-Aldrich (India): turbidity calibration Standard-Formazing (C₆H₁₂N₄ and N₂H₆O₄S, 4000 NTU) and urea (CH₄N₂O, 99%). Magnesium sulfate heptahydrate (MgSO₄·7H₂O, 99%) from Scharlau (Spain). Uric acid (C₅H₄N₄O₃, 99%), from VWR Chemicals (Belgium). Potassium chloride standard conductivity (KCl, 0.010 mol/L) from Crison, Spain. Solutions were prepared with "ultrapure Type 1" water (Milli-Q, Millipore, 18.2 mS cm⁻¹).

Equipment

To measure the turbidity of the solutions after adding oxalate in order to follow the formation of precipitate, a spectrophotometer UV-Vis (UV-2 200 040610 Unicam, United Kingdom) with a tungsten lamp was used and the absorbance of the samples at 620 nm (1200 nm/s) was measured. All the parameters and measures were controlled by the VISIONpro software. A pH-meter (MicropH 2002 Crison, Spain) with a pH electrode (52-21 Crison, Spain) was used to measure and adjust the pH of the samples. A Calcium Ion Selective Electrode (Calcium ISE, 9320BN Thermo, Netherlands) and a reference Ag/AgCl electrode (52-41 Crison, Spain), both connected to a potentiometer, were used to control the calcium measurements in the samples. In order to characterize the solid samples of the different experiments, an Infrared Spectrophotometer Tensor 27, equipped with an Attenuated Total Reflectance module (ATR-FTIR, Bruker, Ettlingen, Germany), with a resolution of 4 cm⁻¹, was used. To study the morphology of the crystals, a Field Emission-Scanning Electron Microscope MERLIN (FE-SEM, Zeiss), with a 1.4 nm resolution, 1 kV 4 pA-100 nA probe current and 0.2-30 kV accelerating voltage, was used. The IR data treatment was performed with the Unscrambler X[®] software. The MEDUSA (Make Equilibrium Diagrams Using Sophisticated Algorithms) program (Sweden, 2010)¹⁶ was used to draw the chemical equilibrium diagrams. The EQUIL 1.4b program (University of Florida)¹¹ to calculate the RSS of urine. OriginPro[®] 2016 (OriginLab Corporation, Northampton, MA, USA) program was used to make the fitting of the data and the graphic representations.

Synthesis of calcium oxalate hydrates

The synthesis of the calcium oxalate hydrates used in this work was previously optimized in our research group⁶.

Preparation of the Artificial Human Urine (AHU)

The artificial human urine AHU used in this study is based in the one developed by Grases et. al. (1998)¹⁷ with the addition of other components usually found in the urine medium, such as uric acid, urea, creatinine and citrate and modifying the concentrations in order to adjust to the desired RSS. Briefly, equal volumes of solutions A and B (composition detailed in Table 1) were mixed at a flow rate of 0.3 ml/min, under constant stirring and the pH of the final solution was adjusted to 6, immediately before use. The individual solutions can be stored at 4°C for one week. The chosen components concentrations are in the normal range found in urine¹⁸⁻

²⁰ but the individual values of the calcium oxalate stones promoters (calcium and oxalate) and inhibitors (phosphate and citrate) have been modified to obtain different RSS values for COM stone formation. The RSS of each AHU prepared were selected to include values from healthy (1.29 to 8.40) and stone formers (2.37 to 11.81 and above), including the wide grey zone of values (2.37 to 8.40)¹². Moreover, to test if the promoters/inhibitors ratio affects the risk of calculi formation, two AHU with the same RSS value (9.5) and different promoters/inhibitors ratio were prepared and calculated as $([Ca] \cdot [Ox]) / ([Phos] \cdot [Cit])$. The final concentration (mol/L) of the promoters and inhibitors can be seen on Table 2.

Table 1. Concentration of the compounds (in each solution) used to prepare the Artificial Human Urines (AHU) at the different Relative Supersaturation (RSS) values for COM stones. The pH of the mixture of solutions A and B was adjusted to 6.

		RSS (COM)						
		2.7	5.3	9.5(1)	9.5(2)	9.8	11.6	13.4
Solution A (g/L)	Na ₂ SO ₄	4.823						
	MgSO ₄ ·7H ₂ O	1.084						
	NH ₄ Cl	1.819						
	KCl	12.197						
	Ca(NO ₃) ₂ ·4H ₂ O	1.417	2.361	2.834	2.361	2.361	2.598	2.598
	Uric acid	0.303						
Solution B (g/L)	NaH ₂ PO ₄ ·2H ₂ O	0.744	0.744	0.744	0.595	0.595	0.744	0.595
	Na ₂ HPO ₄ ·2H ₂ O	0.931	0.931	0.931	0.745	0.745	0.931	0.745
	NaCl	14.281						
	Na ₂ Ox	0.054	0.054	0.08	0.08	0.094	0.107	0.107
	Na ₃ Cit·2H ₂ O	3.529	2.941	2.941	1.765	2.647	2.941	1.765
	Creatinine	2.398						
	Urea	23.398						

Table 2. Final concentration of calcium oxalate kidney stones promoters (calcium and oxalate) and inhibitors (citrate and phosphate), and the promoters/inhibitors ratios, in each Artificial Human Urine (AHU) to obtain the different Relative Supersaturation (RSS) values for COM stones.

	RSS (COM)						
	2.7	5.3	9.5(1)	9.5(2)	9.8	11.6	13.4
Calcium (mol/L)	0.003	0.005	0.006	0.005	0.005	0.006	0.0055
Oxalate (mol/L)	0.0002	0.0002	0.0003	0.0003	0.00035	0.00035	0.0004
Citrate (mol/L)	0.006	0.005	0.005	0.003	0.0045	0.0045	0.003
Phosphate (mol/L)	0.005	0.005	0.005	0.004	0.004	0.004	0.004
Ca/Ox	15.0	25.0	20.0	16.7	14.3	17.1	13.8
(Ca · Ox)/(Phos · Cit)	0.020	0.040	0.072	0.125	0.097	0.117	0.183

Transformation of COD crystals in the different media

The monitoring of the crystalline conversion of COD into the monohydrated species was performed following the process described in previous studies^{6,21}, but using AHU as medium for the incubations. In brief, tubes with 10 mg of synthetic COD and 2 mL of AHU were incubated at 37°C, then, one sample and its replicate were filtered with a 0.22 µm GVPP Millipore filter (Durapore membrane filter, Germany), taking them after the adjusted time for each medium. AHU was replaced by water, as control experiments. In order to monitor the transformation process, the incubated and filtered crystals were analyzed by ATR-FTIR spectroscopy. From the collected data at the different transformation stages, a Savitzky-Golay second derivative, followed by a Maximum Normalization, was applied in the region from 1000 to 820 cm⁻¹. Subsequently, a Multivariate Curve Resolution (MCR) analysis was performed, following the decrease in the 912 cm⁻¹ peak, corresponding to the ν(C-C) + δi(COO) scissoring + ν(M-O) vibrations of COD, and the appearance of peaks at 883 and 948 cm⁻¹ corresponding to the δi(COO) scissoring + ν(M-O) and water libration, respectively, of COM⁶. To calculate the half-time transformation ($t_{1/2}$), a sigmoidal fitting (Boltzmann function) was performed to the Relative Concentration of the MCR corresponding to the loss of COD peak contribution. The $t_{1/2}$ of COD in each AHU was calculated respect to water (Equation 1), where $t_{1/2}(\text{medium})$ and $t_{1/2}(\text{water})$ are the half-time transformation in AHU and in water respectively^{6,21}.

$$\text{Rel. } t_{1/2} = t_{\frac{1}{2}}(\text{medium}) - t_{\frac{1}{2}}(\text{water}) \quad \text{Equation 1}$$

Nucleation test

The induction of the calcium oxalate precipitation was carried out by performing four additions, one every 30 min, of 400 µL of 0.1 M oxalate (from Na₂Ox) or calcium (from Ca(NO₃)₂) to 10 mL of sample (AHU with different RSS), under constant stirring and maintained at 37°C. After the four additions, the final concentration added of both components is 0.016 M, which is a great excess for both²². Each induction was performed by triplicate. The relative nucleation (Rel. Nuc.) was calculated by measuring the absorbance of each sample and its replicate (by triplicate) at 620 nm and applying Equation 2, where A_s is the sample absorbance, A_c is the absorbance of the water used as control.

$$\text{Rel. Nuc.} = A_s - A_c \quad \text{Equation 2}$$

After the analysis, the solutions containing the crystals were centrifuged at 2500 rpm for 10 min, and then washed twice with 5 mL of water, and twice with 5 mL of ethanol, repeating the centrifugation process after each wash.

Determination of the Urine Inhibitory Capacity (UIC)

In order to verify that there was a linear relationship between turbidity and absorbance, a series of turbidity standards were measured, with concentrations between 60 and 800 NTU (Nephelometric Turbidity Units). This calibration curve can be found in the Support Information (SI). The induction of the CaOx precipitation in the AHU by the addition of oxalate in 50 mL of sample was performed with a continuous methodology. The sample (artificial urine) was

circulated on the system, with the use of a peristaltic pump at a flow rate of 4.3 ± 0.2 mL/min. Fifteen additions of 100 μ L of 0.05 mol/L of oxalate, followed by additions of 100 μ L of 0.1 mol/L of oxalate, were performed until the potential of the calcium ISE was lower than -40.0 mV (limit for linearity). To reproduce the physiological conditions, the beaker containing the sample was maintained at 37°C during the assay by using a thermostatic bath with a pump (Figure 1). The turbidity (in the form of absorbance) was measured one minute after every addition by triplicate, with a difference of 30 seconds between each one. All samples were tested by duplicate.

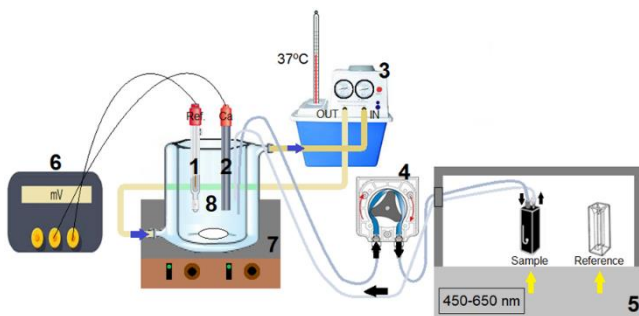


Figure 1. Continuous system assembly. (1) Reference Ag/AgCl electrode, (2) Calcium ISE, (3) Thermostatic bath, (4) Peristaltic pump, (5) Spectrophotometer UV-Vis, (6) Potentiometer, (7) Stirring plate, and (8) Beaker for the sample. The flux is indicated with different color arrows.

To determine the urine inhibitory capacity (UIC) of the samples, the sigmoidal curves obtained by the representation of the relative absorbance at 620 nm in the y-axis and the oxalate concentration added in the x-axis, were fitted by using the Boltzmann function (Equation 3). In this equation, A_1 and A_2 correspond to the asymptotic values of y (Rel. Absorbance) at infinitely small and large x (oxalate concentration added) respectively, x_0 correspond to the center of the Boltzmann sigmoid and dx correspond to the deviation of x around x_0 .

$$y = \frac{A_1 - A_2}{1 + e^{(x - x_0)/dx}} + A_2 \quad \text{Equation 3}$$

The inflection point value of the sigmoidal curve is defined as First Turning Point (FTP) and was calculated by using the Equation 4²³, being the parameters the same as in Equation 3.

$$FTP = x_0 - 2dx \quad \text{Equation 4}$$

Since the slope of the sigmoidal curve is not related to any parameter, it is replaced by the maximum value when $x = x_0$, whose inverse is directly proportional to the maximum slope that occurs at x_0 ²⁴. Hence, with the parameters of the non-linear fitting, the Maximum Slope was calculated using Equation 5²⁴ being the parameters the same as in Equation 2.

$$Max.Slope = Slope(x_0) = \frac{A_2}{4dx}$$

Equation 5 The Urine Inhibitory Capacity (UIC) has been calculated from the combination of the FTP and the Max. Slope, described in Equation 6.

$$UIC = FTP \cdot Max.Slope = \frac{(x_0 - 2dx)A_2}{4dx} \quad \text{Equation 6}$$

Finally, an illustration showing the different parameters needed to calculate the UIC can be found in Figure 2.

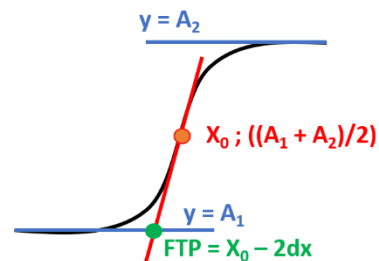


Figure 2. Example of the sigmoidal curve fitting with Boltzmann function and its parameters. A_1 and A_2 correspond to the asymptotic values of y at infinitely small and large x respectively, x_x is the center of the Boltzmann sigmoid, dx is the deviation of x around x_x , and FTP means First Turning Point.

RESULTS AND DISCUSSION

Transformation of COD crystals in the different media

The relative-half-time transformation (Rel. $t_{1/2}$) of COD in the AHU samples with different RSS values are represented in Figure 3. The obtained results can be compared to the ones described in a previous work²¹, since the methodology followed is the same. The first thing to notice are the high values obtained, but being below the Rel. $t_{1/2}$ of 48 hours, which is lower than the one described in the previous work as the maximum Rel. $t_{1/2}$ (120 hours) of experiment where some of the samples did not present transformation. However, it is important to take into account that AHU is a complex matrix, since it tries to simulate human urine, hence, there are much more components that can interfere in

the inhibition of the COD crystalline conversion. Nevertheless, all of the components, with the exception of promoters (calcium and oxalate) and inhibitors (phosphate and citrate) were kept constants (see Table 1), which means that these components should interfere equally in all samples.

Regarding the results observed in Figure 3, the Rel. $t_{1/2}$ does not follow the RSS tendency. In order to evaluate if the effect was due to the present of inhibitors that complex calcium, Equation 7 has been applied (see Support Information (SI2) for the developed equation). The results for the equation (Figure 3) show the same tendency than the Rel. $t_{1/2}$, meaning that, as higher the obtained calcium complexation value ($Ca_{complex}$ in Equation 7), higher is the capacity of the inhibitors that not only complex the free calcium, but also interact with the calcium of the COD structure. This could be explained as the fact that COD transformation could be inhibited by the “protection” of the zeolitic channel, preventing the decomposition of the COD crystalline structure and its crystalline rearrangement produced by the alteration of the “zeolitic water” channel site occupancy^{4,6}. This protective effect could be achieved by the interaction of the mentioned inhibitors with the (200) plane of the COD crystal.

$$Ca_{Complex} = [|CaCit^-| + |CaHCit| + |CaH_2Cit^+|] \cdot [|CaH_2PO_4^+| + |CaHPO_4| + |Ca_5(PO_4)_3OH|]$$

Equation 7

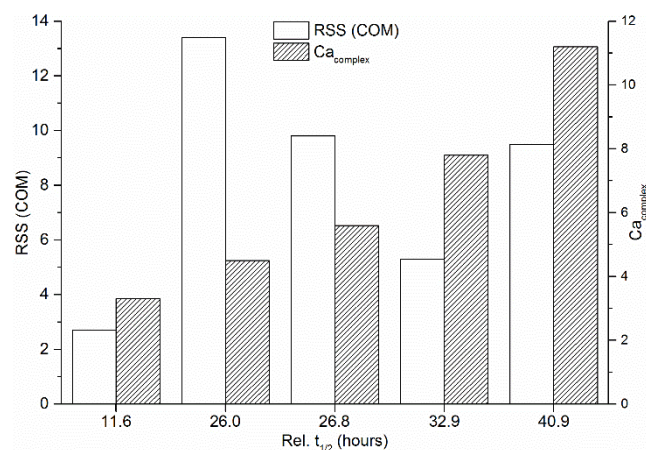


Figure 3. Comparison of the Rel. half-time transformation (Rel. $t_{1/2}$) of COD in the different Artificial Human Urine (AHU) samples with different Relative Supersaturation (RSS) and $Ca_{complex}$ values.

Nucleation test

After the induction of the precipitation by the addition of calcium or oxalate to the AHU samples with

different RSS values, it can be clearly observed in Figure 3 that calcium does not affect the relative nucleation of CaOx, while oxalate clearly forces its precipitation. These differences can be explained by the average concentration of both analytes in the samples (and in urine). As it has been described previously, urine is saturated with respect to calcium oxalate, being the average calcium concentration ten times higher than the oxalate one. Furthermore, after the oxalate additions, an increase in the relative nucleation is observed with respect to the RSS values. Considering these results, a continuous analysis of the induction of calcium oxalate by the addition of oxalate is performed in the next section.

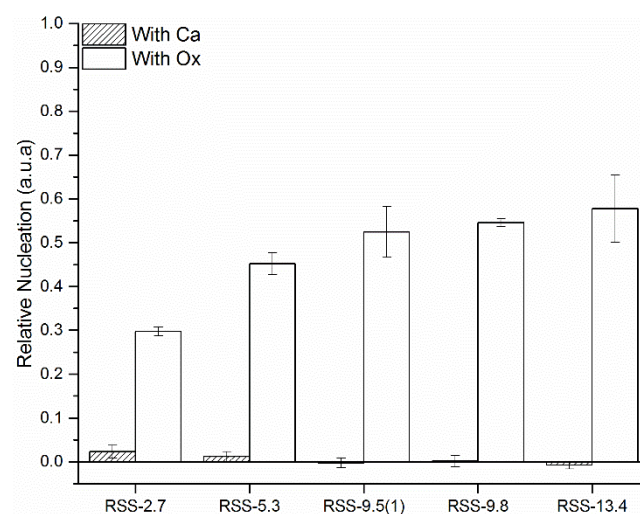


Figure 4. Relative Nucleation of CaOx in Artificial Human Urines (AHU) with different Relative Supersaturation (RSS) after the precipitation induction with calcium (dense columns) or oxalate (white columns).

Regarding the crystals morphology after the inductions with oxalate, SEM images for the different samples are shown in Figure 4. As can be seen, all samples precipitate mainly COM crystallites with the characteristic monoclinic structure, with the exception of RSS-5.3 where tetragonal bipyramid crystallites are observed, characteristic structure of COD. This difference could be related to the Ca/Ox concentration ratio (Table 2), being the mentioned sample the one that presents a higher value, since an excess of calcium in the urine, hypercalciuria, is a known common pathology related to the formation of COD kidney stones²⁵. Another two important features observed are the crystal size and the aggregates formed. Sample RSS-2.7 shows the biggest crystallites, followed by RSS-9.8; however, these are rather loose in comparison. The most aggregated are samples RSS-5.3 and RSS-9.5, being the

last one the smaller, with its bigger clusters of around 4 μm of length and width. Moreover, even sample RSS-13.4 presents the higher relative nucleation, its crystallites are the smallest, more flat and again, rather loose of the ones described in this experiment. This could be related

to the higher saturation of the sample, which means that, at saturations abnormally high, crystallites are continuously forming at a fast rate, leaving less time for their aggregation.

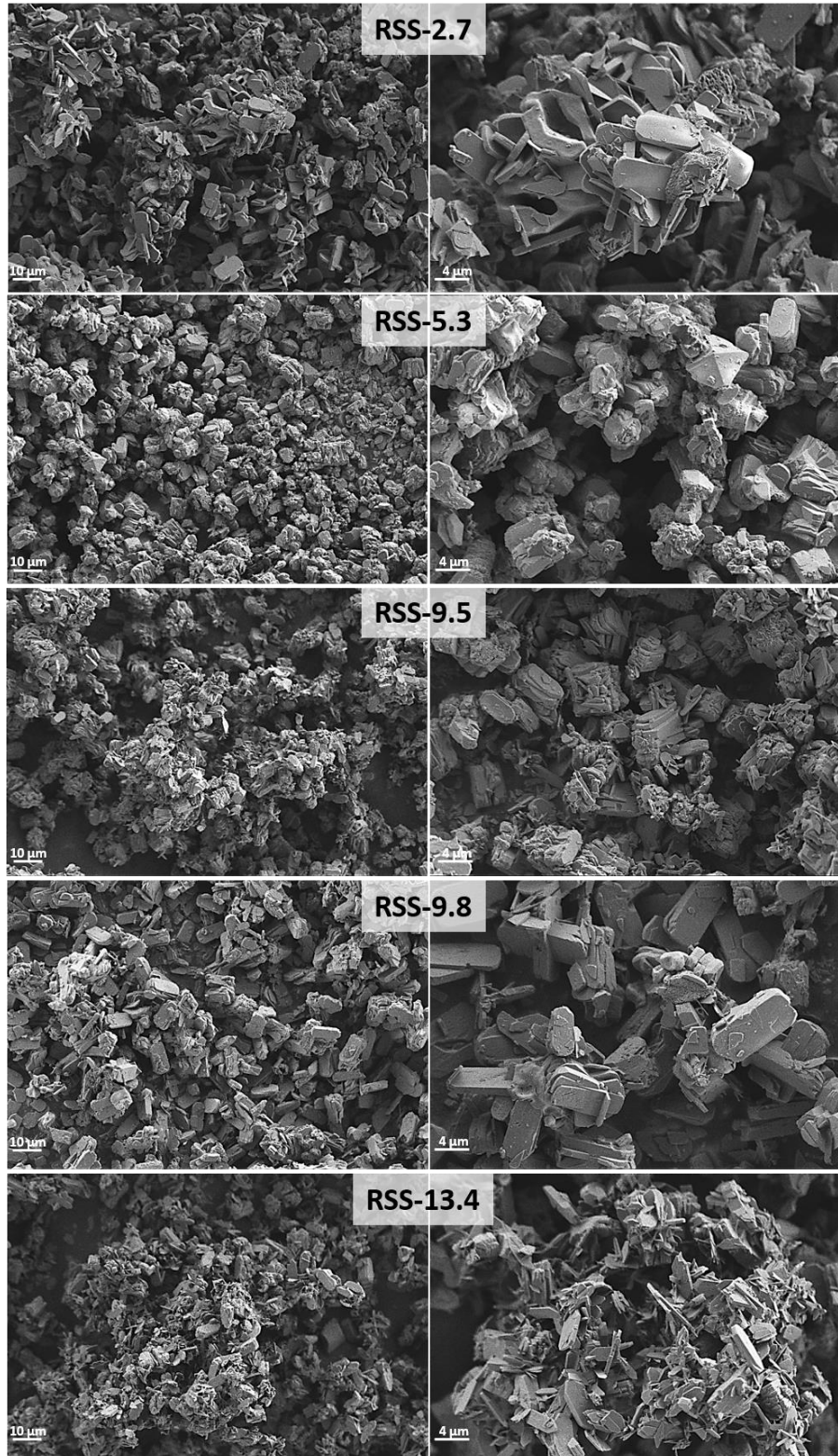


Figure 5. SEM images of the calcium oxalate crystals formed after their precipitation induction by oxalate addition in the Artificial Human Urine (AHU) with different Relative Supersaturation (RSS) values. Scale bar on the left panel is 10 μm and in the right panel is 4 μm .

Determination of the Urine Inhibitory Capacity (UIC)

To determine the risk of a saturated urine to develop a CaOx kidney stone, a continuous method of its precipitation by the addition of oxalate has been developed. For this experiment, two extra urines have been added with the goal of having more variety on the stone formers region of the RSS, and to have two urines with the same RSS value (9.5) but with a different ratio promoters/inhibitors, being 0.072 and 0.125 for RSS-9.5(1) and RSS-9.5(2) respectively (see Table 2 for the rest of samples).

The representation of the sigmoidal curves used to obtain the necessary parameters to calculate the UIC (Equation 6) are shown in Figure 6 (Left panel). As can be observed, all the samples present different FTP and Max. slope, which makes them difficult to compare visually, therefore, the direct relationship between both (UIC) is proposed to perform the comparison.

What can be described from them is that, RSS-2.7 clearly needs a higher concentration of oxalate to induce the start of the precipitation (a higher value of the FTP), as expected, since the lower the RSS, the lower the risk of suffering a kidney stone. On the other hand, the two samples with the same RSS (RSS-9.5(1) and RSS-9.5(2)) do not present similar curves, what would be expected

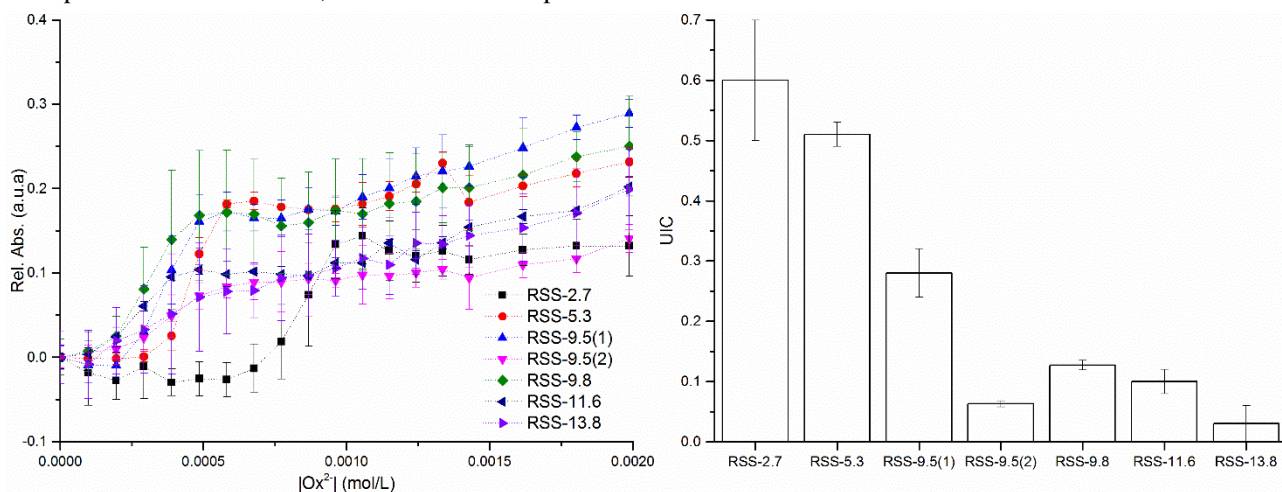


Figure 6. Representation of the Rel. Abs. (a.u.a) in the y-axis with respect to the concentration of oxalate added (mol/L) in the x-axis, for the Artificial Human Urine (AHU) at different Relative Supersaturation (RSS) values (Left panel). Column bars graph representing the Urine Inhibitory Capacity (UIC) calculated with Equation 5 (Right panel).

since both have the same RSS. However, the sigmoidal curve for RSS-9.5(2) is more resembled to the one for RSS-13.4. To better compare the results, the UIC values are represented in Figure 6 (Right panel), where the calculated UIC value is inversely correlated to the RSS values. Nevertheless, as it has just been explained, sample RSS-9.5(2) do not follow the RSS tendency and present a similar UIC value than RSS-13.8, being 0.063 ± 0.005 and 0.03 ± 0.03 respectively, taking into account that the UIC value for RSS-9.5 is 0.28 ± 0.04 . If these tendencies (Figure 6, left panel) are compared with the values obtained for the ratio promoters/inhibitors ($|\text{Ca}| \cdot |\text{Ox}| / |\text{Phos}| \cdot |\text{Cit}|$) from Table 2, it can be observed that the sample with RSS-9.5(2) has a ratio value between samples RSS-11.6 and RSS-13.8, confirming the necessity to consider the present ratio.

With the presented results, it can be determined that the UIC is related to the amount of promoters and inhibitors present in the urine, and in their real capacity to interact to each other. It is important to take into account that this is a first approach with artificial urine, but it could be extrapolated to a much complex system such as healthy or stone formers urine, since it will not be necessary to determine which other inhibitors (like organic matter) are present in the matrix; all of these factors will be taken into account in the UIC calculation.

CONCLUSIONS

This work presents a wide study on the nucleation, and crystalline conversion of calcium oxalate hydrates in an urine like medium designed with Relative Supersaturation (RSS) values of COM that comprising the range between healthy and stone formers. Regarding the nucleation, the first helps to determine how to perform the continuous experiment, by performing oxalate additions to the medium, since all urine have ten times more calcium than oxalate. Moreover, it concluded, with the help of the SEM images, that the composition of the AHU used, more precisely the different Ca/Ox concentration ratios and saturation levels, directly affect the type, size, morphology and level of aggregation of the formed crystallites. The continuous nucleation method was used to determine the Urine Inhibitory Capacity (UIC), which can be described as the risk of a saturated urine to develop a kidney stone, in this case a CaOx one. The UIC is related with the capacity of the urine inhibitors to interact with the promoters and avoid the formation of the crystals. That is why the use of two AHU with the same RSS but different promoters/inhibitors was used, proving that the wide grey zone between healthy and stone formers urine of the RSS could be solved with the application of the UIC. This is possible since this parameter does not only consider a set of measured components with a mathematical approach, but the capacity of the total components in the urine to avoid the CaOx precipitation.

Furthermore, the effect of the different RSS values on the COD crystalline conversation was also studied, concluding that saturation does not affect the transformation time, being this influenced by the calcium complexation with the urine inhibitors. This effect could be explained by the stabilization of the zeolitic channel, which prevent the decomposition of the COD crystalline structure.

To conclude, this work presents a comparison of the relationship between the urine RSS and the CaOx nephroliths formation. With these comparisons it can be concluded that, even being a helpful tool on the lithiasic patients follow up¹⁵, it does not give a complete information about the risk of having a kidney stone, due to its wide grey zone of cases¹², as well as how the urine promoters/inhibitors can affect the formation process. Hence, the application of a methodology based on the direct measure of the urine capacity to avoid the

formation of the stones, the UIC, could be useful to perform a fast and affordable characterization of patients' urine. Nonetheless, it is important to take into account that the UIC of this work has been only applied to CaOx stones, and further studies are needed to adapt it to the rest of the nephroliths of the classification.

ASSOCIATED CONTENT

Supporting Information.

S11: Comparison of the calibration curve between the static and the continuous method to measure turbidity

S12: Equation 7 development (calcium complexation by the urine inhibitors) and constant values

AUTHOR INFORMATION

Corresponding Author

* montserrat.lopez.mesas@uab.cat

Author Contributions

The manuscript was written through contributions of all authors. / All authors have given approval to the final version of the manuscript.

ACKNOWLEDGMENT

The authors want to acknowledge the financial support from the Ministerio de Economía y Competitividad (Spanish Project CMT 2015-65414-C2-1-R). Iris H. Valido acknowledges funding support from the Universitat Autònoma de Barcelona (PIF-2016 grant). All the authors are grateful to the Serveis de Suport a la Investigació of the UAB (Servei d'Anàlisi Química and Servei de Microscòpia).

ABBREVIATIONS

AHU, artificial human urine; ATR-FTIR, Attenuated total reflectance Fourier transform infrared spectroscopy; BRI, BONN-Risk index; CaOx, calcium oxalate hydrates; Cit, citrate; COD, calcium oxalate dihydrate; COM, calcium oxalate monohydrate; HAP, hydroxyapatite; NTU, Nephelometric turbidity units Ox, oxalate; Phos, phosphate; RRFA, Robertson Risk Factor Algorithms; RSS, Relative Supersaturation ; SEM, Scanning Electron Microscopy; SS, Supersaturation; $t_{1/2}$, half-time; UIC, Urine Inhibitory Capacity; ULM, Upper Limit Metastability; UV-Vis, Ultraviolet-Visible.

REFERENCES

- (1) Curhan, G. C. Epidemiology of Stone Disease. *Urol. Clin. North Am.* **2007**, *34* (3), 287–293.
- (2) Bartoletti, R.; Cai, T.; Mondaini, N.; Melone, F.; Travaglini, F.; Carini, M.; Rizzo, M. Epidemiology and Risk Factors in Urolithiasis. *Urol. Int.* **2007**, *79* (SUPPL. 1), 3–7.
- (3) Lorenzo, V.; Torres, A.; Hernández, D.; Ayus, J. C. *Manual de Nefrología*, 2nd ed.; Elsevier, España, 2002.
- (4) Conti, C.; Brambilla, L.; Colombo, C.; Dellasega, D.; Gatta, G. D.; Realini, M.; Zerbi, G. Stability and Transformation Mechanism of Weddellite Nanocrystals Studied by X-Ray Diffraction and Infrared Spectroscopy. *Phys. Chem. Chem. Phys.* **2010**, *12* (43), 14560–14566.
- (5) Conti, C.; Casati, M.; Colombo, C.; Realini, M.; Brambilla, L.; Zerbi, G. Phase Transformation of Calcium Oxalate Dihydrate-Monohydrate: Effects of Relative Humidity and New Spectroscopic Data. *Spectrochim. Acta - Part A Mol. Biomol. Spectrosc.* **2014**, *128*, 413–419.
- (6) H.Valido, Iris; Rius-Bartra, Joaquim M^a; Boada, Roberto; Resina-Gallego, Montserrat; Valiente, Manuel; Lopez-Mesas, M. Characterization of Calcium Oxalate Hydrates and the Transformation Process. *ChemPhysChem* **2020**.
- (7) Iris H. Valido Montserrat Resina-Gallego Ibraheem Yousef Maria Pilar Luque-Gálvez Manuel Valiente Montserrat López-Mesas. Calcium Oxalate Kidney Stones, Where Is the Organic Matter?: A Synchrotron Based Infrared Microspectroscopy Study. *J. Biophotonics* **2020**.
- (8) H.Valido, Iris; Fuentes-Cebrian, Victor; Boada, Roberto; Vallcorba, Oriol; Resina-Gallego, Montserrat; Valiente, Manuel; López-Mesas, M. Discriminating the Formation Origin of Calcium Oxalate Monohydrate in Kidney Stones via Synchrotron Microdiffraction. *Unpublished*.
- (9) Robertson, W. G. Methods for Diagnosing the Risk Factors of Stone Formation. *Arab J. Urol.* **2012**, *10* (3), 250–257.
- (10) Werness, P. G.; Brown, C. M.; Smith, L. H.; Finlayson, B. Equil 2: A BASIC Computer Program for the Calculation of Urinary Saturation. *J. Urol.* **1985**, *134* (6), 1242–1244.
- (11) Brown, C. M.; Purich, D. L.; Ackermann, D. K. EQUIL 93: A Tool for Experimental and Clinical Urolithiasis. *Urol. Res.* **1994**, *22* (2), 119–126.
- (12) Rodgers, A. L. Urinary Saturation: Casual or Causal Risk Factor in Urolithiasis? *BJU Int.* **2014**, *114* (1), 104–110.
- (13) Asplin, J. R.; Parks, J. H.; Coe, F. L. Dependence of Upper Limit of Metastability on Supersaturation in Nephrolithiasis. *Kidney Int.* **1997**, *52* (6), 1602–1608.
- (14) Robertson, W. G.; Jones, J. S.; Heaton, M. A.; Stevenson, A. E.; Markwell, P. J. Predicting the Crystallization Potential of Urine from Cats and Dogs with Respect to Calcium Oxalate and Magnesium Ammonium Phosphate (Struvite). *J. Nutr.* **2002**, *132* (6 SUPPL. 1), 1637–1641.
- (15) Williams, J. C.; Gambaro, G.; Rodgers, A.; Asplin, J.; Bonny, O.; Costa-Bauzá, A.; Ferraro, P. M.; Fogazzi, G.; Fuster, D. G.; Goldfarb, D. S.; Grases, F.; Heilberg, I. P.; Kok, D.; Letavernier, E.; Lippi, G.; Marangella, M.; Nouvenne, A.; Petrarulo, M.; Siener, R.; Tiselius, H. G.; Traxer, O.; Trinchieri, A.; Croppi, E.; Robertson, W. G. Urine and Stone Analysis for the Investigation of the Renal Stone Former: A Consensus Conference. *Urolithiasis* **2020**, No. 0123456789.
- (16) Puigdomenech, I. Make Equilibrium Diagrams Using Sophisticated Algorithms (MEDUSA). *Inorg. Chem.* **2004**.
- (17) Grases, F.; Llobera, A. Experimental Model to Study Sedimentary Kidney Stones. *Micron* **1998**, *29* (2–3), 105–111.
- (18) Chutipongtanate, S.; Thongboonkerd, V. Systematic Comparisons of Artificial Urine Formulas for in Vitro Cellular Study. *Anal. Biochem.* **2010**, *402* (1), 110–112. <https://doi.org/10.1016/j.ab.2010.03.031>.
- (19) Borghi, L.; Meschi, T.; Amato, F.; Briganti, A.; Novarini, A.; Giannini, A. Urinary Volume, Water and Recurrences in Idiopathic Calcium Nephrolithiasis: A 5-Year Randomized Prospective Study. *J. Urol.* **1996**, *155* (3), 839–843.
- (20) Daudon, M.; Letavernier, E.; Frochot, V.; Haymann, J. P.; Bazin, D.; Jungers, P. Respective Influence of Calcium and Oxalate Urine Concentration on the Formation of Calcium Oxalate Monohydrate or Dihydrate Crystals. *Comptes Rendus Chim.* **2016**, *19* (11–12), 1504–1513.
- (21) H.Valido, Iris; Fuentes-Cebrian, Victor; Valiente, Manuel; López-Mesas, M. Understanding the

- Crystalline Conversion of Oxalocalcic Kidney Stones: Effect of Common Urine Inhibitors in Vitro. *Unpublished*.
- (22) Barros, M. E.; Schor, N.; Boim, M. A. Effects of an Aqueous Extract from *Phyllanthus Niruri* on Calcium Oxalate Crystallization in Vitro. *Urol. Res.* **2003**, *30* (6), 374–379.
- (23) Li, T.; Ci, T.; Chen, L.; Yu, L.; Ding, J. Salt-Induced Reentrant Hydrogel of Poly(Ethylene Glycol)-Poly(Lactide-Co- Glycolide) Block Copolymers. *Polym. Chem.* **2014**, *5* (3), 979–991.
- (24) Mockaitis, G. Supplementary Information : Development of a Modified Boltzmann Sigmoidal Equation. **2016**, No. February 2015.
- (25) Bazin, D.; Leroy, C.; Tielens, F.; Bonhomme, C.; Bonhomme-Coury, L.; Damay, F.; Le Denmat, D.; Sadoine, J.; Rode, J.; Frochot, V.; Letavernier, E.; Haymann, J. P.; Daudon, M. Hyperoxaluria Is Related to Whewellite and Hypercalciuria to Weddellite: What Happens When Crystalline Conversion Occurs? *Comptes Rendus Chim.* **2016**, *19* (11–12), 1492–1503.

Support Information of the manuscript:

“In vitro study of the ratio promoters/inhibitors influence in oxalocalcic nephroliths formation: Approach for the development of Urine Inhibitory Capacity (UIC) as a risk index”

Authors: Iris H.Valido, Daniel Patilla-Gutiérrez, Manuel Valiente, Montserrat López-Mesas*

^a Centre Grup de Tècniques de Separació en Química (GTS), Departament de Química, Universitat Autònoma de Barcelona, Facultat de Ciències. Edifici CN. 08193, Bellaterra, Barcelona, Spain

**montserrat.lopez.mesas@uab.cat*

SI1: Comparison of the calibration curve between the static and the continuous method to measure turbidity

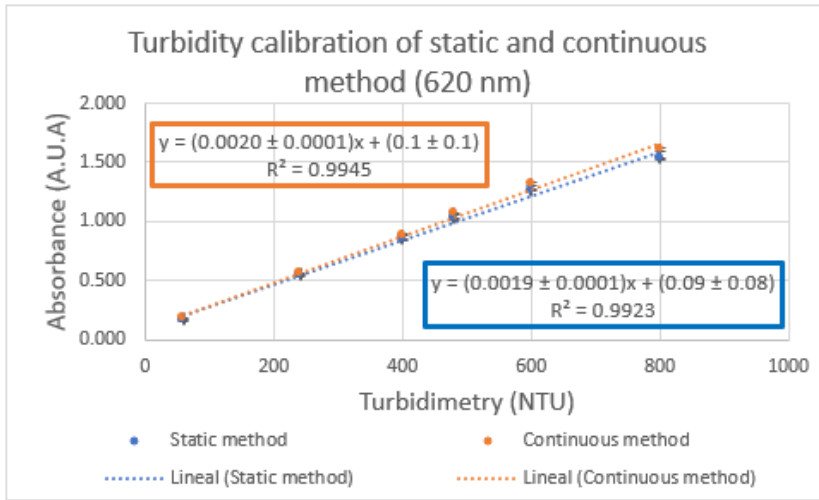


Figure 18. Calibration curve of the turbidity standards between 60 and 800 NTU measured by absorbance for the two methods, static (blue) and continuous (orange).

For the two methods used, static and continuous, the calibration results (Figure 18) show a linear correlation between turbidity (measured in NTU) and absorbance. To validate the equivalence between static and continuous method, t student test was applied. In this case, first was necessary to check the condition of equality of variances; if the standard deviations of the residuals of each $(S_{y/x})_1$ and $(S_{y/x})_2$ were significantly the same (H_0) or different (H_1). A Fisher test was performed to know if there were significant differences in the precision between both calibration curves (Equation 1). If the value of F_{exp} was less or equal to $F_{critical}$ for the level of significance desired and n_1-1 and n_2-1 degrees of freedom, then we accepted the hypothesis of equality of variances. For equality of variances, t_{exp} is calculated by Equation 2 and for inequality of variances, t_{exp} is calculated by Equation 3.

$$F_{exp} = \frac{(S_{y/x})_1^2}{(S_{y/x})_2^2} \quad \text{Equation 1}$$

$$t_{exp} = \frac{|b_1 - b_2|}{S_{b_1 - b_2}} \quad \text{Equation 2}$$

$$t_{exp} = \frac{|b_1 - b_2|}{\sqrt{S_{b_1}^2 + S_{b_2}^2}} \quad \text{Equation 3}$$

The F_{exp} was calculated using Equation 1. As $F_{exp} \leq F_{critical}$ for $\alpha = 0.05$ (95%), $(n_1-1) gl_1$, and $(n_2-1) gl_2$, are no significant differences in the precision between both calibration curves and hence the hypothesis of equal variances (H_0) is fulfilled. Then t_{exp} was calculated using Equation 2. Hence, from the results it can be concluded that there are no significant differences between both methods as $t_{exp} \leq t_{table}$ for $\alpha = 0.05$ (95%).

SI2: Equation 7 development (calcium complexation by the urine inhibitors) and constant values

$$[|CaCit^-| + |CaHCit| + |CaH_2Cit^+|] \cdot [|CaH_2PO_4^+| + |CaHPO_4| + |Ca_5(PO_4)_3OH|] = X \cdot Y$$

$$X = \left[\frac{|Ca^{2+}||Cit^{3-}|}{A} (\beta_{CaCit^-} \cdot B + \beta_{CaHCit} \cdot C + \beta_{CaH_2Cit^+}) \right]$$

$$Y = \left[\frac{|Ca^{2+}||PO_4^{3-}|_T}{D} \left(\beta_{CaH_2PO_4^+} + \beta_{CaHPO_4} \cdot E + \beta_{HAP} |Ca^{2+}|^4 \cdot F \cdot G^3 \cdot \left(\frac{|PO_4^{3-}|_T}{D} \right)^2 \right) \right]$$

$$A; D \equiv 1 + \frac{k_{a3}k_{a2}}{10^{-2pH}} + \frac{k_{a2}}{10^{-pH}} + \frac{10^{-pH}}{k_{a1}}$$

$$B; G \equiv \frac{k_{a3}k_{a2}}{10^{-2pH}}$$

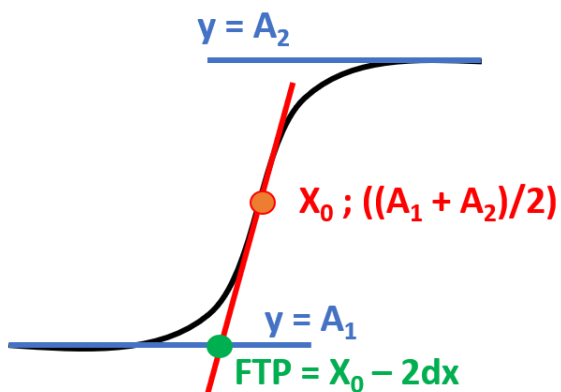
$$C; E \equiv \frac{k_{a2}}{10^{-pH}}$$

$$F \equiv \frac{k_w}{10^{-pH}}$$

	Use in: A, B or C	Use in: D, E, F or G
	Citrate	Phosphate
k_{a1}	$7.08 \cdot 10^{-4}$	$6.90 \cdot 10^{-3}$
k_{a2}	$1.70 \cdot 10^{-5}$	$6.20 \cdot 10^{-8}$
k_{a3}	$3.98 \cdot 10^{-7}$	$9.80 \cdot 10^{-13}$
k_w	$1 \cdot 10^{-14}$	

	log β	β	Reference
CaH₂PO₄⁺	1.45	28	L. Giocondi, B. S. El-Dasher, G. H. Nancollas, C. A. Orme, Molecular mechanism of crystallization impacting calcium phosphate cements. Phil. Trans. R. Soc. A (2010) 368, 1937-1961
CaHPO₄	2.77	589	
Ca₁₀(PO₄)₆(OH)₂	7.82	66069345	A. López-Macipe, J. Gómez-Morales, R. Rodríguez-Clemente, Nanosized Hydroxyapatite precipitation from homogeneous Calcium/Citrate/Phosphate solutions using microwave and conventional heating. Adv. Mater. 1998, 10 No.1
CaOx	3	1000	Lange's Handbook of Chemistry.
MgOx	3.43	2692	
MgH₂PO₄⁺	1.51	32	P. W. Linder, J. C. Little, Formation constants for the complexes of orthophosphate with magnesium and hydrogen ions. Talanta, Vol. 32, No. 1, pp 83-85, 1985
MgHPO₄	1.94	87	
MgPO₄⁻	3.13	1349	
CaCit⁻	4.86	72444	K. N., Pearce, Formation constants for magnesium and calcium citrate complexes. Aust. J. Chem., 1980, 33, 1511-7
CaHCit	2.92	832	
CaH₂Cit⁺	1.45	28	
MgCit⁻	4.85	70795	
MgHCit	2.67	468	
MgH₂Cit⁺	1	10	

S13: Illustration of the parameters needed to calculate the Urine Inhibitory Capacity (UIC)




$$y = \frac{A_1 - A_2}{1 + e^{(x-x_0)/dx}} + A_2$$

$$FTP = x_0 - 2dx$$

$$Max. Slope = Slope(x_0) = \frac{A_2}{4dx}$$

$$UIC = FTP \cdot Max. Slope = \frac{(x_0 - 2dx)A_2}{4dx}$$

Figure 19. Example of a sigmoidal curve fitting with Boltzmann function and its parameters. In the equations, A_1 and A_2 correspond to the asymptotic values of y (Rel. Absorbance) at infinitely small and large x (oxalate concentration added) respectively, x_x correspond to the center of the Boltzmann sigmoid and dx correspond to the deviation of x around x_x . FTP means First Turning Point; Max. Slope is the maximum slope of the curve; and UIC means Urine Inhibitory Capacity.



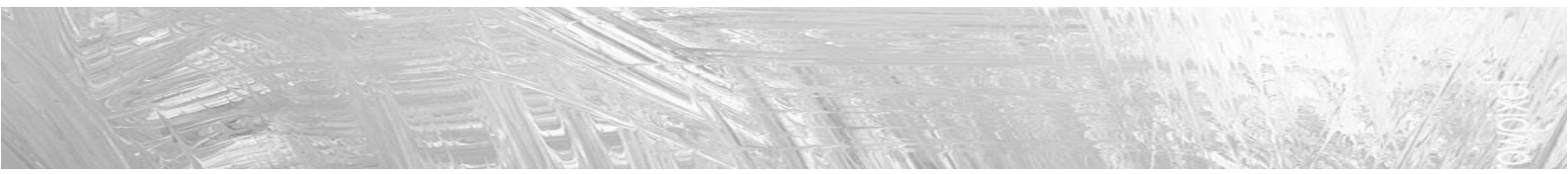
**A comparative study of the *Lepidium latifolium*
(*Rompepiedras*) extracts effects on calcium
oxalate crystallization *in vitro***

Iris H. Valido, Paula Cairó-Ballester, Manuel Valiente, and Montserrat López-Mesas*

Centre Grup de Tecniques de Separacio en Quimica (GTS), Departament de Quimica, Universitat Autònoma de Barcelona, Facultat de Ciències, Edifici CN. 08193, Bellaterra, Barcelona, Spain

**Montserrat.lopez.mesas*

Unpublished



A comparative study of the *Lepidium latifolium* (Rompepiedras) extract effects on calcium oxalate crystallization *in vitro*

Iris H. Valido, Paula Cairó-Ballester, Manuel Valiente, Montserrat López-Mesas*

Centre Grup de Tècniques de Separació en Química (GTS), Departament de Química, Universitat Autònoma de Barcelona, Facultat de Ciències, Edifici CN, 08193, Belaterra, Spain.

KEYWORDS: kidney stones; calcium oxalate; *Lepidium latifolium*; inhibition; antioxidant; polyphenols; flavonoids; alkaloids; fixed oils

ABSTRACT: *Lepidium latifolium* is a plant traditionally used in the folk medicine of Canary Islands for the treatment of renal affections such as lithiasis, being known as “Rompepiedras” (Stone breaker). Moreover, it has been reported to be used as stomach tonic, diuretic and anti-hypertensive among others, but its capacity as anti-lithiasic has not been previously tested. Hence, in this work the potential of several extracts from the leaves of this plant on the inhibition of calcium oxalate crystals formation *in vitro* using Artificial Human Urine as precipitating medium was studied, as well as their cytotoxic properties and the antioxidant potential of the powdered dry leaves and aqueous extract. The results showed a higher antioxidant capacity when compared with the same extract from the plant collected in India, as well as an inhibitory effect of the oxalocalcic formation produced by polyphenols and fixed oils, while flavonoids and alkaloids promoted its precipitation. Furthermore, the cytotoxic screening revealed that the extract studied present a good IC₅₀ (0.8-5.3 mg/mL) that could be related with the high content of the flavonoid anthocyanin that has been reported elsewhere. The results of this work show that extracts of this plant present a high potential to be used as prophylactic treatment against calcium oxalate nephroliths in order to avoid their formation and/or prevent the recurrence.

INTRODUCTION

Kidney stones have a prevalence of 7-15% in men and 3-6% in women worldwide¹, being notably higher in industrially developed countries². Moreover, it presents a high, and increasing, recurrent rate of 30-50% in the next 5 to 10 years after the first episode, and up to 75% after 20 years^{3,4}. From the seven types of nephroliths, the ones formed by calcium oxalate present the higher incidence (66%)⁵. Thus, preventing its formation in the kidneys with the use of prophylactic treatments would be of great interest to prevent the disease of its recurrence.

There are many reviews and research papers listing the herbal medicines used in different regions for the treatment of renal affections with the preparation methods used and properties⁶⁻²⁰. From those, there are two that had showed to be effective on the inhibition of calcium oxalate stones in *in vitro* experiments, in rat models, and in some studies with calcium stone forming

patients: *Phyllanthus niruri*, from the Euphorbiaceae family and widely used in folk medicine in Brazil to treat urolithiasis²¹⁻²⁶; and *Herniaria hirsuta*, from the Caryophyllaceae family and used in Morocco to treat kidney stones²⁷⁻³⁰. Furthermore, there is a plant traditionally used in the folk medicine of the Canary Islands, as well as in other regions such as India³¹⁻³³, to treat such affections, *Lepidium latifolium* from the Brassicaceae family. It is known in the Canary Islands as “Rompepiedra” (Stone breaker) for its antilithiasic properties, which use knowledge has been collected from the old generations in a series of interviews performed in Gran Canaria³⁴. This plant has been also reported for its use as stomach tonic, diuretic, anti-hypertensive, against renal lithiasis and other kidney disorders and against prostatic hyperplasia³², as well as for its antitumor³⁵ and antimicrobial³⁶ activity, being its aqueous extract diuretic properties just fully studied on one research paper³¹, to the knowledge of the authors of this work.

The objective of this work is to study the possible effect of *Lepidium latifolium* extract in different fractions (polyphenols, flavonoids, alkaloids and fixed oils) as inhibitors of the oxalocalcic formation *in vitro*.

MATERIALS AND METHODS

Reagents

All the chemicals in this project were of analytical grade. From Merck (Germany): petroleum ether (75%), diethyl ether ($\geq 99.5\%$), n-hexane anhydrous (95%), ammonium chloride (99.5%), calcium nitrate tetrahydrate (99%), sodium citrate dihydrate (99%) and creatinine (99%). From VWR (Belgium): methanol ($\geq 99\%$), ammonium hydroxide (25%), and chloroform (99%), uric acid (99%). From Scharlau (Spain): ethanol (96%), sulfuric acid (95-98%), and ascorbic acid (99.7%), magnesium sulfate heptahydrate (99%). From Sigma-Aldrich (India): ethyl acetate ($\geq 99.5\%$), and 2,2-diphenyl-1-picrylhydrazyl (DPPH), urea (99%). From Fluka (Germany): 2,4,6-Tris(2-pyridyl)-s-triazine (TPTZ), iron (III) chloride anhydrous (97%). From Panreac (Spain): sodium acetate trihydrate (99%), potassium chloride (99.5%), sodium chloride (95%), sodium dihydrogen phosphate dihydrate (95%), sodium hydrogen phosphate dihydrate (95%), sodium oxalate (95%), and sodium sulfate (99%).

The reagents used for the cell culture and the cytotoxic screening were: DMEM (Dulbecco's Modified Eagle Medium, ThermoFisher Scientific, Waltham, USA), fetal bovine serum (FBS; ThermoFisher Scientific) and penicillin-streptomycin (Sigma-Aldrich). Cell proliferation reagent WST-1 (Sigma-Aldrich). HEK-293 (human embryonic kidney) cells were obtained from ATCC (American Type Culture Collection).

Equipment

To measure the absorbances, a spectrophotometer UV-Vis (UV-2 200 040610 Unicam, United Kingdom) with a tungsten lamp to measure the absorbance of the samples at 620 nm (1200 nm/s) was used. All the parameters and measures were controlled by the VISIONpro software. A pH-meter (MicroPH 2002 Crison, Spain) with a pH electrode (52-21 Crison, Spain) was used to measure and adjust the pH of the samples. To characterize the solid samples, an Infrared Spectrophotometer Tensor 27, equipped with an Attenuated Total Reflectance module (ATR-FTIR, Bruker, Ettlingen, Germany), with a resolution of 4 cm⁻¹,

was used, and a Field Emission-Scanning Electron Microscope MERLIN (FE-SEM, Zeiss), with a 1.4 nm resolution, 1 kV 4 pA-100 nA probe current and 0.2-30 kV accelerating voltage, was used to study the morphology of the crystals. The EQUIL 1.4b program (University of Florida)³⁷ to calculate the RSS of urine. OriginPro® 2016 (OriginLab Corporation, Northampton, MA, USA) program was used to make the fitting of the data and the graphic representations. The OriginLab software (OriginLab Corp., Northampton, MA, USA) was used for the graphical representation and the treatment of the results.

Samples

Dried bundles of *Lepidium latifolium* L. were purchased from a "yerbero" (person who is dedicated to selling medicinal herbs) market stall in Gran Canaria. The taxonomic identification was confirmed and a sample has been deposited in the "Colección de Referencia Botánica" of the Universidad de las Palmas de Gran Canaria, with the entry number ULP-811.

The plant bundles were dried at 45-50°C for 12 hours, after which the leaves were separated from the stems and seeds, and were powdered with the use of an automatic mortar. The powdered dried leaves were storage at room temperature in sealed containers.

Aqueous extract

The aqueous extract was prepared by following the procedure described by Navarro et al. (1994)³¹ with some modifications. Briefly, 120 grams of the powdered sample was mixed with 800 mL of Milli-Q water, and was boiled by reflux for 12 hours. The mixture was allowed to cool down at room temperature, and then vacuum filtered. The filtrate was concentrated by rotary evaporation at 50°C until a syrupy residue was obtained with an overall extraction of 44% (w/w).

Polyphenols extract

Polyphenols were extracted with the method described by Kaur et al. (2013)³⁸. Briefly, 25 grams of the powdered sample was mixed with 500 mL of methanol (80%), keeping the ratio sample/methanol at 0.05 g/mL and heated at 40°C with a reflux and constant stirring for 8 hours. The mixture was vacuum filtered using Nylon filters with a 0.45 µm pore size, and then concentrated by rotary evaporation at 40°C until dry, with an overall extraction of 23% (w/w).

Flavonoids extract

For the extraction of flavonoids, the method described by Guyot et al. (1997)³⁹ was the one used with some modifications. Briefly, 10 mL of hexane were added to 1.5 g of the powdered sample and mixed in an ultrasonic bath for 15 min at 40°C, followed by a 5 min centrifugation at 3000 rpm. The supernatant was then discarded to remove the non-polar organic compounds (mainly lipids, carotenoids and chlorophylls). This process was repeated for a total of three times. Afterwards, the same steps were followed, but adding 10 mL of methanol in order to remove the sugars, organic acids and phenolic compounds of low molecular weight. Finally, the same steps were repeated again, but adding 10 mL of a mixture acetone:water (60:40), and this time keeping the supernatants. These three last supernatants were collected, mixed together and dried with a rotary evaporator, obtaining an overall extraction of 14% (w/w).

Alkaloids extract

The alkaloid extraction was performed following the method described by Djilani et al. (2006)⁴⁰. The process starts with the addition of 4 mL of NH₄OH (25%, w/w) to 2.5 grams of the powdered sample, followed by 75 mL of ethyl acetate, keeping the mixture at room temperature for 72 hours while homogenizing it twice per day. After the indicated time passed, the mixture was filtered using Nylon filters (0.45 µm pore size) and the solvent was evaporated at 40°C in a rotary evaporator. The obtained residue was then dissolved in 20 mL Milli-Q water and acidified until pH 3-4 with H₂SO₄ (1M). The separation of the alkaloid fraction was performed by liquid/liquid separation following the process described in Figure 1, being the overall extraction of 0.46% (w/w).

Fixed oils extract

The methods used by Le et al. (2004)⁴¹ and Abushama et al. (2014)⁴² were adapted to extract the fixed oils from the powdered samples with the use of ultrasonic bath and reflux. This process begins with the addition of 100 mL of petroleum ether to 15 g of the powdered sample, and keeping the mixture on a ultrasonic bath (42 ± 6 KHz and 100 W) for 1 hour at 40°C. This mixture was then heated with a reflux for four additional hours at 40°C. When the time passed, the mixture was filtrated and concentrated in a rotary evaporator, obtaining an overall extraction of 2% (w/w).

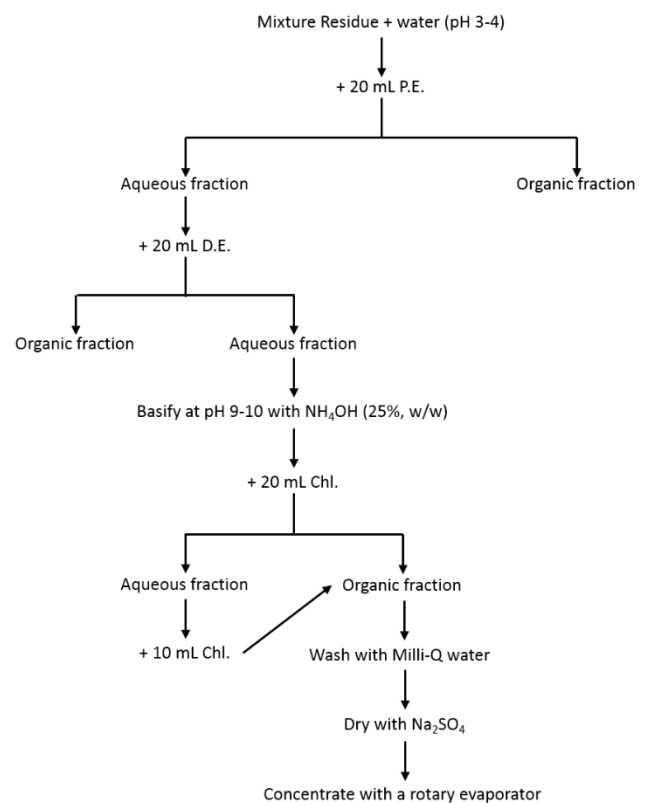


Figure 1. Schematic representation for the separation of alkaloids, starting with the acidified mixture of the residue obtained in the extraction, with ethyl acetate, with water. The abbreviations used in the scheme correspond to: petroleum ether (P.E.), diethyl ether (D.E.) and chloroform (Chl.).

Determination of the antioxidant activity of the powdered dry leaves and aqueous extract

Ethanol pretreatment

This pretreatment was performed following a similar method to the one described by Chaieb et al. (2011)⁴³. Briefly, 15 mL of ethanol (70%) were added to 1 g of powdered plant or aqueous extract, being subjected to rotary agitation for one hour, and then centrifuged for 10 min at 2500 rpm. The supernatant was collected, and the process was repeated two more times with the addition of 2.5 mL of ethanol (70%), followed by 30 min of rotary agitation and centrifugation. The three supernatants were collected and mixed together.

Methanol pretreatment

This pretreatment was performed following the ISO 14502-1:2005 for the determination of the total content of polyphenols in tea⁴⁴. Briefly, 5 mL of methanol (70%) at 70°C were added to 0.2 g of powdered plant or aqueous extract, keeping it at 70°C for 10 min and

performing vortex agitation every 5 min. Samples were cooled down at room temperature, and then centrifuged for 10 min at 3000 rpm. The supernatant was collected, and the same process was repeated one more time over the sediment. Both supernatants were mixed in a 10 mL volumetric flask and made up to the mark with methanol (70%).

DPPH assay

The DPPH (2,2-diphenyl-1-picrylhydrazyl) free radical scavenging activity of the powdered sample and the aqueous extract was determined following the method described elsewhere^{43,45}. A 240 ppm stock solution of DPPH in methanol was prepared and kept at 4°C until use. To prepare the working solution of the radical, the DPPH stock solution was diluted in methanol until an absorbance of 0.98 ± 0.02 at 517 nm was obtained. To perform the assay, 3 mL of the DPPH working solution were added to a test tube and mixed with 100 µL of the samples from the ethanolic or methanolic pretreatments (10 mg/mL). The mixture was kept in dark for 30 min and then the absorbance was measured at 517 nm. A control solution was prepared using 100 µL of methanol instead of sample, as well as a control for the samples in where 100 µL of the same samples were mixed with 3 mL of methanol. In order to determine the antioxidant or radical scavenging activity (%), the Equation 1⁴³ was used, where A_0 is the absorbance of the control solution (DPPH + methanol), A_i is the absorbance of the samples with DPPH, and A_S is the absorbance of the sample control (sample + methanol).

$$\% \text{Antioxidant activity} = \frac{A_0 - (A_i - A_S)}{A_0} \cdot 100 \quad \text{Equation 1}$$

FRAP assay

Ferric reducing antioxidant potential (FRAP) of the samples from ethanolic and methanolic pretreatments was determined following the method described elsewhere^{43,45}. Briefly, the FRAP reagent was prepared by mixing solutions of 10mM of TPTZ, 20 mM of FeCl₃ and 0.3 M of acetate buffer (pH 3.6) in a v/v proportion of 1:1:10. The FRAP reagent was incubated at 37°C for 15 min prior to its use. Dilutions of the samples were performed before the analysis, using final concentrations of 4 and 3 mg/mL of the ethanolic solution from the powdered sample and the aqueous extract respectively, and 3 mg/L for both methanolic solution. Ascorbic acid was used as

standard in the range between 0.01 to 0.05 mg/mL in methanol. To perform the assay, 150 µL of sample was mixed with 2.85 mL of the incubated FRAP reagent, being kept in the dark for 30 min. After this period, the absorbance was measured at 593 nm. The results are expressed as mg of ascorbic acid equivalents per mL (AAE mg/mL).

Effect of the different extracts on the *in vitro* induction of CaOx in artificial urine

The artificial human urine (AHU) used in this study is based in the ones developed in a previous study⁴⁶, and adapted to have a RSS (COM) of 7.4 (in the middle of the range). To prepare the AHU, equal volumes of two solutions (A and B) were mixed at a flow rate of 0.3 mL/min, under constant stirring and adjusting the pH of the mixture to six. Solution A contains: 4.860 g of Na₂SO₄, 1.020 g of MgSO₄·7H₂O, 1.819 g of NH₄Cl, 12.197 g of KCl, 2.239 g of Ca(NO₃)₂·4H₂O and 0.303 g of uric acid. While Solution B contains: 0.595 g of NaH₂PO₄·2H₂O, 0.745 g of Na₂HPO₄·2H₂O, 14.281 g NaCl, 0.075 g of Na₂C₂O₄, 2.706 g of Na₃C₆H₅O₇·2H₂O, 2.398 g of creatinine and 23.063 g of urea.

The precipitation of calcium oxalate was induced by performing four additions of 800 µL of sodium oxalate (0.1 M), one every 30 min, into 20 mL of AHU at 37°C and under constant stirring, achieving a final concentration of added oxalate in the medium of 0.016 M²³. For the inductions in the presence of *Lepidium latifolium* extracts, these were added to the sample 30 min prior to the process²³, corresponding to 0.5 mL of each fraction (polyphenols, flavonoids, alkaloids, and fixed oils) re-suspended in ethanol (equivalent to 25 ppm (mg extract/L ethanol) in the AHU, being 0.5 mL of ethanol used as control which is a common concentration used in the literature to determine different properties of plant extracts⁴⁷⁻⁴⁹). Each induction was performed by triplicate.

When the incubation experiment was finished, the absorbance of each sample was measured in triplicate at 590 nm, and the Relative Nucleation (Rel. Nuc.) was calculated using Equation 2, where A_S corresponds to the absorbance of the incubation with extract and A_C corresponds to the absorbance of the control incubation.

$$\text{Rel. Nuc} = A_S - A_C \quad \text{Equation 2}$$

After the analysis, the solutions containing the crystals were centrifuged at 2500 rpm for 10 min, then washed twice with 5 mL of water, and twice with 5 mL of ethanol, repeating the centrifugation process after each wash.

Cytotoxic screening

Human embryonic kidney cells (HEK-293) were used for cytotoxicity screening of the *Lepidium latifolium* leaves extracts. The cell line was cultured in DMEM supplemented with FBS (10%, v/v), penicillin (100 unit/mL) and streptomycin (100 µg/mL) and incubated at 37°C and 5% CO₂. The extracts were diluted with cell culture medium till target concentration range (from 0.05 to 20 mg/mL). For the cytotoxic screening, the HEK-293 cells were seeded in 96-well plates (10⁴ cells/well) and were left to attach for 24 hours prior treatment at 37°C (5% CO₂). After the incubation period, the medium was discarded and 100 µL of the extract solution in the cell medium was added to each well. The cells were incubated for another 24 hours under the same conditions, and then 10 µL of the Cell Proliferation Reagent WST-1 was added to determine the cell viability. After 2 hours of incubation, the plates were shaken and the absorbance was measured at 440 nm (maximum absorbance of the formazan product) and at 650 nm (as reference wavelength)⁵⁰. The percentage of cell viability was calculated using Equation 3, where A_S corresponds to the sample absorbance, A_{NC} corresponds to negative control absorbance (the sample without WST-1) and A_{PC} corresponds to the positive control absorbance (absorbance without sample)⁵¹.

$$\text{Viability (\%)} = \frac{A_S - A_{NC}}{A_{PC} - A_{NC}} \cdot 100 \quad \text{Equation 3}$$

The extract concentration needed to inhibit 50% of the cell viability (IC₅₀) was calculated by the Dose Response fitting (on the OriginLab software) of the logarithm of the concentration, in the x-axis, vs. the percentage of cell death (100 – viability), in the y-axis.

RESULTS AND DISCUSSION

Antioxidant activity of the powdered dry leaves and aqueous extract

Since the leaves of *Lepidium latifolium* are consumed in folk medicine as an infusion, which are also sold by companies as dried leaves in vacuum packs³¹, the antioxidant capacity of the aqueous extract and the

powdered dry leaves, were determined by the DPPH and FRAP assays. The results of the mentioned antioxidant capacities are summarized in Table 1. As can be seen, the pretreatment on methanol achieved a higher antioxidant capacity than the ones in ethanol, being in both cases higher for the aqueous extract than for the direct powdered leaves extraction, since the aqueous extract is a concentrate of plant components. The differences between pretreatments could be related to the effectiveness of both solvent to extract components such as polyphenols, which are well known for their antioxidant properties, being usually extracted with methanol as solvent⁴⁴.

Table 1. Antioxidant capacity of the powdered dry leaves and the aqueous extract of *Lepidium latifolium* calculated by two methods: DPPH scavenging capacity (%) and Ferric reducing antioxidant potential, or FRAP (AAE mg/g), and using two solvents as pretreatment (methanol and ethanol).

	Solvent	Powdered dry leaves	Aqueous extract
DPPH scavenging capacity (%)	Ethanol	13.4 ± 0.1	25.32 ± 0.01
	Methanol	19.4 ± 0.4	29.5 ± 0.5
FRAP assay (AAE mg/g)	Ethanol	4.6 ± 0.2	7.0 ± 0.3
	Methanol	5.9 ± 0.3	8.0 ± 0.3

The methanolic extract (10 mg/mL) from the dried leaves of *Lepidium latifolium* collected in Gran Canaria, show a DPPH scavenging capacity of 19.4±0.4%. This value is higher than the one reported for the same type of extract and plant, but collected in the Ladakh region of India, which presented an average DPPH scavenging capacity of 9.8% for the same concentration (reported in the literature, for a concentration of 40 mg/mL, as 39.1%)³⁸. The differences regarding the antioxidant capacities could be due to the environmental conditions surrounding the plant growth, being Gran Canaria well known for its warm temperature along the whole year, while Ladakh is a cold and arid region with severe conditions such as sub-zero temperatures³⁸.

Effect of the different extractions on the *in vitro* induction in artificial urine

The relative nucleation of calcium oxalate after the induction of its precipitation on AHU in the presence of the different extracts can be seen in Figure 2. Negative

values of Rel. Nuc. represent a lower precipitation in the sample than in the control, inhibitory potential, while positive values represent more crystals in the sample than in the control, promoter potential. As can be seen, flavonoids and alkaloids promote the precipitation of calcium oxalate, whereas polyphenols and fixed oils inhibit it, being the latter the one with the highest inhibitory capacity. This can be related with the inhibitory potential of lipids, since they have a strong binding capacity with calcium ions^{52,53}, making them less available to interact with oxalate in the urine. Moreover, lipids were found in the surface of quiescent calcium oxalate kidney stones in a previous study⁵⁴. On the other hand, a study where the inhibition potential of gallic acid on calcium oxalate nucleation⁵⁵, the authors propose an inhibition mechanism that comprehend the formation of amorphous calcium oxalate (ACO).

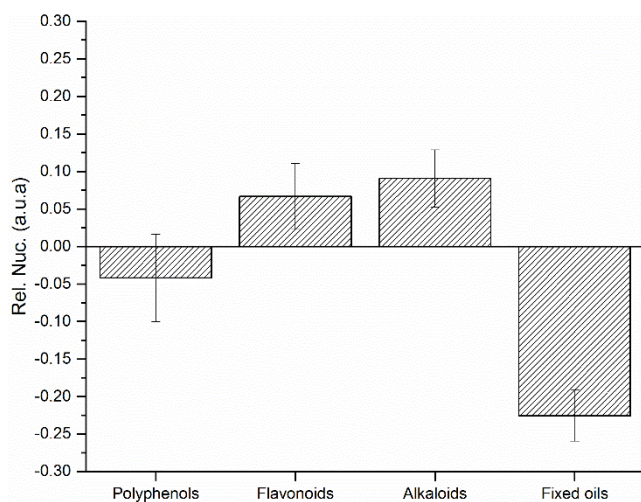


Figure 2. Relative nucleation of calcium oxalate after the induction by oxalate addition in the Artificial Human Urine (AHU) medium, in the presence of different extract fractions (polyphenols, flavonoids, alkaloids and fixed oils).

The SEM images showing the morphologies of the calcium oxalate crystals after the precipitation

induction in AHU in the presence of different extract fractions can be seen in Figure 3. The control (Figure 3 A) presents a mixture of smaller and non well-defined COM crystals and COD crystals morphologies that could be produced by the presence of ethanol in the AHU medium: cross-shaped, with four sharp branches⁵⁶, and a twisted-shape than comes from the twist growth of instable COD⁵⁷. In the SEM image that corresponds to the presence of polyphenols (Figure 3 B) similar morphologies than in the control are observed, with the addition of more amorphous material between them, which could be related with the study previously presented where the inhibition of calcium oxalate was caused by the formation of ACO⁵⁵. Despite having flavonoids in the medium promotes the formation of oxalocalcic crystals (Figure 2), smaller and less defined crystallites are observed (Figure 3 C), that could avoid their aggregation and facilitate their expulsion in the urine. The IR spectra from crystals obtained in the flavonoid extract (Figure 4, left panel) presents two peaks 1184 and 1119 cm^{-1} , corresponding to the asymmetric stretching of the $\text{C}=\text{C}-\text{O}-\text{C}_{\text{aliphatic}}$ and CO (or $\text{C}-\text{OH}$) vibrations on the phenolic ring respectively, that could indicate a strong interaction between flavonoids and crystals surface. The crystals formed in the presence of alkaloids (Figure 3 D) are the most similar to the control, presenting more twisted crystals. Finally, the crystals induced in the medium with the fixed oil extract present smaller crystals more similar to the small and not well-defined COM crystals of the control (Figure 3 E). In this case, the IR spectra (Figure 4, right panel) show three peaks, 2962, 2922 and 2851 cm^{-1} that correspond to the asymmetric stretching of $-\text{CH}_3$ and $-\text{CH}_2$ and the symmetric stretching of $-\text{CH}_2$ respectively, which are in the lipidic region of the spectra. This could also indicate a strong interaction between the components of the fixed oil extract and the surface of the crystals.

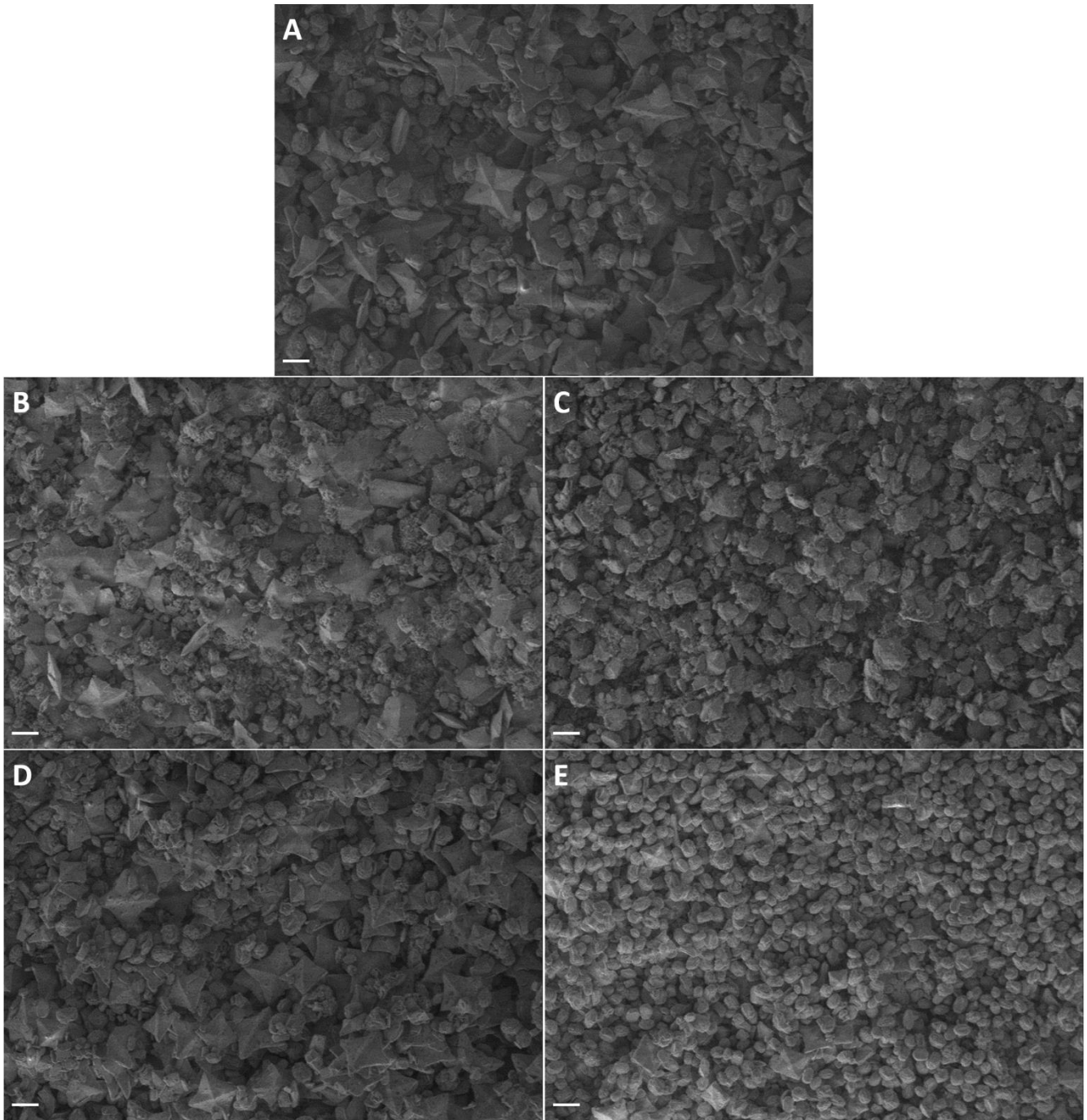


Figure 3. SEM images of the calcium oxalate precipitated after the induction by oxalate addition in the Artificial Human Urine (AHU) medium in the presence of different extract fractions: A) control with ethanol; B) polyphenols; C) flavonoids; D) alkaloids; and E) fixed oils. Scale bar on all images is 10 μm .

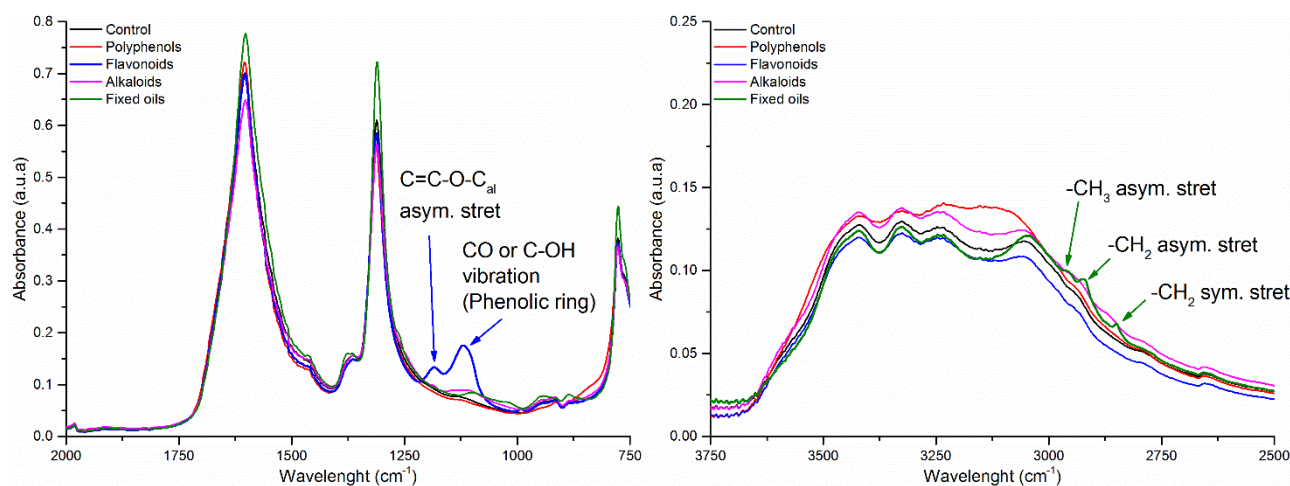


Figure 4. ATR-FTIR spectra of the calcium oxalate crystals after the precipitation induction in Artificial Human Urine (AHU) in the absence (control, black) and presence of different *Lepidium latifolium* leaves extracts: polyphenols (red), flavonoids (blue), alkaloids (pink) and fixed oils (green). The characteristic bands observed for flavonoids (left panel) and fixed oils (right panel) are marked with arrows.

Cytotoxic screening

The extract concentration needed to inhibit 50% of the HEK-293 cell viability (IC_{50}) was determined for the different fractions tested in this study (¡Error! No se encuentra el origen de la referencia.). As can be observed, flavonoids and alkaloids present the higher IC_{50} , being less lethal (a higher concentration is needed to kill 50% of the cells) than the other extracts, while polyphenols and fixed oils present the lower IC_{50} values, or the more lethal ones. The aqueous extract presents an intermediate value when compared with the rest, which is related to its composition (it is a mixture of all the components).

The IC_{50} values of the extracts from *Lepidium latifolium* leaves presented in this work are in the range between 0.8 and 5.3 mg/mL. These concentrations presents a low cytotoxicity for the HEK-293 cell lines, since it has been reported IC_{50} values in the range of 25 to 60 $\mu\text{g/mL}$ for other plants leaves extracts (e.g. 25.7 $\mu\text{g/mL}$ for *Solanum coagulans*⁵⁸, 53.5 $\mu\text{g/mL}$ for *Acacia laeta*⁵⁹ and 60.3 $\mu\text{g/mL}$ for *Phoenix paludosa*⁶⁰). However, lower cytotoxicity effect has been found in the aqueous extract of *Grewia asiatica* (53.34 mg/mL), which is a plant commonly used by Native Americans for its antioxidant and anti-inflammatory properties⁶¹ and has been recently studied for its antilithiasic activity⁶². It is interesting that both, *Grewia asiatica*⁶¹ and *Lepidium latifolium*⁶³, are rich in anthocyanin, a flavonoid, presenting flavonoids one of the highest IC_{50} in the present study, which could mean that this phytochemical group is less toxic to the renal cells.

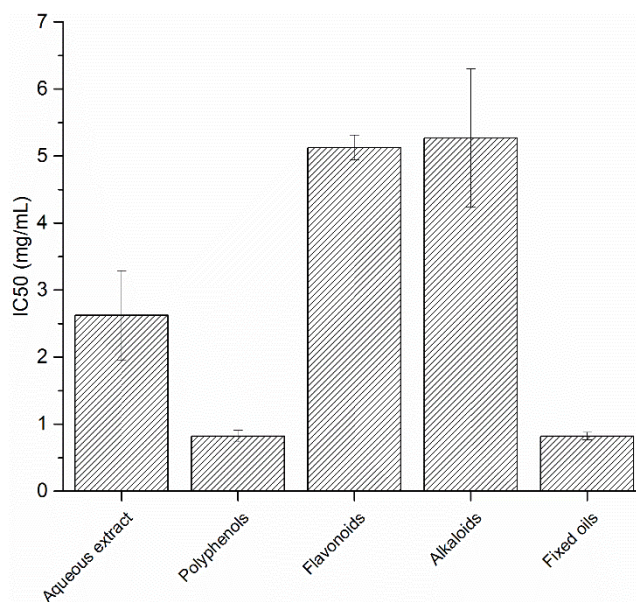


Figure 5. Extract concentration needed to inhibit 50% of the cell viability (IC_{50}) for the different extract fractions (aqueous extract, polyphenols, flavonoids, alkaloids and fixed oils).

CONCLUSIONS

The higher antioxidant capacity achieved for the methanolic extract in both the powdered leaves and the aqueous extract could be related to the higher extraction of polyphenols with the mentioned solvent when compared with ethanol. Moreover, the methanolic pretreatment from dried leaves of *Lepidium latifolium* collected in Gran Canaria presented a higher antioxidant activity that the one from the Ladakh region of India and reported in the literature³⁸, which could be due to environmental conditions surrounding the plant

growth. Moreover, the potential of the different extracts (polyphenols, flavonoids, alkaloids and fixed oils) to inhibit the formation of calcium oxalate crystal on Artificial Human Urine (AHU) with and intermediate Relative Supersaturation for COM (RSS = 7.4) was evaluated. After the induction of the precipitation, it was observed that flavonoids and alkaloids presented a promoter potential while polyphenols and fixed oils were inhibitors, presenting the latter the highest capacity that has been related to the strong binding capacity of lipids to calcium ions^{52,53}, what corroborates the results from previous analysis performed with synchrotron based FTIR microspectroscopy on kidney stones⁵⁴. The inhibitory potential of polyphenols has been related with the formation of amorphous calcium oxalate (ACO)⁵⁵. These effects were corroborated by the SEM images as well as the ATR-FTIR spectra. Moreover, flavonoids extract presents smaller and less defined crystallites in the SEM images, which could be associated with the strong interaction of the flavonoids with the crystal surface as it was shown in the ATR-FTIR bands analysis. Regarding the cytotoxic screening performed on the HEK-293 cell line, it was concluded that the studied extracts from the leaves of *Lepidium latifolium* present high IC₅₀ values when compared with other plant extracts, which could be due to the high content of anthocyanin, a flavonoid. The results of this work show that *Lepidium latifolium* is a promising plant for the prophylactic treatment of nephrolithiasis, as it is believed by the folk in Gran Canaria. However, further studies are needed to understand the role of the different extracts on the inhibition of calcium oxalate, as well as to determine which components of each fraction arrive to the kidneys after the digestion and absorption in the body.

AUTHOR INFORMATION

Corresponding Author

* montserrat.lopez.mesas@uab.cat

Author Contributions

The manuscript was written through contributions of all authors. / All authors have given approval to the final version of the manuscript.

ACKNOWLEDGMENT

The authors want to acknowledge the financial support from the Ministerio de Economía y Competitividad

(Spanish Project CMT 2015-65414-C2-1-R). This project has received funding from the European Union's Horizon 2020 research and innovation programme under the Marie Skłodowska-Curie grant agreement No.778325). Iris H.Valido acknowledges funding support from the Universitat Autònoma de Barcelona (PIF-2016 grant. All the authors are grateful to the Serveis de Suport a la Investigació of the UAB (Servei d'Anàlisi Química and Servei de Microscòpia). The authors want to acknowledge to Dr. Jacob Morales and Pedro Henríquez-Valido for the help on the botanical identification and deposition of the plant on the registry. The authors want to acknowledge to Prof. Moustapha Hassan and Dr. Ying Zhao from Karolinska Institutet for the material and help given to perform the cell experiments.

ABBREVIATIONS

AAE, ascorbic acid equivalents; AHU, artificial human urine; ATCC, American Type Culture Collection; ATR-FTIR, Attenuated Total Reflectance Fourier Transform Infrared spectroscopy; CaOx, calcium oxalate hydrates; COD, calcium oxalate dihydrate; COM, calcium oxalate monohydrate; DPPH, 2,2-diphenyl-1-picrylhydrazyl; FBS, fetal bovine serum; FRAP, Ferric reducing antioxidant potential; noHEK, human embryonic kidney; IR, infrared; RSS, relative Supersaturation; SEM, scanning electron microscopy.

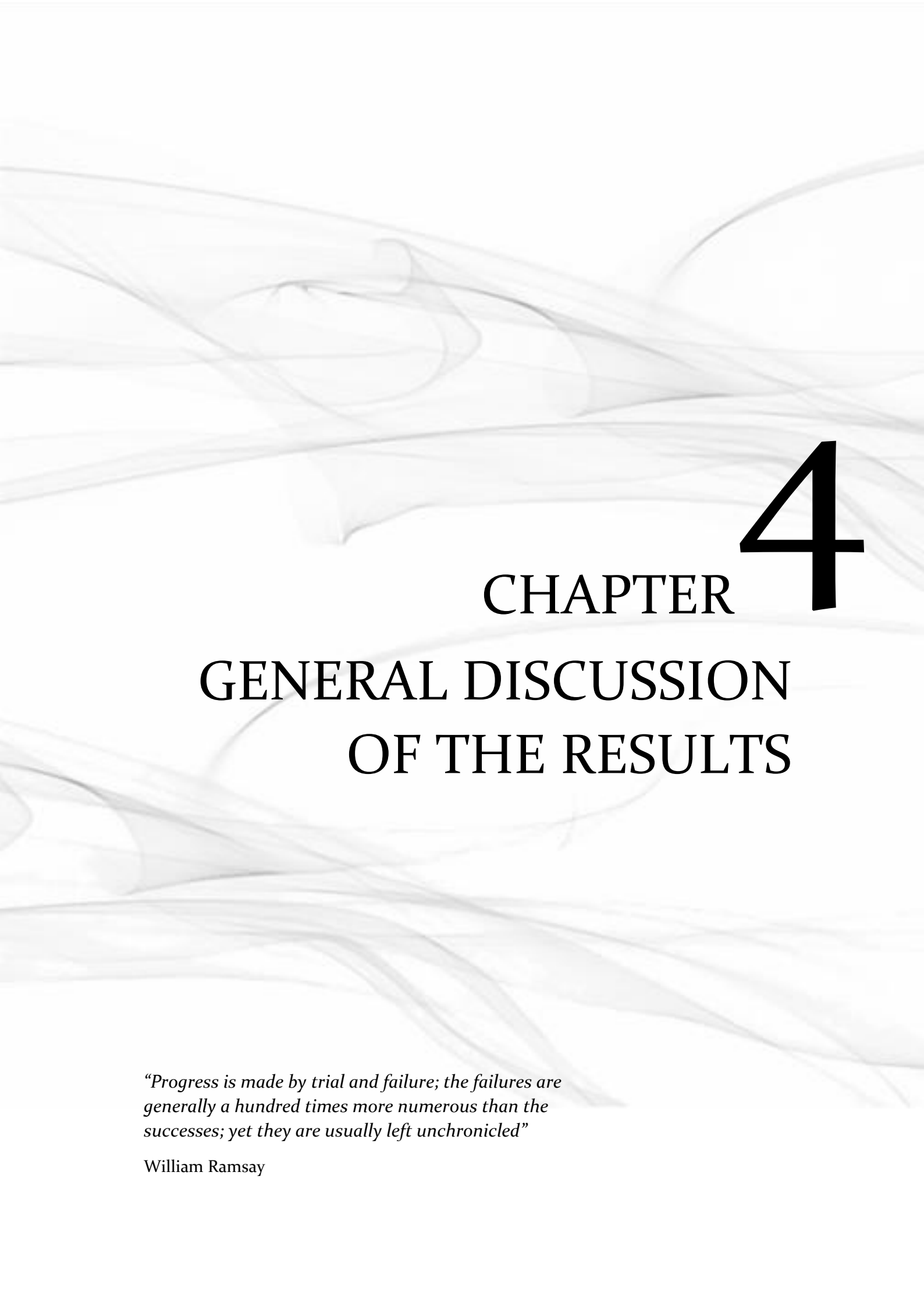
REFERENCES

- (1) Ferrari, P.; Piazza, R.; Ghidini, N.; Bisi, M.; Galizia, G.; Ferrari, G. Lithiasis and Risk Factors. *Urol. Int.* **2007**, *79* (SUPPL. 1), 8–15. <https://doi.org/10.1159/000104435>.
- (2) Robertson, W. G. Is Prevention of Stone Recurrence Financially Worthwhile? *Urol. Res.* **2006**, *34* (2), 157–161.
- (3) Curhan, G. C. Epidemiology of Stone Disease. *Urol. Clin. North Am.* **2007**, *34*, 287–293.
- (4) Alelign, T.; Petros, B. Kidney Stone Disease: An Update on Current Concepts. *Adv. Urol.* **2018**, Feb 4.
- (5) Lorenzo, V.; Torres, A.; Hernández, D.; Ayus, J. C. *Manual de Nefrología*, 2nd ed.; Elsevier, España, 2002.
- (6) González, A. F.; Pieters, L.; Hernández, R. D. Effectiveness of Herbal Medicine in Renal Lithiasis: A Review. *Siriraj Med. J.* **2020**, *72* (2), 188–194.
- (7) Beto, J. A. *Herbal Use in the Nutrition Management of Kidney Stones*; Han, H.; Mutter, W.; Nasser, S., Ed.; Cham Humana, 2019.

- (8) Miyaoka, R.; Monga, M. Use of Traditional Chinese Medicine in the Management of Urinary Stone Disease. *Int. Braz J Urol* **2009**, *35* (4), 396–405.
- (9) Butterweck, V.; Khan, S. R. Herbal Medicines in the Management of Urolithiasis: Alternative or Complementary? *Planta Med.* **2009**, *75* (10), 1095–1103.
- (10) Kieley, S.; Dwivedi, R.; Monga, M. Ayurvedic Medicine and Renal Calculi. *J. Endourol.* **2008**, *22* (8),
- (11) Ballabh, B.; Chaurasia, O. P.; Ahmed, Z.; Singh, S. B. Traditional Medicinal Plants of Cold Desert Ladakh-Used against Kidney and Urinary Disorders. *J. Ethnopharmacol.* **2008**, *118* (2), 331–339.
- (12) Gürocak, S.; Küpeli, B. Consumption of Historical and Current Phytotherapeutic Agents for Urolithiasis: A Critical Review. *J. Urol.* **2006**, *176* (2), 450–455.
- (13) Dhole, A. R.; Yeligar, V. C. Urolithiasis and Its Herbal Remedies. *Int. J. Sci. Res. Sci. Technol.* **2018**, *4* (11), 150–156.
- (14) Nirumand, M. C.; Hajialyani, M.; Rahimi, R.; Farzaei, M. H.; Zingue, S.; Nabavi, S. M.; Bishayee, A. Dietary Plants for the Prevention and Management of Kidney Stones: Preclinical and Clinical Evidence and Molecular Mechanisms. *Int. J. Mol. Sci.* **2018**, *19* (3).
- (15) Kasote, D. M.; Jagtap, S. D.; Thapa, D.; Khyade, M. S.; Russell, W. R. Herbal Remedies for Urinary Stones Used in India and China: A Review. *J. Ethnopharmacol.* **2017**, *203*, 55–68.
- (16) Bahmani, M.; Baharvand-Ahmadi, B.; Tajeddini, P.; Rafieian-Kopaei, M.; Naghdi, N. Identification of Medicinal Plants for the Treatment of Kidney and Urinary Stones. *J. Ren. Inj. Prev.* **2016**, *5* (3), 129–133.
- (17) Ahmed, S.; Hasan, M. M.; Alam, Z. In-Vitro Urolithiasis Models: An Evaluation of Prophylactic Management against Kidney Stones. *J. Pharmacogn. Phytochem.* **2016**, *5* (3), 28–35.
- (18) Delfan, B.; Baharvand-Ahmadi, B.; Bahmani, M.; Mohseni, N.; Saki, K.; Rafieian-Kopaei, M.; Shahsavari, S.; Naghdi, N.; Taherikalani, M.; Ghafourian, S. An Ethnobotanical Study of Medicinal Plants Used in Treatment of Kidney Stones and Kidney Pain in Lorestan Province, Iran. *J. Chem. Pharm. Sci.* **2015**, *8* (4), 693–699.
- (19) Sharma, N.; Tanwer, B. S.; Vijayvergia, R. Study of Medicinal Plants in Aravali Regions of Rajasthan for Treatment of Kidney Stone and Urinary Tract Troubles. *Int. J. PharmTech Res.* **2011**, *3* (1), 110–113.
- (20) NOUMI, E. Potentiality of Medicinal Plants in Treating Urinary Lithiasis in Littoral Region, Cameroon. *European J. Med. Plants* **2011**, *1* (3), 74–87.
- (21) Freitas, A. M.; Schor, N.; Boim, M. A. The Effect of Phyllanthus Niruri on Urinary Inhibitors of Calcium Oxalate Crystallization and Other Factors Associated with Renal Stone Formation. *BJU Int.* **2002**, *89* (9), 829–834.
- (22) Barros, M. E.; Lima, R.; Mercuri, L. P.; Matos, J. R.; Schor, N.; Boim, M. A. Effect of Extract of Phyllanthus Niruri on Crystal Deposition in Experimental Urolithiasis. *Urol. Res.* **2006**, *34* (6), 351–357.
- (23) Barros, M. E.; Schor, N.; Boim, M. A. Effects of an Aqueous Extract from Phyllanthus Niruri on Calcium Oxalate Crystallization in Vitro. *Urol. Res.* **2003**, *30* (6), 374–379.
- (24) Nishiura, J. L.; Campos, A. H.; Boim, M. A.; Heilberg, I. P.; Schor, N. Phyllanthus Niruri Normalizes Elevated Urinary Calcium Levels in Calcium Stone Forming (CSF) Patients. *Urol. Res.* **2004**, *32* (5), 362–366.
- (25) Pucci, N. D.; Marchini, G. S.; Mazzucchi, E.; Reis, S. T.; Srougi, M.; Evazian, D.; Nahas, W. C. Effect of Phyllanthus Niruri on Metabolic Parameters of Patients with Kidney Stone: A Perspective for Disease Prevention. *Int. Braz J Urol* **2018**, *44* (4), 758–764.
- (26) Boim, M. A.; Heilberg, I. P.; Schor, N. Phyllanthus Niruri as a Promising Alternative Treatment for Nephrolithiasis. *Int. Braz J Urol* **2010**, *36* (6), 657–664.
- (27) Atmani, F.; Khan, R. Effects of an Extract from Herniaria Hirsuta on Calcium Oxalate Crystallization in Vitro. **2000**, 621–625.
- (28) Atmani, F.; Slimani, Y.; Mimouni, M.; Hacht, B. Prophylaxis of Calcium Oxalate Stones by Herniaria Hirsuta on Experimentally Induced Nephrolithiasis in Rats. *BJU Int.* **2003**, *92* (1), 137–140.
- (29) Atmani, F.; Farell, G.; Lieske, J. C. Extract from Herniaria Hirsuta Coats Calcium Oxalate Monohydrate Crystals and Blocks Their Adhesion to Renal Epithelial Cells. *J. Urol.* **2004**, *172* (4 I), 1510–1514.
- (30) Fouada, A.; Yamina, S.; Nait, M. A.; Mohammed, B.; Abdlekrim, R. In Vitro and in Vivo Antilithiasic Effect of Saponin Rich Fraction Isolated from Herniaria Hirsuta. *J. Bras. Nefrol.* **2006**, *28* (4), 199–203.
- (31) Navarro, E.; Alonso, J.; Rodriguez, R.; Trujillo, J.; Boada, J. Diuretic Action of an Aqueous Extract of

- Lepidium Latifolium L. *J. Ethnopharmacol.* **1994**, *41* (1–2), 65–69.
- (32) Verma, A. K.; Goyal, Y.; Dev, K. Medicinal Value and Mechanism of Light Adaptation in Lepidium Latifolium in Ladakh Region. **2019**, *20* (3), 49–55.
- (33) Tabassum, N.; Ahmad, F. Role of Natural Herbs in the Treatment of Hypertension. **2011**, *5* (9).
- (34) González, J. G. Estudio de Los Usos Culturales de Las Plantas Silvestres En Los Campos de Gran Canaria. **2017**, *111*.
- (35) Conde-Rioll, M.; Gajate, C.; Fernández, J. J.; Villa-Pulgarin, J. A.; Napolitano, J. G.; Norte, M.; Mollinedo, F. Antitumor Activity of Lepidium Latifolium and Identification of the Epithionitrile 1-Cyano-2,3-Epithiopropene as Its Major Active Component. *Mol. Carcinog.* **2018**, *57* (3), 347–360.
- (36) Blažević, I.; Đulović, A.; Maravić, A.; Čikeš Čulić, V.; Montaut, S.; Rollin, P. Antimicrobial and Cytotoxic Activities of Lepidium Latifolium L. Hydrodistillate, Extract and Its Major Sulfur Volatile Allyl Isothiocyanate. *Chem. Biodivers.* **2019**, *16* (4).
- (37) Brown, C. M.; Purich, D. L.; Ackermann, D. K. EQUIL 93: A Tool for Experimental and Clinical Urolithiasis. *Urol. Res.* **1994**, *22* (2), 119–126.
- (38) Kaur, T.; Hussain, K.; Koul, S.; Vishwakarma, R.; Vyas, D. Evaluation of Nutritional and Antioxidant Status of Lepidium Latifolium Linn.: A Novel Phytofood from Ladakh. *PLoS One* **2013**, *8* (8), 1–9.
- (39) Guyot, S.; Doco, T.; Souquet, J. M.; Moutounet, M.; Drilleau, J. F. Characterization of Highly Polymerized Procyanidins in Cider Apple (*Malus Sylvestris* Var. Kermerrien) Skin and Pulp. *Phytochemistry* **1997**, *44* (2), 351–357.
- (40) Djilani, A.; Legseir, B.; Soulimani, R.; Dicko, A.; Younos, C. New Extraction Technique for Alkaloids. *J. Braz. Chem. Soc.* **2006**, *17* (3), 518–520.
- (41) Le, P. M.; Benhaddou-Andaloussi, A.; Elimadi, A.; Settaf, A.; Cherrah, Y.; Haddad, P. S. The Petroleum Ether Extract of *Nigella Sativa* Exerts Lipid-Lowering and Insulin-Sensitizing Actions in the Rat. *J. Ethnopharmacol.* **2004**, *94* (2–3), 251–259.
- (42) Abushama, M. Lethality and Antioxidant Activity of Some Sudanese Medicinal Plants' Fixed Oils. *European J. Med. Plants* **2014**, *4* (5), 563–570.
- (43) Chaieb, N.; González, J. L.; López-Mesas, M.; Bouslama, M.; Valiente, M. Polyphenols Content and Antioxidant Capacity of Thirteen Faba Bean (*Vicia Faba* L.) Genotypes Cultivated in Tunisia. *Food Res. Int.* **2011**, *44* (4), 970–977.
- (44) Standard, I. INTERNATIONAL STANDARD Content of Total Polyphenols in Tea — Colorimetric Method Using Folin-Ciocalteu Reagent. **2005**.
- (45) Ahmed, D.; Khan, M. M.; Saeed, R. Comparative Analysis of Phenolics, Flavonoids, and Antioxidant and Antibacterial Potential of Methanolic, Hexanic and Aqueous Extracts from *Adiantum Caudatum* Leaves. *Antioxidants* **2015**, *4* (2), 394–409.
- (46) H. Valido, Iris; Patilla-Gutiérrez, Daniel; Valiente, Manuel; López-Mesas, M. In Vitro Study of the Promoters/Inhibitors Influence in Oxalocalcic Nephroliths Formation: Approach for the Development of Urine Inhibitory Capacity (UIC) as a Risk Index. *Unpublished*.
- (47) Jayaprakasha, G. K.; Selvi, T.; Sakariah, K. K. Antibacterial and Antioxidant Activities of Grape (*Vitis Vinifera*) Seed Extracts. *Food Res. Int.* **2003**, *36* (2), 117–122.
- (48) Negi, P. S.; Jayaprakasha, G. K. Antioxidant and Antibacterial Activities of *Punica Granatum* Peel Extracts. *J. Food Sci.* **2003**, *68* (4), 1473–1477.
- (49) Sugiwati, S.; Setiasih, S.; Afifah, E. Antihyperglycemic Activity of The Mahkota Dewa (*Phaleria Macrocarpa* (Scheff.) Boerl.) Leaf Extracts as an Alpha-Glucosidase Inhibitor. *Makara Kesehat.* **2009**, *13* (2), 74–78.
- (50) Zheng, W.; Boada, R.; He, R.; Xiao, T.; Ye, F.; Simonelli, L.; Valiente, M.; Zhao, Y.; Hassan, M. Extracellular Albumin Covalently Sequesters Selenocompounds and Determines Cytotoxicity. *Int. J. Mol. Sci.* **2019**, *20* (19).
- (51) Ngamwongsatit, P.; Banada, P. P.; Panbangred, W.; Bhunia, A. K. WST-1-Based Cell Cytotoxicity Assay as a Substitute for MTT-Based Assay for Rapid Detection of Toxicogenic *Bacillus* Species Using CHO Cell Line. *J. Microbiol. Methods* **2008**, *73* (3), 211–215.
- (52) Melcrová, A.; Pokorna, S.; Pullanchery, S.; Kohagen, M.; Jurkiewicz, P.; Hof, M.; Jungwirth, P.; Cremer, P. S.; Cwiklik, L. The Complex Nature of Calcium Cation Interactions with Phospholipid Bilayers. *Sci. Rep.* **2016**, *6*, 1–12.

- (53) Huster, D.; Arnold, K.; Gawrisch, K. Strength of Ca^{2+} Binding to Retinal Lipid Membranes: Consequences for Lipid Organization. *Biophys. J.* **2000**, *78* (6), 3011–3018.
- (54) H. Valido, Iris; Resina-Gallego, Montserrat; Yousef, Ibraheem; Luque-Gálvez, Maria Pilar; Valiente, Manuel; López-Mesas, M. Calcium Oxalate Kidney Stones, Where Is the Organic Matter?: A Synchrotron Based Infrared Microspectroscopy Study. *J. Biophotonics* **2020**.
- (55) Li, S.; Tang, W.; Shi, P.; Li, M.; Sun, J.; Gong, J. A New Perspective of Gallic Acid on Calcium Oxalate Nucleation. *Cryst. Growth Des.* **2020**, *20* (5), 3173–3181.
- (56) Sun, X. Y.; Ouyang, J. M.; Xu, M. Synthesis, Characterization, and Cytotoxicity Assay of Calcium Oxalate Dihydrate Crystals in Various Shapes. *CrystEngComm* **2016**, *18* (29), 5463–5473.
- (57) Nenow, D.; Vitkov, L. Effect of the Opposite Directions on the Crystal Face upon the Growth Kinetics of Weddellite. *J. Cryst. Growth* **1997**, *182* (3–4), 461–464.
- (58) Alajmi, M. F.; Alam, P.; Rehman, M. T.; Husain, F. M.; Khan, A. A.; Siddiqui, N. A.; Hussain, A.; Kalam, M. A.; Parvez, M. K. Interspecies Anticancer and Antimicrobial Activities of Genus *Solanum* and Estimation of Rutin by Validated UPLC-PDA Method. *Evidence-based Complement. Altern. Med.* **2018**, 2018.
- (59) Alajmi, M. F.; Alam, P.; Alqasoumi, S. I.; Ali Siddiqui, N.; Basudan, O. A.; Hussain, A.; Mabood Husain, F.; Ali Khan, A. Comparative Anticancer and Antimicrobial Activity of Aerial Parts of *Acacia Salicina*, *Acacia Laeta*, *Acacia Hamulosa* and *Acacia Tortilis* Grown in Saudi Arabia. *Saudi Pharm. J.* **2017**, *25* (8), 1248–1252.
- (60) Samarakoon, S. R.; Shanmuganathan, C.; Ediriweera, M. K.; Tennekoon, K. H.; Piyathilaka, P.; Thabrew, I.; de Silva, E. D. In Vitro Cytotoxic and Antioxidant Activity of Leaf Extracts of Mangrove Plant, *Phoenix Paludosa* Roxb. *Trop. J. Pharm. Res.* **2016**, *15* (1), 127–132.
- (61) Bhavna, M.; Keyur H., D.; Dharmik D., P.; Pinal D., P.; Divya, P.; Maulik P., S.; Vipul P., P.; Sunil B., B. In-Vitro Cytotoxicity Evaluation of Aqueous Fruit and Leaf Extracts of *Grewia Asiatica* Using MTT Assay. *Der Pharma Chem.* **2011**, *3* (3), 282–287.
- (62) Veeresh Babu, P.; Vamsi Krishna, M.; Ashwini, T.; Ganga Raju, M. Antilithiatic Activity of *Grewia Asiatica* in Male Rats. *Int. J. Pharm. Sci. Res.* **2017**, *8* (3), 1326–1335.
- (63) Hajiboland, R.; Bahrami-Rad, S.; Zeinalzade, N.; Atazadeh, E.; Akhiani, H.; Poschenrieder, C. Differential Functional Traits Underlying the Contrasting Salt Tolerance in *Lepidium* Species. *Plant Soil* **2020**, *448* (1–2), 315–334.



CHAPTER 4

GENERAL DISCUSSION OF THE RESULTS

“Progress is made by trial and failure; the failures are generally a hundred times more numerous than the successes; yet they are usually left unchronicled”

William Ramsay

Since the work carried out to develop the present Thesis has been presented in the form of six manuscripts (two already published), the general discussion of the results is divided in six sections in order to facilitate its reading and understanding.

4.1. “Characterization of calcium oxalate hydrates and the transformation process”

To confirm the crystallographic phases of the synthetic samples, profile matching refinement of the diffraction patterns obtained was performed by starting with the structures reported in the literature for COD (weddelite) and COM (whewellite) determined from single crystal fragments extracted from kidney stones. It was determined that COM correspond to the monoclinic, $P2_1/c$ (low temperature structure, COM-LT), and COD correspond to the tetragonal (bipyramidal), $I4/m$.

Moreover, the local coordination environment of calcium in the two calcium oxalate hydrates was studied by X-ray absorption spectroscopy (XAS) as a short-range order study. According to the literature, the crystalline structure of the dihydrated species contains equivalent planar units of oxalate (symmetry group C_{2v}), while the monohydrated species contains one planar (symmetry group C_{2h}) and other barely twisted (symmetry group D_{2h}), with a shorted C-C distance, oxalate. This information has been considered in the DFT computational study performed for the vibrational frequencies assignment, as well as the results described from the XRD and XAS analysis, since it proves that the structures from the literature reproduce the results obtained from the long and short ranges structural characterization.

With the aim of monitoring the transformation process from the dihydrated to the monohydrated calcium oxalate, a Multivariate Curve Resolution (MCR) analysis of the IR spectra collected at different stages of the transformation was performed. This analysis was carried out in the region where both species present the larger spectral differences, between 100 and 820 cm^{-1} , being the peak at 912 cm^{-1} ($\nu(\text{C-C}) + \delta_i(\text{COO})$ scissoring + $\nu(\text{M-O})$) characteristic of COD, and the peaks at 883 cm^{-1} ($\delta_i(\text{COO})$ scissoring + $\nu(\text{M-O})$) and 948 cm^{-1} (water libration) characteristic of

COM. The half-time ($t_{1/2}$) transformation in water has been determined by non-linear (sigmoidal) fitting of the MCR component concentration that correspond to COD. By comparing, with the application of LeBail fitting, the diffractograms from the transformed weddellite (TRA) with the synthetic COM and COD, it was determined that it is the same as synthetic COM, but with peaks less intense.

The transformation process has been characterized by a first step corresponding to the decomposition of the COD crystalline structure, produced by the alteration of the “zeolitic water” channel site occupancy, which promotes the structural rearrangement (closing the channel). Moreover, there is a second step in which, during the cell reorganization, the $\nu(\text{C-C})$ of the COD oxalate is gradually restrained (associated with the symmetric $\delta_i(\text{COO})$ scissoring+ $\nu(\text{M-O})$), ending in an asymmetric scissoring of the COM $\delta_i(\text{COO})$ + $\nu(\text{M-O})$, corresponding to the more stable symmetries of the oxalate coordination. Taking into account the described transformation, it can be deduced that there are some aspects that could stabilize the COD structure, such as: larger crystal sizes, elements that “protects” the zeolitic channel (like organic matter or big ligands that interact with the (001) plane in order to avoid the zeolitic water exchange with the medium) and elements that could interact with (stabilize) the (200) plane (like common calcium oxalate inhibitors present in the urine as citrate and phosphate among others).

4.2. “Calcium oxalate kidney stones, where is the organic matter?: A synchrotron based infrared spectroscopy study”

To differentiate between calcium oxalate species, the measurements performed in reflectance mode with SR- μ FTIR of three different set of samples (COD, COM and TRA) were analyzed by applying PCA. It is possible to differentiate between monohydrated and dihydrated species but it is difficult to distinguish between COM and TRA. It is possible to observe differences between them, but due to high variability of each species individually, as was described by the PCA and ANOVA analysis, it is not possible to distinguish them.

By studying the intensity ratios between the peaks corresponding to the asymmetric stretching of the aliphatic $-\text{CH}_2/-\text{CH}_3$, it is possible to differentiate

between proteins and lipids, since the presence of long $-CH_2-$ chains in the lipids structures means a higher $-CH_2/-CH_3$ ratio, being the opposite for proteins. Considering the spectra collected from non-transformed COD, as well as from nephroliths undergoing the transformation process, it was observed that the organic matter found in the non-transformed COD crystallites is mostly represented by lipids, while crystallites undergoing the transformation process, or already transformed, presented mainly proteins. Moreover, the distribution of the organic matter throughout COM was studied by selecting crystals from the nucleus and surface of quiescent COM kidney stones (without white/grayish film on their surface), where proteins were located in the nucleus and lipids in the surface by comparing the same mentioned peaks in a PCA analysis. The location of the lipids, as well as their presence in non-transformed COD crystallites, suggest that they could act as inhibitors of the formation of COM and the stabilization of the crystalline conversion of COD.

There are works in the literature that described proteins as promoters of the stone formation, while other suggest they are inhibitor, or that the role of promoters or inhibitors depend on the type of protein. In the presented study, the proteins found in the nucleus of COM stones have not been identified. However, it could be related with low-molecular-weight proteins (LMWP) that, as it has been described in the literature, could be also derived from an oxidative stress produced in the kidney during the stone formation process, with generates reactive oxygen species (ROS). The oxidative stress in the kidney could favor the calcium oxalate stone formation by two different means: the loss of an inhibitory potential (lipids breakdown), and the formation of promoters (products of the lipid peroxidation and the formation of LMWP).

4.3. “Discriminating the formation origin of calcium oxalate monohydrate in kidney stones via synchrotron microdiffraction”

The first step of this study was to analyze a representative number of the selected kidney stones samples by ATR-FTIR. It was expected that samples classified by morpho-constitutional analysis as COD or COM should have a relative concentration of 100% of the respective oxalocalcic species, which was observed in

a sample classified as COM, but not in the ones classified as COD. In samples classified as COD, where the presence of its characteristic crystals (by shape and color) were observed with the stereomicroscope, a relative CaOx concentration of 100% COM was observed, which indicates that those stones were, in fact, totally transformed. On the other hand, two samples classified as COD with HAP between crystals presented a relative CaOx concentration of a COM:COD mixture. These results suggest that stones formed as COD with HAP between crystals are less transformed or more stable over the formation/development time. Furthermore, these results show the great difficulty to differentiate between COM and those CaOx monohydrated that come from the crystalline conversion of the unstable COD (named TRA) by using ATR-FTIR, as reported in the second article of this Thesis work.

The synthetic CaOx samples were analyzed by powder diffraction in the same synchrotron beamline, while the selected oxalocalcic stones were analyzed by through-the-substrate micro X-ray diffraction (tts- μ XRD). By comparing the diffraction patterns of the synthetic samples with the stones, it was observed that CaOx nephroliths presented the most common reflections characteristics of each species. However, not all the reflections were present in the renal calculi due to the preferential orientation of the crystallites in the stone as a consequence of its formation/growth.

In order to determine if there are significant differences between the diffraction patterns of COM and TRA from kidney stones, a PCA was performed in the region of interest ($2\theta = 2.5-9.5^\circ$). As a result, COD was easily separated from the monohydrated species by its characteristic reflections (200) and (222) in the negative region of PC-3, while the principal contribution in its positive region was the reflection (021) of the monohydrated CaOx. However, COM and TRA were mixed over PC-1 and PC-2, which indicates that it is not possible to differentiate between them, since both are the same crystallographic phase (space group, $P2_1/c$).

The collected 2D μ XRD images provided also information regarding the sample texture, orientation degree and graininess affecting how the intensity of the reflections are distributed along the Debye rings. In this aspect, differences can be

observed in the 2D diffraction images of four representative points of CaOx stones previously classified by morpho-constitutional analysis: for COD, individual reflections appear as small spots, characteristic of single crystals at a specific orientation; for COM, the image shows elongated spots following partially the Debye ring and representing a distribution of close orientations, corresponding to a textured sample with a clear distribution of orientation; for TRA, the intensity of the reflections are more distributed along the Debye ring, approaching the behavior of random oriented polycrystalline samples; finally, MIX was defined as a point where both species are present since there is a contribution of signals of weddellite (COD) and whewellite (COM or TRA). Hence, it seems to be possible to differentiate between COM and TRA by their level of texture.

In order to have a better representation and a systematic method to analyze the observed differences, the evolution of the azimuthal intensity of selected reflections ((100) and (040)) has been plotted to obtain a linear representation of the pixel intensity evolution along the ellipse specified by the 2θ angle (Debye ring). There are clear differences between COM and TRA, since the elongated spots observed in the 2D μ XRD images, in the case of COM, are represented in the azimuthal plot by patterns repeated every 180° in the azimuthal angle, while no pattern is observed for TRA. The same analysis has been applied to a stone classified as papillary COM with HAP and organic matter in the nucleus (S33), which raised doubts about its formation origin when it was examined with the stereomicroscopy, since there were areas that presented different textures. By representing the azimuthal plot of the analyzed lines, it was determined that the stone was formed by a mixture of COM and TRA, which was correlated with the previous observation with the stereomicroscope.

Furthermore, an MCR analysis was performed to study the evolution of the different components throughout the collected diffractogram patterns along each measured line from the surface to the inside of the samples, allowing to solve the mixture composition of the sample along the analyzed line. It is well known that COD is transformed over time in the medium, therefore the transformation occurs along the crystal growth (oldest sections are more transformed) what is described

in this work as a Correlated transformation, since it is proportional to the formation time. This behavior has been observed in superficial deposits of COD over COM stones (e.g. S27 and S24). However, another transformation behavior has been observed, and since it is not proportional to the formation time, it has been described in this work as non-Correlated. It has been observed in samples classified as COD with HAP between crystals (e.g. S29). These two different features found in nephroliths classified as COD suggest that the level of transformation is not only related with the time after the formation of the crystal (or the contact with the medium), but also with the presence of certain components that could act as stabilizers of the dihydrated species.

4.4. “Understanding the crystalline conversion of oxalocalcic kidney stones: effect of common urine inhibitors *in vitro*”

Rather flat tetragonal bipyramid shapes represent COD crystallites. After a total transformation in water at 37°C and pH 6, the observed shape corresponds to the one observed for COM/whewellite crystals, monoclinic shaped crystallites. However, when the transformation takes place in water at 37°C and pH 7, the crystallites are slightly bigger and flatter in comparison. Nevertheless, in both cases the transformed COD crystals have the typical morphology and crystal habit found on the direct formation of COM. The half time transformation ($t_{1/2}$) in water can vary depending on the environment and the synthetic conditions, being between 16-34 hours of incubation at the mentioned conditions in this study. Hence, with the objective of performing a comparative study, the $t_{1/2}$ of the different experiments presented in this work are calculated with respect to the $t_{1/2}$ of COD in water, as control, being the results represented as Relative $t_{1/2}$ (Rel. $t_{1/2}$).

The first step of this work was to compare the inhibitory potential of the different individual components (phosphate, citrate, magnesium and phytate) at pH 6. It was observed that phosphate presents a promoting factor while increasing the concentration, while citrate does not promote or inhibits the transformation by itself. However, the combination of both in a 1:1 ratio decrease the promoting effect observed in the incubation with phosphate. These effects have been explained by the species present in solution at the mentioned conditions, being the dihydrogen

phosphate (H_2PO_4^-) the majoritarian species of phosphate, which has to compete with HCit^{2-} , when citrate is added, having the calcium citrate complexes a higher formation constant than the calcium phosphate ones. Having magnesium in the medium increase the Rel. $t_{1/2}$, but this is not altered by increasing its concentration. The case of phytate is particularly interesting, since it presents the higher inhibitory capacity of the individual components studied, which increases at higher concentrations, being the COD not totally transformed after five days of incubation in the medium with $4.5 \mu\text{M}$ of phytate. This effect could be related to the molecular structure of phytate, since, as has been reported in the literature and in a previous section, the alteration of the “zeolitic water” channel in the COD structure is what promotes the structural rearrangement and, hence, the crystalline conversion.

The morphology of the totally transformed crystals in the different media was studied by SEM. The shape of the crystals in the phosphate medium resembles the ones described in the literature as the “possible equilibrium shape of whewellite”, which could be caused by the faster transformation time in comparison, having a smaller crystal size when the phosphate concentration is increased. The crystallites incubated in the citrate medium presented an elongated hexagonal platelets shape, which has been previously described in studies described in the literature for the CaOx crystallization in synthetic urine (180 mg/L of calcium, 35 mg/L of oxalate and 600 mg/L of citrate) and with the structure reported in the literature for the growth of whewellite in the presence of citric acid. Similar behavior was observed in the incubation with the average concentration of magnesium (2 mM), while at the higher concentration (4 mM) a diamond-shaped like crystals were observed, being similar to the ones formed in the presence of bovine serum albumin (BSA), which binds to (12-1) and (021) faces reducing the crystal aspect ratio. The same shape has been also reported as “rhomboid” with a dominant pinacoid (100) and an additional facet (010) in whewellite crystals found in *Cactaceae*. Finally, the crystals transformed in the medium with the average concentration of phytate ($1.7 \mu\text{M}$) were similar to the one carried out in water, while when the concentration is increased ($4.5 \mu\text{M}$), a mixture of COM and COD

crystallites was observed, which is caused by the lack of a total transformation, as mentioned before.

It is common to find phosphate in CaOx kidney stones, usually as HAP, being a promoter of COM in the form of Randall's Plaques, or promoter of the formation of COD crystals in the form of colloidal phosphate, and being also found that HAP is present in stabilized COD, as described in the previous section. However, in the incubation with the individual components, phosphate was found to be a promoter of the crystalline conversion rather than an inhibitor. Hence, the combinations of calcium and magnesium with phosphate at two different pH values were studied, keeping the concentrations of Ca (5 mM) and magnesium (2 mM) constants and using two different concentrations of phosphate (5 and 50 mM). The Rel. $t_{1/2}$ of these combinations showed that the higher inhibitory capacity was achieved by the medium Ca:Phos-pH6-1:1, which could be related with the *in situ* formation of colloidal HAP. This result was corroborated with the IR spectra of the total transformed COD in the mentioned medium, which presented the characteristic bands that corresponds to HAP that is formed after the crystalline conversion of ACP. The inhibitory effect is considerably lost when the concentration of phosphate is increased (Ca:Phos-pH6-1:10), which could be related, once again, to the presence of H_2PO_4^- and the absence of colloidal HAP. There is also a loss in the inhibitory effect when the pH is increased from 6 to 7 at both phosphate concentrations, being possibly related to the higher stability of HAP at pH 7. In the case of the incubation in the Mg:Phos-pH6-1:2.5 medium, there is no inhibition or promotion of the crystalline conversion due to the formation of soluble magnesium phosphate complexes. However, when the magnesium concentration was increased (ratio 1:25), an increase on Rel. $t_{1/2}$ was observed, which could be associated to the formation of colloidal newberyite ($\text{MgHPO}_4 \cdot 3\text{H}_2\text{O}$), mineral also found in renal stones.

Regarding the morphologies of the crystals transformed on the media formed by the combinations of calcium or magnesium with phosphate, the results has been correlated with the ones performed on the individual components media. For example, the crystallites transformed in the Ca:Phos-pH6-1:10 presents similar

morphology and size the ones incubated with only phosphate, being caused by the presence of H_2PO_4^- ; the crystals incubated in the Ca:Phos media with the 1:1 ratio are elongated hexagonal platelets being similar to the ones transformed on the citrate medium.

Since urine is a complex medium, synergistic effects between different compounds are expected, that is why the effect of the combination of calcium and phosphate with magnesium or citrate has been studied. The high inhibitory effect presented by the Ca:Phos incubation at pH 6 present some lost when magnesium is added to the medium since it inhibits the crystallization of HAP by being adsorbed in the surface of its precursor (ACP). Moreover, due to the higher stability of the formed HAP in comparison with newberyite, no differences were observed when the pH was increased to 7 in the mixture with magnesium. On the other hand, when only citrate was added to the medium, no effect was observed, while when adding it to the Ca:Phos mixture, there was a remarkable improvement of the inhibition when comparing with its absence. This is related to the capacity of citrate to promote HAP nucleation while inhibiting its crystal growth, being also an aid in the stabilization of HAP hydrocolloids. These findings could mean that the HAP involved in the COD stabilization (found in stabilized kidney stones COD crystallites), are small colloids of certain characteristics. Regarding the crystalline morphologies observed on the transformation of these combinations, the Ca:Cit:Phos ratios present mostly COD crystals (with the exception of the Ca:Cit:Phos-pH7-1:1:10), which showed better inhibitory effect when compared with the same combinations without citrate, presenting also similar crystal morphologies that the ones transformed in the 8 mM citrate medium, being related, as explained before, to the interaction of citrate with the excess of phosphate in the medium. The crystals incubated in the medium mixed with magnesium showed similar morphologies than the ones carried out without calcium (Mg:Phos), with the exception of the Ca:Mg:Phos-pH6-1:1:1 medium, which results are similar of the ones performed for the same ratio without magnesium, indicating that it does not play a role, or it is not as significant as the Ca:Phos combination, on the crystalline conversion in the mentioned media.

4.5. “*In vitro* study of the promoters/inhibitors influence in oxalocalcic nephroliths formation: approach for the development of Urine Inhibitory Capacity (UIC) as a risk index”

The Artificial Human Urine (AHU) used as medium in this work is a complex matrix prepared to simulate the human urine under different COM Relative Supersaturation (RSS) conditions. The first part of the study was to monitor the crystalline conversion in the AHU in order to determine which parameters have a higher influence in the process. Hence, the relative half-time transformation (Rel. $t_{1/2}$) of COD in the different media was determined and compared with respect the RSS of each sample as well as the capacity of the inhibitors to complex calcium (Ca_{complex}). It was observed that the Rel. $t_{1/2}$ did not follow the same tendency that the RSS, while it did follow the one from Ca_{complex} , which means that, as higher the obtained calcium complexation value, higher is the capacity of the inhibitors to not only complex the free calcium, but also to interact with the calcium of the COD structure. This protective effect could be achieved by the interaction of the mentioned inhibitors with the (200) plane of the COD crystals, “protecting” the zeolitic channing and therefore preventing the decomposition of the COD crystalline structure.

Furthermore, an induction of the precipitation of calcium oxalate on the different AHU was performed by additions of calcium or oxalate. It was observed that the calcium inductions did not affect the relative nucleation of CaOx, while oxalate clearly forced its precipitation, increasing the relative nucleation in proportion with the RSS values. These differences can be explained by the average concentration of both analytes in the samples (and in urine), being the calcium concentration ten times higher than the oxalate one. Regarding the crystals morphologies after the inductions with oxalate, all samples precipitated mainly COM crystallites with the characteristic monoclinic structure, with the exception of RSS-5.3 where tetragonal bipyramid crystallites (characteristic of COD) were observed. This difference could be related to the Ca/Ox concentration ratio, being the mentioned sample the one with the higher value, since an excess of calcium in

the urine (hypercalciuria) is a known common pathology related to the formation of COD kidney stones.

Finally, to determine the risk of a saturated urine to develop a CaOx kidney stone, a continuous method of its precipitation by the addition of oxalate has been developed. The graphical representation of the oxalate concentration added (x-axis) vs. the relative absorbance measured (y-axis) has the form of sigmoidal curves, in which the characteristic parameters calculated after performing a Boltzmann fitting are the maximum slope of the curve (Max. Slope) and the concentration of oxalate needed to start the precipitation (named First Turning Point, FTP). What can be observed from these parameters is that the sample with the lower RSS (2.7) presents a higher FTP value, while two samples with the same RSS (9.5) do not present similar curves, being the one with the higher promoters/inhibitors ratio more similar to the AHU with the higher RSS (13.4). In order to determine if it is possible to differentiate the behaviors of those samples with the same RSS, the direct relationship between the FTP and Max. Slope of the sigmoidal curves, which has been defined as Urine Inhibitory Capacity (UIC) is proposed to perform the comparison. If the samples with RSS-9.5 are not considered, the calculated UIC values are inversely correlated to the RSS values. However, when the UIC of all samples is compared with the promoters/inhibitors ratio, it became a perfect match, proving the correlation of the proposed parameter with the capacity of the matrix components to prevent or favor the crystals formation.

4.6. “A comparative study of the *Lepidium latifolium* (Rompepiedras) extracts effect on calcium oxalate crystallization *in vitro*”

Since the leaves of *Lepidium latifolium* are consumed in folk medicine as an infusion and are sold for they use as dried leaves in vacuum packs, the antioxidant capacity of the aqueous extract and the powdered dry leaves were determined by DDPH and FRAP assays after performing a pretreatment with methanol or ethanol as solvent. It has been determined that the methanol pretreatment achieved a higher antioxidant capacity in both assays, which could be related to the effectiveness of both solvents to extract components such as polyphenols, which

are well known for their antioxidant properties, being usually extracted with methanol as solvent. Moreover, when the results from the powdered dry leaves, performed with methanol as solvent, of *Lepidium latifolium* collected in Gran Canaria were compared with a similar study reported in the literature with the same plant collected in the Ladakh region of India, a higher DPPH scavenging capacity has been observed. The difference in antioxidant capacity between the plants on both locations could be due to environmental conditions.

The relative nucleation of calcium oxalate after the induction of its precipitation on AHU in the presence of different *Lepidium latifolium* extracts (polyphenols, flavonoids, alkaloids and fixed oils) as evaluated. It was observed that flavonoids and alkaloids promote the precipitation of calcium oxalate (more crystals in the sample than in the control), while polyphenols and fixed oils inhibit it (less crystals in the sample than in the control), being the latter the one with the highest inhibitory capacity. The inhibition produced by the polyphenols extract was associated to the formation of amorphous calcium phosphate (ACO), since amorphous material was observed in the SEM images and it was reported in the literature as a possible mechanism for the inhibition by gallic acid. Furthermore, the inhibition produced by the fixed oils extract can be related with the inhibitory potential of lipids, since they have a strong binding capacity with calcium ions, making them less available to interact with oxalate in the urine. This strong interaction is observed in the ATR-FTIR spectra of the crystals after the induction, since three characteristic peaks of the lipids are observed, 2962, 2922 and 2851 cm^{-1} , corresponding to the asymmetric stretching of $-\text{CH}_3$ and $-\text{CH}_2$ and the symmetric stretching of $-\text{CH}_2$ respectively.

The cytotoxic screening of the different extracts performed with a human embryonic cell line (HEK-293) showed that flavonoids is the less lethal of the extracts (higher IC_{50}). These values are high when compared with other plants extracts, having IC_{50} on the range of the ones reported for *Grewia asiatica* extracts, which is a plant, as *Lepidium latifolium*, rich in anthocyanin, a flavonoid.



CHAPTER 5

CONCLUSIONS

*“What we know is a drop, what we
don’t know is an ocean”*

Isaac Newton

The following points summarize the conclusions from the presented thesis dissertation:

Characterization of calcium oxalate hydrates

- The long-range (XRD) and short-range (XAS) order characterization of the synthetic oxalocalcic species, COM and COD, agrees with the structures reported in the literature for Whewellite and Weddellite respectively.
- The characteristic bands from the vibrational spectra (IR and Raman), from COD and COM, gathered from the literature, have been unified by assigning each peak to the corresponding vibration and oxalate symmetries with the application of a DFT computational analysis of the mentioned structures.

Crystalline conversion of COD

- The application of the Multivariate Curve Resolution (MCR) analysis to the SR- μ XRD results made possible to analyze the crystalline conversion of COD *in situ*, concluding that the transformation level is not only related with the crystal time in the medium, but it is also affected by the presence of other components (e.g. HAP), that could stabilize the dihydrated species.
- The *in vitro* crystalline conversion of COD into the monohydrate species has been monitored by the application of MCR analysis to the IR spectra. This method has been used to calculate the half-time ($t_{1/2}$) transformation in water and to characterize the process.
- The *in vitro* study of the COD crystalline conversion on the presence of common oxalocalcic inhibitors found in the urine showed that phytate presents the major inhibitory capacity, while phosphate promotes the transformation due to the presence of H_2PO_4^- in the medium.
- The results of the Ca:Phos combinations indicate that the formation of small HAP colloids is the responsible of the COD stabilization.
- The formation of HAP colloids is favored by the addition of citrate to the medium and it is inhibited by the addition of magnesium.

- The transformation of COD on urine like media with different Relative Supersaturation (RSS) values has been correlated with the complexation of calcium by urine inhibitors, which could prevent the decomposition of the COD crystalline structure by the stabilization of the zeolitic channel.

Distribution of the organic matter on oxalocalcic stones

- The organic matter distribution throughout calcium oxalate nephroliths was studied with SR- μ FTIR in transmittance mode, by analyzing the asymmetric stretching of the aliphatic $-\text{CH}_2-$ and $-\text{CH}_3$, making possible to differentiate between proteins and lipids.
- It was possible to determine that lipids participate in the stabilization of COD crystallites and as possible inhibitors of the COM formation/development.
- Proteins could act as promoters of the COM formation since they were found in the nucleus.
- The results in the present study are in agreement with the hypothesis that the formation of kidney stones could be related with an oxidative stress process, where LMWP (low molecular weight proteins) and the products of lipid peroxidation could act as promoters of the calculi formation.

Formation origin of calcium oxalate monohydrate

- By applying SR- μ FTIR in reflectance mode to oxalocalcic kidney stones, it is possible to differentiate between mono- and dihydrated species.
- However, due to the high variability on the calcium oxalate spectra, the slight differences observed between COM and TRA are not considered significant enough to distinguish them with the used technique.
- The use of SR- μ XRD is a useful tool to improve the knowledge applied to perform the morpho-constitutional analysis used to classify oxalocalcic kidney stones.
- Since COM and TRA are chemically and crystallographically the same, it is not possible to determine which is the formation origin of the monohydrated species (COM or the crystalline conversion of COD) by μ XRD.

- Nevertheless, it is possible to distinguish them by studying their crystalline texture degree in renal calculi with the qualitative analysis of the azimuthal plots of the selected reflections from the 2D μ XRD data.
- This new approach has shown that nephroliths originally formed as COM have well oriented structures, while TRA does not present the same level of texture, making possible to correlate the obtained results with the observations of the samples with the stereomicroscope.

Urine Inhibitory Capacity (UIC) as a risk index

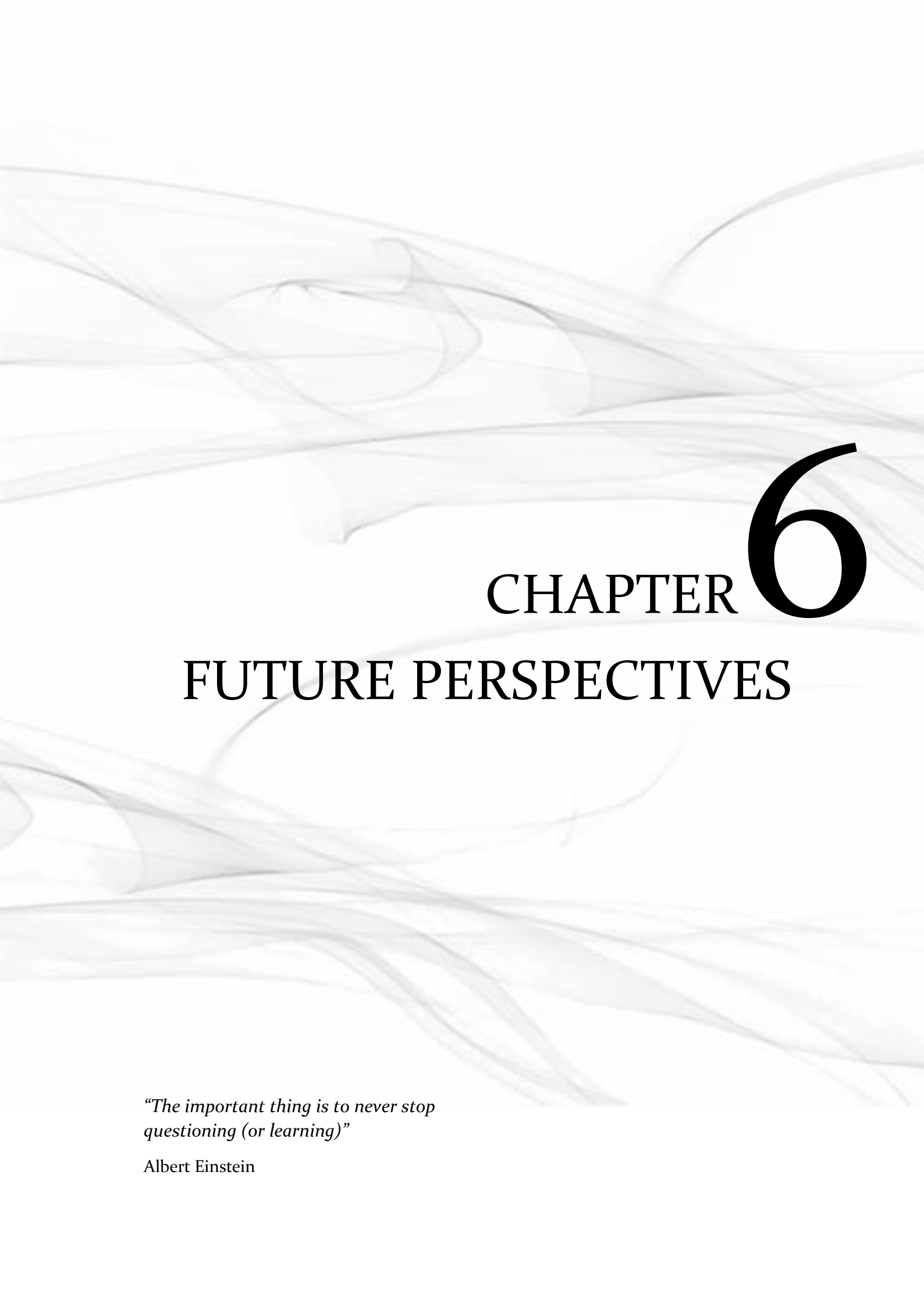
- The *in vitro* study of the formation and crystalline conversion of calcium oxalate crystals in a urine like medium, with different values of Relative Supersaturation (RSS), proved the importance of the promoters/inhibitors ratio for the stone formation process.
- The transformation of COD has been correlated with the complexation of calcium by urine inhibitors, which could prevent the decomposition of the COD crystalline structure by the stabilization of the zeolitic channel.
- Preliminary experiments to develop a new fast and affordable risk index have been performed, named Urine Inhibitory Capacity (UIC), based on the induction of the precipitation of calcium oxalate, and the measurement of the turbidity formed.
- The UIC is related with the capacity of the urine inhibitors to interact with the promoters and avoid the formation of the crystals. Since it is an *in situ* measurement, this parameter does not only consider a set of measured components with a mathematical approach, but the capacity of all the urine components to avoid the CaOx precipitation.
- UIC could help to differentiate between urines with the same RSS values but different risk of forming a stone, as well as to reduce the cost of the analysis.

***Lepidium latifolium* (Rompepedras) extracts**

- The methanolic pretreatment from the powdered dry leaves of *Lepidium latifolium* collected in Gran Canaria presented a higher antioxidant activity

that the one from the Ladakh region of India reported in the literature, which could be due to environmental conditions surrounding the plant growth.

- Flavonoids and alkaloids extracts presented a promoter potential while polyphenols and fixed oils extract were inhibitors, presenting the latter the highest capacity, of the *in vitro* formation of calcium oxalate crystals on a urine like medium at an intermediate RSS.
- The higher inhibitory capacity of the fixed oils extract has been related to the strong binding capacity of lipids to calcium ions and corroborates the results from previous analysis.
- Furthermore, the inhibitory potential of polyphenols has been related with the formation of amorphous calcium oxalate (ACO) reported in the literature and corroborated by the SEM images and the ATR-FTIR spectra.
- From the cytotoxic screening performed on a human embryonic kidney cell line (HEK-293), it was concluded that the studied extracts from the leaves of *Lepidium latifolium* present high IC_{50} values when compared with other plant extracts in the literature, which could be due to the high content of anthocyanin, a flavonoid.



CHAPTER 6

FUTURE PERSPECTIVES

*“The important thing is to never stop
questioning (or learning)”*

Albert Einstein

Considering the results described in the presented thesis, further insights can be divided in three branches as:

- Stone:

- After proving that it is possible to differentiate between COM and TRA by their level of texture, it will be necessary a wider correlation of these texture levels with the different transformed stones. It will be even more interesting if the mentioned correlation could be performed in a laboratory basis, allowing the analyst to perform a proper systematic classification.
- Moreover, it will be necessary, after analyzing a large population of samples, to introduce TRA into the morpho-constitutional analysis, as well the different degrees of transformation and the knowledge of how the different inhibitors affect their crystalline formation.
- After the analysis of the mentioned samples, and with the help of the knowledge gathered by the present study, it may be possible to correlate the transformation with pathologies, or with urine conditions, which will help to treat patients and decrease the recurrence rate.

- Urine:

- After observing that the Urine Inhibitory Capacity (UIC) can be considered as a risk index, it will be fundamental to determine the ranges in which the urine can be considered as healthy or from a stone former. Hence, it will be necessary to analyze samples from both groups with the developed methodology.
- Furthermore, it could be useful to have and automated system for the continuous induction on the UIC analysis. With this purpose, and automatic titrator and a turbidity probe could be used, trying to use the same computer software and to reduce the complexity of the system (there will not be necessary the use of different tubes to move the sample into the spectrophotometer).

- Treatment:

- Regarding the *Lepidium Latifolium*, further *in vitro* experiments will be necessary to demonstrate the efficacy of the different extracts analyzed in the present work. As an example, the different extracts could be digested by simulating the human metabolism, which means, apply the acids and enzymes of the salivary, gastric and intestinal digestions in order to determine which fractions arrive to the kidneys.
- Try to correlated the findings of the present work with other traditionally used treatments with the objective of determining a common inhibitory component (or group of components) that could be used as a treatment for the prevention or inhibition of the calcium oxalate nephroliths formation